



**HAL**  
open science

# Dissecting the role of calcium signaling in Fragile X syndrome

Sara Castagnola

► **To cite this version:**

Sara Castagnola. Dissecting the role of calcium signaling in Fragile X syndrome. Cellular Biology. COMUE Université Côte d'Azur (2015 - 2019), 2019. English. NNT : 2019AZUR4043 . tel-03273176

**HAL Id: tel-03273176**

**<https://theses.hal.science/tel-03273176>**

Submitted on 29 Jun 2021

**HAL** is a multi-disciplinary open access archive for the deposit and dissemination of scientific research documents, whether they are published or not. The documents may come from teaching and research institutions in France or abroad, or from public or private research centers.

L'archive ouverte pluridisciplinaire **HAL**, est destinée au dépôt et à la diffusion de documents scientifiques de niveau recherche, publiés ou non, émanant des établissements d'enseignement et de recherche français ou étrangers, des laboratoires publics ou privés.

# THÈSE DE DOCTORAT

## Le rôle de la signalisation calcique dans le Syndrome de l'X fragile

**Sara CASTAGNOLA**

Institut de pharmacologie moléculaire et cellulaire

**Présentée en vue de l'obtention  
du grade de docteur en Sciences de la Vie  
et de la Santé  
de l'Université Côte d'Azur  
Dirigée par le Dr. Barbara BARDONI  
Soutenue le : 28 Juin 2019**

**Devant le jury, composé de :**  
Barbara BARDONI, DR, IPMC UCA  
Alessandra FOLCI, Post-Doc, Istituto  
Clinico Humanitas  
Nicoletta LANDSBERGER, Professeur,  
Università degli Studi di Milano  
Séverine MASSENET, CRCN CNRS,  
Université de Lorraine  
Thomas MAURIN, Post-Doc, IPMC UCA  
Michèle STUDER, DR, IBV UCA

# **Le rôle de la signalisation calcique dans le Syndrome de l'X Fragile**

Jury :

Président du jury

Mme Michèle STUDER, DR INSERM, HDR, Institut de Biologie Valrose (IBV), Université Côte d'Azur (UCA), Nice (France)

Rapporteurs

Mme Nicoletta LANDSBERGER, Professeur, Dipartimento di Biotecnologie Mediche e Medicina Translazionale, Università degli Studi di Milano, Milano (Italie)

Mme Séverine MASSENET, CRCN CNRS, HDR, Bipôle de l'Université de Lorraine, Vandoeuvre Les Nancy (France)

Examineurs

M. Thomas MAURIN, Post-Doc, Institut de Pharmacologie Moléculaire et Cellulaire (IPMC), Valbonne (France)

Mme Alessandra FOLCI, Post-Doc, Laboratorio di Farmacologia e Patologia del Sistema Nervoso, Istituto Clinico Humanitas, Milano (Italie)

## **Titre : Le rôle de la signalisation calcique dans le Syndrome de l'X Fragile**

**Resumé :** Le syndrome de l'X fragile (FXS) est la forme héréditaire la plus commune de retard mental (RM) et la première cause de troubles du spectre de l'autisme (TSA). Il est causé par la perte d'expression du gène *FMR1* qui code la protéine Fragile X Mental Retardation Protein (FMRP). FMRP est une protéine capable de se lier aux ARNs, et elle est impliquée dans différentes étapes du métabolisme de l'ARN allant du transport des ARNs au contrôle de la traduction des ARNm au niveau du soma et des synapses. Pour identifier les différents ARNm ciblés par FMRP, nous avons séquencé à haut-débit les ARNs isolés par « crosslinking » immunoprécipitation (HITS-CLIP ou CLIP-seq). Cette technique nous a permis d'identifier 1065 ARNm liés par FMRP avec une forte affinité. Un nombre remarquable de ces ARNm code des régulateurs de l'homéostasie ionique, et plus particulièrement l'homéostasie calcique.

A partir de ces données, j'ai développé le premier axe de ma thèse, ciblé sur la compréhension de l'homéostasie du  $Ca^{2+}$  dans le FXS. Je me suis plus particulièrement focalisée sur l'une des cibles principales de FMRP, appelée *Cacna1a*. Ce gène code la sous-unité formant le pore du canal calcique voltage-dépendant de type P/Q (VGCC)  $Ca_v2.1$ , qui est localisé dans les neurones au niveau du compartiment somato-dendritique et de l'axone. Le canal  $Ca_v2.1$  laisse entrer le calcium dans le cytosol des neurones lors de la dépolarisation de la membrane, et de nombreux changements intracellulaires découlent de cet influx de calcium, en particulier la libération de neurotransmetteurs et la transcription calcium-dépendante. Mon but était d'analyser la corrélation entre l'absence de FMRP et l'expression de *Cacna1a* dans des cultures primaires de neurones afin de déterminer le rôle de ce gène et de cette protéine dans la physiopathologie du FXS. Pour cela, j'ai réalisé une analyse fonctionnelle de la régulation calcique en utilisant une méthode d'imagerie calcique sur des neurones en culture *Fmr1*-Knock-Out (KO) corticaux et hippocampaux. J'ai ainsi pu observer que ces neurones ont un influx de calcium plus faible et plus lent que les neurones sauvages (WT) en réponse à une dépolarisation KCl-dépendante. De plus, j'ai également montré que la protéine codée par *Cacna1a* a une activité et une synthèse réduite à la membrane plasmique des souris *Fmr1*-KO par rapport aux wild-type (WT). Mes résultats mettent donc en évidence un nouveau phénotype pour les neurones *Fmr1*-KO en culture et montrent que le défaut d'homéostasie calcique est un nouveau biomarqueur de ce modèle cellulaire.

Dans le second axe de mon travail, j'ai étudié le rôle de l'homéostasie calcique dans les différentes populations cellulaires qui composent le cerveau en présence et en absence de FMRP. Pour mieux décrire la diversité des différents types cellulaires observés en imagerie calcique et définir quelles caractéristiques moléculaires appartiennent à chaque sous-groupe neuronal, j'ai développé un nouvel outil d'analyse appelé aiFACS pour « agonist-induced Functional Analysis and Cell Sorting ». Cette technique permet de stimuler individuellement les neurones et d'analyser leur réponse à un agoniste pharmacologique et de les trier simultanément. Différentes analyses «-omics» permettent ensuite de définir l'identité des différentes cellules et les éléments moléculaires qui caractérisent la réponse des neurones WT par rapport aux *Fmr1*-KO. Grâce à cette méthode, j'ai mis en évidence une dérégulation de l'excitabilité des interneurones, ce qui permet de mieux caractériser le schéma chimique du cerveau de ces souris.

**Mots-clés :** Syndrome de l'X Fragile, retard mental, troubles du spectre de l'autisme, FMRP, signalisation calcique,  $Ca_v2.1$ , hétérogénéité, interneurones, agonist-induced Functional Analysis and Cell Sorting (aiFACS)

## **Title: Dissecting the role of calcium signaling in Fragile X syndrome**

**Abstract:** Fragile X Syndrome (FXS) is the most common form of inherited intellectual disability (ID) and the primary cause of autism spectrum disorder (ASD). It originates from the lack of expression of the *Fragile X Mental Retardation 1 (FMR1)* gene which encodes the Fragile X Mental Retardation Protein (FMRP). FMRP is an RNA-binding protein involved in different steps of RNA metabolism, ranging from RNA transport to translational control of mRNAs at soma and at synapses. To identify the repertoire of mRNA targets of FMRP, we used the high-throughput sequencing of RNAs isolated by crosslinking immunoprecipitation (HITS-CLIP or CLIP-seq), resulting in the identification of 1065 mRNAs bound by FMRP with high affinity. Remarkably, a number of them encode regulators of ion homeostasis and, in particular, several calcium homeostasis players.

I started from these findings to develop the first axis of my thesis focused on the understanding of  $\text{Ca}^{2+}$  homeostasis in FXS. In particular, I focused on one of the most enriched mRNA targets of FMRP, namely *Cacna1a*. This gene encodes the pore-forming subunit of the P/Q type Voltage-Gated Calcium Channel (VGCC)  $\text{Ca}_v2.1$ , which is particularly expressed in neurons, both in axon terminal and somato-dendritic compartments. The  $\text{Ca}_v2.1$  channel allows the entry of calcium in the cytosol of neurons upon membrane depolarization and several intracellular changes derive from this calcium influx, notably neurotransmitter release and calcium-dependent gene transcription. My goal was to analyze the correlation between the lack of FMRP and the expression of *Cacna1a* in primary neuronal cultures, in order to define the role of this gene and its protein in the pathophysiology of FXS. For this purpose, I carried out a functional analysis of calcium regulation using a calcium-imaging approach in mouse cultured *Fmr1*-Knock-Out (KO) cortical/hippocampal neurons, and I observed that these neurons display a weaker and slower  $\text{Ca}^{2+}$  response to KCl-dependent depolarization than wild-type (WT) neurons. Consistent with these findings, I also showed that the protein product of *Cacna1a* has a reduced activity/expression at the plasma membrane of mutant mice compared to WT. Altogether, my results pinpoint a new phenotype for cultured *Fmr1*-KO neurons and describe calcium homeostasis impairment as a new biomarker in this cellular model.

In the second axis of my work, my interest further expanded toward the study of the role of  $\text{Ca}^{2+}$  homeostasis in different cellular populations that compose the brain in the presence and in the absence of FMRP. To better describe the cell type diversity observed during the previous neuronal imaging and define which molecular characteristics belong to which neuronal sub-group, I developed a new powerful tool called "agonist-induced Functional Analysis and Cell Sorting" (aiFACS). This technique allows to stimulate and analyze a neuronal response to a pharmacological agonist at a single-cell level and to simultaneously sort cells accordingly. Subsequent "-omic" investigation can then define the cell identity and the molecular determinants that characterize the response of WT versus *Fmr1*-KO neurons. By doing so, I was able to highlight a marked deregulation of interneuron excitability, which adds a step in the direction of drawing a detailed chemical map of the rodent brain.

**Keywords:** Fragile X syndrome, intellectual disability, autism spectrum disorder, FMRP, calcium signaling,  $\text{Ca}_v2.1$ , heterogeneity, interneurons, agonist-induced Functional Analysis and Cell Sorting (aiFACS)

# Acknowledgements

I would like to acknowledge the thesis committee members, who kindly agreed to evaluate my work. In particular, I am appreciative of Dr. Michèle STUDER for accepting to be the president of the jury, as well as of Dr. Nicoletta LANDSBERGER and Dr. Séverine MASSENET for their eagerness to be reviewers of my work. In addition, I thank Dr. Alessandra FOLCI and Dr. Thomas MAURIN for agreeing to examine my thesis.

I thank my thesis director, Dr. Barbara BARDONI for the opportunity she offered me of working in her laboratory in a warm and welcoming environment. Thank you, Barbara, for granting me your trust, respect and encouragement all along these past years.

I address my dearest gratitude to Dr. Thomas MAURIN, without whom my PhD wouldn't have been the same. Thank you, TomTom, for the endless help, precious knowledge and comforting words you accorded me throughout this long/rough/fun/complex/exciting journey.

A big "thank you" goes to the rest of my lab partners, the whole "BB team": both past and present members filled my PhD with great memories.

I thank all my friends, those who have been there from day one and those who joined me along the way. You don't need to be mentioned to know who you are.

And finally, to my family: your love and support never ceases to amaze me.

# Summary

RESUMÉ EN FRANÇAIS

ENGLISH ABSTRACT

ACKNOWLEDGEMENTS

ABBREVIATIONS

INTRODUCTION

## CHAPTER 1 – INTELLECTUAL DISABILITY

1. The definition of intellectual disability
2. The rise and fall of intellectual disability – a historical perspective
3. Neurodevelopmental disorders – moving away from IQ score
4. Intellectual disability – epidemiology and causes
5. Intellectual disability vs. Autism Spectrum Disorders (ASD)

## CHAPTER 2 – FRAGILE X SYNDROME

1. Fragile X syndrome – the history of its discovery
2. Fragile X syndrome – the disorder
3. Fragile X syndrome – an unusual X-linked condition
4. Fragile X syndrome – the phenotype
  - 4.1. Intellectual disability
  - 4.2. Physical features
  - 4.3. Epilepsy
  - 4.4. The behavioral phenotype
5. Fragile X syndrome – the genetics
  - 5.1. The *FMR1* gene
  - 5.2. From polymorphism to full mutation
  - 5.3. *FMR1* mutations and their implications in disease
6. Fragile X syndrome – the FMRP protein
  - 6.1. The FMRP family
  - 6.2. FMRP – the structure
  - 6.3. FMRP – the functions
7. Animal models of FXS
  - 7.1. *Danio rerio*
  - 7.2. *Drosophila melanogaster*
  - 7.3. *Rattus norvegicus*
  - 7.4. *Mus musculus*

## CHAPTER 3 – ALTERED SIGNALING IN FRAGILE X SYNDROME

1. Excitation and inhibition in Fragile X syndrome – the importance of balance
  - 1.1. Cortical GABAergic interneurons

## **2. Therapeutic strategies for FXS**

- 2.1. The glutamatergic pathway
- 2.2. The GABAergic pathway
- 2.3. The insulin pathway
- 2.4. The matrix metalloproteinases pathway
- 2.5. The endocannabinoid pathway
- 2.6. The serotonin pathway
- 2.7. The oxytocin pathway
- 2.8. The cAMP/cGMP pathway

## **3. Ion channel dysfunctions in FXS – other aberrant pathways in FXS**

- 3.1. FMRP regulation of ion homeostasis players
- 3.2. Calcium impairment in neurons
- 3.3. The important role of calcium in neurons
- 3.4. Voltage-gated calcium channels (VGCCs)

## **AIMS OF THE THESIS**

## **MATERIALS & METHODS**

## **RESULTS**

### **1. Search and characterization of target mRNAs of FMRP**

### **2. Validation of the main FMRP targets obtained by HITS-CLIP**

- 2.1. The Phosphodiesterase 2A (PDE2A)
- 2.2. The Ca<sub>v</sub>2.1 channel

### **3. Identification of genome expression alterations in FXS with aiFACS**

- 3.1. aiFACS sorted cells are amenable to genomic/cell biology experiments
- 3.2. aiFACS selection through AMPA stimulation enriches sorted cells in interneurons
- 3.3. aiFACS selection through AMPA stimulation unveils *Meis2* interneuron deficiencies in the absence of FMRP expression

## **DISCUSSION**

### **1. The search and characterization of FMRP mRNA targets**

### **2. Molecular characterization of FMRP function**

- 2.1. Full characterization of FMRP binding sequences in brain
- 2.2. Identification of new FMRP-binding coding regions enriched in the GAC codon
- 2.3. Understanding of how FMRP modulates mRNA translation
- 2.4. Description of the role of FMRP in mRNA transport

### **3. Pathophysiology of FXS**

- 3.1. The PDE2A pathway
- 3.2. The calcium pathway

### **4. aiFACS and cell heterogeneity**

### **5. Final considerations**

## **BIBLIOGRAPHY**

## **ANNEXES**

# Abbreviations

**3'-UTR:** 3'-UnTranslated Region

**5'-UTR:** 5'-UnTranslated Region

**5-HT:** 5-HydroxyTryptamine

**aa:** amino acid

**AAIDD:** American Association on Intellectual and Developmental Disabilities

**ADHD:** Attention-Deficit/Hyperactivity Disorder

**ASD:** Autism Spectrum Disorder

**CDC:** Center for Disease Control

**CICR:** Calcium-Induced Calcium Release

**CNS:** Central Nervous System

**dFMR1:** Fragile X Mental Retardation gene 1 (*Drosophila melanogaster*)

**DSM:** Diagnostic and Statistical Manual of mental disorders

**E/I:** Excitation/Inhibition

**ECM:** ExtraCellular Matrix

**eCS:** endoCannabinoid System

**FMR1:** Fragile X Mental Retardation gene 1 (human)

**Fmr1:** Fragile X Mental Retardation gene 1 (mouse)

**FMRP:** Fragile X mental Retardation Protein

**FMRP-mRNP:** FMRP-bound mRNAs

**FXPOI:** Fragile X-associated premature ovarian failure

**FXR1:** Fragile X mental retardation syndrome-Related protein 1

**FXR2:** Fragile X mental retardation syndrome-Related protein 2

**FXS:** Fragile X Syndrome

**FXTAS:** Fragile X-associated Tremor Ataxia Syndrome

**GABA:** Gamma-AminoButyric Acid

**hnRNPC:** heterogeneous nuclear RiboNucleoProtein C

**ID:** Intellectual Disability

**IDD:** Intellectual Developmental Disorders

**IGF-1:** Insulin-like Growth factor 1

**IP3R:** Inositol Triphosphate Receptor  
**KH domain:** K Homology domain  
**KO:** Knock-Out  
**LTD:** Long-Term Depression  
**MMP:** MetalloProteinase  
**MR:** Mental Retardation  
**NES:** Nuclear Export Signal  
**NDD:** NeuroDevelopmental Disorder  
**NLS:** Nuclear Localization Signal  
**PB:** P-Body  
**PDE2A:** PhosphoDiEsterase 2A  
**PMCA:** Plasma Membrane Ca<sup>2+</sup> ATPase  
**PND:** Post-Natal Day  
**RyR:** Ryanodine Receptor  
**SERCA:** Sarco-Endoplasmic Reticulum Ca<sup>2+</sup> ATPase  
**VGCC:** Voltage-Gated Calcium Channel  
**WT:** Wild Type  
**XLID:** X-linked

# Introduction

## CHAPTER 1 – INTELLECTUAL DISABILITY

### 1. The definition of intellectual disability

*“Intellectual Disability is a disability characterized by significant limitations in both intellectual functioning and in adaptive behavior, which covers many everyday social and practical skills. This disability originates before the age of 18.”*

Definition given by the American Association on Intellectual and Developmental Disabilities (AAIDD).

It is common between individuals to make comparisons based on each other's abilities and the observation can take into account several attributes, one of them being the faculty of accomplishing tasks based on intellectual and adaptive functioning, what is called Intellectual Ability (IA). The intellect is indeed defined as the capacity of reasoning and understanding objectively, and more in general to take in, compare and recall data. When an individual lacks this ability we talk about Intellectual Disability (ID) or, as was preferred in the past, Mental Retardation (MR).

ID/MR is a cluster of developmental syndromes and disorders characterized by significant impairment of cognitive functions and associated limitations in several areas or domains of function, such as cognitive, language, motor and auditory skills, moral judgment, psychosocial and adaptive behavior (Pratt and Greydanus, 2007). The most recent definition that takes in consideration the wide spectrum of disorders covered by

these troubles, is Intellectual Developmental Disorders (IDD), and it is founded on two aspects:

- 1) on one side ID/MR is considered a health condition by the World Health Organization (WHO), as reported in the International Classification of Diseases and Related Health Problems (category F.70);
- 2) on the other side, because of the patient's impairments in intellectual functions, ID/MR is classified as a part of disability, according to WHO's International Classification of Functioning, Disability and Health (ICF) (Salvador-Carulla et al., 2011).

This general description takes into account the patient's deficits affecting development, cognition and intellectual ability, which appear during the developmental period (from birth to late adolescence) and that are manifested concurrently with deficiencies in adaptive behavior and functioning as well as in intellectual performance. These defects can range from mild to severe (Pratt and Greydanus, 2007).

## **2. The rise and fall of intellectual disability – a historical perspective**

In ancient times, during Greek and Roman civilization, courage, temperance, justice and wisdom were the cardinal virtues advocated, as opposed to intelligence and physical strength that were only considered secondary. The lack of noteworthy predispositions in babies led to eugenic beliefs accompanied by a high rate of infanticides.

Various centuries later, in the medieval era, the mentally impaired served as jesters and fools or were left wandering the streets under the name of "les enfants du Bon Dieu" (children of the Good God), without receiving any support by physicians who did not consider educating them as their responsibility.

During the Renaissance two different approaches counter-posed: on one side, the flourishing of exploration into arts and science allowed the bettering of medical care, while on the other side magic, divinity and amulets were still largely used to treat diseases.

The 17<sup>th</sup> and 18<sup>th</sup> centuries brought significant changes in the understanding of nature through empirical observation, so that mentally retarded individuals could be considered diseased rather than immoral or wicked, and it's with the advent of the 1800's that medical concern really started to be oriented towards educational approaches for these patients. In particular, during the second half of the century, the unitary concept of mental deficiency was broken, leaving room for a wider analysis of the disease. Indeed, what was until then known as a homogeneous condition, was now categorized in sub-classifications; for instance, the "Mongolian type of idiocy" was described for the first time, leading the way for a deeper analysis of what is nowadays referred to as Down syndrome (Crissey, 1975; Mirabi, 1985).

However, despite the big efforts of physicians and educators, half a century later, in the early years of the 20<sup>th</sup> century, movements of social Darwinism provided justification for the eugenics movement, an example of which being Goddard's work "The Kallikak Family: A Study in the Heredity of Feeble-Mindedness" released in 1912 (Goddard, 1942). The conclusion of this study was that a variety of mental traits are hereditary, so the "feeble-minded" should be prevented from reproducing and segregated in institutions. Clearly, as a result, the general perception of mental illness got distorted and retarded individuals began to be regarded as a menace. This concept, as wrong and out of proportion as it was, grew stronger and extremely persuasive among the

populations and later became Hitler's rationale for the extermination of countless "incurables and mental defectives" in Germany.

The early 1900's, in spite of the terrible misconceptions and mistreatments reserved to the intellectually disabled that took place, were the years of some important scientific advances in the field. 1910 was indeed the year in which a new system to measure individual intelligence was invented and introduced in medicine, thanks to the work of the Association of Medical Officers of American Institutions for Idiotic and Feeble-Minded Persons. People that today are known as intellectually disabled were divided in three classifications, posing the bases for what today we call Intelligence Quotient (IQ) test. This tool allowed to somehow create a link between retardation and intelligence abilities, encouraging to view intellectual disability as a heterogeneous condition. **Figure 1** reports a chart adapted from a 1913 New York Times article regarding the classification of 1000 children in New York City schools based on their "defective characteristics". What might be striking for us looking at this graph in 2019 is the terminology used, which might appear harsh and not so subtle. In reality these terms at the time were not perceived as insulting or offensive, because they were proper medical terms used to classify mentally impaired individuals. However, the nomenclature used for deficiencies has always been slippery and in some ways difficult to adjust to, considering the negative identity some terms acquired in non-medical conversations. This is why there has been a step-by-step modification throughout the years to fit the medical terms according to their general perception. Therefore, "mental retardation" became "intellectual disability" and "retarded", "imbecile", "moron" and "idiot" individuals became "mentally impaired" with different abilities (Crissey, 1975; Mirabi, 1985).

As time passed by, the consciousness that individuals with intellectual disability were to be medically neglected grew weaker, and indeed an important twist was observed in 1959 when the concept of “practical skills” was associated with mental ability: this set the bases for concurrent deficits in intelligence on one side and adaptive skills on the other side, which is, as I previously stated, the ultimate definition of intellectual disability.

In 1966 the psychiatrist George Tarjan referred to ID as the “Cinderella” of psychiatry, pointing out the need of finding ways to anticipate and cure intellectual disability; he wrote “will Cinderella and the Prince meet? At the moment Cinderella is waiting and the Prince is probably searching” referring to the urge in prevention and treatment of mental disorders (Tarjan, 1966).

Certainly, it took several centuries to define and understand what is known today, but we have witnessed throughout the years slow but considerable advances in the field, starting from the acceptance of a previously feared condition, to initial educational achievements, and today individuals with ID can receive appropriate personalized support (Crissey, 1975; Goddard, 1942; King et al., 1997; Mirabi, 1985; Tarjan, 1966).

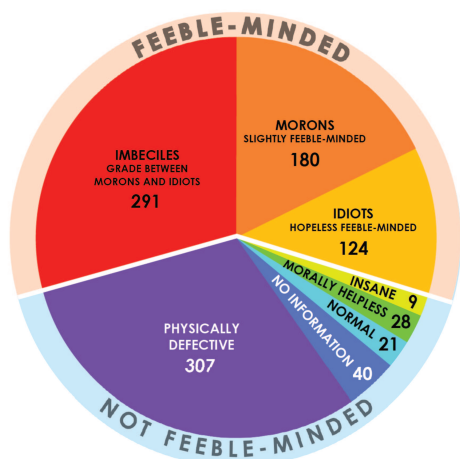


**Figure 1. The classification of 1000 children in New York City schools based on their “defective characteristics”** (adapted from the 1913 New York Times article titled “Nearly 15 000 000 school children are defectives”; <https://timesmachine.nytimes.com/timesmachine/1913/09/28/100407851.pdf>)

### **3. Neurodevelopmental disorders – moving away from IQ score**

In May 2013, the 5<sup>th</sup> edition of the Diagnostic and Statistical Manual of mental disorders (DSM-5) has been released, bringing improved definition and classification of mental disorders. This volume contains the guidelines that clinicians should follow to diagnose, treat and research mentally disabled people. Besides changes and improvements made on the criteria for learning disorders and the addition of “social communication disorders”, which are beyond the purpose of this thesis, there have been modifications in the benchmarks for intellectual disabilities, which were known as “mental retardations” in the previous manual (the DSM-IV).

To give a general definition, NeuroDevelopmental Disorders (NDDs) comprise various conditions associated with the function of the neurological system and brain, which are outlined by a combination of cognitive, communication, behavior and/or motor skill impairments that derive from abnormal brain development. The list of NDDs is quite long and include, among others, autism, intellectual and learning disabilities, and cerebral palsy and Attention-Deficit/Hyperactivity Disorder (ADHD). Some NDDs can be completely resolved over time, but many of them persist throughout life and their symptoms and behaviors can evolve according to the age of the patient. Several treatment options are currently available, despite not being resolute, and they can generally be divided in pharmacological and non-pharmacological interventions. The treatment of election for each disorder is highly linked to both the type of NDD and the symptoms presented by each patient. Treatment strategies often involve a combination of professional therapy, as well as pharmaceuticals and home/school-based programs. For the purpose of this thesis, I will focus on ID/MR and from now on, to avoid confusion, I will refer to ID/MR using only the terms intellectual disability or its acronym ID.

#### **4. Intellectual disability – epidemiology and causes**

Mental disorders are highly prevalent globally, affecting people of any class and status in every region of the world. The introduction of well-calibrated tests and criteria for ID allowed a more precise estimate of several mental disorders. Indeed, the statistical prevalence of ID estimated worldwide is approximately 1% to 3%, although the methodological characteristics of the singular studies can affect the results.

The individuals with more severe forms of intellectual disability typically receive the correct health care service they need. However, it is estimated that among those with milder forms of mental disorder less than half receive mental health support (Johnson and Walker, 2006; Merikangas et al., 2009). Despite the prevalence of ID being overall similar across ages, it has been estimated that as many as 40% of adults with ID are not known to the medical system.

It is noteworthy that ID is not a disease by itself but rather a developmental consequence of several circumstances. Although some causes of ID have been identified and researched upon, in 30-50% of all cases the origin of ID remains unknown. ID can be divided into two subfamilies according to the established risk factors:

- 1) syndromic ID, in which the intellectual defects are associated to other medical symptoms. Various genetic disorders can lead to ID, the most frequent ones being Down syndrome and Fragile X syndrome, accounting for about 30% of all ID cases;
- 2) non-syndromic ID, in which no other medical abnormalities co-occur. The main causative factors of non-syndromic ID are maternal substance abuse during pregnancy (e.g., alcohol abuse causes fetal alcohol syndrome) or exposure to certain infections (e.g., rubella), drugs or chemicals (e.g., valproic acid or

thalidomide; Vargesson, 2015). In addition, environmental factors like socioeconomic status, low parental education and caregiving issues can also lead to non-syndromic ID (Krauss).

## **5. Intellectual disability vs. Autism Spectrum Disorders (ASD)**

ASD is a fairly widespread neurodevelopmental condition affecting around 1 in 160 children worldwide but based on epidemiological studies conducted over the past 50 years this estimate appears to be constantly increasing. Roughly one fifth of all diagnosed cases of ASD are linked to monogenic disorders, among which Fragile X Syndrome (FXS) is the most common.

As for ID, the guidelines for diagnosis of ASD are reported in the DSM-5 and the clinical manifestations of the disease can be grouped in what is known as the autistic triad, that consists of: 1) social interaction deficits; 2) social communication and language problems; 3) stereotyped and repetitive behaviors. Indeed, the persistent deficits in social communication and interaction span across multiple contexts, and restricted, repetitive patterns of behavior, interests or activities complete the complex clinical phenotype of the patients.

The symptoms of ASD must manifest in the early developmental period and should cause significant impairment in social, occupational or other important areas of current functioning. In addition to these core symptoms, other co-occurring conditions can be present, including epilepsy, gastrointestinal problems, sleep disturbances, anxiety, depression and obsessive-compulsive disorder. All these features concur to make ASD a very heterogeneous disorder, with a level of severity that can vary between

affected subjects. Moreover, ASD may occur as a result of genetic predisposition and/or environmental interactions during early development (Chaste and Leboyer, 2012).

No approved treatment is available for ASD to date, however several evidence-based interventions are accessible. Among them occupational therapy, relationship development intervention and speech therapy are some of the most common treatments to improve behavioral and social interaction problems. Furthermore, specific cures for the associated medical conditions (anti-epileptics, anti-depressives, etc.) can also be of help (Ameis et al., 2018).

It is noteworthy that ASD is not an intellectual disability. This misconception is particularly widespread nowadays, but intellectual ability – or lack thereof – is not part of the diagnostic criteria of ASD and in fact, never has been. For instance, a person in the autism spectrum might have an easier and quicker ability to progress in some areas related to adaptive behaviors, while being somewhat differently/unevenly capable in others, but will generally be able to learn, reason, problem solve, think abstractly and apply/transfer learnings, which are skills related to intellectual ability.

It is indeed true that a child can have co-occurring autism and intellectual disability, but this is not the rule and it cannot be said that the two impairments are always found together. Patients who present the combination of the two will likely need an individual support that is different from individuals with only ASD, because they lack both intellectual and adaptive abilities. Presence of an intellectual disability, communication issue, epilepsy or another genetic disorder can be quite common, and in fact 70% of people with ASD are associated with these co-morbidities. A study conducted in 2008 by the Center for Disease Control (CDC) showed that around 38% of children with ASD also had ID. On the other hand, only 10% of individuals with ID also

show autistic traits. In the Third Edition of the America's Children and the Environment (updated October 2015) are presented the data of an ongoing annual survey conducted by the National Center for Health Statistics on U.S. children aged 5 to 17 reported to have ID (for reference, <https://www.epa.gov/ace>).

## CHAPTER 2 – FRAGILE X SYNDROME

### 1. Fragile X syndrome – the history of its discovery

In 1943, James Purdon Martin and Julia Bell described a specific form of ID, by reporting a family case study in which they observed that ID was linked to the X chromosome. Indeed, they observed that this form of ID was inherited from the X-chromosome of a mother carrying the trait or from an affected father. The outcome of their research was published in 1943 (Martin and Bell, 1943) and they detailed and discussed the observations made on a family with a total of eleven male children across two generations who exhibited symptoms of ID. Martin and Bell, after detailing the family's history and interviewing the affected individuals, could conclude that the condition was sex linked and inheritable. Moreover, they hypothesized that the speech deficits affecting the patients could probably be explained by the improper development of specific areas of the brain, like the pre-frontal cortex. Interestingly, they didn't report one of the main recurring features of the disease, the testicle enlargement in males. They named the disease Martin-Bell syndrome.

In 1969, Herbert Lubs observed an unusual "marker X chromosome" on the extremity of the long arm of the X chromosome (Lubs, 1969), which was subsequently addressed as the "fragile site" (Hecht and Kaiser-McCaw, 1979). Lubs also developed the chromosomal test for FXS, which was scarcely used until the late 1970's.

An extensive and more detailed description of the disease, now named Fragile X syndrome, was given in 1985, when Felix F. de la Cruz outlined the main physical, psychological and cytogenic characteristics of FXS (Cruz, 1985), but nothing has been

known about its genetics until 1991. In this year, the causative gene of FXS was identified, sequenced and further characterized (Oberlé et al., 1991; Verkerk et al., 1991): it was named *FMR1*, from Fragile X Mental Retardation 1 gene.

Ten years later, in 2001, the two linked diseases Fragile X-associated tremor/ataxia syndrome (FXTAS) and Fragile X-associated primary ovarian insufficiency (FXPOI) were also recognized to be associated with *Fmr1* (Cronister et al., 1991; Hagerman et al., 2001).

## **2. Fragile X syndrome – the disorder**

Fragile X syndrome ORPHA:908 is a rare genetic condition having a prevalence of 1:4000 males and 1:7000 females worldwide (Brown, 1990; Coffee et al., 2009; Morton et al., 1997; Turner et al., 1996) and, in the majority of affected individuals, this genetic disorder is caused by a CGG trinucleotide repeat expansion in the 5'-untranslated region (UTR) of the *Fmr1* gene. When the expansion surpasses the 200 repetitions, the gene is silenced, and this causes the lack of production of the Fragile X Mental Retardation Protein (FMRP) and the manifestation of the disease.

FXS is characterized by specific clinical characteristics, ranging from cognitive to physical and cellular defects (Berry-Kravis, 2002; McLennan et al., 2011). The physical features of the disease include craniofacial abnormalities, muscle and connective tissue defects and males after puberty often show an augmentation of testicle size, a condition that is named macroorchidism (Schapiro et al., 1995). On the basis of cognitive features, FXS includes ID, language delay, behavioral issues and communication and social interaction problems (Berry-Kravis, 2002; Cornish et al., 2004, 2008; Freund and Reiss, 1991; Hagerman et al., 2009; Hall, 2009; Hall et al., 2012; Kwon et al., 2001; Maes et

al., 1994; Moy et al., 2009). The cellular marker of the disease is the dysmorphogenesis of dendritic spines. Indeed, anatomical studies of post-mortem brains revealed that neurons derived from patients appear longer and thinner than those of matched controls, indicating an impaired mechanism of maturation (Hinton et al., 1991; Irwin et al., 2001; Wisniewski et al., 1991). Moreover, the brains of FXS patients show enlargement of lateral ventricles and increased caudate nucleus volume, as seen in MRI studies (Reiss et al., 1995). The main features of FXS are reported in **Figure 2**.

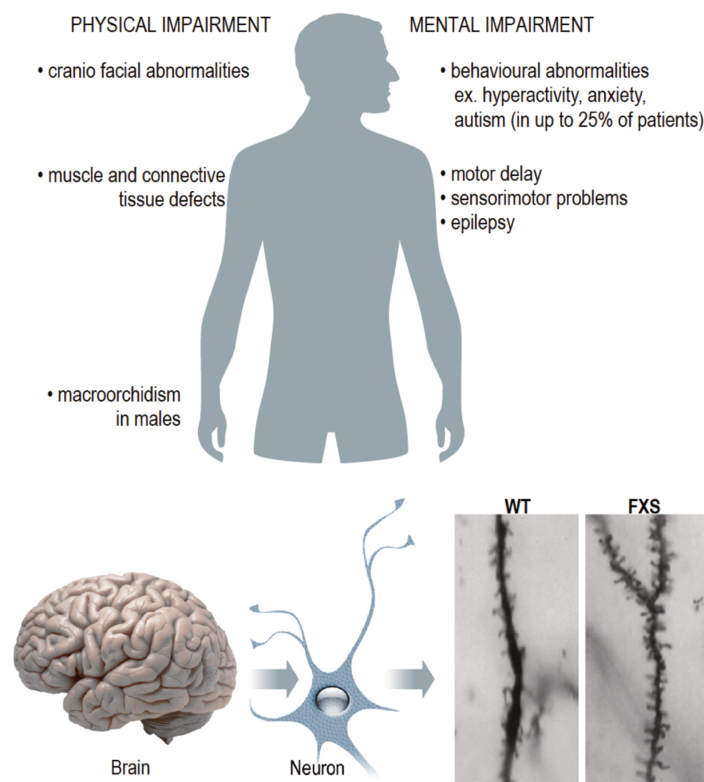


**Figure 2. Main characteristics of Fragile X syndrome.** The most representative features of FXS are reported here and range from physical to mental impairments. Microscopically, dendritic spine dysmorphogenesis is the cellular marker of the disease.

### 3. Fragile X syndrome – an unusual X-linked condition

In the classical pattern of inheritance of X-linked genes, females with one abnormal X chromosome have another that is normal, while males only possess one.

Therefore, when an X-linked gene is deficient, in women it will be compensated by the normal X-linked allele present on the other X chromosome, while males will manifest the pathology. Women are, so to speak, “protected” by the additional X chromosome, which makes them carriers of the disease without showing the symptoms. On the contrary, if a male has a defective X chromosome, he cannot count on the normal counterpart to mask the resulting phenotype (Kirchgessner et al., 1995).

Interestingly, in FXS 30% of female carriers are found to manifest ID, although at a lower grade, and this is due to a mechanism of inactivation (methylation) of the normal X chromosome during early embryogenesis in a given cell that causes its silencing, in the subset of cells deriving from it. Indeed, in healthy females, the inactivation of one of the two X chromosomes causes *Fmr1* to be normally methylated, while the second X chromosome contains the “healthy” allele of the gene. On the other hand, in the presence of the disease, not only one of the two X chromosomes is inactive, but the second one, in a subset of cells, carries the methylation of the CGG triplet expansion, causing the gene to be only partially expressed.

#### **4. Fragile X syndrome – the phenotype**

##### 4.1. Intellectual disability

FXS is the leading identified monogenic source of ASD and a major cause of mental deficiency in our society. It represents the second most common form of chromosome abnormality – after Down syndrome – among the mentally impaired and it is an inherited X-linked ID condition (Hagerman et al., 2010; O’Donnell and Warren, 2002). Indeed, it is known that about 20% more males than females are mentally retarded. About 75% of individuals with Fragile X syndrome show ID as a major symptom, with mild to moderate

ID and IQ scores between 50 and 75 (in the general population about 63% of all test-takers obtain scores from 85 to 115 and about 14% from 70 to 85). The remaining 25% of patients show a higher degree of ID and IQ scores inferior to 50 (Hagerman et al., 2008).

#### 4.2. Physical features

FXS individuals exhibit typical physical manifestations that are present mostly in males and usually tend to be subtle. The main features of the disease might be harder to recognize in babies and young children compared to adolescents and adults. Patients show, at a general body level, muscular hypotonia, connective tissue dysplasia and hyperextensibility of joints. The cranio-facial abnormalities consist of macrocephaly accompanied by a typically long and narrow face with a prominent jaw, large and anteverted ears and a high arched palate. A very common characteristic, displayed by almost every male subject, is testicular enlargement, which becomes evident at puberty. Besides mitral valve prolapse, observed in some patients, no major organ malformations are reported as additional manifestations of the disease. FXS patients can present some recurring minor complications, including ear infections, gastroesophageal reflux, constipation, strabismus and sleep problems, but generally they show a good health status (Kidd et al., 2014). As stated before, in females the physical phenotype, if at all present, is similar to that of males but far less marked (Van Esch, 2006). Dendritic spine dysmorphogenesis, the result of abnormal formation and growth of dendrites, is also a feature of FXS, representing the cellular biomarker of the disease.

### 4.3. Epilepsy

Approximately 20% of FXS individuals show epilepsy (Musumeci et al., 1999), which appears usually between 4 and 10 years of age and disappears, with some exceptions (Sabaratnam et al., 2001), after puberty. Even the proportion of boys not manifesting seizures shows EEG abnormalities (Berry-Kravis, 2002; Berry-Kravis et al., 2010). The usual treatment is done by single-drug antiepileptic therapy during the developmental period and it is usually continued throughout life to avoid seizure relapse in later stages of life.

### 4.4. The behavioral phenotype

The main features that characterize the behavior of FXS patients consist of hyperactivity, anxiety, impulsivity, gaze avoidance, short attention span, continuative speech, hypersensitivity to sensory stimuli (like light and sound inputs), stereotyped and repeated movements, inconvenient emotional manifestations and episodic tantrums (Cornish et al., 2008; Grefer et al., 2016). Although many of these symptoms, especially if combined, cause a general state of stress in patients, in particular “secured” environments (like families) a number of patients can sustain short conversations, behave in an appropriate manner and adapt a positive attitude towards daily activities.

Since FXS represents the most common monogenic cause of ASD, a portion of FXS patients (about 5%) show autistic traits (Budimirovic and Kaufmann, 2011). This is true also for premutation male carriers (Chonchaiya et al., 2012) while female carriers of a full mutation show a milder ASD manifestation (de Vries et al., 1996).

## 5. Fragile X syndrome – the genetics

### 5.1. The *Fmr1* gene

FXS is caused by the silencing of the *FMR1* gene, which was cloned in 1991 (Connor, 1991). Localized on the long arm of the X chromosome, *FMR1* is encoded in 17 exons that span 38 kb of Xq27.3 (Eichler et al., 1993) and encodes a 4.4 kb long mRNA that is subjected to alternative splicing. The products of these events of splicing generate 12 protein isoforms that can be detected in various tissues and that usually span from 70 to 80 kilodaltons (kDa) in size. The *FMR1* gene is evolutionarily well conserved, with homologs found in all vertebrates (e.g., mouse, chicken and frog) and some invertebrates (e.g., the fly *Drosophila melanogaster*).

The CGG repeat is located in the 5'-UTR (the promoter region): this is the site of the expansion that gives rise to FXS. In response to a massive expansion of this CGG triplet *Fmr1* gets highly methylated and this causes the disease.

### 5.2. From polymorphism to full mutation

In the general population, the CGG triplet of the *FMR1* gene is expanded polymorphically to a maximum of 54 repeats and this expansion doesn't produce any deficit. The silencing of the *Fmr1* gene in FXS is due to an expansion of around 200 to more than 1000 units of the CGG repeat in more than 95% of the cases and this event is known as "full" mutation. In rare cases, point mutations and deletions have also been reported to be causative of the disease (Willemsen et al., 2011).

Other two diseases are linked to failures of the normal function of *FMR1*, namely FXPOI and FXTAS (Goodrich-Hunsaker et al., 2011). These two conditions are caused by what's referred to as "premutation" alleles (which are defined by lengths between 55

and 200 repeats). A woman carrying the premutation allele is at ~ 25% risk of FXPOI with a major impact on her reproductive future, while a man who carries the premutation allele is at more than 50% risk of FXTAS, a disorder characterized by tremor, ataxia and cognitive decline. In the case of premutation, the molecular and clinical consequences are different than the ones observed in full mutation, since the CGG expansion in *FMR1* has different effects on gene expression. Indeed, the premutation alleles are linked with a gain-of-function pathogenetic mechanism, since they associate with an increase in *FMR1* gene transcription and a slight reduction of FMRP levels. On the contrary, the full mutation alleles associate with a loss-of-function pathogenetic mechanism, since the gene is silenced and neither RNA nor protein is produced (Willemsen et al., 2011).

Peculiar conditions have been identified in some individuals whose clinical picture appears more complex and whose features belong to both FXS and FXTAS. A limited number of patients manifest a condition called mosaicism (Jiraanont et al., 2017), either carrying both full mutation cells and premutation cells (size mosaicism (Milà et al., 1996) or expressing the full mutation where only a portion of the mutated allele is methylated (methylation mosaicism; (Genç et al., 2000; Hagerman et al., 1994).

### 5.3. *Fmr1* mutations and their implications in disease

FMRP and its network of mRNA targets and interacting proteins contribute to several forms of synaptic plasticity involving learning and memory processes, notably induced by activation of type I metabotropic glutamate receptor (mGluR; (Davidovic et al., 2011). Mice lacking FMRP have impaired long-term potentiation in somatosensory cortex (Li et al., 2002), visual cortex (Wilson and Cox, 2007), olfactory cortex (Larson et al., 2005), cingulate cortex and amygdala (Zhao et al., 2005) and enhanced long-term depression

in hippocampus (Huber et al., 2002). In synaptosomal preparations, stimulation of mGluR results in a FMRP-dependent increase in protein synthesis (Weiler et al., 1997, 2004). It is hypothesized that a decrease in *Fmr1* functionally affects the protein interaction network with direct consequences on the signaling cascade and on cellular metabolism (Davidovic et al., 2011).

Premutations appear to influence translation of *FMR1* mRNA (Feng et al., 1995). In many individuals with premutations, excess *FMR1* mRNA is produced, yet FMRP is synthesized below normal levels (Tassone et al., 2000a, 2000b) and this may contribute to approximately 10% of male and 2–3% of female ASD cases (Wang et al., 2013). Upon female transmission, the premutation can become a full mutation. FXS is caused by full mutation which is 200 trinucleotide repeats, and results in hypermethylation of the gene and transcriptional silencing (Tassone et al., 2000b). This creates an FMRP deficiency in the brain, which leads to FXS presentation (McLennan et al., 2011; Tassone et al., 2000a). Very rarely other mutations in the *FMR1* gene involving deletions (Gedeon et al., 1992) or point mutations (De Boule et al., 1993; Suhl and Warren, 2015) result in symptoms identical or even more severe than FXS.

## **6. Fragile X syndrome – the FMRP protein**

FMRP is a widely distributed protein among adult human tissues, but it is particularly abundant in brain and testes, which are the main affected tissues in FXS. In brain, the expression of FMRP is higher in cortex, hippocampus and cerebellum. At a cellular level, FMRP is produced in the soma and near the synapse and it is an essential protein involved in the shaping of dendritic spines (Berry-Kravis, 2002; Berry-Kravis et al., 2011; Davidovic et al., 2011).

### 6.1. The FMRP family

FMRP is part of a family of proteins that comprises its own orthologues as well as the two FXR1P and FXR2P paralogues (70-80% of identity and 80-90% of similarity at the N-terminal block of 444 residues; no conservation at the C-terminus). FXR1P and FXR2P are conserved in humans, mice and *Xenopus laevis* (Coy et al., 1995; Siomi et al., 1995; Zhang et al., 1995) and they are autosomally encoded (3q28 and 17p13.2 respectively; (Coy et al., 1995). FXR1P is highly expressed in muscles, especially in the heart, where FMRP and FXR2P are substantially absent (Coy et al., 1995; Devys et al., 1993; Khandjian et al., 1995).

### 6.2. FMRP – the structure

FMRP is a medium sized protein (71 kDa) with a full-length genomic sequence of 632 amino acids (aa). This protein has been functionally characterized and its domains have been described (**Figure 3**). FMRP contains:

- several RNA-binding domains, which are typical RNA and single strand DNA binding modules (Nicastro et al., 2015; Valverde et al., 2008). These domains include: 3 KH (K Homology) domains (KH0, KH1, KH2), which are evolutionarily conserved sequences of around 70 aa that can function in RNA recognition;
- the RGG box, which is a 20-25 aa long sequence that contains repeats of arginine-glycine-glycine;
- a Nuclear Localization Signal (NLS) present in the KH0 region, which tags the protein for import from the cytoplasm to the cell nucleus;

- a Nuclear Export Signal (NES), which is a short aa sequence (4 hydrophobic residues) that targets the protein for its export from the nucleus through the nuclear pore complex;
- a Nucleolar Localization Signal (NoLS), which is a short basic motif that localizes the protein to the nucleolus (Ramos et al., 2003; Taha et al., 2014);
- two protein-binding conserved domains, namely Argentin domains or tandem Tudor domains (Tud1 and Tud2) (Ramos et al., 2006);
- an N-terminal domain, also acting as protein-binding (Ramos et al., 2006).

These same functional domains are shared by FXR1P and FXR2P, although their functions still remain elusive.

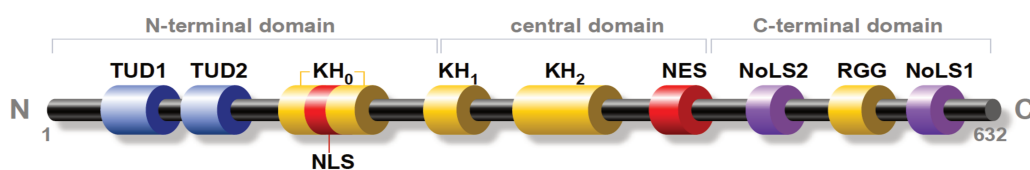


**Figure 3. Structure of the FMRP protein.** The main domains forming the FMRP protein are shown.

### 6.3. FMRP – the functions

FMRP, being ubiquitous, is mainly localized in the cytoplasm. In neurons, it is associated to synaptic polyribosomes and it is a component of RiboNucleoProtein (RNP) granules (Feng et al., 1997). These complexes transport mRNAs along dendrites and axons (Khayachi et al., 2018; Maurin et al., 2014, 2018a).

FMRP has been proposed to enter the nucleus and interact with pre-mRNPs in order to escort them to the cytoplasm. Then, FMRP-bound mRNAs (FMRP-mRNPs) can follow different fates:

- 1) In normal conditions, FMRP-mRNPs are massively associated with actively translating polyribosomes and FMRP is also localized at P-bodies (Pb), consistently with its activity of repressor and activator of translation (Barbee et al., 2006; Stefani et al., 2004);
- 2) During a cellular stress, FMRP-mRNPs (and other mRNAs) are directed to stress granules and FMRP plays an active role in this process (Didiot et al., 2009; Gareau et al., 2013);
- 3) More specifically in neurons, some of the FMRP-mRNP complexes are selectively translocated to distant locations (dendritic spines) within RNA-granules together with other RNA-binding proteins and ribosomes. FMRP was thus proposed to be a link/adaptor between RNA and motor molecules (Davidovic et al., 2007).

FMRP is a multifarious protein, because of its involvement in different steps of RNA metabolism and its interaction with several proteins, mainly implicated in cytoskeleton remodeling (Abekhoukh and Bardoni, 2014; Maurin et al., 2014) and ion channel control (Castagnola et al., 2018; Ferron, 2016). The principal aspects of FMRP that have been investigated over the years are its RNA-binding properties. Indeed, FMRP modulates the expression of thousands of mRNAs primarily at the translational level and, in particular, it has been shown to regulate translation at the synaptic level. This local regulation has pleiotropic effects especially on synaptic functioning.

Over the years, FMRP acquired the reputation of translational repressor, since many studies concluded that this protein has the ability to inhibit protein production from several mRNAs. When taking into consideration all data gathered on the translational modification ability of FMRP, it can be concluded that FMRP is mainly a repressor of

translation, especially during development in mammals, as clearly summarized by my colleagues (Maurin and Bardoni, 2018). In **figure 4** are reported the motifs recognized by FMRP.

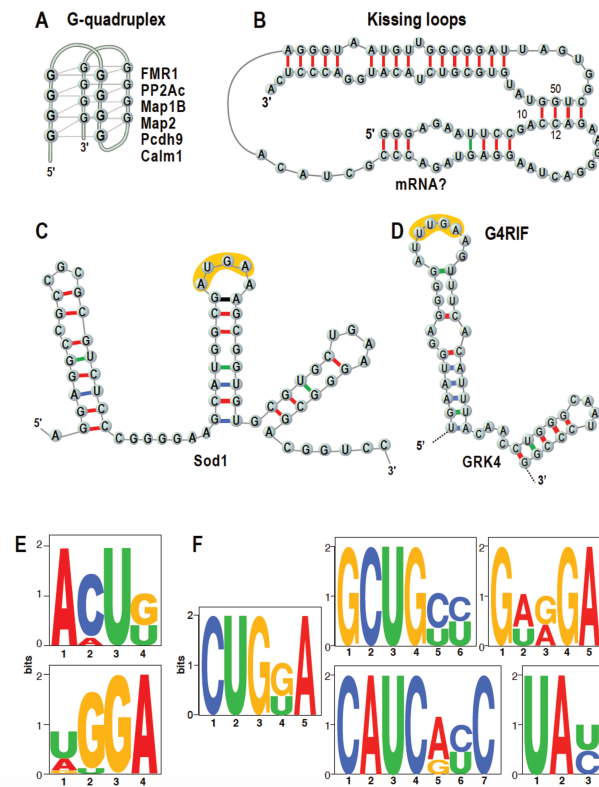


**Figure 4. mRNA motifs bound by FMRP.** Main structures and sequences that are bound by FMRP are listed (from (Maurin and Bardoni, 2018))

During the last 18 years, however, growing data has shown a more complex picture. Indeed, we now have evidence that:

- 1) FMRP can increase the translation level of certain transcripts in the presence of specific enhancers like SoSLIP (Bechara et al., 2009);
- 2) FMRP can control the translation of mRNAs in a specific tissue at a given time point, according to development;

- 3) Certain proteins encoded by targets of FMRP can elude the repression of translation mediated by FMRP (Maurin and Bardoni, 2018).

Thus, not only it is important to investigate the spatio-temporal-dependent manner in which FMRP controls its targets, but also the RNA-binding specificity this protein has. Evidences point out that several target mRNAs of FMRP contain short sequences that are recognized by FMRP only when in the context of a secondary RNA structure, namely single stranded regions or loop sequences of stem loop structures (Maurin et al., 2018a). In addition, FMRP targets show an enrichment of G-quadruplex structures, further suggesting the ability of FMRP to recognize and bind structural motifs (Ascano et al., 2012; Maurin et al., 2018a).

More in detail, the main functions of FMRP are:

- 1) Translational regulation: most of the data obtained up to date point to a critical role of FMRP as a translational regulator by direct interaction with mRNA and being associated to translating polyribosomes. Interestingly, depending on the target mRNA, FMRP acts as a repressor or as an enhancer of translation. Indeed, while G-quadruplex, G4-RIF motif or the ACUK/WGGA have been shown to mediate translational repression, the So-Slip structure is an enhancer of translation (Maurin and Bardoni, 2018). Some mechanisms that have been reported to date to modulate the translation of the FMRP target mRNAs are: I) the inhibition of translation by preventing ribosome scanning via a G-quadruplex structure localized in the 5'UTR of a target mRNA that can be organized by the WGGA sequence or via another structure associated with ACUK/WGGA motifs (Ascano et al., 2012); II) the retention of mRNAs in translationally inactive mRNPs via interaction with the "kissing complex" motif (Darnell et al., 2005); III) the

repression through a polyribosome stalling mechanism (sequences mediating this process have not been identified) (Stefani et al., 2004); IV) the activation via the interaction with the SoSLIP RNA or via a G-quadruplex structure when located at the 3'UTR (Bechara et al., 2009);

- 2) RNA transport: the presence of FMRP in RNA granules and its interaction with at least two kinesins have supported the idea that this protein can have an active role in the transport of mRNAs. Our laboratory has shown that FMRP interacts with *Kif3*, representing a link between RNA and the molecular motor for dendritic/axonal transport (Davidovic et al., 2007). Furthermore, the kinesin *Kif5* has been observed to coimmunoprecipitate with FMRP (Dichtenberg et al., 2008). mRNAs copurified with *Kif5* have been analyzed by RT-qPCR, showing that among them many target mRNAs of FMRP are present (*Pp2ac*, *Camk1la*, *Sapap4*, and *Map1b*) and differentially associated with *Kif5* depending on the presence of FMRP. Altogether, these findings suggest that FMRP facilitates dendritic/axonal transport by mediating the interaction between molecular motors and RNA. However, this enhancing function is not systematic and depends on the FMRP mRNA target. For example, the G-quadruplex RNA structure has properties of a zip-code when located in the 3'-UTR of the *Psd95* and *Camk1l* mRNAs, but the dendritic transport of these mRNAs was not described as FMRP-dependent. On the other side, an increase in *Bdnf* mRNA in dendrites of *Fmr*-Knock-Out (KO) mice under resting conditions was observed. In our laboratory it has been demonstrated that FMRP binds the 3'-UTR of the *Bdnf* mRNA, directly implicating FMRP in the regulation of the trafficking of this mRNA (Vicario et al., 2015). Thus, in the absence of FMRP, an increased dendritic transport of some of its targets

could be associated with an increased expression level at the synapse of their encoded proteins.

- 3) Intracellular trafficking: between FMRP and heterogeneous nuclear ribonucleoprotein C1/C2 (hnRNPC) there is a competition for binding the mRNA of Amyloid Precursor Protein (APP): this suggested that FMRP represses translation by recruiting APP mRNA to processing bodies, whereas hnRNPC promotes APP mRNA translation by displacing FMRP. Even if an altered association with polyribosomes was observed for other targets of FMRP in FXS cells, the specific mechanism shown for the mRNA of APP was never validated for any other target of FMRP (Lee et al., 2010);
- 4) Nucleocytoplasmic shuttling: FMRP is a predominantly cytoplasmic protein but it harbors domains promoting import to the nucleus or export to the cytoplasm. Consistently, endogenously expressed FMRP molecules are detected in nuclear fractions upon subcellular fractionation experiments using HeLa or human lymphoblastoid cells or visualized in the nucleus by immunostaining in response to replication stress or during early developmental period in *Xenopus tropicalis* and zebrafish embryos. A specific FMRP isoform generated by alternative splicing and lacking the NES has been revealed in the nucleus associated with Cajal bodies in a transfected cell line. However, the effective localization of this protein has never been demonstrated. In brain, using immunogold staining, which provided sufficient sensitivity and resolution, few FMRP-labeled particles were detected in the nucleus of cortical and hippocampal neurons (Filippini et al., 2017). It has been proposed that FMRP is recruited early on its target mRNAs in the nucleus and may participate to their nuclear export to the cytoplasm. However, the

effective addressing of FMRP to the nucleus in neurons, its regulation and its nuclear functions still remain open questions.

## 7. Animal models of FXS

FXS is a natural occurring human disease that doesn't manifest spontaneously in other species, therefore in order to get an animal model for the disease it has been necessary to genetically modify several species. To date, a number of model organisms have been generated to study FXS, and they include both vertebrate (mammalian and non-mammalian) and invertebrate species.

The main non-mammalian species used are the fruit fly *Drosophila melanogaster* and the zebra fish *Danio rerio*, which generally serve as a first source of fast answers, especially about gene function. If, on one side, the central nervous system (CNS) of these animals is relatively simple compared to the one of humans, it is also known in better detail and much easier to handle and can give important information. Clearly, more complex organisms are needed when turning to biomedical research, since they can give robust experimental foundation. For this purpose, rats (*Rattus norvegicus*) and mice (*Mus musculus*) are the most popular rodent models for FXS that have extensively been used in the study of this disorder.

### 7.1. *Danio rerio*

For the study of embryonic development in a vertebrate system, the zebra fish *Danio rerio* has proven to be a very convenient animal model. Genetically modified animals are obtained by random mutagenesis (den Broeder et al., 2009) or morpholino KO (Truszkowski et al., 2016) and show impairment in several FXS-related neuronal

phenotypes and behaviors (Kim et al., 2014; Ng et al., 2013). It is commonly assumed that the KO obtained through morpholino injection is potentially derived by experimental artifacts (Schulte-Merker and Stainier, 2014), but nevertheless the valuable potential of zebra fish as a complementary vertebrate model is unquestionable, especially for the first stages of development.

### 7.2. *Drosophila melanogaster*

*dFMR1*, the *Drosophila* homolog of *FMR1*, was identified in 2000 by Wan *et al.* and its sequence is highly conserved, with the two KH domains being 75% identical between the human and the fruit fly genes (Wan et al., 2000). The gene, which codes the dFMRP protein, is widely expressed throughout *Drosophila* embryos, but particularly in the brain, CNS (mushroom bodies, the centers for learning and memory), ventral nerve cord and muscle precursors, while in larvae we find it present also in testes (Lee et al., 2003; Schenck et al., 2002). In fly adults, dFMRP is present mainly in brain and its associated neural projections, but also in other non-neuronal areas, where it exerts different functions.

Interestingly, *Drosophila dFMR1* mutants show phenotypes that recall human FXS symptoms, like motor impairment and social behavior (for more details, refer to the review by (Drozd et al., 2018).

### 7.3. *Rattus norvegicus*

Rats have proven to be a good model for experimentation, and more so for neuroscience studies, since their brains are bigger than the ones of mice. Moreover, compared to their rodent counterpart, rats have a milder nature, are able to learn more sophisticated

behaviors and show finer social skills, which makes them a very good model to mimic the complex phenotypes of FXS patients. However, their purchase and maintenance come at a higher price and they are less genetically amenable than mice and flies, therefore these two latter models are generally preferred for biochemical and molecular analysis, while rats are used mostly for behavioral tests (Dahlhaus, 2018).

#### 7.4. *Mus musculus*

The Knock-Out (KO) mouse model is the first FXS model ever created (The Dutch-Belgian Fragile X Consortium, 1994). The generation of this model was done by homologous recombination of a targeting vector into the mouse germline using embryonic stem cells. In its early days, it showed a problem related to the remaining activity of the promoter of the *Fmr1* gene, which was still active and caused an abnormal production of RNA. To avoid this issue, two different KO models were developed in parallel: the conditional KO, where the gene is only expressed in the tissue of interest (Mientjes et al., 2006), and the constitutive *Fmr1*-KO, where there is total absence of the protein in the whole animal, which is the one I used for my thesis (C57Bl6 background). In this model, differently from the original one, the absence of production of FMRP is accompanied by the absence of RNA transcript.

Noticeably, it is not possible to use a model which recreates the full CGG expansion present in the human gene, since in mice the same modification doesn't provoke the methylation and consequent silencing of the gene as it happens in humans (Brouwer et al., 2007).

For the moment, the mouse model is in general considered the best model for FXS because it recapitulates a large number of FXS phenotypes, like deficits in learning and

memory (for review (Melancia and Trezza, 2018), anxiety (Heulens et al., 2012; Liu and Smith, 2009; Peier et al., 2000), repetitive behaviors (Kramvis et al., 2013; Pietropaolo et al., 2011; Spencer et al., 2011), hyperactivity (Peier et al., 2000; Pietropaolo et al., 2011), social interaction and communication (Dahlhaus and El-Husseini, 2010; Gholizadeh et al., 2014; McNaughton et al., 2008; Pietropaolo et al., 2011; Rotschafer et al., 2012; Roy et al., 2012), altered volumes of specific brain regions (Gothelf et al., 2008; Hoeft et al., 2010), dendritic spine dysmorphogenesis (Galvez and Greenough, 2005; Grossman et al., 2006), and macroorchidism (Slegtenhorst-Eegdeman et al., 1998).

## CHAPTER 3 – ALTERED SIGNALING IN FRAGILE X SYNDROME

### 1. Excitation and inhibition in Fragile X syndrome – the importance of balance

The two main classes of neurons that form the cerebral cortex are pyramidal cells and interneurons, which respectively use glutamate and Gamma-AminoButyric Acid (GABA) as neurotransmitters. In the adult brain, glutamatergic pyramidal cells are excitatory while GABAergic interneurons exert inhibitory functions. These two systems are responsible for maintaining an excitatory/inhibitory (E/I) balance of neurotransmission to allow the correct functioning of the cerebral cortex and, by extension, of the brain.

FXS, as well as other neurological disorders, is characterized by profound alterations in this E/I balance of neurotransmission. In addition, in FXS cortical E/I imbalance is often associated to impairments of neurotransmission that affect other brain areas, therefore leading to the typical symptoms of the disease. Indeed, visual and somatosensory cortex impairment cause the failure of sensory system neuronal processing, while cerebellar defects have been linked to motor learning deficits. Moreover, impaired behavior-processing neuronal circuits in the amygdala are associated with emotion recognition and auditory deficits.

The intricate networks of cortical FXS neurons are characterized by hyperresponsiveness and hyperexcitability and the explanation of the severe impact that an exaggerated response to the metabotropic glutamate receptor (mGluR) activation has on the psychiatric and neurological aspects of FXS is clearly given by the “mGluR theory”, which describes an unbalanced mGluR-mediated protein translation in the absence of FMRP (Bear et al., 2004). On the other hand, it is important to define the role of the stream counterpart of excitation, which is inhibition; the analysis of its balancing activity

is indeed crucial to have a better understanding on how this equilibrium works. The main CNS inhibiting neuronal network is represented by the GABA pathway, which, as mentioned above, is deregulated in FXS (Adusei et al., 2010).

In order to maintain a “healthy” neuronal transmission, it is of utmost importance the activity of a so-far-neglected population of neurons: the inhibitory interneurons family. This broad and varied cell population constitutes local inhibiting circuits and provides control over excitatory neuronal networks (Cea-Del Rio and Huntsman, 2014).

### 1.1. Cortical GABAergic interneurons

Although being a relatively restricted neuronal population, interneurons are the most diverse set of neurons present in the forebrain and the multifarious morphologies, connectivity and physiological properties account for their great neuronal variety. By definition, cortical interneurons are short-axon cells that don't project outside of the neocortex, as opposed to cortical neurons, that for the most part are pyramidal cells with long axons projecting towards the white matter. However, there can be projecting neurons with interneuron characteristics and *vice versa*.

GABAergic interneurons usually have axons that remain close to the soma and project locally to control and synchronize the output of pyramidal neuron microcircuits. They constitute around 10 to 30% of the total neuronal population and they are morphologically, biochemically and physiologically diversified neurons located in all layers of the cortex. Despite the difficult and sometimes controversial classification of interneuron subtypes, today it is largely accepted that GABAergic interneurons mainly possess inhibitory activity.

GABAergic interneurons are of great importance for neuronal development and functioning and in the neonate the correct formation of these circuits is paramount. Indeed, defects in interneuron activity have been linked to delay in the maturation of GABAergic interneurons in different animal models and for different brain areas. For instance, in the mouse brain, multiple laboratories have shown developmental delays of the sensory cortex, which is caused by the reduced functionality of interneurons that in turn results in hyperexcitability and increased frequency of the global neuronal activity (Ethridge et al., 2017; Nomura et al., 2017). In the same animal model, hippocampus defects in the functioning of interneurons have been described in *Fmr1*-KO brains, with neuronal network synchronization being compromised and leading to cognitive impairment (Arbab et al., 2018). In rat brains, the regulation of the visual cortex is controlled by inhibitory connectivity that is impaired and contributes to disrupted attention and sensory processing (Berzhanskaya et al., 2016). Interestingly, an augmentation of GABA release from Basket cells (interneurons) in the cerebellum of mice is responsible for a decreased firing frequency of Purkinje cells in *Fmr1*-KO brains, which is a recurring feature of autism (Yang et al., 2018). The analysis of the olfactory bulb in *Drosophila* mutants showed an impairment of GABAergic inhibition of excitatory neurons, and this is causative of defective olfactory behaviors and computation (Franco et al., 2017).

## **2. Therapeutic strategies for FXS**

In the past 20 years, an active exploration of the FXS physiopathology has gone hand in hand with the extensive analysis of FMRP targets in order to clarify the molecular determinants of the disease. The definition of many deregulated pathways paved the way

for putative treatment strategies that over the years have been widely examined (Berry-Kravis et al., 2011). However, even if the efforts of basic research set high hopes for the availability of efficient human therapies in the immediate future, clinical trials have constantly failed to succeed.

Among the putative targets analyzed, the glutamatergic and GABAergic pathways were the first in time to be investigated. Indeed, the excitation/inhibition imbalance in FXS is a well-known phenotype of the disease. Therefore, the therapeutic approaches targeting these pathways were aimed at either inhibiting the mGluR-dependent signaling or stimulating the GABAergic-dependent signaling, but unfortunately, despite the great work conducted in preclinical and clinical research, no promising results derived from targeting these two systems.

In addition to these two pathways, other therapeutic targets have then been considered for the treatment of FXS (**Figure 5**), since in recent years a big number of studies were pointed toward the identification of novel strategies to treat FXS. I will only give a summary of the most promising pathways that have been studied in recent years, but to have a more in-depth description of the most recent significant discoveries, refer to the Annexes section, Publication 1.

### 2.1. The glutamatergic pathway

The mGluR theory of FXS states that the lack of FMRP exaggerates the activation of the mGluR pathway, causing an hyperexcitation of neurons. Indeed, it has been shown that an overactive signaling through group 1 and 5 mGluRs contributes to many FXS features, as FMRP negatively regulates mGluR-dependent protein synthesis (Bear et al., 2004). In turn, the lack of FMRP is responsible for the absence of down-regulation of this excitatory

pathway therefore causing the hyperstimulation of neurons. Although the molecular details of this unbalance are not fully understood, extensive research has been conducted in order to develop a strategy to pharmacologically rescue the mGluR pathway.

### 2.2. The GABAergic pathway

The GABAergic system is the main inhibitory pathway of neurons in the Central Nervous System (CNS) and is necessary to maintain an equilibrium in neuronal activation. In FXS this system is deregulated, since an altered expression of GABA receptor subunits and a drop in the production of GABA have been observed (Adusei et al., 2010; Davidovic et al., 2011). This impairment concurs in the arousal of several FXS features like oversensitivity to sensory stimuli, seizures and anxiety.

The acquired knowledge on the role of GABA signaling in FXS allowed for the designing and application of several approaches and compounds to be used in clinical trials (for review: (Lozano et al., 2014).

### 2.3. The insulin pathway

The insulin pathway has been studied in association with FXS and ASD in different animal models, like the fly (Bu and Zhang, 2017; Monyak et al., 2017; Viollet et al., 2012) and mouse (Wise, 2017) models. Abnormalities in this pathway are associated to several deficits, like aberrant cognitive abilities and circadian regulation. Imbalances in the Insulin-like Growth factor 1 (IGF-1) pathways have been shown to lead to neuronal developmental impairments that in turn cause autistic features.

#### 2.4. The matrix metalloproteinases pathway

The extracellular matrix (ECM) is a scaffolding structure that surrounds neurons and glia in the extracellular space, providing not only support to the neuronal network but also guidance in neuronal plasticity. The matrix metalloproteinases (MMPs) are collagenases that can cleave and modify the structure of the ECM (for review: (Reinhard et al., 2015). More specifically, MMP-9 is an ECM-remodeling collagenase that in brain can control learning and memory formation (Ganguly et al., 2013; Knapska et al., 2013). Evidently, the hyperactivation of MMP-9 may promote the degradation of the ECM, in turn causing defects in the function and maturation of synapses.

FMRP is a negative regulator of MMP-9 transcription. In FXS, the absence of FMRP cannot guarantee the regulation of the activity of this collagenase, therefore pre-clinical and clinical studies have focused on inhibiting MMP-9 to rescue the abnormal phenotype.

#### 2.5. The endocannabinoid pathway

The endocannabinoid system (eCS) consists of neuromodulatory lipids and their receptors, and in the brain it plays a role in synaptic plasticity, modulating nociception, cognition, anxiety and susceptibility to seizures. The impaired functioning of the eCS pathway in glutamatergic synapses has been linked to the absence of FMRP in FXS, therefore a number of drugs have been developed for the rescue of this system (Jung et al., 2012)

### 2.6. The serotonin pathway

Deregulation of the serotonin signaling system (also referred to as 5-HydroxyTryptamine system, 5-HT) has been linked to ASD by observing the levels and availability of serotonin as well as of its precursors (*i.e.*, tryptophan) in patients (Boccutto et al., 2013; Chugani et al., 1999). In addition, animal models of autism also display alterations in the serotonin pathway that can be partially rescued by the stimulation of 5-HT receptors (Costa et al., 2012, 2015; Muller et al., 2016). A recent study from the Malenka laboratory shows that the release of serotonin in the nucleus accumbens plays an important role in enhancing sociability, and this effect is obtained through the activation of specific 5-HT receptors present in this brain area. Conversely, the inhibition of the 5-HT pathway reduces social interactions, suggesting that 5-HT action in the nucleus accumbens is necessary for normal levels of sociability (Walsh et al., 2018).

### 2.7. The oxytocin pathway

The oxytocin system has been proposed as a therapeutic target of FXS as early as 1989, when it has been shown to play a key role in the balance between excitation and inhibition of neuronal activity (Ben-Ari et al., 1989). Indeed, oxytocin can control the effect of GABA stimulation, particularly in the perinatal period when oxytocin mediates the switch of the GABA system from excitatory to inhibitory (Tyzio et al., 2006) and dysfunctions in this neuropeptide's pathway can lead to autism, as reported in different human studies (Domes et al., 2007; Ishak et al., 2011; Winslow and Insel, 2004).

### 2.8. The cAMP/cGMP pathway

A novel therapeutic target to treat FXS is represented by the cAMP/cGMP system. Indeed, recent data published by our laboratory and colleagues (Maurin et al., 2018, refer to the Annexes, Publication 3) show that the mRNA encoding the phosphodiesterase 2A (PDE2A), an enzyme involved in the metabolism of cAMP and cGMP, is a prominent target of FMRP. In the study, High Throughput Sequencing-Cross Linking Immunoprecipitation (HITS-CLIP) was performed on various mouse brain regions in order to determine FMRP RNA targets and it allowed to identify the *Pde2a* mRNA as the main target of FMRP in the mouse cortex at postnatal day (PND) 13, an early stage of development when FMRP is most highly expressed and synaptogenesis peaks.

Subsequent combinations of *in vitro*, *ex vivo* and *in vivo* approaches revealed that PDE2A pharmacological inhibition restores the dendritic spine morphology and mGluR-dependent long-term depression (LTD) while rescuing altered social behaviors. Therefore, this pathway can be considered a novel therapeutic target for the treatment of FXS patients (Maurin et al., 2018b), refer to the Annexes, Publication 4).

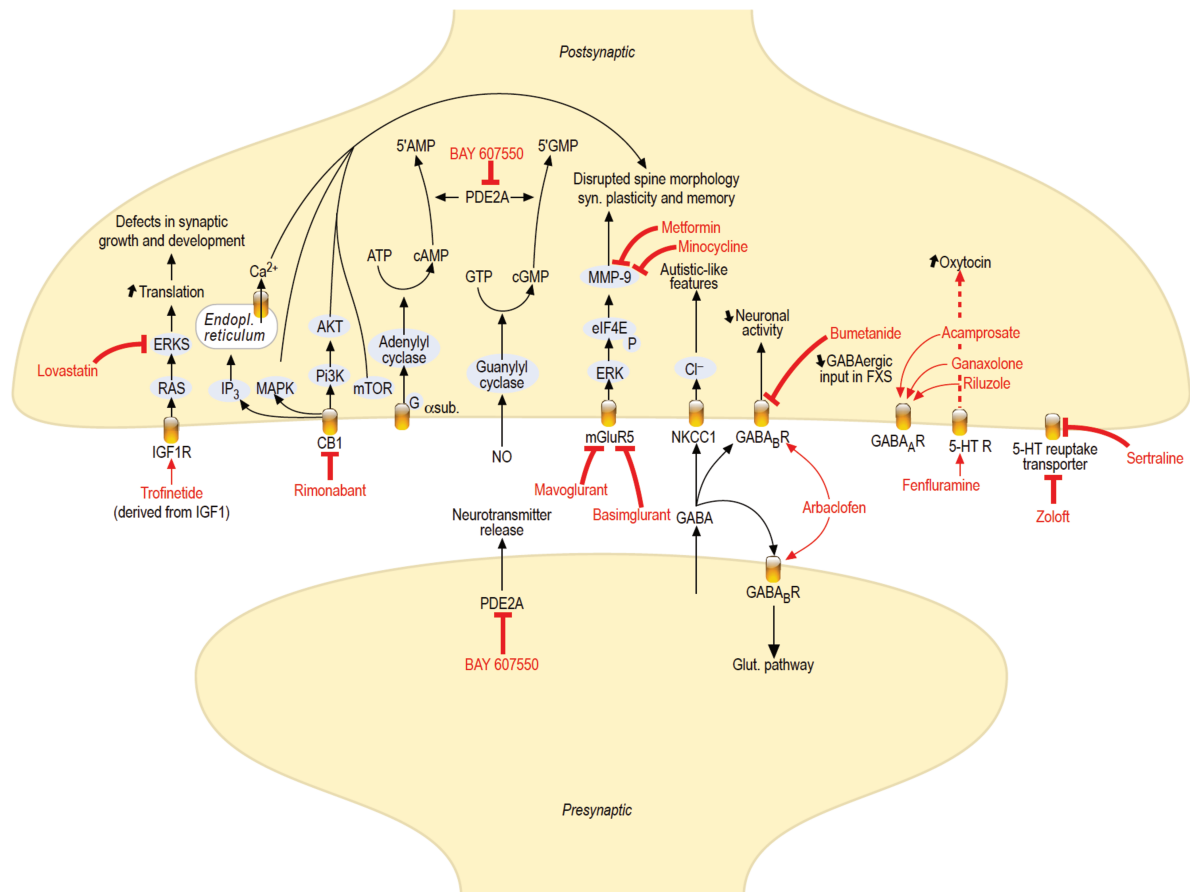


**Figure 5. Overview of the main deregulated pathways in FXS.** Due to the unsuccessful attempts to find pharmacological strategies to treat FXS, no treatment is available to date. Nevertheless, with the intent of finding new treatments for this genetic disorder many scientific advances have been made, better describing a number of pathways that are implicated in different aspects of the disease. Here is a schematic representation of the most important therapeutic trials that have been conducted until now in the FXS field.

### **3. Ion channel dysfunctions in FXS – other aberrant pathways in FXS**

#### 3.1. FMRP regulation of ion homeostasis players

The brain transcriptome associated with FMRP contains a broad spectrum of potential mRNA targets that include a number of ion homeostasis regulators and in particular ion channels (Ascano et al., 2012; Brager and Johnston, 2014; Brown and Kaczmarek, 2011; Darnell et al., 2011; Ferron, 2016; Maurin et al., 2018a; Miyashiro et al., 2003). Among them, those encoding the voltage-gated potassium channels  $K_v3.1b$  and  $K_v4.2$  (Gross et al., 2011; Lee et al., 2011; Strumbos et al., 2010).

FMRP has also been shown to directly bind ion channel proteins and the first data obtained were published by the Brown group on the sodium-activated potassium channel Slack (Brown et al., 2010). Subsequently, many more channels have been identified as targets of FMRP (reviewed in (Ferron, 2016), namely the large conductance  $Ca^{2+}$ -activated potassium BK channel (Deng et al., 2013) and the Voltage-Gated Calcium Channels (VGCCs)  $Ca_v2.2$  (Ferron et al., 2014) and  $Ca_v2.1$  (Castagnola et al., 2018).

#### 3.2. Calcium impairment in neurons

Calcium homeostasis impairment in FXS has been demonstrated by several laboratories since Chen *et al.* first showed an alteration in some VGCCs (Chen et al., 2003) in the frontal cortex of *Fmr1*-KO mice. Indeed, impairment in ion homeostasis has been pointed out in many studies (Achuta et al., 2018; Contractor et al., 2015; Deng et al., 2013; Ferron et al., 2014; Meredith et al., 2007; Wahlstrom-Helgren and Klyachko, 2015; Zhang et al., 2014), in particular in association with calcium deregulation (Brown et al., 2001; Catterall and Few, 2008; Maurin et al., 2018a; Miyashiro et al., 2003). For instance, FMRP has been shown to repress the translation of  $K_v3.1b$   $K^+$  channels in mice and

activate the translation of L-type  $\text{Ca}^{2+}$  channels in human cells. Furthermore, FMRP has been reported to directly bind ion channels *via* direct protein/protein interactions thereby modulating their pore conductivity and affecting neural activity by regulating  $\text{Ca}^{2+}$  signaling. This has been shown for  $\text{K}^+$  channels, including  $\text{Na}^+$ -activated Slack and  $\text{Ca}^{2+}$ -activated BK channels. Also, FMRP indirectly controls presynaptic N-type  $\text{Ca}^{2+}$  channel levels by acting on proteasomal degradation (for review, (Davis and Broadie, 2017)). Recently, FMRP has also been shown to directly interact with two members of the VGCC family, namely  $\text{Ca}_v2.1$  and  $\text{Ca}_v2.2$  (Ferron et al., 2014).

Ion channel gene defects have been characterized in association with ASD and VGCCs is a well-recognized channel family involved in channelopathy diseases and ASD (Chemin et al., 2018; Damaj et al., 2015; Schmunk and Gargus, 2013).

Deregulation in the calcium pathway has been observed in both ASD-comorbid syndromes, namely FXS and tuberous sclerosis types 1 and 2 (Schmunk et al., 2015) and in subjects with sporadic ASD (Schmunk et al., 2017).

### 3.3. The important role of calcium in neurons

Calcium ions are universal second messengers guiding a wide range of important cell functions, such as gene transcription, regulation of metabolic activity, cell growth and neurotransmitter release, controlling virtually every aspect of cell life. Neurons, which are extremely sensitive to calcium concentration unbalances, are profoundly altered in their activity when defects in  $\text{Ca}^{2+}$  homeostasis occur and this can lead to destructive consequences. Therefore, calcium regulation is a finely organized process that involves the activity of multiple protein complexes that compose the  $\text{Ca}^{2+}$  signaling toolkit of neurons (Carafoli, 2002).

The cytosolic calcium concentration is set by the balance between calcium influx and efflux as well as by the exchange of calcium with internal stores. In mammals, the extracellular calcium concentration is in the millimolar range, while at the intracellular level it is at nanomolar levels, due to buffering and sequestration into stores. Indeed, upon plasma membrane channel opening,  $\text{Ca}^{2+}$  flows in the cytosol thanks to its concentration gradient, and these transient increases of intracellular  $\text{Ca}^{2+}$  are perceived by the cell as signals to regulate cell function. In order to restore basal  $\text{Ca}^{2+}$  levels, the intervention of pumps and transporters is necessary. More specifically, in neurons calcium entry is stimulated by an action potential that activates the VGCCs placed on the plasma membrane. The ions flowing in the cytosol then stimulate secondary release of calcium from cellular stores activating the Ryanodine receptors (RyR) placed on the endoplasmic reticulum through a mechanism called “calcium-induced calcium release” (CICR). Alternatively to VGCCs, also NMDA or AMPA glutamatergic receptors allow the entry of  $\text{Ca}^{2+}$  from the extracellular space. The release of calcium from intracellular stores can also be triggered by extracellular ligands such as histamine, insulin or adrenaline, which activate the Inositol trisphosphate receptor (IP3R) via intracellular signaling pathways (IP3R/Phospholipase C pathways; (Ackerman and Clapham, 1997; Clapham, 2007).

$\text{Ca}^{2+}$  levels in the cytosol must decrease very rapidly, due to the toxicity of the ion, and this depletion is performed by plasma membrane  $\text{Ca}^{2+}$  ATPases (PMCAs) and  $\text{Na}/\text{Ca}^{2+}$  exchangers placed on the plasma membrane, and by sarco-endoplasmic reticulum  $\text{Ca}^{2+}$  ATPases (SERCAs).

Finally, calcium sensors present in the cytosol (e.g., calmodulin) are able to finely regulate the concentration of this ion.

Through HITS-CLIP experiments, our laboratory and others were able to identify a number of calcium homeostasis players as FMRP targets. Among them, we remember: ionotropic glutamate receptor NMDA- and AMPA-type, intracellular calcium level sensors, proteins regulating calcium-dependent transcription, intracellular calcium store proteins, calcium transporters, PMCAs, SERCAs, proteins involved in the calcium signaling pathway, and VGCCs (Maurin et al., 2018a).

#### 3.4. Voltage-gated calcium channels (VGCCs)

VGCCs are membrane integral proteins that form ionic channels allowing the selective flow of  $\text{Ca}^{2+}$  cations through the plasma membrane according to their electrochemical gradient. As mentioned previously, in the cytosol the  $\text{Ca}^{2+}$  concentration is usually tightly regulated to remain in the nanomolar range and this regulation is of utmost importance in order to avoid toxicity for the cells. VGCCs can be found in various cell types, and in neurons are particularly important to accomplish tasks like gene expression, initiation of synaptic transmission and neurotransmitter release. The trigger that causes the opening of these channels is a change in the voltage of the plasma membrane (also called membrane potential). This electric signal of the action potential is then converted by the VGCCs into a chemical signal consisting of an intracellular  $\text{Ca}^{2+}$  transient.

From the point of view of structure, they consist of a transmembrane pore-forming  $\alpha 1$  subunit, composed of four domains (I-IV) each of which is constituted by six transmembrane segments (S1-S6) and a phosphate-binding loop (P-loop) that re-enters the membrane (**Figure 6**). This subunit gives specificity to the channel and differs among all the subtypes of VGCCs. The channel is also composed of an intracellular  $\beta$ -subunit,

an extracellular  $\alpha 2$ -  $\delta$  subunit and for some channels of the family a  $\gamma$ -subunit (Zamponi et al., 2015).

VGCCs can be found in several cell types, where they regulate different intracellular processes; in endocrine cells, VGCCs regulate secretion of hormones, in cardiomyocytes contraction and in the CNS neurotransmitter release (Catterall et al., 2005). The main types of VGCCs found in endocrine cells, cardiomyocytes, retina cells and cochlear hair cells are L-types (and T-types in muscle cells), while neuronal cells show a wide spectrum of  $Ca_v$  expression, including L-, T-, R- types both in soma and post-synaptic terminals and N- and P/Q-types in pre- and post-synaptic terminals (for review, (Schampel and Kuersten, 2017)).

The VGCC subtypes are characterized by specific  $Ca^{2+}$  currents defined by physiological and pharmacological properties that differentiate them from one another. In neurons, the most prominent calcium currents are the N-, P/Q- and R-type, which have specific sensitivity to, respectively,  $\omega$ -conotoxin GVIA,  $\omega$ -agatoxin IVA and SNX-482 (for the latter, it is only true for some cell types).

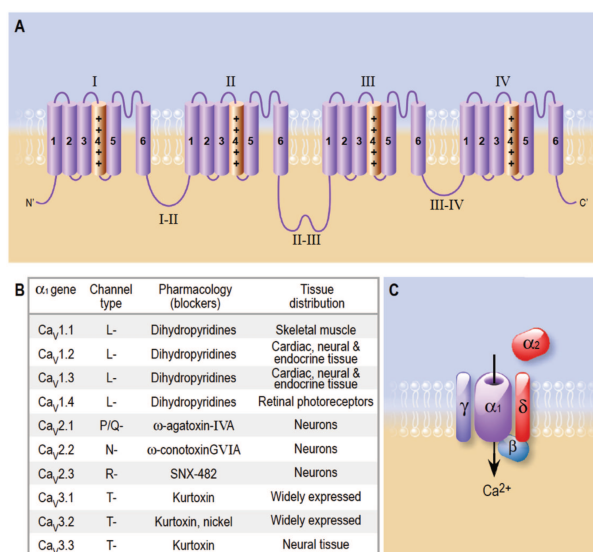


**Figure 6. Structure of a Voltage-Gated Calcium Channel.** **A)** Representation of the domains that compose the protein. **B)** Table reporting each VGCC subtype with their  $\alpha 1$  subunit gene names, pharmacological antagonists and tissue distribution. **C)** Organization of a typical VGCC with its accessory subunits.

# Aims of the thesis

Unraveling the complexity of the molecular networks that play a role in the pathophysiology of FXS is of utmost importance to identify a therapeutic approach for this syndrome. The identification of a therapy for FXS is intimately linked to the definition of the precise function of FMRP and its targets (RNAs & proteins). This search characterized the activity of Dr. Bardoni's laboratory during the last 20 years. Indeed, when I started my stage of thesis at the end of 2015, the HITS-CLIP was already set up and the analyses of the results were in progress. Quickly, it was possible to expose the deregulation of two main pathways in FXS, namely the Phosphodiesterase 2A (PDE2A)-dependent cAMP/cGMP and the calcium homeostasis pathways. From this, the main aims of my work were to:

1. Validate the two most prominent targets of FMRP we found in cortex and hippocampus (*Pde2A* and *Cacna1a*);
2. Study the homeostasis of  $\text{Ca}^{2+}$  in cultured cortical neurons and in neurons obtained by brain dissociation in the absence of FMRP.

Furthermore, according to the HITS-CLIP results, the expression of mRNAs regulated by FMRP varies not only on the basis of the brain region but also according to the cell type, as we observed by comparing our dataset with the analysis in the somatosensory cortex and the hippocampus single-cell transcriptomic datasets. Thus, an additional aim was to study the differential role exerted by FMRP on signaling modulation in distinct cell types of the brain that can contribute to the heterogeneity of cells that compose this complex organ. To answer to this need, I set-up the aiFACS assay and I

applied it to GABAergic interneurons, a wide class of inhibitory interneurons present in the forebrain whose deregulation has been observed in several neurodevelopmental disorders and studied in different animal models.

# Materials & Methods

The majority of materials and methods used are fully disclosed in the articles included in the Annexes at the end of this thesis. For the latest unpublished results, in order to allow a fuller comprehension of a new technique prototyped by our laboratory (aiFACS), the materials and methods are listed below.

**Brain dissociation and neuron isolation.** Full brains were dissected from PND 18 mice. A brief wash with complete D-PBS (supplemented with 0.5% bovine serum albumin, 1% pyruvate and 15 mM glucose) was performed before cutting the brains sagittally in 6 equally thick sections (2 mm) using a mouse brain matrix slicer (CellPoint Scientific) and 5 razorblades. The brain slices were dissociated mechanically using a gentleMACS™ octodissociator and enzymatically using the Adult Brain Dissociation kit (Miltenyi Biotec) following the manufacturer's instructions. The Neuron Isolation Kit (Miltenyi Biotec) was used for magnetic selection of neuronal cells.

**Neuron labeling.** Neuronal suspensions were labeled with the following combination of dyes: the Fluo-4 calcium indicator (5 µg; Invitrogen) and either the Wheat Germ Agglutinin 594 (WGA 594; Invitrogen) for WT cells or the WGA 647 for *Fmr1*-KO cells (5 µg; Invitrogen). The labelling was performed in complete D-PBS for 30 and 10 min, respectively. The Fluo-4 labelling allowed to follow the changes in calcium flux upon

stimulation, while the WGA labelling allowed the multiplexing of samples, which consisted in injecting simultaneously in the FACS two neuronal populations, namely WT and *Fmr1*-KO, each labelled with a different WGA, so that both of them would be subjected to the same treatment condition at the same time.

**Flow cytometry and cell sorting.** Cells are sorted with a 100  $\mu\text{m}$  nozzle on a FACSAria III (BDBiosciences) equipped with 4 lasers. Fluo-4, alexa-fluor594, DAPI, alexa-fluor647 and APC-Cy7 are collected respectively upon 488nm, 561nm, 405nm and 633nm, through BP530/30, BP610/20, BP450/40, BP660/20 and BP780/60 filters. The sorter is implemented with a homemade injection system. The sample line is replaced by a different sample line connected with an injection system composed of two syringes and a micro-pump that are placed just after the solenoid valve. D-PBS buffer is put in the first syringe. A 2X agonist solution is prepared and APC-CY7-labeled compbeads (BD Biosciences) are added to the solution prior to connecting the second injection syringe. The minipuls3 pump (Gilson) and the cytometer flow rate are set to 39  $\mu\text{l}/\text{min}$ . The baseline acquisition and sorting are done with the open syringe containing D-PBS buffer. Once the syringe containing the agonist is opened, the D-PBS buffer syringe is closed. The agonist solution occurring in flow cell is monitored with the appearance of beads. At this moment the agonist-responding cells start to be sorted. Cells are collected in D-PBS buffer. Data are analyzed with the BD FACSDiva v6 software (BD Biosciences).

**RNA preparation and RT-qPCR.** Total RNA from aiFACS-sorted cells was extracted using Trizol reagent (Sigma) according to the manufacturer's instructions. In each experimental sample 5000 cells per condition were used. RNAs were purified with 500  $\mu\text{l}$  of Trizol

reagent and precipitated from the aqueous phase with 500 µl of Isopropanol (VWR Medicals) and 1 µg of glycogen (Invitrogen). RNAs were resuspended in 11 µl of RNase-free H<sub>2</sub>O that were directly added to the RT reaction. RT was performed with the Superscript IV synthesis kit (Invitrogen). An initial amplification was done with a denaturation step at 65°C for 5 min, followed by oligo d(T) annealing at 23°C for 10 min, primer annealing at 53°C for 10 min and primer extension at 80°C for 10 min. Upon completion of the cycling steps, the reactions were stored at 4°C.

Quantitative PCR (qPCR) was performed on a Light Cycler 480 (Roche) with MasterMix SYBRGreen (Roche) following the manufacturer's instructions and according to the MIQE guidelines (Bustin et al., 2009). The primer sequences for *Meis2* are the following: *Meis2\_F*, GCCAAGGAGCAGCGTATAGT; *Meis2\_R*, ATTCCAATCATGGGTCCTGC.

**Immunocytochemistry on FACS-sorted neurons.** FACS-sorted neurons were plated on ornithine-coated glass coverslips (35 mm diameter) and cultivated in complete medium: Neurobasal (Invitrogen) supplemented with B-27 (Invitrogen) and glutamax (Invitrogen) as previously described (Maurin et al., 2018b).

**Droplet-based scRNA-seq.** Single-cell suspensions were converted to barcoded scRNA-seq libraries by using the Chromium Single Cell 3' Library, Gel Bead & Multiplex Kit and Chip Kit (10x Genomics), aiming for an estimated 2000 cells per library and following the manufacturer's instructions. Samples were processed using kits pertaining to V2 barcoding chemistry of 10x Genomics. Libraries were sequenced on an Illumina

NextSeq500, and mapped to the mouse genome (build mm10) using CellRanger (10x Genomics). Gene positions were annotated as per Ensembl build 84.

### **Single-cell gene expression quantification and determination of the major cell types.**

Raw gene expression matrices generated per sample using CellRanger (version 2.0.0) were loaded and processed in R (version 3.4.3). Samples were analyzed independently within the Seurat workflow using the Seurat R package (version 3.0.0). First, all cells that had either over 40% UMIs derived from ribosomal RNAs, over 95% dropouts and over 50000 UMIs were removed. From the remaining cells, gene expression matrices were normalized to the median of cellular UMI count, variably expressed genes were selected as having a normalized expression over 0.1, and a quantile-normalized variance exceeding 0.25. To reduce dimensionality of each dataset, the resulting variably expressed genes were summarized by principle component analysis, and the first 11 principle components further summarized using tSNE dimensionality reduction using the default settings of the RunTSNE function. The three independent analysis were then aggregated using FindIntegrationAnchors and IntegrateData functions. Seurat workflow was then re-run with integrated object using the first 30 PCs. Cell clusters in the resulting tSNE two-dimensional representation were annotated to known biological cell types using canonical marker genes.

**Statistics.** The non-parametric Mann-Whitney test was applied to data of two unpaired samples. Data are expressed as mean  $\pm$  SEM, and the P values (or adjusted P values)  $<$  0.05 were considered statistically significant. The statistical analysis was performed using Prism Software 7 version (GraphPad Software, Inc.).

# Results

## 1. Search and characterization of target mRNAs of FMRP

During mouse brain development, the highest expression of FMRP occurs at PND 13. In this time window synaptogenesis reaches a peak. Our research work was oriented to find targets of FMRP during this early developmental stage and in different mouse brain regions (cortex, hippocampus and cerebellum) in order to better define the function of FMRP and its effect on a variety of neuronal pathways. For this purpose, we performed High Throughput Sequencing of RNAs isolated by Cross Linking Immunoprecipitation (HITS-CLIP; **Figure 7**) and we were able to identify the largest dataset of FMRP mRNA targets available in mouse so far, including over 1600 new genes, defining also their cellular origins. We confirmed that FMRP is involved in more functions than just translational regulation and that it interacts with different RNAs during different metabolic steps. Furthermore, we could confirm that the G-quadruplex forming structure is enriched in our dataset and it is the main motif mediating the interaction of mRNAs with FMRP. We defined four novel motifs, which are able to negatively regulate translation, and we validated them to be present in the context of single strand RNA regions (likely loop structures). With our results we were also able to understand how FMRP modulates mRNA translation by defining the role of this protein as an enhancer of translation and not only as repressor (as it was mainly considered so far). Lastly, by analyzing the implication of FMRP in the regulation of RNAs expressed in specific brain regions, we identified the Phosphodiesterase 2A (PDE2A) enzyme as the prominent target

of FMRP, showing that in the absence of this protein, the level of PDE2A is elevated. This allowed us to characterize a novel FMRP mechanism of action.

For the full article, refer to the Annexes – article 3 (Maurin et al., 2018a).

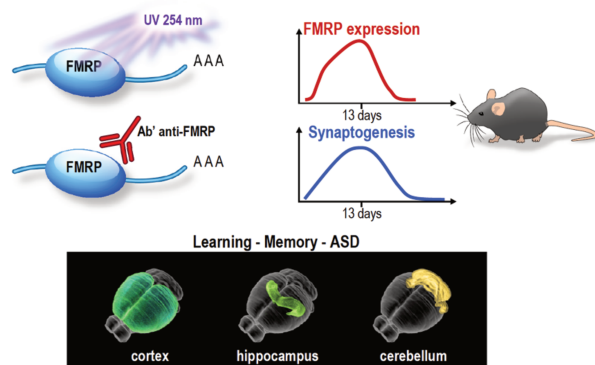


**Figure 7. Representation of the HITS-CLIP experiment.** To isolate mRNAs associated with FMRP *in vivo*, frozen and grinded brain regions are irradiated with UV light to induce UV-crosslinking and FMRP is immunoprecipitated. CLIP samples are subsequently sequenced. The procedure is performed at PND 13, during brain development, at the period of maximum FMRP expression and at the peak of synaptogenesis. The mouse brain regions analyzed are cortex, hippocampus and cerebellum, which are the sites responsible for learning and memory and are compromised in ASD.

My implications in the study: I took care of the differential expression of *Pde2A* in brain and helped define the role of the different binding motifs in the regulation of translation.

## 2. Validation of the main FMRP targets obtained by HITS-CLIP

### 2.1. The Phosphodiesterase 2A (PDE2A)

We found that, at PND 13, the mRNA coding PDE2A is a prominent target of FMRP, which negatively regulates its translation and dendritic transport in the mouse brain (both in cortex and hippocampus). PDE2A is mainly a synaptic enzyme involved in cGMP-dependent degradation of both cAMP and cGMP exerting both pre- and post-synaptic functions. cAMP and cGMP are second messengers at the crossroad of numerous signaling pathways that modulate memory and cognition. In FXS the level of PDE2A is increased and, consequently, the abundance of both cAMP and cGMP is reduced. With

the aim to understand the role of PDE2A in brain development and in the pathophysiology of FXS and ASD, we performed the pharmacological inhibition of PDE2A in *Fmr1*-KO mice using acute and chronic injections of a specific, powerful and commercially available PDE2A inhibitor (Bay 60-7550; **Figure 8**) and we observed that the inhibition of PDE2A:

- a) restores the normal length of growing axon (that is reduced in FXS) and improves the morphology of dendritic spines in *Fmr1*-KO primary cultured neurons;
- b) rescues the exaggerated mGluR-dependent LTD in hippocampal slice that is a hallmark of *Fmr1*-KO brain;
- c) rescues the deficit of social interaction and cognition in newborn and adolescent *Fmr1*-KO mice.

Therefore, the inhibition of PDE2A represents a novel therapeutic approach for FXS.

For the full article, refer to the Annexes – article n°4 (Maurin et al., 2018b).

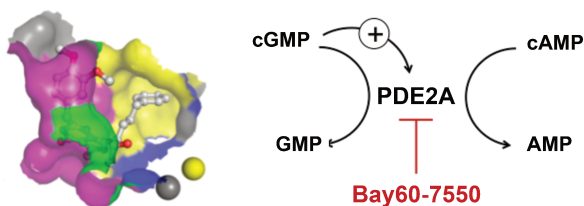


**Figure 8. Mechanism of action of PDE2A in the hydrolysis of cGMP and cAMP.** On the left is illustrated the PDE2A enzyme in its working conformation with Bay60-7550 (in white) in its action site. On the right is reported a schema illustrating the ability of PDE2A to degrade both cAMP and cGMP. PDE2A is selectively inhibited by the drug Bay60-7550.

My implications in the study: I took part in a number of mice behavioral tests.

## 2.2. The Ca<sub>v</sub>2.1 channel

Another notable target of FMRP found with the HITS-CLIP assay is *Cacna1a*, encoding the  $\alpha 1$  subunit (the pore-forming subunit) of the P/Q-type VGCC Ca<sub>v</sub>2.1. This channel protein is involved in the pathophysiology of ASD and FXS, being a key player in the E/I balance of cortical and hippocampal circuits (Schmunk and Gargus, 2013). In recent years, several groups showed the binding of FMRP to mRNAs encoding regulators of ion homeostasis. Also, FMRP can directly interact with proteins, and more specifically with VGCCs. In order to investigate calcium homeostasis defects in FXS, we performed ratiometric calcium imaging recordings on *Fmr1*-KO neurons from mice. We carried out this functional approach to analyze calcium regulation and we were able to observe differences in the levels of calcium between WT and *Fmr1*-KO neurons. We showed that neurons lacking FMRP:

- a) have a deregulated homeostasis of calcium at basal levels and an altered entry of calcium upon a depolarizing stimulus;
- b) are more sensitive to Ca<sub>v</sub>2.2 inhibition and less sensitive to Ca<sub>v</sub>2.1 inhibition compared to WT;
- c) have an impaired membrane expression of Ca<sub>v</sub>2.1.

With our results we underlie the important role played by the Ca<sub>v</sub>2.1 channel in the maintenance of Ca<sup>2+</sup> homeostasis, and we uncover a novel cellular biomarker for cultured *Fmr1*-KO neurons (**Figure 9**).

For the full article, refer to the Annexes – article n°5 (Castagnola et al., 2018).

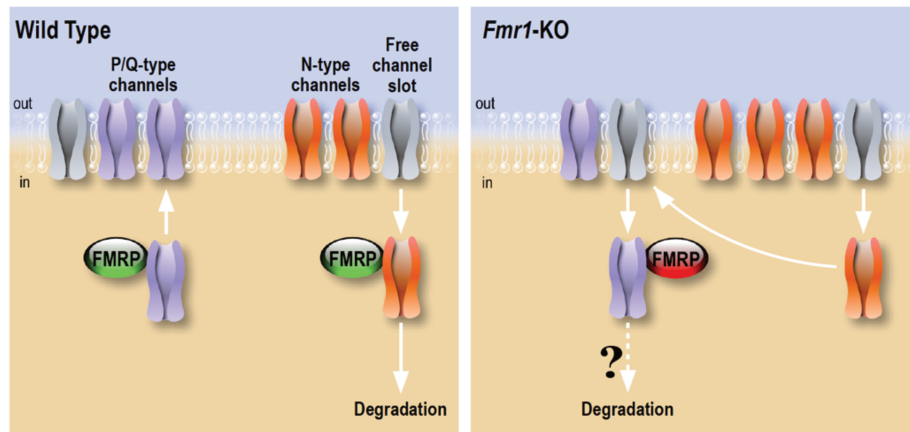


**Figure 9. Our working model of FMRP-mediated regulation of VGCC developmental switch.** In WT cells, N-type channels (in orange), that are expressed first, are inserted in the plasma membrane and occupy most of the available N- and P/Q-preferring “channel slots” (in grey) at the synapse. We hypothesize that upon development and probably upon specific stimuli, FMRP could contribute to the replacement of N- by P/Q-type (in purple) VGCCs. In *Fmr1*-KO neurons, this replacement could be impaired resulting in an altered plasma membrane expression ratio between P/Q- and N-type channels (adapted from the article).

### 3. Identification of genome expression alterations in FXS with aiFACS

In order to get more insight into the role played by FMRP in different cell types and brain regions, we designed and optimized the agonist-induced Functional Analysis and Cell Sorting (aiFACS) prototype. With this tool we could simultaneously stimulate, record and sort cells upon a specific pharmacological stimulation, all of this in real time and with viable cells (**Figure 10A-C**). The aiFACS sorted cells are subsequently amenable to genomic/cell biology experiments that can elucidate the molecular determinants at the base of genotypical and phenotypical cell differences. The coupling of aiFACS with single cell transcriptomic analysis allowed us to molecularly characterize the cell response derived from the stimulus applied to the neurons during the protocol and to define the differential behavior of cells lacking or not FMRP.

Using the Miltenyi neuron isolation kit, we freshly dissociated mouse PND 18 brains to obtain RNA from the neuronal and non-neuronal collected fractions that we used to measure the expression of several neuronal markers by RT-qPCR. The neuronal

fraction is enriched for interneurons (*Gad2*) and pyramidal cells (*Itpr1*), and depleted in microglial markers (*Gm*), immature neurons (*Sox2*) and astrocytes (*Gfap*). Oligodendrocytes (*Mog2*) and endothelial cells (*Rapgef4*) were not significantly removed using this magnetic separation procedure (**Figure 10B**).

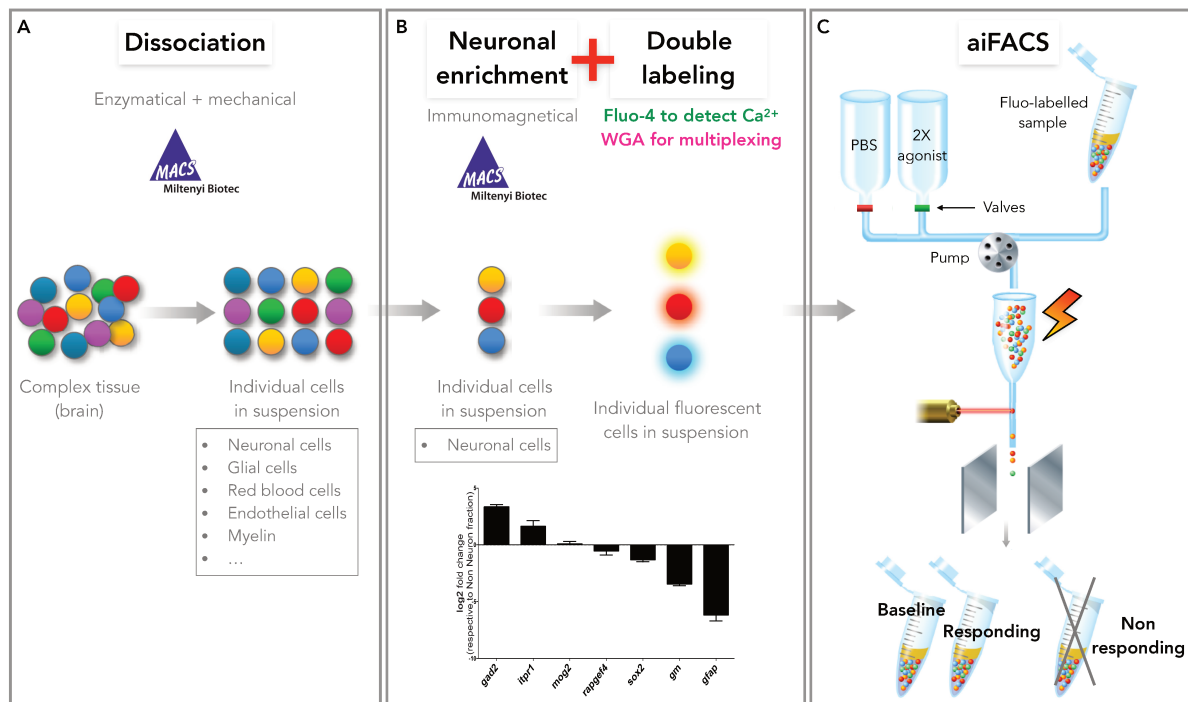


**Figure 10. aiFACS enables the dynamic characterization of heterogeneous samples.** aiFACS pipeline: **A**) Brains from PND 18 mice were dissected and processed with the adult brain dissociation kit (Miltenyi Biotech). **B**) Neuronal and non-neuronal fractions were separated with the Neuron isolation kit (Miltenyi Biotech) and a magnetic negative selection. RNAs were purified from each cell suspension and the expression of canonical markers for various cell populations were analyzed by RT-qPCR. Neurons were loaded with a calcium fluorescent dye (Fluo-4) to monitor their activation. Fluorescent lectin labeling (WGA) allows to mix up to 3 independent samples. **C**) Labeled cells were mixed together and injected in a FACS Aria3 equipped with the aiFACS device that allows to mix cells with a pharmacological agonist. Cells responding to the pharmacological stimulation were selected and sorted and are amenable to subsequent cellular and molecular analysis.

### 3.1. aiFACS sorted cells are amenable to genomic/cell biology experiments

We injected the neuron population labelled with a calcium indicator (Fluo-4) in the FACS supplying the cell flow with a PBS neutral calcium recording solution (baseline

condition). After 3 minutes of recording, we stimulated cells with a high KCl solution (50 mM) to which fluorescently labeled beads were added in order to monitor the pharmacological stimulus (**Figure 11A**). We observed a simultaneous increase in Fluo-4 fluorescence synchronous to the appearance of beads fluorescence. We sorted the cells that displayed increased Fluo-4 fluorescence in the presence of KCl from the non-responding cells. Among the responding cells, we were able to discriminate between morphologically different cells, that we labelled as “small” and “big” cells, and RT-qPCR analysis of sorted cell markers showed that the small cell population is enriched in *Gad2*- and *Calb2*-expressing cells compared to the big cell population, which highlights that the FACS gating strategy favors interneuron selection (**Figure 11B, C**). Remarkably, post-aiFACS neurons are viable (>90%) and capable to grow neurites after 48h in culture as shown by MAP2 immunostaining (**Figure 11D**).

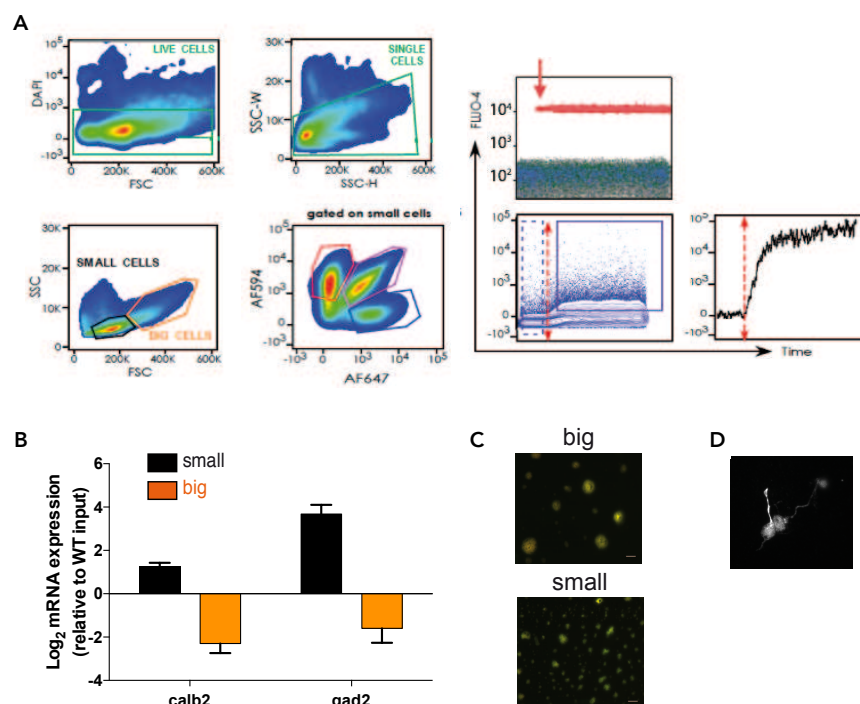


**Figure 11. aiFACS enables the dynamic characterization of heterogeneous samples. A)** FACS gating strategy - Dead cells were excluded by DAPI staining, single cells were isolated then big and small cells

were separated according to their size/structure. Membrane labeling with fluorescent lectins allowed the multiplexing of several samples. The pharmacological stimulation is applied in real time and is monitored through the recording of the fluorescence of standard beads. Cell activation is monitored with the Fluo-4 probe in real time and responding cells are sorted from non-responding cells (blue gate). **B**) Markers from small and big populations - RNAs were purified from big and small cell suspensions and were analyzed by RT-qPCR. The graph shows mRNA expression relative to the neuron suspension (input cells). **C**) Big and small cell populations were immediately imaged after the aiFACS sort. **D**) DIV 6 neuron, MAP2 staining. Sorted neurons can grow neurites *in vitro*: KCl stimulated/sorted neurons were plated on L-ornitin coated glass coverslips, cultivated for up to 6 days in complete neurobasal medium and analyzed by immunocytochemistry.

### 3.2. aiFACS selection through AMPA stimulation enriches sorted cells in interneurons

We prepared fresh neuronal suspensions from PND 18 mice whole brains, sorted them with aiFACS either in the absence (WT) or in the presence of 50 $\mu$ M  $\alpha$ -amino-3-hydroxy-5-methyl-4-isoxazolepropionic acid (AMPA; WT AMPA) and single cell transcriptomics was performed with the 10x Genomics Chromium and Illumina sequencing platform. After quality control, we analyzed 2196 cells (874 WT and 1322 WT AMPA).

The canonical correspondence analysis (CCA) of the three aggregated samples led to the identification of 10 cell clusters, broadly split into inhibitory (*Dcx*, *Gad1*, *Gad2*, *Dlx6*, *Dlx1*, *Dlx5*, *Dlx2*) and excitatory neurons (*Slc17a7*, *Slc17a6*, *Nrn1*, *Neurod1*, *Neurod2*) (**Figure 12A-E**).

We identified 2 clusters of cycling progenitors (*Top2a*, *Ube2c*, *Mki67*, *Hmgb2*, *Cenpf*) already engaged toward the inhibitory (*Dlx1*, *Dlx5*, *Dlx2*) or excitatory lineages (*Selm*, *Meis1*, *Pax6*, *E2f1*, *Cog7*, *Cd63*). Inhibitory neurons were split in 3 main populations that express *Meis2* in combination with other markers: *Tiam2/Nrxn3*, *Pbx1/Sox4* and *Synpr/Calb2/Pbx3*.

We also identified two inhibitory neuron clusters further advanced in their maturation process, "*Sema3c*" (*Calb2*, *Sema3c*, *Id2*, *Cnr1*) that are *Vip* neuron precursors

and cluster of inhibitory mature neurons “*Rora*” (*Cldn3*, *Akap7*, *Cttnbp2*, *Gad1*, *Gad2*) that may give rise to CCK interneurons (**Figure 12A-D**).

Next, we identified a continuum of 3 excitatory cell clusters, separated by their differentiation status: ventricular zone or dentate gyrus granule cells intermediate progenitors (*Hes6* and *Ccnd2*) and two clusters of further differentiated cells (*Neurod1*, *Neurod2*, *Apc*, *Nrxn1*, *Rbfox3*, and *Map1b*), that could be split according to their intermediate or final maturation as indicated by the expression of pre- and post-synaptic proteins expression (*Snap25*, *Grin2b*, *Pclo*), cytoskeletal (*Mapt*) and potassium channel expression (*Kcnb2* or *Kcna1*, *Kcnk2-Trek1*).

The stimulation with AMPA also selected a small proportion of *Olig1*-expressing cells (**Figure 12A, E**). Indeed, these cell types are well known to express AMPA receptors (Bergles et al., 2000) and were sorted together with the neurons in our experiment. In order to focus our analysis exclusively on neurons, we excluded these cells from downstream analysis.

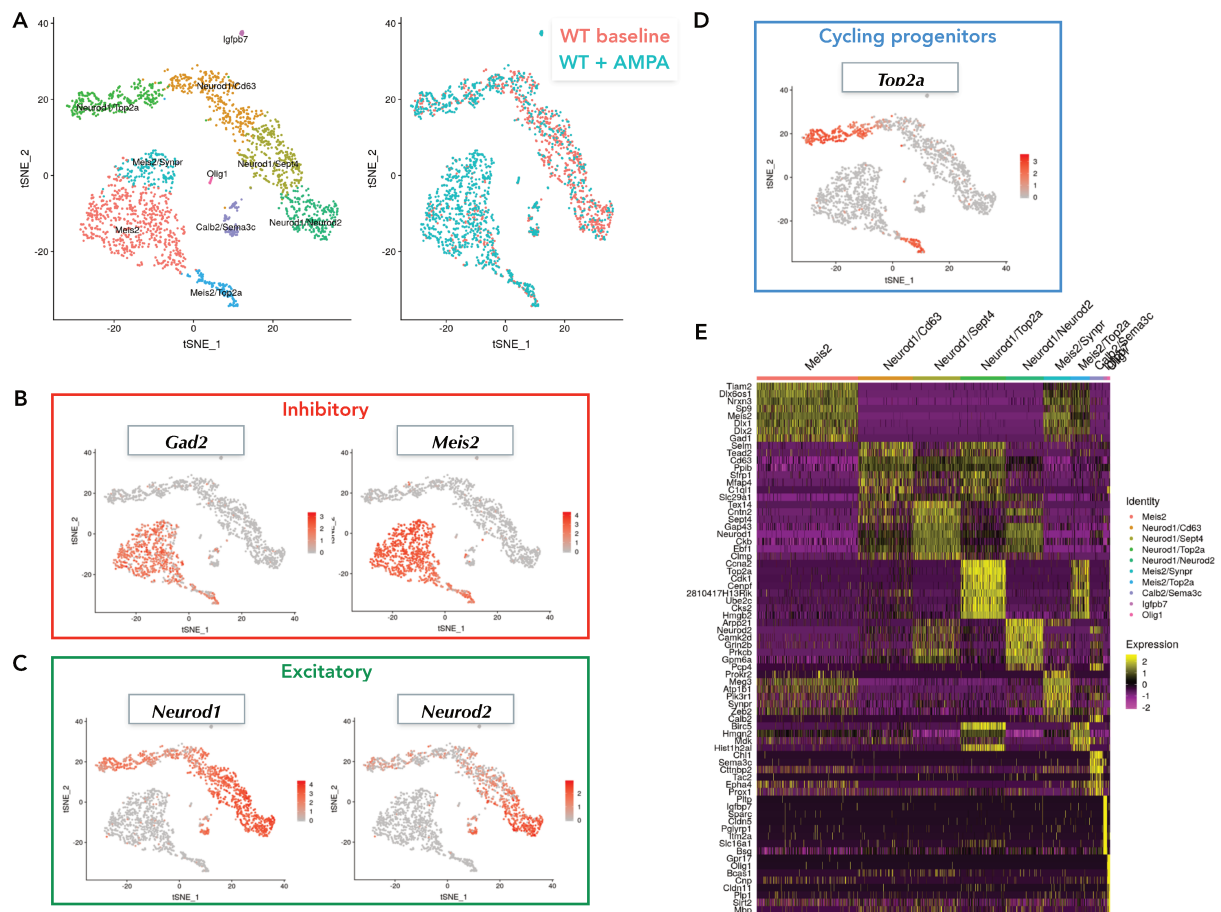


**FIGURE 12. Single cell transcriptomics highlights interneuron population deficits in freshly dissociated neurons from WT brains.** **A)** t-SNE analysis of the two aggregated samples WT-baseline and WT-AMPA. **B)** *Gad2*- and *Meis2*-expressing inhibitory cell clusters. **C)** *Neurod1*- and *Neurod2*-expressing excitatory cell clusters. **D)** *Top2a*-expressing neuronal precursors, representing a less mature cell cluster in the cycling phase. **E)** Heatmap of marker gene expression for the 10 identified cell clusters in the aggregated dataset.

The repartition of the cell types in the stimulated vs. non-stimulated samples clearly shows that AMPA stimulation allowed for the positive selection of *Meis2* interneurons (**Figure 13**). Our results are consistent with previous reports that show that AMPA stimulation selects migrating interneurons (Le Magueresse and Monyer, 2013) expressing *Meis2*. AMPA stimulation promotes a drastic *Meis2* interneuron selection at the expense of excitatory cells (**Figure 13**).

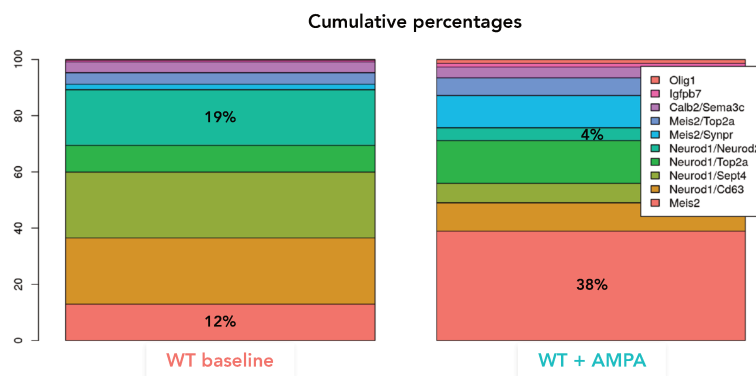


**FIGURE 13. AMPA stimulation positively selects *Meis2* interneurons.** Cell repartition by cluster type for individual samples. This analysis reveals that AMPA selection promotes an enrichment in all *Meis2* neuron types and a decrease in *Neurod1* and *Neurod2* excitatory cells in the WT sample.

We focused on *Meis2* cells and validated the previous results performing a RT-qPCR analysis. We observed that the *Meis2* marker is enriched in WT cells after stimulation with AMPA (**Figure 14A**).

To characterize the phenotype associated with the *Fmr1*-KO neuron counterpart, we analyzed the expression of *Meis2* in AMPA-unstimulated and -stimulated *Fmr1*-KO cells. Our results suggest that the stimulation does not induce a differential expression of the marker in the two fractions (**Figure 14B**), suggesting a deregulation of this type of interneurons in *Fmr1*-KO brains. In addition, the set of KCl stimulations performed previously by our laboratory (Castagnola et al., 2018) also point in the direction of an impaired ability of *Fmr1*-KO neurons to respond correctly to stimulation.

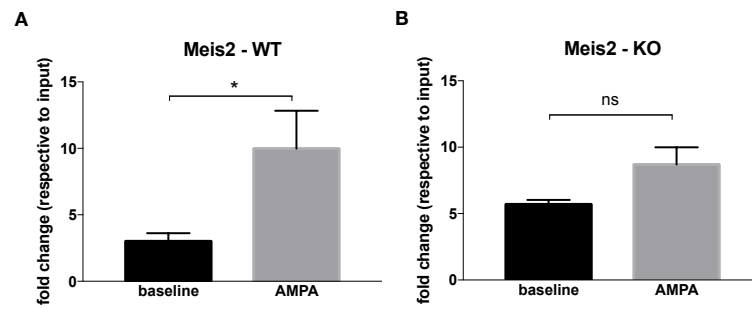


**FIGURE 14. WT and *Fmr1*-KO neurons show different responses to AMPA stimulation.** **A)** Quantification of *Meis2* levels in WT neurons before and after AMPA stimulation. Baseline condition neurons (unstimulated) and 50  $\mu$ M AMPA stimulated neurons show a significant difference. **B)** Quantification of *Meis2* levels in KO neurons before and after AMPA stimulation. Baseline condition neurons (unstimulated) and 50  $\mu$ M AMPA stimulated neurons don't show a significant difference. The "input" neuronal fractions not subjected to aiFACS were used as reference for both genotypes. Results are presented as the mean  $\pm$  SEM, Mann-Whitney test: \* $P = 0.0238$ ; ns = not significant ( $P = 0650$ ).

### 3.3. aiFACS selection through AMPA stimulation unveils *Meis2* interneuron deficiencies in the absence of FMRP expression

We compared by RT-qPCR analysis the expression of *Meis2* in unstimulated and stimulated WT and *Fmr1*-KO neurons. Although these results are preliminary, *Meis2*-expressing *Fmr1*-KO interneurons show a higher baseline than their WT counterparts (**Figure 15**) consistently with previous reports for other types of *Fmr1*-KO neurons (Le Magueresse, 2013).

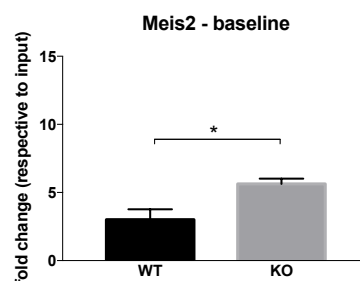


**FIGURE 15. *Meis2* interneurons response to AMPA stimulation is impaired in *Fmr1*-KO neurons.** The expression of *Meis2* in baseline conditions (unstimulated) was quantified by RT-qPCR in WT and *Fmr1*-KO neuron samples. Results are presented as the mean  $\pm$  SEM, Mann-Whitney test: \* $P = 0.0177$ .

# Discussion

## 1. The search and characterization of FMRP mRNA targets

With the aim to better understand the physiopathology of FXS in various brain regions, we performed a High Throughput Sequencing and CrossLinking Immuno-Precipitation (HITS-CLIP) assay from three mouse brain regions (cortex, hippocampus and cerebellum) in the temporal window of active synaptogenesis and when FMRP expression peaks in the brain at PND 13. This resulted in the identification of 1065 FMRP-associated mRNA targets (Maurin et al., 2018a): 872 of them are overlapping with previous studies (Ascano et al., 2012; Darnell et al., 2011) while 192 are novel mRNA targets. The results found are highly relevant because our experiment was performed precisely at the time where a phenotypic effect is seen in *Fmr1*-KO animals. Strikingly, 188 transcripts were also strongly associated with ASD (<https://www.sfari.org/resource/sfari-gene/>), confirming the strong implication of FMRP in the pathophysiology of this disorder. These findings are critical to understand the mechanism of action of FMRP and the pathophysiology of FXS.

## 2. Molecular characterization of FMRP function

### 2.1. Full characterization of FMRP binding sequences in brain

Our analysis clearly shows that the CTGKA, GWRGA and UAY motifs present in regions bound by FMRP are not engaged in Watson-Crick pairing (Maurin and Bardoni, 2018; Maurin et al., 2018a). We conclude that FMRP prevalently recognizes motifs that are presented in single stranded regions or loop sequences of stem loop structures;

## 2.2. Identification of new FMRP-binding coding regions enriched in the GAC codon

The GAC codon is decoded by the m38C\_tRNA \_Asp, a highly modified tRNA harboring a GUC anticodon whose Guanosine is hyper modified by Queuine (Q). Q is solely provided by the gut microbiota and is used to modify tRNAs. Q deprivation stalls ribosomes at GAC codons and to a smaller extent at near-cognate codons (Tuorto et al., 2018). Collectively these findings lead to the hypothesis that FMRP stalls polyribosomes – one of the mechanisms proposed to explain the role of translational repressor of FMRP (Darnell et al., 2011; Maurin et al., 2014) – by affecting m38C\_tRNA \_Asp metabolism (Maurin and Bardoni, 2018);

## 2.3. Understanding of how FMRP modulates mRNA translation

The CLIP results definitively help to define the role of FMRP as enhancer of translation and not only as repressor as it was mainly considered so far (Maurin and Bardoni, 2018);

## 2.4. Description of the role of FMRP in mRNA transport

While it was reported that in the absence of FMRP, the transport of mRNA targets to the synapses is reduced (Dictenberg et al., 2008), we have shown that the transport of *Pde2a* mRNA is enhanced in *Fmr1*-KO neurons (Maurin et al., 2018a). These data suggest a heterogeneous role of FMRP in mRNA localization. This function of FMRP has been poorly studied so far, as most works have focused on translational regulation.

### 3. Pathophysiology of FXS

Several pathways in the brain are targeted by FMRP, as revealed by gene ontology analysis, and in order to validate the FMRP targets obtained by CLIP, we focused specifically on the two most prominent and representative pathways that show deregulation in the *Fmr1*-KO mouse brain: the phosphodiesterase 2A (PDE2A) pathway and the calcium (Ca<sup>2+</sup>) pathway.

#### 3.1. The PDE2A pathway

We found that, at PND 13, the mRNA coding PDE2A is a prominent target of FMRP that negatively modulates its translation and dendritic transport in the mouse brain (both in cortex and hippocampus) (Maurin et al., 2018a). PDE2A is a synaptic enzyme – the only PDE located in docked synaptic vesicles (Boyken et al., 2013)– involved in the degradation of both cAMP and cGMP (Rosman et al., 1997) that modulates a wide array of intracellular processes and related neurobehavioral functions, including memory and cognition. We showed that the level of PDE2A is increased in FXS mouse neurons and that the abundance of both cAMP and cGMP is reduced (Maurin et al., 2018b). Among the several PDE2A inhibitors characterized so far, we selected the specific, powerful and commercially available BAY60-7550 (Boess et al., 2004) that efficiently crosses the blood-brain barrier (Wang et al., 2017). We found that pharmacological inhibition of PDE2A with BAY60-7550 resulted in the rescue of *in vitro* (dendrites and axon phenotypes), *ex-vivo* (exaggerated mGlu-R dependent LTD) and *in vivo* (deficit of social behavior) phenotypes characterizing FXS.

In conclusion, our data confirm that the *Pde2A* mRNA is a critical target involved in the pathophysiology of FXS and suggest that altered expression of PDE2A is a new putative cause of ASD, thus validating our CLIP strategy.

In the future, it will be interesting to perform genetic and chronic pharmacological reduction of PDE2A in *Fmr1*-KO mice in order to validate the pathophysiological role of PDE2A in various FXS phenotypes and to define a PDE2A-based therapy for FXS.

### 3.2. The calcium pathway

Several reports have shown that multiple FMRP mRNA targets encode regulators of ion homeostasis, particularly in the calcium pathway, by different mechanisms (Ascano et al., 2012; Brown et al., 2001; Darnell et al., 2011; Maurin et al., 2018a; Miyashiro et al., 2003). In particular, FMRP has been shown to directly interact with two members of the VGCC family, namely  $Ca_v2.1$  and  $Ca_v2.2$  (Ferron et al., 2014). VGCCs are key players in neurons since they regulate membrane excitability, neurotransmitter release and gene expression modulation (Zamponi et al., 2015) and their altered expression at the plasma membrane leads to several conditions, namely ataxia, ID, ASD and epilepsy (Damaj et al., 2015).

Interestingly, the mRNA of *Cacna1a*, which encodes the pore-forming  $\alpha 1$  subunit of the  $Ca_v2.1$  P/Q type VGCC, is the second most prominent gene we found in our CLIP analysis. This protein is a presynaptic  $Ca^{2+}$  channel involved in the pathophysiology of ASD and FXS that has a key role in the excitation/inhibition balance in hippocampal circuits, which is affected in the ASD phenotype (Schmunk and Gargus, 2013). I showed that FMRP binds both the *Cacna1a* mRNA and its encoded protein and also that the absence of FMRP does not alter the abundance of this protein in the total cellular fraction

but reduces its plasma membrane localization in cultured *Fmr1*-KO neurons. I also showed that the inhibition of both  $Ca_v2.1$  and  $Ca_v2.2$  (N-type VGCC) affects the KCl-mediated entry of calcium in neurons, promoting respectively a lower and a higher entry of calcium in *Fmr1*-KO neurons compared to WT. This suggests that the activity of both channels is deregulated when FMRP is not present. Indeed, FMRP has been already shown to regulate N-type expression by targeting this channel to the proteasome (Ferron et al., 2014), so it is tempting to speculate that FMRP is a molecular adaptor regulating the relative plasma membrane localization of N- and P/Q-type channels. The working model I propose is illustrated in **Figure 9**: N-type channels (in orange) are expressed first in development and are inserted in the plasma membrane occupying most of the available “channel slots” (in grey) at the synapse (Cao and Tsien, 2010; Cao et al., 2004). I hypothesize that upon development, and probably upon specific stimuli, FMRP could contribute to the replacement of N- by P/Q-type (in purple) VGCCs. In *Fmr1*-KO neurons, however, due to the lack of FMRP, this replacement could be impaired resulting in an altered plasma membrane ratio between P/Q- and N-type channels, as already shown in the case of familial hemiplegic migraine (Cao and Tsien, 2010). Moreover, the ability of FMRP to regulate the subcellular localization of its target mRNAs, and specifically that of  $Ca_v2.1$ , may be responsible for the actual presence of the channel at the plasma membrane (Castagnola et al., 2018).

Several reports suggest that there is an altered cytoskeleton organization in different FXS cell lines (Abekhoukh and Bardoni, 2014; Abekhoukh et al., 2017; Davydova et al., 2014) and this might explain the aberrant expression of  $Ca_v2.1$  at the plasma membrane. On the other side, as already mentioned, the Ferron group proposed an implication of the proteasome (Ferron et al., 2014).

Last but not least, the impairment of calcium homeostasis, according to our results, can be considered a new cellular biomarker for cultured *Fmr1*-KO neurons, while to date the only available cellular biomarker for in *Fmr1*-KO cultured neurons is represented by the immaturity of dendritic spines (Castagnola et al., 2018).

In the future I think that it will be interesting, on one side, to test the impact on  $\text{Ca}^{2+}$  homeostasis of various drugs having a positive effect on the FXS phenotype; on the other side, to study calcium homeostasis in iPS-derived neurons obtained from FXS patients and compare them with control cells.

#### **4. aiFACS and cell heterogeneity**

By performing  $\text{Ca}^{2+}$  imaging I realized that a huge heterogeneity of  $\text{Ca}^{2+}$  levels is present among the different neurons. These observations led me to the question “What makes a cell look different from its neighbors?”. Even if I do not think to be able to provide a complete answer for the moment, I decided to get a better insight into the study of the heterogeneity of neurons both in brain and *in vitro*, taking advantage of the new single cell sequencing technique available in our Institute.

Thus, starting from this issue and keeping in mind the need to validate my data of  $\text{Ca}^{2+}$  homeostasis already obtained *in vitro* in brain-derived neurons (Castagnola et al., 2018), I set up a new technique together with Dr. Thomas Maurin and the Imaging platform of IPMC, adapting to our needs the FACS machinery. This technique, called agonist-induced Functional Analysis and Cell Sorting (aiFACS for short), allows to couple neuronal stimulation (in real time) and collection with omics or single cell sequencing analysis. aiFACS provides new information on the targeted cell population of a given pharmacological compound and on the molecular specificities that drive the

heterogeneity of the cell response. By using aiFACS not only I validated my *in vitro* data by showing that *Fmr1*-KO interneurons are hypoexcitable, but after single cell analysis of dissociated WT neurons either stimulated or not by AMPA, I was capable of identifying a new cell FXS phenotype involving a previously neglected interneuron subclass. Indeed, the impaired response to AMPA seems associated with a defective function of a specific group of inhibitory cells, the *Meis2* interneurons. The study of *Fmr1*-KO brains with aiFACS allowed me to highlight the implication of this previously underestimated subclass of interneurons in the pathophysiology of FXS. Furthermore, in the *Fmr1*-KO mouse brain the composition of cellular subtypes appears different from that of the WT counterpart. Altogether, my results suggest that it will be possible to create a “chemical” map of the brain in health and disease and in the future it will be interesting to apply aiFACS to other forms of ID and ASD.

Finally, it is important to stress that aiFACS is a highly versatile tool: to date, our understanding of neuron response to pharmacological stimulation has lacked high throughput methodology that strongly impacted different research and medical areas other than neuroscience, but with aiFACS fields like immunology and cancer research can also benefit of its potentiality.

## 5. Final Considerations

In conclusion, I consider my PhD work successful at different levels, since it allowed me to better detail the pathophysiology of FXS and, by extension, of ID. Indeed, I could:

- 1) Define and characterize PDE2A as a promising pharmacological target that represents a novel therapeutic strategy for FXS;

- 2) Identify calcium homeostasis deregulation as a new phenotype of cultured *Fmr1*-KO neurons. This phenotype can be considered a new cellular biomarker, easily manageable to screen small molecules and to robustly monitor drug efficiency. This can ultimately lead to the identification of new drugs to treat FXS;
- 3) Describe a new cell phenotype of FXS during post-natal development involving the deregulation of *Meis2* inhibitory interneurons.

Because of the vital importance of finding new treatments for FXS, I hope to be able to further investigate the signaling pathways that are deregulated in the absence of FMRP, which would allow to gain more insight in this rare but serious disease. In addition, I strongly believe in the future application of the aiFACS technology in the study of other syndromes and disorders associated with mental retardation, as well as in the investigation of other scientific areas, like cancer research.

# Bibliography

- Abekhoukh, S., and Bardoni, B. (2014). CYFIP family proteins between autism and intellectual disability: links with Fragile X syndrome. *Front. Cell. Neurosci.* *8*, 81.
- Abekhoukh, S., Sahin, H.B., Grossi, M., Zongaro, S., Maurin, T., Madrigal, I., Kazue-Sugioka, D., Raas-Rothschild, A., Doulazmi, M., Carrera, P., et al. (2017). New insights into the regulatory function of CYFIP1 in the context of WAVE- and FMRP-containing complexes. *Dis. Model. Mech.* *10*, 463–474.
- Achuta, V.S., Möykkynen, T., Peteri, U.-K., Turconi, G., Rivera, C., Keinänen, K., and Castrén, M.L. (2018). Functional changes of AMPA responses in human induced pluripotent stem cell-derived neural progenitors in fragile X syndrome. *Sci. Signal.* *11*, eaan8784.
- Ackerman, M.J., and Clapham, D.E. (1997). Ion channels--basic science and clinical disease. *N. Engl. J. Med.* *336*, 1575–1586.
- Adusei, D.C., Pacey, L.K.K., Chen, D., and Hampson, D.R. (2010). Early developmental alterations in GABAergic protein expression in fragile X knockout mice. *Neuropharmacology* *59*, 167–171.
- Ameis, S.H., Kasee, C., Corbett-Dick, P., Cole, L., Dadhwal, S., Lai, M.-C., Veenstra-VanderWeele, J., and Correll, C.U. (2018). Systematic review and guide to management of core and psychiatric symptoms in youth with autism. *Acta Psychiatr. Scand.* *138*, 379–400.
- Arbab, T., Pennartz, C.M.A., and Battaglia, F.P. (2018). Impaired hippocampal representation of place in the *Fmr1* -knockout mouse model of fragile X syndrome. *Sci. Rep.* *8*, 8889.
- Ascano, M., Mukherjee, N., Bandaru, P., Miller, J.B., Nusbaum, J.D., Corcoran, D.L., Langlois, C., Munschauer, M., Dewell, S., Hafner, M., et al. (2012). FMRP targets distinct mRNA sequence elements to regulate protein expression. *Nature* *492*, 382–386.
- Barbee, S.A., Estes, P.S., Cziko, A.-M., Hillebrand, J., Luedeman, R.A., Coller, J.M., Johnson, N., Howlett, I.C., Geng, C., Ueda, R., et al. (2006). Staufen- and FMRP-Containing Neuronal RNPs Are Structurally and Functionally Related to Somatic P Bodies. *Neuron* *52*, 997–1009.
- Bear, M.F., Huber, K.M., and Warren, S.T. (2004). The mGluR theory of fragile X mental retardation. *Trends Neurosci.* *27*, 370–377.
- Bechara, E.G., Didiot, M.C., Melko, M., Davidovic, L., Bensaid, M., Martin, P., Castets, M., Pognonec, P., Khandjian, E.W., Moine, H., et al. (2009). A novel function for fragile X mental retardation protein in translational activation. *PLoS Biol.* *7*, e16.
- Ben-Ari, Y., Cherubini, E., Corradetti, R., and Gaiarsa, J.L. (1989). Giant synaptic potentials in immature rat CA3 hippocampal neurones. *J. Physiol.* *416*, 303–325.
- Bergles, D.E., Roberts, J.D., Somogyi, P., and Jahr, C.E. (2000). Glutamatergic synapses on oligodendrocyte precursor cells in the hippocampus. *Nature* *405*, 187–191.
- Berry-Kravis, E. (2002). Epilepsy in fragile X syndrome. *Dev. Med. Child Neurol.* *44*, 724–728.
- Berry-Kravis, E., Raspa, M., Loggin-Hester, L., Bishop, E., Holiday, D., and Bailey, D.B. (2010). Seizures in Fragile X Syndrome: Characteristics and Comorbid Diagnoses. *Am. J. Intellect. Dev. Disabil.* *115*, 461–472.

- Berry-Kravis, E., Knox, A., and Hervey, C. (2011). Targeted treatments for fragile X syndrome. *J. Neurodev. Disord.* 3, 193–210.
- Berzhanskaya, J., Phillips, M.A., Shen, J., and Colonnese, M.T. (2016). Sensory hypoexcitability in a rat model of fetal development in Fragile X Syndrome. *Sci. Rep.* 6, 30769.
- Boccuto, L., Chen, C.-F., Pittman, A.R., Skinner, C.D., McCartney, H.J., Jones, K., Bochner, B.R., Stevenson, R.E., and Schwartz, C.E. (2013). Decreased tryptophan metabolism in patients with autism spectrum disorders. *Mol. Autism* 4, 16.
- Boess, F.G., Hendrix, M., van der Staay, F.-J., Erb, C., Schreiber, R., van Staveren, W., de Vente, J., Prickaerts, J., Blokland, A., and Koenig, G. (2004). Inhibition of phosphodiesterase 2 increases neuronal cGMP, synaptic plasticity and memory performance. *Neuropharmacology* 47, 1081–1092.
- Boyken, J., Grønborg, M., Riedel, D., Urlaub, H., Jahn, R., and Chua, J.J.E. (2013). Molecular profiling of synaptic vesicle docking sites reveals novel proteins but few differences between glutamatergic and GABAergic synapses. *Neuron* 78, 285–297.
- Brager, D.H., and Johnston, D. (2014). Channelopathies and dendritic dysfunction in fragile X syndrome. *Brain Res. Bull.* 103, 11–17.
- den Broeder, M.J., van der Linde, H., Brouwer, J.R., Oostra, B.A., Willemsen, R., and Ketting, R.F. (2009). Generation and characterization of FMR1 knockout zebrafish. *PLoS One* 4, e7910.
- Brouwer, J.R., Mientjes, E.J., Bakker, C.E., Nieuwenhuizen, I.M., Severijnen, L.A., Van der Linde, H.C., Nelson, D.L., Oostra, B.A., and Willemsen, R. (2007). Elevated Fmr1 mRNA levels and reduced protein expression in a mouse model with an unmethylated Fragile X full mutation. *Exp. Cell Res.* 313, 244–253.
- Brown, W.T. (1990). The fragile X: progress toward solving the puzzle. *Am. J. Hum. Genet.* 47, 175–180.
- Brown, M.R., and Kaczmarek, L.K. (2011). Potassium channel modulation and auditory processing. *Hear. Res.* 279, 32–42.
- Brown, A.M., Westenbroek, R.E., Catterall, W.A., and Ransom, B.R. (2001). Axonal L-type Ca<sup>2+</sup> channels and anoxic injury in rat CNS white matter. *J. Neurophysiol.* 85, 900–911.
- Brown, M.R., Kronengold, J., Gazula, V.-R., Chen, Y., Strumbos, J.G., Sigworth, F.J., Navaratnam, D., and Kaczmarek, L.K. (2010). Fragile X mental retardation protein controls gating of the sodium-activated potassium channel Slack. *Nat. Neurosci.* 13, 819–821.
- Bu, B., and Zhang, L. (2017). A New Link Between Insulin Signaling and Fragile X Syndrome. *Neurosci. Bull.* 33, 118–120.
- Budimirovic, D.B., and Kaufmann, W.E. (2011). What can we learn about autism from studying fragile X syndrome? *Dev. Neurosci.* 33, 379–394.
- Cao, Y.-Q., and Tsien, R.W. (2010). Different Relationship of N- and P/Q-Type Ca<sup>2+</sup> Channels to Channel-Interacting Slots in Controlling Neurotransmission at Cultured Hippocampal Synapses. *J. Neurosci.* 30, 4536–4546.
- Cao, Y.-Q., Piedras-Rentería, E.S., Smith, G.B., Chen, G., Harata, N.C., and Tsien, R.W. (2004). Presynaptic Ca<sup>2+</sup> channels compete for channel type-preferring slots in altered neurotransmission arising from Ca<sup>2+</sup> channelopathy. *Neuron* 43, 387–400.
- Carafoli, E. (2002). Calcium signaling: a tale for all seasons. *Proc. Natl. Acad. Sci. U. S. A.* 99, 1115–1122.
- Castagnola, S., Delhay, S., Folci, A., Paquet, A., Brau, F., Duprat, F., Jarjat, M., Grossi, M., Béal, M., Martin, S., et al. (2018). New Insights Into the Role of Cav2 Protein Family

- in Calcium Flux Deregulation in Fmr1-KO Neurons. *Front. Mol. Neurosci.* *11*.
- Catterall, W.A., and Few, A.P. (2008). Calcium channel regulation and presynaptic plasticity. *Neuron* *59*, 882–901.
- Catterall, W.A., Perez-Reyes, E., Snutch, T.P., and Striessnig, J. (2005). International Union of Pharmacology. XLVIII. Nomenclature and structure-function relationships of voltage-gated calcium channels. *Pharmacol. Rev.* *57*, 411–425.
- Cea-Del Rio, C.A., and Huntsman, M.M. (2014). The contribution of inhibitory interneurons to circuit dysfunction in Fragile X Syndrome. *Front. Cell. Neurosci.* *8*.
- Chaste, P., and Leboyer, M. (2012). Autism risk factors: genes, environment, and gene-environment interactions. *Dialogues Clin. Neurosci.* *14*, 281–292.
- Chemin, J., Siquier-Pernet, K., Nicouleau, M., Barcia, G., Ahmad, A., Medina-Cano, D., Hanein, S., Altin, N., Hubert, L., Bole-Feysot, C., et al. (2018). De novo mutation screening in childhood-onset cerebellar atrophy identifies gain-of-function mutations in the CACNA1G calcium channel gene. *Brain J. Neurol.* *141*, 1998–2013.
- Chen, L., Yun, S.W., Seto, J., Liu, W., and Toth, M. (2003). The fragile X mental retardation protein binds and regulates a novel class of mRNAs containing U rich target sequences. *Neuroscience* *120*, 1005–1017.
- Chonchaiya, W., Au, J., Schneider, A., Hessel, D., Harris, S.W., Laird, M., Mu, Y., Tassone, F., Nguyen, D.V., and Hagerman, R.J. (2012). Increased prevalence of seizures in boys who were probands with the FMR1 premutation and co-morbid autism spectrum disorder. *Hum. Genet.* *131*, 581–589.
- Chugani, D.C., Muzik, O., Behen, M., Rothermel, R., Janisse, J.J., Lee, J., and Chugani, H.T. (1999). Developmental changes in brain serotonin synthesis capacity in autistic and nonautistic children. *Ann. Neurol.* *45*, 287–295.
- Clapham, D.E. (2007). Calcium signaling. *Cell* *131*, 1047–1058.
- Coffee, B., Keith, K., Albizua, I., Malone, T., Mowrey, J., Sherman, S.L., and Warren, S.T. (2009). Incidence of Fragile X Syndrome by Newborn Screening for Methylated FMR1 DNA. *Am. J. Hum. Genet.* *85*, 503–514.
- Connor, J.M. (1991). Cloning of the gene for the fragile X syndrome: implications for the clinical geneticist. *J. Med. Genet.* *28*, 811–813.
- Contractor, A., Klyachko, V.A., and Portera-Cailliau, C. (2015). Altered neuronal and circuit excitability in Fragile X Syndrome. *Neuron* *87*, 699–715.
- Cornish, K., Sudhalter, V., and Turk, J. (2004). Attention and language in fragile X. *Ment. Retard. Dev. Disabil. Res. Rev.* *10*, 11–16.
- Cornish, K., Turk, J., and Hagerman, R. (2008). The fragile X continuum: new advances and perspectives. *J. Intellect. Disabil. Res. JIDR* *52*, 469–482.
- Costa, L., Spatuzza, M., D'Antoni, S., Bonaccorso, C.M., Trovato, C., Musumeci, S.A., Leopoldo, M., Lacivita, E., Catania, M.V., and Ciranna, L. (2012). Activation of 5-HT7 serotonin receptors reverses metabotropic glutamate receptor-mediated synaptic plasticity in wild-type and Fmr1 knockout mice, a model of Fragile X syndrome. *Biol. Psychiatry* *72*, 924–933.
- Costa, L., Sardone, L.M., Lacivita, E., Leopoldo, M., and Ciranna, L. (2015). Novel agonists for serotonin 5-HT7 receptors reverse metabotropic glutamate receptor-mediated long-term depression in the hippocampus of wild-type and Fmr1 KO mice, a model of Fragile X Syndrome. *Front. Behav. Neurosci.* *9*.
- Coy, J.F., Sedlacek, Z., Bächner, D., Hameister, H., Joos, S., Lichter, P., Delius, H., and Poustka, A. (1995). Highly conserved 3' UTR and expression pattern of FXR1 points to a divergent gene regulation of FXR1 and FMR1. *Hum. Mol. Genet.* *4*, 2209–2218.

- Crissey, M.S. (1975). Mental retardation: Past, present, and future. *Am. Psychol.* *30*, 800–808.
- Cronister, A., Schreiner, R., Wittenberger, M., Amiri, K., Harris, K., and Hagerman, R.J. (1991). Heterozygous fragile X female: historical, physical, cognitive, and cytogenetic features. *Am. J. Med. Genet.* *38*, 269–274.
- Cruz, D.L. (1985). Fragile X Syndrome. *Am. J. Ment. Defic.* *90*, 119–123.
- Dahlhaus, R. (2018). Of Men and Mice: Modeling the Fragile X Syndrome. *Front. Mol. Neurosci.* *11*.
- Dahlhaus, R., and El-Husseini, A. (2010). Altered neuroligin expression is involved in social deficits in a mouse model of the fragile X syndrome. *Behav. Brain Res.* *208*, 96–105.
- Damaj, L., Lupien-Meilleur, A., Lortie, A., Riou, É., Ospina, L.H., Gagnon, L., Vanasse, C., and Rossignol, E. (2015). CACNA1A haploinsufficiency causes cognitive impairment, autism and epileptic encephalopathy with mild cerebellar symptoms. *Eur. J. Hum. Genet. EJHG* *23*, 1505–1512.
- Darnell, J.C., Fraser, C.E., Mostovetsky, O., Stefani, G., Jones, T.A., Eddy, S.R., and Darnell, R.B. (2005). Kissing complex RNAs mediate interaction between the Fragile-X mental retardation protein KH2 domain and brain polyribosomes. *Genes Dev.* *19*, 903–918.
- Darnell, J.C., Van Driesche, S.J., Zhang, C., Hung, K.Y.S., Mele, A., Fraser, C.E., Stone, E.F., Chen, C., Fak, J.J., Chi, S.W., et al. (2011). FMRP stalls ribosomal translocation on mRNAs linked to synaptic function and autism. *Cell* *146*, 247–261.
- Davidovic, L., Jaglin, X.H., Lepagnol-Bestel, A.-M., Tremblay, S., Simonneau, M., Bardoni, B., and Khandjian, E.W. (2007). The fragile X mental retardation protein is a molecular adaptor between the neurospecific KIF3C kinesin and dendritic RNA granules. *Hum. Mol. Genet.* *16*, 3047–3058.
- Davidovic, L., Navratil, V., Bonaccorso, C.M., Catania, M.V., Bardoni, B., and Dumas, M.-E. (2011). A metabolomic and systems biology perspective on the brain of the Fragile X syndrome mouse model. *Genome Res.* *21*, 2190–2202.
- Davis, J.K., and Broadie, K. (2017). Multifarious Functions of the Fragile X Mental Retardation Protein. *Trends Genet. TIG* *33*, 703–714.
- Davydova, D., Marini, C., King, C., Klueva, J., Bischof, F., Romorini, S., Montenegro-Venegas, C., Heine, M., Schneider, R., Schröder, M.S., et al. (2014). Bassoon specifically controls presynaptic P/Q-type Ca<sup>2+</sup> channels via RIM-binding protein. *Neuron* *82*, 181–194.
- De Boulle, K., Verkerk, A.J., Reyniers, E., Vits, L., Hendrickx, J., Van Roy, B., Van den Bos, F., de Graaff, E., Oostra, B.A., and Willems, P.J. (1993). A point mutation in the FMR-1 gene associated with fragile X mental retardation. *Nat. Genet.* *3*, 31–35.
- Deng, P.-Y., Rotman, Z., Blundon, J.A., Cho, Y., Cui, J., Cavalli, V., Zakharenko, S.S., and Klyachko, V.A. (2013). FMRP regulates neurotransmitter release and synaptic information transmission by modulating action potential duration via BK channels. *Neuron* *77*, 696–711.
- Devys, D., Lutz, Y., Rouyer, N., Bellocq, J.P., and Mandel, J.L. (1993). The FMR-1 protein is cytoplasmic, most abundant in neurons and appears normal in carriers of a fragile X premutation. *Nat. Genet.* *4*, 335–340.
- Dictenberg, J.B., Swanger, S.A., Antar, L.N., Singer, R.H., and Bassell, G.J. (2008). A direct role for FMRP in activity-dependent dendritic mRNA transport links filopodial-spine morphogenesis to fragile X syndrome. *Dev. Cell* *14*, 926–939.

- Didiot, M.-C., Subramanian, M., Flatter, E., Mandel, J.-L., and Moine, H. (2009). Cells lacking the fragile X mental retardation protein (FMRP) have normal RISC activity but exhibit altered stress granule assembly. *Mol. Biol. Cell* *20*, 428–437.
- Domes, G., Heinrichs, M., Michel, A., Berger, C., and Herpertz, S.C. (2007). Oxytocin improves “mind-reading” in humans. *Biol. Psychiatry* *61*, 731–733.
- Drozd, M., Bardoni, B., and Capovilla, M. (2018). Modeling Fragile X Syndrome in *Drosophila*. *Front. Mol. Neurosci.* *11*, 124.
- Eichler, E.E., Richards, S., Gibbs, R.A., and Nelson, D.L. (1993). Fine structure of the human FMR1 gene. *Hum. Mol. Genet.* *2*, 1147–1153.
- Ethridge, L.E., White, S.P., Mosconi, M.W., Wang, J., Pedapati, E.V., Erickson, C.A., Byerly, M.J., and Sweeney, J.A. (2017). Neural synchronization deficits linked to cortical hyper-excitability and auditory hypersensitivity in fragile X syndrome. *Mol. Autism* *8*, 22.
- Feng, Y., Zhang, F., Lokey, L.K., Chastain, J.L., Lakkis, L., Eberhart, D., and Warren, S.T. (1995). Translational suppression by trinucleotide repeat expansion at FMR1. *Science* *268*, 731–734.
- Feng, Y., Gutekunst, C.A., Eberhart, D.E., Yi, H., Warren, S.T., and Hersch, S.M. (1997). Fragile X mental retardation protein: nucleocytoplasmic shuttling and association with somatodendritic ribosomes. *J. Neurosci. Off. J. Soc. Neurosci.* *17*, 1539–1547.
- Ferron, L. (2016). Fragile X mental retardation protein controls ion channel expression and activity. *J. Physiol.* *594*, 5861–5867.
- Ferron, L., Nieto-Rostro, M., Cassidy, J.S., and Dolphin, A.C. (2014). Fragile X mental retardation protein controls synaptic vesicle exocytosis by modulating N-type calcium channel density. *Nat. Commun.* *5*, 3628.
- Filippini, A., Bonini, D., Lacoux, C., Pacini, L., Zingariello, M., Sancillo, L., Bosisio, D., Salvi, V., Mingardi, J., La Via, L., et al. (2017). Absence of the Fragile X Mental Retardation Protein results in defects of RNA editing of neuronal mRNAs in mouse. *RNA Biol.* *14*, 1580–1591.
- Franco, L.M., Okray, Z., Linneweber, G.A., Hassan, B.A., and Yaksi, E. (2017). Reduced Lateral Inhibition Impairs Olfactory Computations and Behaviors in a *Drosophila* Model of Fragile X Syndrome. *Curr. Biol. CB* *27*, 1111–1123.
- Freund, L.S., and Reiss, A.L. (1991). Cognitive profiles associated with the fra(X) syndrome in males and females. *Am. J. Med. Genet.* *38*, 542–547.
- Galvez, R., and Greenough, W.T. (2005). Sequence of abnormal dendritic spine development in primary somatosensory cortex of a mouse model of the fragile X mental retardation syndrome. *Am. J. Med. Genet. A.* *135*, 155–160.
- Ganguly, K., Rejmak, E., Mikosz, M., Nikolaev, E., Knapska, E., and Kaczmarek, L. (2013). Matrix metalloproteinase (MMP) 9 transcription in mouse brain induced by fear learning. *J. Biol. Chem.* *288*, 20978–20991.
- Gareau, C., Houssin, E., Martel, D., Coudert, L., Mellaoui, S., Huot, M.-E., Laprise, P., and Mazroui, R. (2013). Characterization of fragile X mental retardation protein recruitment and dynamics in *Drosophila* stress granules. *PLoS One* *8*, e55342.
- Gedeon, A.K., Baker, E., Robinson, H., Partington, M.W., Gross, B., Manca, A., Korn, B., Poustka, A., Yu, S., and Sutherland, G.R. (1992). Fragile X syndrome without CCG amplification has an FMR1 deletion. *Nat. Genet.* *1*, 341–344.
- Genç, B., Müller-Hartmann, H., Zeschneigk, M., Deissler, H., Schmitz, B., Majewski, F., von Gontard, A., and Doerfler, W. (2000). Methylation mosaicism of 5'-(CGG)(n)-3' repeats in fragile X, premutation and normal individuals. *Nucleic Acids Res.* *28*, 2141–2152.

- Gholizadeh, S., Arsenault, J., Xuan, I.C.Y., Pacey, L.K., and Hampson, D.R. (2014). Reduced Phenotypic Severity Following Adeno-Associated Virus-Mediated Fmr1 Gene Delivery in Fragile X Mice. *Neuropsychopharmacology* 39, 3100–3111.
- Goddard, H.H. (1942). IN DEFENSE OF THE KALLIKAK STUDY. *Science* 95, 574–576.
- Goodrich-Hunsaker, N.J., Wong, L.M., McLennan, Y., Srivastava, S., Tassone, F., Harvey, D., Rivera, S.M., and Simon, T.J. (2011). Young adult female fragile X premutation carriers show age- and genetically-modulated cognitive impairments. *Brain Cogn.* 75, 255–260.
- Gothelf, D., Furfaro, J.A., Hoeft, F., Eckert, M.A., Hall, S.S., O'Hara, R., Erba, H.W., Ringel, J., Hayashi, K.M., Patnaik, S., et al. (2008). Neuroanatomy of Fragile X Syndrome Is Associated with Aberrant Behavior and the Fragile X Mental Retardation Protein (FMRP). *Ann. Neurol.* 63, 40–51.
- Grefer, M., Flory, K., Cornish, K., Hatton, D., and Roberts, J. (2016). The emergence and stability of attention deficit hyperactivity disorder in boys with fragile X syndrome. *J. Intellect. Disabil. Res. JIDR* 60, 167–178.
- Gross, C., Yao, X., Pong, D.L., Jeromin, A., and Bassell, G.J. (2011). Fragile X mental retardation protein regulates protein expression and mRNA translation of the potassium channel Kv4.2. *J. Neurosci. Off. J. Soc. Neurosci.* 31, 5693–5698.
- Grossman, A.W., Elisseou, N.M., McKinney, B.C., and Greenough, W.T. (2006). Hippocampal pyramidal cells in adult Fmr1 knockout mice exhibit an immature-appearing profile of dendritic spines. *Brain Res.* 1084, 158–164.
- Hagerman, R., Hoem, G., and Hagerman, P. (2010). Fragile X and autism: Intertwined at the molecular level leading to targeted treatments. *Mol. Autism* 1, 12.
- Hagerman, R.J., Hull, C.E., Safanda, J.F., Carpenter, I., Staley, L.W., O'Connor, R.A., Seydel, C., Mazzocco, M.M., Snow, K., and Thibodeau, S.N. (1994). High functioning fragile X males: demonstration of an unmethylated fully expanded FMR-1 mutation associated with protein expression. *Am. J. Med. Genet.* 51, 298–308.
- Hagerman, R.J., Leehey, M., Heinrichs, W., Tassone, F., Wilson, R., Hills, J., Grigsby, J., Gage, B., and Hagerman, P.J. (2001). Intention tremor, parkinsonism, and generalized brain atrophy in male carriers of fragile X. *Neurology* 57, 127–130.
- Hagerman, R.J., Rivera, S.M., and Hagerman, P.J. (2008). The fragile X family of disorders: A model for autism and targeted treatments. *Curr. Pediatr. Rev.* 4, 40–52.
- Hagerman, R.J., Berry-Kravis, E., Kaufmann, W.E., Ono, M.Y., Tartaglia, N., Lachiewicz, A., Kronk, R., Delahunty, C., Hessel, D., Visootsak, J., et al. (2009). Advances in the treatment of fragile X syndrome. *Pediatrics* 123, 378–390.
- Hall, S.S. (2009). Treatments for fragile X syndrome: a closer look at the data. *Dev. Disabil. Res. Rev.* 15, 353–360.
- Hall, S.S., Lightbody, A.A., McCarthy, B.E., Parker, K.J., and Reiss, A.L. (2012). Effects of intranasal oxytocin on social anxiety in males with fragile X syndrome. *Psychoneuroendocrinology* 37, 509–518.
- Hecht, F., and Kaiser-McCaw, B. (1979). The importance of being a fragile site. *Am. J. Hum. Genet.* 31, 223–225.
- Heulens, I., D'Hulst, C., Van Dam, D., De Deyn, P.P., and Kooy, R.F. (2012). Pharmacological treatment of fragile X syndrome with GABAergic drugs in a knockout mouse model. *Behav. Brain Res.* 229, 244–249.
- Hinton, V.J., Brown, W.T., Wisniewski, K., and Rudelli, R.D. (1991). Analysis of neocortex in three males with the fragile X syndrome. *Am. J. Med. Genet.* 41, 289–294.
- Hoeft, F., Carter, J.C., Lightbody, A.A., Hazlett, H.C., Piven, J., and Reiss, A.L. (2010).

- Region-specific alterations in brain development in one- to three-year-old boys with fragile X syndrome. *Proc. Natl. Acad. Sci.* *107*, 9335–9339.
- Huber, K.M., Gallagher, S.M., Warren, S.T., and Bear, M.F. (2002). Altered synaptic plasticity in a mouse model of fragile X mental retardation. *Proc. Natl. Acad. Sci. U. S. A.* *99*, 7746–7750.
- Irwin, S.A., Patel, B., Idupulapati, M., Harris, J.B., Crisostomo, R.A., Larsen, B.P., Kooy, F., Willems, P.J., Cras, P., Kozlowski, P.B., et al. (2001). Abnormal dendritic spine characteristics in the temporal and visual cortices of patients with fragile-X syndrome: a quantitative examination. *Am. J. Med. Genet.* *98*, 161–167.
- Ishak, W.W., Kahloon, M., and Fakhry, H. (2011). Oxytocin role in enhancing well-being: a literature review. *J. Affect. Disord.* *130*, 1–9.
- Jiraanont, P., Kumar, M., Tang, H.-T., Espinosa, G., Hagerman, P.J., Hagerman, R.J., Chutabhakdikul, N., and Tassone, F. (2017). Size and methylation mosaicism in males with Fragile X syndrome. *Expert Rev. Mol. Diagn.* *17*, 1023–1032.
- Johnson, C.P., and Walker, W.O. (2006). Mental retardation: management and prognosis. *Pediatr. Rev.* *27*, 249–255; quiz 256.
- Jung, K.-M., Sepers, M., Henstridge, C.M., Lassalle, O., Neuhofer, D., Martin, H., Ginger, M., Frick, A., DiPatrizio, N.V., Mackie, K., et al. (2012). Uncoupling of the endocannabinoid signalling complex in a mouse model of fragile X syndrome. *Nat. Commun.* *3*, 1080.
- Khandjian, E.W., Fortin, A., Thibodeau, A., Tremblay, S., Côté, F., Devys, D., Mandel, J.L., and Rousseau, F. (1995). A heterogeneous set of FMR1 proteins is widely distributed in mouse tissues and is modulated in cell culture. *Hum. Mol. Genet.* *4*, 783–789.
- Khayachi, A., Gwizdek, C., Poupon, G., Alcor, D., Chafai, M., Cassé, F., Maurin, T., Prieto, M., Folci, A., De Graeve, F., et al. (2018). Sumoylation regulates FMRP-mediated dendritic spine elimination and maturation. *Nat. Commun.* *9*, 757.
- Kidd, S.A., Lachiewicz, A., Barbouth, D., Blitz, R.K., Delahunty, C., McBrien, D., Visootsak, J., and Berry-Kravis, E. (2014). Fragile X syndrome: a review of associated medical problems. *Pediatrics* *134*, 995–1005.
- Kim, L., He, L., Maaswinkel, H., Zhu, L., Sirotkin, H., and Weng, W. (2014). Anxiety, hyperactivity and stereotypy in a zebrafish model of fragile X syndrome and autism spectrum disorder. *Prog. Neuropsychopharmacol. Biol. Psychiatry* *55*, 40–49.
- King, B.H., State, M.W., Shah, B., Davanzo, P., and Dykens, E. (1997). Mental Retardation: A Review of the Past 10 Years. Part I. *J. Am. Acad. Child Adolesc. Psychiatry* *36*, 1656–1663.
- Kirchgessner, C.U., Warren, S.T., and Willard, H.F. (1995). X inactivation of the FMR1 fragile X mental retardation gene. *J. Med. Genet.* *32*, 925–929.
- Knapska, E., Liudyno, V., Kiryk, A., Mikosz, M., Górkiewicz, T., Michaluk, P., Gawlak, M., Chaturvedi, M., Mochol, G., Balcerzyk, M., et al. (2013). Reward learning requires activity of matrix metalloproteinase-9 in the central amygdala. *J. Neurosci. Off. J. Soc. Neurosci.* *33*, 14591–14600.
- Kramvis, I., Mansvelter, H.D., Loos, M., and Meredith, R. (2013). Hyperactivity, perseveration and increased responding during attentional rule acquisition in the Fragile X mouse model. *Front. Behav. Neurosci.* *7*.
- Kwon, H., Menon, V., Eliez, S., Warsofsky, I.S., White, C.D., Dyer-Friedman, J., Taylor, A.K., Glover, G.H., and Reiss, A.L. (2001). Functional neuroanatomy of visuospatial working memory in fragile X syndrome: relation to behavioral and molecular measures. *Am. J. Psychiatry* *158*, 1040–1051.

- Larson, J.R., Jessen, R.E., Kim, D.K.Y., Fine, A.-K.S., and Hoffmann, J. du (2005). Age-dependent and selective impairment of long-term potentiation in the anterior piriform cortex of mice lacking the fragile X mental retardation protein. *J. Neurosci. Off. J. Soc. Neurosci.* *25*, 9460–9469.
- Lee, A., Li, W., Xu, K., Bogert, B.A., Su, K., and Gao, F.-B. (2003). Control of dendritic development by the *Drosophila* fragile X-related gene involves the small GTPase Rac1. *Dev. Camb. Engl.* *130*, 5543–5552.
- Lee, E.K., Kim, H.H., Kuwano, Y., Abdelmohsen, K., Srikantan, S., Subaran, S.S., Gleichmann, M., Mughal, M.R., Martindale, J.L., Yang, X., et al. (2010). hnRNP C promotes APP translation by competing with FMRP for *APP* mRNA recruitment to P bodies. *Nat. Struct. Mol. Biol.* *17*, 732–739.
- Lee, H.Y., Ge, W.-P., Huang, W., He, Y., Wang, G.X., Rowson-Baldwin, A., Smith, S.J., Jan, Y.N., and Jan, L.Y. (2011). Bidirectional regulation of dendritic voltage-gated potassium channels by the fragile X mental retardation protein. *Neuron* *72*, 630–642.
- Le Magueresse, C., and Monyer, H. (2013). GABAergic Interneurons Shape the Functional Maturation of the Cortex. *Neuron* *77*, 388–405.
- Li, J., Pelletier, M.R., Perez Velazquez, J.-L., and Carlen, P.L. (2002). Reduced cortical synaptic plasticity and GluR1 expression associated with fragile X mental retardation protein deficiency. *Mol. Cell. Neurosci.* *19*, 138–151.
- Liu, Z.-H., and Smith, C.B. (2009). Dissociation of social and nonsocial anxiety in a mouse model of fragile X syndrome. *Neurosci. Lett.* *454*, 62–66.
- Lozano, R., Hare, E.B., and Hagerman, R.J. (2014). Modulation of the GABAergic pathway for the treatment of fragile X syndrome. *Neuropsychiatr. Dis. Treat.* *10*, 1769–1779.
- Lubs, H.A. (1969). A marker X chromosome. *Am. J. Hum. Genet.* *21*, 231–244.
- Maes, B., Fryns, J.-P., Walleghe, M.V., and Berghe, H.V. den (1994). Cognitive functioning and information processing of adult mentally retarded men with fragile-X syndrome. *Am. J. Med. Genet.* *50*, 190–200.
- Martin, J.P., and Bell, J. (1943). A PEDIGREE OF MENTAL DEFECT SHOWING SEX-LINKAGE. *J. Neurol. Psychiatry* *6*, 154–157.
- Maurin, T., and Bardoni, B. (2018). Fragile X Mental Retardation Protein: To Be or Not to Be a Translational Enhancer. *Front. Mol. Biosci.* *5*.
- Maurin, T., Zongaro, S., and Bardoni, B. (2014). Fragile X Syndrome: from molecular pathology to therapy. *Neurosci. Biobehav. Rev.* *46 Pt 2*, 242–255.
- Maurin, T., Lebrigand, K., Castagnola, S., Paquet, A., Jarjat, M., Popa, A., Grossi, M., Rage, F., and Bardoni, B. (2018a). HITS-CLIP in various brain areas reveals new targets and new modalities of RNA binding by fragile X mental retardation protein. *Nucleic Acids Res.* *46*, 6344–6355.
- Maurin, T., Melancia, F., Jarjat, M., Castro, L., Costa, L., Delhaye, S., Khayachi, A., Castagnola, S., Mota, E., Di Giorgio, A., et al. (2018b). Involvement of Phosphodiesterase 2A Activity in the Pathophysiology of Fragile X Syndrome. *Cereb. Cortex N. Y. N 1991.*
- McLennan, Y., Polussa, J., Tassone, F., and Hagerman, R. (2011). Fragile x syndrome. *Curr. Genomics* *12*, 216–224.
- McNaughton, C.H., Moon, J., Strawderman, M.S., Maclean, K.N., Evans, J., and Strupp, B.J. (2008). Evidence for social anxiety and impaired social cognition in a mouse model of fragile X syndrome. *Behav. Neurosci.* *122*, 293–300.
- Melancia, F., and Trezza, V. (2018). Modelling fragile X syndrome in the laboratory setting: A behavioral perspective. *Behav. Brain Res.* *350*, 149–163.

- Meredith, R.M., Holmgren, C.D., Weidum, M., Burnashev, N., and Mansvelder, H.D. (2007). Increased threshold for spike-timing-dependent plasticity is caused by unreliable calcium signaling in mice lacking fragile X gene FMR1. *Neuron* 54, 627–638.
- Merikangas, K.R., Nakamura, E.F., and Kessler, R.C. (2009). Epidemiology of mental disorders in children and adolescents. *Dialogues Clin. Neurosci.* 11, 7–20.
- Mientjes, E.J., Nieuwenhuizen, I., Kirkpatrick, L., Zu, T., Hoogeveen-Westerveld, M., Severijnen, L., Rifé, M., Willemsen, R., Nelson, D.L., and Oostra, B.A. (2006). The generation of a conditional Fmr1 knock out mouse model to study Fmrp function in vivo. *Neurobiol. Dis.* 21, 549–555.
- Milà, M., Castellví-Bel, S., Sánchez, A., Lázaro, C., Villa, M., and Estivill, X. (1996). Mosaicism for the fragile X syndrome full mutation and deletions within the CGG repeat of the FMR1 gene. *J. Med. Genet.* 33, 338–340.
- Mirabi, M. (1985). Psychiatry and Mental Retardation: A Historical Perspective. In *Child and Adolescent Psychiatry, Mental Retardation, and Geriatric Psychiatry*, P. Pichot, P. Berner, R. Wolf, and K. Thau, eds. (Boston, MA: Springer US), pp. 177–181.
- Miyashiro, K.Y., Beckel-Mitchener, A., Purk, T.P., Becker, K.G., Barret, T., Liu, L., Carbonetto, S., Weiler, I.J., Greenough, W.T., and Eberwine, J. (2003). RNA cargoes associating with FMRP reveal deficits in cellular functioning in Fmr1 null mice. *Neuron* 37, 417–431.
- Monyak, R.E., Emerson, D., Schoenfeld, B.P., Zheng, X., Chambers, D.B., Rosenfelt, C., Langer, S., Hinchey, P., Choi, C.H., McDonald, T.V., et al. (2017). Insulin signaling misregulation underlies circadian and cognitive deficits in a *Drosophila* fragile X model. *Mol. Psychiatry* 22, 1140–1148.
- Morton, J.E., Bunday, S., Webb, T.P., MacDonald, F., Rindl, P.M., and Bullock, S. (1997). Fragile X syndrome is less common than previously estimated. *J. Med. Genet.* 34, 1–5.
- Moy, S.S., Nadler, J.J., Young, N.B., Nonneman, R.J., Grossman, A.W., Murphy, D.L., D’Ercole, A.J., Crawley, J.N., Magnuson, T.R., and Lauder, J.M. (2009). Social approach in genetically engineered mouse lines relevant to autism. *Genes Brain Behav.* 8, 129–142.
- Muller, C.L., Anacker, A.M.J., and Veenstra-VanderWeele, J. (2016). The serotonin system in autism spectrum disorder: from biomarker to animal models. *Neuroscience* 321, 24–41.
- Musumeci, S.A., Hagerman, R.J., Ferri, R., Bosco, P., Dalla Bernardina, B., Tassinari, C.A., De Sarro, G.B., and Elia, M. (1999). Epilepsy and EEG findings in males with fragile X syndrome. *Epilepsia* 40, 1092–1099.
- Ng, M.-C., Yang, Y.-L., and Lu, K.-T. (2013). Behavioral and Synaptic Circuit Features in a Zebrafish Model of Fragile X Syndrome. *PLoS ONE* 8.
- Nicastro, G., Taylor, I.A., and Ramos, A. (2015). KH-RNA interactions: back in the groove. *Curr. Opin. Struct. Biol.* 30, 63–70.
- Nomura, T., Musial, T.F., Marshall, J.J., Zhu, Y., Remmers, C.L., Xu, J., Nicholson, D.A., and Contractor, A. (2017). Delayed Maturation of Fast-Spiking Interneurons Is Rectified by Activation of the TrkB Receptor in the Mouse Model of Fragile X Syndrome. *J. Neurosci.* 37, 11298–11310.
- Oberlé, I., Rousseau, F., Heitz, D., Kretz, C., Devys, D., Hanauer, A., Boué, J., Bertheas, M.F., and Mandel, J.L. (1991). Instability of a 550-base pair DNA segment and abnormal methylation in fragile X syndrome. *Science* 252, 1097–1102.
- O’Donnell, W.T., and Warren, S.T. (2002). A decade of molecular studies of fragile X syndrome. *Annu. Rev. Neurosci.* 25, 315–338.

- Peier, A.M., McIlwain, K.L., Kenneson, A., Warren, S.T., Paylor, R., and Nelson, D.L. (2000). (Over)correction of FMR1 deficiency with YAC transgenics: behavioral and physical features. *Hum. Mol. Genet.* *9*, 1145–1159.
- Pietropaolo, S., Guilleminot, A., Martin, B., D'Amato, F.R., and Crusio, W.E. (2011). Genetic-background modulation of core and variable autistic-like symptoms in Fmr1 knock-out mice. *PLoS One* *6*, e17073.
- Pratt, H.D., and Greydanus, D.E. (2007). Intellectual disability (mental retardation) in children and adolescents. *Prim. Care* *34*, 375–386; abstract ix.
- Ramos, A., Hollingworth, D., and Pastore, A. (2003). G-quartet-dependent recognition between the FMRP RGG box and RNA. *RNA N. Y. N* *9*, 1198–1207.
- Ramos, A., Hollingworth, D., Adinolfi, S., Castets, M., Kelly, G., Frenkiel, T.A., Bardoni, B., and Pastore, A. (2006). The structure of the N-terminal domain of the fragile X mental retardation protein: a platform for protein-protein interaction. *Struct. Lond. Engl.* *14*, 21–31.
- Reinhard, S.M., Razak, K., and Ethell, I.M. (2015). A delicate balance: role of MMP-9 in brain development and pathophysiology of neurodevelopmental disorders. *Front. Cell. Neurosci.* *9*.
- Reiss, A.L., Abrams, M.T., Greenlaw, R., Freund, L., and Denckla, M.B. (1995). Neurodevelopmental effects of the FMR-1 full mutation in humans. *Nat. Med.* *1*, 159.
- Rosman, G.J., Martins, T.J., Sonnenburg, W.K., Beavo, J.A., Ferguson, K., and Loughney, K. (1997). Isolation and characterization of human cDNAs encoding a cGMP-stimulated 3',5'-cyclic nucleotide phosphodiesterase. *Gene* *191*, 89–95.
- Rotschafer, S.E., Trujillo, M.S., Dansie, L.E., Ethell, I.M., and Razak, K.A. (2012). Minocycline treatment reverses ultrasonic vocalization production deficit in a mouse model of Fragile X Syndrome. *Brain Res.* *1439*, 7–14.
- Roy, S., Watkins, N., and Heck, D. (2012). Comprehensive analysis of ultrasonic vocalizations in a mouse model of fragile X syndrome reveals limited, call type specific deficits. *PLoS One* *7*, e44816.
- Sabaratnam, M., Vroegop, P.G., and Gangadharan, S.K. (2001). Epilepsy and EEG findings in 18 males with fragile X syndrome. *Seizure* *10*, 60–63.
- Salvador-Carulla, L., Reed, G.M., Vaez-Azizi, L.M., Cooper, S.-A., Martinez-Leal, R., Bertelli, M., Adnams, C., Cooray, S., Deb, S., Akoury-Dirani, L., et al. (2011). Intellectual developmental disorders: towards a new name, definition and framework for “mental retardation/intellectual disability” in ICD-11. *World Psychiatry Off. J. World Psychiatr. Assoc. WPA* *10*, 175–180.
- Schampel, A., and Kuerten, S. (2017). Danger: High Voltage-The Role of Voltage-Gated Calcium Channels in Central Nervous System Pathology. *Cells* *6*.
- Schapiro, M.B., Murphy, D.G., Hagerman, R.J., Azari, N.P., Alexander, G.E., Mizejeski, C.M., Hinton, V.J., Horwitz, B., Haxby, J.V., and Kumar, A. (1995). Adult fragile X syndrome: neuropsychology, brain anatomy, and metabolism. *Am. J. Med. Genet.* *60*, 480–493.
- Schenck, A., Van de Bor, V., Bardoni, B., and Giangrande, A. (2002). Novel features of dFMR1, the Drosophila orthologue of the fragile X mental retardation protein. *Neurobiol. Dis.* *11*, 53–63.
- Schmunk, G., and Gargus, J.J. (2013). Channelopathy pathogenesis in autism spectrum disorders. *Front. Genet.* *4*, 222.
- Schmunk, G., Boubion, B.J., Smith, I.F., Parker, I., and Gargus, J.J. (2015). Shared functional defect in IP<sub>3</sub>R-mediated calcium signaling in diverse monogenic autism

- syndromes. *Transl. Psychiatry* 5, e643.
- Schmunk, G., Nguyen, R.L., Ferguson, D.L., Kumar, K., Parker, I., and Gargus, J.J. (2017). High-throughput screen detects calcium signaling dysfunction in typical sporadic autism spectrum disorder. *Sci. Rep.* 7.
- Schulte-Merker, S., and Stainier, D.Y.R. (2014). Out with the old, in with the new: reassessing morpholino knockdowns in light of genome editing technology. *Dev. Camb. Engl.* 141, 3103–3104.
- Siomi, M.C., Siomi, H., Sauer, W.H., Srinivasan, S., Nussbaum, R.L., and Dreyfuss, G. (1995). FXR1, an autosomal homolog of the fragile X mental retardation gene. *EMBO J.* 14, 2401–2408.
- Slegtenhorst-Eegdeman, K.E., de Rooij, D.G., Verhoef-Post, M., van de Kant, H.J., Bakker, C.E., Oostra, B.A., Grootegoed, J.A., and Themmen, A.P. (1998). Macroorchidism in FMR1 knockout mice is caused by increased Sertoli cell proliferation during testicular development. *Endocrinology* 139, 156–162.
- Spencer, C.M., Alekseyenko, O., Hamilton, S.M., Thomas, A.M., Serysheva, E., Yuva-Paylor, L.A., and Paylor, R. (2011). Modifying behavioral phenotypes in Fmr1KO mice: genetic background differences reveal autistic-like responses. *Autism Res. Off. J. Int. Soc. Autism Res.* 4, 40–56.
- State, M.W., King, B.H., and Dykens, E. (1997). Mental Retardation: A Review of the Past 10 Years. Part II. *J. Am. Acad. Child Adolesc. Psychiatry* 36, 1664–1671.
- Stefani, G., Fraser, C.E., Darnell, J.C., and Darnell, R.B. (2004). Fragile X mental retardation protein is associated with translating polyribosomes in neuronal cells. *J. Neurosci. Off. J. Soc. Neurosci.* 24, 7272–7276.
- Strumbos, J.G., Brown, M.R., Kronengold, J., Polley, D.B., and Kaczmarek, L.K. (2010). Fragile X mental retardation protein is required for rapid experience-dependent regulation of the potassium channel Kv3.1b. *J. Neurosci. Off. J. Soc. Neurosci.* 30, 10263–10271.
- Suhl, J.A., and Warren, S.T. (2015). Single-Nucleotide Mutations in FMR1 Reveal Novel Functions and Regulatory Mechanisms of the Fragile X Syndrome Protein FMRP. *J. Exp. Neurosci.* 9, 35–41.
- Taha, M.S., Nouri, K., Milroy, L.G., Moll, J.M., Herrmann, C., Brunsveld, L., Piekorz, R.P., and Ahmadian, M.R. (2014). Subcellular fractionation and localization studies reveal a direct interaction of the fragile X mental retardation protein (FMRP) with nucleolin. *PLoS One* 9, e91465.
- Tarjan, G. (1966). Cinderella and the prince: mental retardation and community psychiatry. *Am. J. Psychiatry* 122, 1057–1059.
- Tassone, F., Hagerman, R.J., Taylor, A.K., Gane, L.W., Godfrey, T.E., and Hagerman, P.J. (2000a). Elevated levels of FMR1 mRNA in carrier males: a new mechanism of involvement in the fragile-X syndrome. *Am. J. Hum. Genet.* 66, 6–15.
- Tassone, F., Hagerman, R.J., Loesch, D.Z., Lachiewicz, A., Taylor, A.K., and Hagerman, P.J. (2000b). Fragile X males with unmethylated, full mutation trinucleotide repeat expansions have elevated levels of FMR1 messenger RNA. *Am. J. Med. Genet.* 94, 232–236.
- The Dutch-Belgian Fragile X Consortium (1994). Fmr1 knockout mice: a model to study fragile X mental retardation. The Dutch-Belgian Fragile X Consortium. *Cell* 78, 23–33.
- Truskowski, T.L.S., James, E.J., Hasan, M., Wishard, T.J., Liu, Z., Pratt, K.G., Cline, H.T., and Aizenman, C.D. (2016). Fragile X mental retardation protein knockdown in the developing *Xenopus* tadpole optic tectum results in enhanced feedforward inhibition and

- behavioral deficits. *Neural Develop.* 11.
- Tuorto, F., Legrand, C., Cirzi, C., Federico, G., Liebers, R., Müller, M., Ehrenhofer-Murray, A.E., Dittmar, G., Gröne, H., and Lyko, F. (2018). Queuosine-modified tRNAs confer nutritional control of protein translation. *EMBO J.* 37.
- Turner, G., Webb, T., Wake, S., and Robinson, H. (1996). Prevalence of fragile X syndrome. *Am. J. Med. Genet.* 64, 196–197.
- Tyzio, R., Cossart, R., Khalilov, I., Minlebaev, M., Hübner, C.A., Represa, A., Ben-Ari, Y., and Khazipov, R. (2006). Maternal Oxytocin Triggers a Transient Inhibitory Switch in GABA Signaling in the Fetal Brain During Delivery. *Science* 314, 1788–1792.
- Valverde, R., Edwards, L., and Regan, L. (2008). Structure and function of KH domains. *FEBS J.* 275, 2712–2726.
- Van Esch, H. (2006). The Fragile X premutation: new insights and clinical consequences. *Eur. J. Med. Genet.* 49, 1–8.
- Vargesson, N. (2015). Thalidomide-induced teratogenesis: History and mechanisms. *Birth Defects Res.* 105, 140–156.
- Verkerk, A.J., Pieretti, M., Sutcliffe, J.S., Fu, Y.H., Kuhl, D.P., Pizzuti, A., Reiner, O., Richards, S., Victoria, M.F., and Zhang, F.P. (1991). Identification of a gene (FMR-1) containing a CGG repeat coincident with a breakpoint cluster region exhibiting length variation in fragile X syndrome. *Cell* 65, 905–914.
- Vicario, A., Colliva, A., Ratti, A., Davidovic, L., Baj, G., Gricman, Ł., Colombrita, C., Pallavicini, A., Jones, K.R., Bardoni, B., et al. (2015). Dendritic targeting of short and long 3' UTR BDNF mRNA is regulated by BDNF or NT-3 and distinct sets of RNA-binding proteins. *Front. Mol. Neurosci.* 8.
- Viollet, B., Guigas, B., Sanz Garcia, N., Leclerc, J., Foretz, M., and Andreelli, F. (2012). Cellular and molecular mechanisms of metformin: an overview. *Clin. Sci. Lond. Engl.* 1979 122, 253–270.
- de Vries, B.B., Wiegers, A.M., Smits, A.P., Mohkamsing, S., Duivenvoorden, H.J., Fryns, J.P., Curfs, L.M., Halley, D.J., Oostra, B.A., van den Ouweland, A.M., et al. (1996). Mental status of females with an FMR1 gene full mutation. *Am. J. Hum. Genet.* 58, 1025–1032.
- Wahlstrom-Helgren, S., and Klyachko, V.A. (2015). GABAB receptor-mediated feed-forward circuit dysfunction in the mouse model of fragile X syndrome. *J. Physiol.* 593, 5009–5024.
- Walsh, J.J., Christoffel, D.J., Heifets, B.D., Ben-Dor, G.A., Selimbeyoglu, A., Hung, L.W., Deisseroth, K., and Malenka, R.C. (2018). 5-HT release in nucleus accumbens rescues social deficits in mouse autism model. *Nature* 560, 589–594.
- Wan, L., Dockendorff, T.C., Jongens, T.A., and Dreyfuss, G. (2000). Characterization of dFMR1, a *Drosophila melanogaster* Homolog of the Fragile X Mental Retardation Protein. *Mol. Cell. Biol.* 20, 8536–8547.
- Wang, J.Y., Hessel, D., Iwahashi, C., Cheung, K., Schneider, A., Hagerman, R.J., Hagerman, P.J., and Rivera, S.M. (2013). Influence of the fragile X mental retardation (FMR1) gene on the brain and working memory in men with normal FMR1 alleles. *NeuroImage* 65, 288–298.
- Wang, Y.I., Abaci, H.E., and Shuler, M.L. (2017). Microfluidic blood-brain barrier model provides in vivo-like barrier properties for drug permeability screening. *Biotechnol. Bioeng.* 114, 184–194.
- Weiler, I.J., Irwin, S.A., Klintsova, A.Y., Spencer, C.M., Brazelton, A.D., Miyashiro, K., Comery, T.A., Patel, B., Eberwine, J., and Greenough, W.T. (1997). Fragile X mental

- retardation protein is translated near synapses in response to neurotransmitter activation. *Proc. Natl. Acad. Sci. U. S. A.* *94*, 5395–5400.
- Weiler, I.J., Spangler, C.C., Klintsova, A.Y., Grossman, A.W., Kim, S.H., Bertaina-Anglade, V., Khaliq, H., de Vries, F.E., Lambers, F.A.E., Hatia, F., et al. (2004). Fragile X mental retardation protein is necessary for neurotransmitter-activated protein translation at synapses. *Proc. Natl. Acad. Sci. U. S. A.* *101*, 17504–17509.
- Willemsen, R., Levenge, J., and Oostra, B.A. (2011). CGG repeat in the FMR1 gene: size matters. *Clin. Genet.* *80*, 214–225.
- Wilson, B.M., and Cox, C.L. (2007). Absence of metabotropic glutamate receptor-mediated plasticity in the neocortex of fragile X mice. *Proc. Natl. Acad. Sci. U. S. A.* *104*, 2454–2459.
- Winslow, J.T., and Insel, T.R. (2004). Neuroendocrine basis of social recognition. *Curr. Opin. Neurobiol.* *14*, 248–253.
- Wise, T.L. (2017). Changes in insulin-like growth factor signaling alter phenotypes in Fragile X Mice. *Genes Brain Behav.* *16*, 241–249.
- Wisniewski, K.E., Segan, S.M., Mizejeski, C.M., Sersen, E.A., and Rudelli, R.D. (1991). The Fra(X) syndrome: neurological, electrophysiological, and neuropathological abnormalities. *Am. J. Med. Genet.* *38*, 476–480.
- Yang, Y.-M., Arsenault, J., Bah, A., Krzeminski, M., Fekete, A., Chao, O.Y., Pacey, L.K., Wang, A., Forman-Kay, J., Hampson, D.R., et al. (2018). Identification of a molecular locus for normalizing dysregulated GABA release from interneurons in the Fragile X brain. *Mol. Psychiatry* *1*.
- Zamponi, G.W., Striessnig, J., Koschak, A., and Dolphin, A.C. (2015). The Physiology, Pathology, and Pharmacology of Voltage-Gated Calcium Channels and Their Future Therapeutic Potential. *Pharmacol. Rev.* *67*, 821–870.
- Zhang, Y., O'Connor, J.P., Siomi, M.C., Srinivasan, S., Dutra, A., Nussbaum, R.L., and Dreyfuss, G. (1995). The fragile X mental retardation syndrome protein interacts with novel homologs FXR1 and FXR2. *EMBO J.* *14*, 5358–5366.
- Zhang, Y., Bonnan, A., Bony, G., Ferezou, I., Pietropaolo, S., Ginger, M., Sans, N., Rossier, J., Oostra, B., LeMasson, G., et al. (2014). Dendritic channelopathies contribute to neocortical and sensory hyperexcitability in *Fmr1(-/y)* mice. *Nat. Neurosci.* *17*, 1701–1709.
- Zhao, M.-G., Toyoda, H., Ko, S.W., Ding, H.-K., Wu, L.-J., and Zhuo, M. (2005). Deficits in trace fear memory and long-term potentiation in a mouse model for fragile X syndrome. *J. Neurosci. Off. J. Soc. Neurosci.* *25*, 7385–7392.

# Annexes

# Publication 1



# The Search for an Effective Therapy to Treat Fragile X Syndrome: Dream or Reality?

Sara Castagnola<sup>1</sup>, Barbara Bardoni<sup>2\*</sup> and Thomas Maurin<sup>1</sup>

<sup>1</sup>Université Côte d'Azur, CNRS, Institut de Pharmacologie Moléculaire et Cellulaire (IPMC), Valbonne, France,

<sup>2</sup>Université Côte d'Azur, INSERM, CNRS, Institut de Pharmacologie Moléculaire et Cellulaire (IPMC), Valbonne, France

Fragile X Syndrome (FXS) is the most common form of intellectual disability and a primary cause of autism. It originates from the lack of the Fragile X Mental Retardation Protein (FMRP), which is an RNA-binding protein encoded by the Fragile X Mental Retardation Gene 1 (*FMR1*) gene. Multiple roles have been attributed to this protein, ranging from RNA transport (from the nucleus to the cytoplasm, but also along neurites) to translational control of mRNAs. Over the last 20 years many studies have found a large number of FMRP mRNA targets, but it is still not clear which are those playing a critical role in the etiology of FXS. So far, no therapy for FXS has been found, making the quest for novel targets of considerable importance. Several pharmacological approaches have been attempted, but, despite some promising preclinical results, no strategy gave successful outcomes, due either to the induction of major side effects or to the lack of improvement of the phenotypes. However, these studies suggested that, in order to measure the effectiveness of a specific treatment, trials should be redesigned and new endpoints defined in FXS patients. Nevertheless, the search for new therapeutic targets for FXS is very active. In this context, the advances in animal modeling, coupled with better understanding of neurobiology and physiopathology of FXS, are of crucial importance in developing new selected treatments. Here, we discuss the pathways that were recently linked to the physiopathology of FXS (mGluR, GABAR, insulin, Insulin-like Growth Factor 1 (IGF-1), MPP-9, serotonin, oxytocin and endocannabinoid signaling) and that suggest new approaches to find an effective therapy for this disorder. Our goal with this review article is to summarize some recent relevant findings on FXS treatment strategies in order to have a clearer view of the different pathways analyzed to date emphasizing those shared with other synaptic disorders.

## OPEN ACCESS

### Edited by:

Hansen Wang,  
University of Toronto, Canada

### Reviewed by:

Christina Gross,  
Cincinnati Children's Hospital Medical  
Center, United States

Emily Osterweil,  
University of Edinburgh,  
United Kingdom

Lucia Ciranna,  
Università degli Studi di Catania, Italy

### \*Correspondence:

Barbara Bardoni  
bardoni@ipmc.cnrs.fr

**Received:** 02 August 2017

**Accepted:** 16 October 2017

**Published:** 06 November 2017

### Citation:

Castagnola S, Bardoni B and  
Maurin T (2017) The Search for an  
Effective Therapy to Treat Fragile X  
Syndrome: Dream or Reality?  
*Front. Synaptic Neurosci.* 9:15.  
doi: 10.3389/fnsyn.2017.00015

**Keywords:** Fragile X Syndrome, *FMR1*, ASD, MMP-9, IGF-1, endocannabinoid system, oxytocin, serotonin

## INTRODUCTION

### Fragile X Syndrome

Fragile X syndrome (FXS) is the most common form of inherited intellectual disability (ID) and a primary genetic cause of autism. Due to its X-linked nature, it occurs in around 1:4000 males and 1:7000 females and one in three FXS patients display Autism Spectrum Disorders (ASD). Furthermore, the syndrome is characterized by delay in development and intellectual capacity, which impairs cognitive, executive and language performance. The severity of the symptoms can be very different among patients, and some of the most common features of the disease

include repetitive behaviors, hyperactivity, anxiety, mood disorders and epilepsy (Hagerman et al., 2009). At the cellular level, there are abnormalities in neuronal maturation and pruning (Bassell and Warren, 2008; Scotto-Lomassese et al., 2011). In the brain of FXS patients as well as in FXS animal models (*Fmr1*-KO mouse and *dFMR1*-KO flies), dendritic spines have an altered morphology, and they appear longer, thinner and more tortuous than normal (Bassell and Warren, 2008). The morphological abnormalities are associated with deregulated synaptic plasticity: in mouse hippocampal mGluR dependent Long Term Depression (LTD) is increased (Huber et al., 2002), while Long Term Potentiation (LTP) is reduced in somatosensory and anterior cingulate cortex (Desai et al., 2006) as well as in amygdala (Suvrathan and Chattarji, 2011) and in the CA1 region (Lauterborn et al., 2007; Seese et al., 2012).

FXS arises from a mutation in a single gene called Fragile X Mental Retardation Gene 1 (*FMR1*). The 5' UTR of *FMR1* contains a CGG trinucleotide repeat that is polymorphic in the population. Once the repeats exceed 200 in number, methylation of the promoter is triggered, and this in turn causes the lack of expression of the gene and translation of its encoded protein, the Fragile X Mental Retardation Protein (FMRP; Bardoni et al., 2000). FMRP is an RNA-binding protein involved in different steps of mRNA metabolism, such as translational control (in soma and dendritic spines) and RNA transport (Maurin et al., 2014).

## Therapeutic Strategies for FXS

Exploration of the physiopathology of FXS as well as the search for targets of FMRP have been very active over the last 20 years. These targets include mRNAs and proteins. Most proteins interacting with FMRP are RNA-binding protein components of FMRP-containing ribonucleoproteic particles. However, interactors of FMRP are also ion channels, molecular motors and proteins involved in cytoskeleton remodeling pathways (Menon et al., 2004; Bardoni et al., 2006; Davidovic et al., 2007; Abekhouk and Bardoni, 2014; Maurin et al., 2014, 2015; Ferron, 2016; Abekhouk et al., 2017; Bienkowski et al., 2017). This effort resulted in the identification of multiple putative targets for the treatment of FXS. However, so far no efficient therapy is available for this disorder (reviewed in Maurin et al., 2014). For instance, the imbalance between excitatory and inhibitory systems in FXS has been known for 20 years, and it has been thought to be the key target for therapy. Indeed, the first ever therapeutic strategies to be tested for FXS in clinical trials targeted the glutamatergic system (the excitatory pathway known to be up-regulated in FXS; Bear et al., 2004; Berry-Kravis et al., 2016) and the  $\gamma$ -aminobutyric acid (GABA) system (the inhibitory pathway also dysregulated in the disease; D'Antuono et al., 2003).

The mGluR theory regarding the pathophysiology of FXS states that the lack of FMRP hyperactivates the mGluR5-mediated pathway leading to the most prominent features of FXS (Bear et al., 2004). Even if the molecular reasons of this exaggerated activation are not completely clear, many efforts

have been done based on this theory in order to develop an effective strategy for both pharmacological and genetic rescue through the inhibition of the mGluR pathway (Bear et al., 2004). In the mammalian FXS animal model (*Fmr1*-KO mouse), the treatment with specific antagonists of the mGluR5 resulted in the rescue of cellular (dendritic spine morphology), synaptic (exaggerated LTD) and behavioral defects, but these successes were not translated to the human treatments. Indeed, no beneficial effects of mavoglurant (AFQ056, a previous mGluR5 well-characterized antagonist) were observed in a 12-weeks, double-blind study involving a large cohort of adolescent and adult FXS patients (Bailey et al., 2016; Berry-Kravis et al., 2016). A similar new clinical trial was performed in a cohort of 183 FXS using basimglurant, a potent and selective mGluR5-negative allosteric modulator (NAM), already administrated as a treatment of depression (Quiroz et al., 2016). Again, according to the evaluation of the ADAMS score, no improvement in patients' behavior was observed (Youssef et al., 2017).

GABA is the main inhibitory neurotransmitter of the Central Nervous System (CNS). Based on an altered expression of GABA receptor subunits in the absence of FMRP (Adusei et al., 2010) and a reduced production of GABA (Davidovic et al., 2011), it has been shown that an impairment of the GABAergic system is involved in FXS (D'Hulst and Kooy, 2007; Braat et al., 2015). Direct administration of GABA to the patients is not possible, partly because of its poor brain penetration. Thus, to restore the normal inhibition rate of the CNS and consequently reverse some major phenotype features of the disease, investigators have tried to treat FXS patients with GABA receptor agonists. So far, compounds like Acamprosate, Ganaxolone, Arbaclofen and Riluzole have been tested, but, despite the very mild side effects and good tolerability, they have caused very limited improvements in preliminary studies (Berry-Kravis et al., 2012; Erickson et al., 2014a,b; Ligsay et al., 2017).

Besides Glutamate and GABA, other deregulated pathways have been identified in FXS. Recent pre-clinical studies revealed that modulating other signaling pathways could ameliorate FXS symptoms in the mouse model of FXS. Our goal with this review is to summarize some recent relevant findings on FXS treatment strategies, focusing on promising molecular pathways that are altered not only in FXS but also in other forms of synaptic disorders that might lead to the discovery of a future treatment for neurodevelopmental diseases. In addition to those described here, other therapeutic targets for future treatment of FXS can be considered, for example, Amyloid Precursor Protein (APP), Brain-Derived Neurotrophic Factor (BDNF), cAMP and *N*-methyl-D-aspartate (NMDA) receptor as illustrated in several recent reviews (Wei et al., 2012; Castrén and Castrén, 2014; Androschuk et al., 2015; Tian et al., 2015; Westmark et al., 2016).

## Insulin and Insulin-Like Growth Factor 1 Pathway

Transcriptomic analysis of cultured hippocampal neurons obtained from WT and *Fmr1*-KO embryos showed that at

the top of the list of enriched gene expression pathways was the “Insulin signaling pathway” (Prilutsky et al., 2015). In *dFMR1-KO* flies insulin signaling is altered due to an elevated expression of *Drosophila insulin-like peptide 2 (Dilp2)* gene in the insulin-producing cells (IPCs) of the brain. Administration of metformin, an FDA-approved anti-diabetic drug, to *dFMR1-KO* flies (Viollet et al., 2012), leads to an amelioration of memory defects (Monyak et al., 2017). In this context it is interesting to notice that recent studies have clearly demonstrated the improvement of different *in vitro/in vivo* hallmarks in *Fmr1-KO* mice (Gantois et al., 2017) and in seven FXS patients (Dy et al., 2017) using metformin treatment. The precise mechanism of action of metformin has not been deciphered yet, but it has been shown that this drug inhibits the mitochondrial respiratory-chain, specifically at the complex I level, without affecting any other steps of the mitochondrial machinery. This leads to a reduction in proton-driven synthesis of ATP from ADP and inorganic phosphate. In addition, through AMPK-dependent and -independent regulation, metformin can lead to the inhibition of glucose production by disrupting gluconeogenesis gene expression (Viollet et al., 2012). In *Fmr1-KO* mice, metformin treatment inhibited the mTORC1 and ERK pathways, that resulted in the compensation of up-regulated translation, a hallmark of FXS (Maurin et al., 2014; Gantois et al., 2017). Indeed, in *Fmr1*-null neurons an increased level of phosphorylation of the serine/threonine kinase S6K1 has been observed. S6K1 is a common target of the mTORC1 and ERK pathways that are deregulated in the absence of FMRP (Sharma et al., 2010; Bhattacharya et al., 2012; Gross and Bassell, 2014; Gross et al., 2015a,b). It is interesting to notice here that two inhibitors of S6K1 (PF-4708671 and FS-115) were used in preclinical studies in mouse improving aberrant social interaction and behavioral inflexibility in Y-maze (for review see Gross and Bhattacharya, 2017). On the other side, also reducing the activation of the ERK pathway with lovastatin (a drug that inhibits the Ras-ERK1/2 activation by interfering with Ras recruitment to the membrane) or rimonabant (see endocannabinoid pathway) resulted in an improvement of *Fmr1-KO* cognition (Busquets-Garcia et al., 2013; Osterweil et al., 2013).

Obesity is often a co-morbid issue observed in FXS patients (Tounian et al., 1999; Raspa et al., 2010). Importantly, metformin has been used to treat seven obese FXS patients who showed improved cognition, language behavior along with obesity condition (Dy et al., 2017) proving to be an effective treatment for the FXS patients.

Insulin-like Growth Factor 1 (IGF-1) is a hormone primarily secreted by hepatocytes in response to Growth Hormone (GH) and, like insulin, promotes a decrease of glycaemia. IGF-1 promotes anabolic processes and tissue growth throughout life and it is a central factor for pathways involved in cell development and survival, proliferation and renewal. IGF-1 exerts its function by interacting with its receptor IGF receptor 1 (IGF1R; Costales and Kolevzon, 2016). In the CNS, IGF-1 plays a role in growth and development of all major CNS cell types and their synapse maturation. Imbalances in the IGF-1

pathway are associated to neuronal developmental impairment and, in particular, to ASD (Vahdatpour et al., 2016). Indeed, recombinant IGF-1, as well as some related compounds, have emerged as potential therapeutics to treat neurodevelopmental disorders and, indeed, clinical trials for ASD are in progress with these molecules (Wrigley et al., 2017).

In the mouse model of FXS, decreasing the levels of IGF1R corrects a number of phenotypic features (Deacon et al., 2015). Trofinetide is a neurotrophic peptide derived from IGF-1 that shows a long half-life and is well tolerated. A chronic treatment of *Fmr1-KO* mice with trofinetide corrected learning and memory deficits, hyperactivity and social interaction deficits displayed by these animals. At the microscopic level, abnormal dendritic spine density was rescued (Deacon et al., 2015). Considering this promising premise, a phase II clinical trial for trofinetide was performed and after only 28 days of treatment, improvements in higher sensory tolerance, reduced anxiety, better self-regulation and more social engagement were observed. No serious side effects were reported. Interestingly, Neuren Pharmaceuticals reported that trofinetide had significant clinical benefits in a Phase II clinical trial in 5–15 years old girls affected by Rett syndrome, another form of neurodevelopmental disorder characterized by ASD and intellectual disability (Bedogni et al., 2014)<sup>1</sup>.

## Matrix Metalloproteinases Pathway

Matrix metalloproteinases (MMPs) are endopeptidases implicated in both physiological and pathological remodeling of tissues, and their activity is dependent on the zinc ion of their catalytic site. The MMPs family counts 25 members (22 of them found in humans), which can cleave both extracellular matrix (ECM) components and non-ECM elements. MMP-9 is a 92 kD collagenase involved in a broad spectrum of remodeling events of the ECM and plays a major proteolytic role in many cell types. Indeed, it acts during embryo implantation, cardiac tissue development and immune cell functioning (Yabluchanskiy et al., 2013). In the brain, MMP-9 controls synaptic plasticity, and thus learning and memory formation (Ganguly et al., 2013; Knapska et al., 2013).

Until recently, brain disorders associated to defects in MMP-9 has been linked uniquely to its involvement in inflammatory and immune responses. Nevertheless, a hyperactivation of MMP-9 in neurons may cause a massive degradation of the ECM surrounding them that could have severe consequences on function and maturation of synapses. So far, misregulated activation of this enzyme has been implicated in a number of neurodegenerative disorders, including traumatic brain injury, multiple sclerosis and Alzheimer’s disease but also in neurodevelopmental disorders (Reinhard et al., 2015).

The mRNA coding MMP-9 is a target of FMRP, which negatively modulates its expression. Indeed, in the absence of FMRP the expression levels and the activity of MMP-9 are increased. Interestingly this abnormal activity as well as the aberrant dendritic spines could be rescued by treating

<sup>1</sup><https://www.fraxa.org/tag/trofinetide/>

neuronal cultures with minocycline (Bilousova et al., 2009). This drug is an FDA-approved broad-spectrum antibiotic that shows two major effects: (1) it increases the phosphorylation of GluR1; (2) it promotes the membrane insertion of AMPA receptors (Imbesi et al., 2008). With its action, minocycline lowers the abnormally elevated levels of MMP-9 in FXS, and, when used *in vivo* on *Fmr1*-KO mice, reduces anxiety and reverses the deficit in ultrasonic vocalizations (Rotschafer et al., 2012). Genetic reduction of MMP-9 was obtained by crossing the viable MMP-9 KO mice with *Fmr1*-KO mice. Double KO mice lacked the typical major symptoms of FXS observed in *Fmr1*-KOs (Sidhu et al., 2014).

Until now, minocycline has been shown to be successful in two different clinical trials (Paribello et al., 2010; Leigh et al., 2013) and, importantly, treatment with minocycline resulted in the improvement of some event-related potentials compared with placebo (Schneider et al., 2013). However, the presence of side effects reduces the enthusiasm for the utilization of this molecule in clinic. It is worth to note that the relevance of MMP-9 levels for the physiopathology of FXS has been recently underlined by the rescue of several FXS related behaviors after a chronic treatment of *Fmr1*-KO with metformin that, interestingly, resulted in the reduction of MMP-9 levels in the *Fmr1*-KO mouse brain (Gantois et al., 2017).

## Endocannabinoid Pathway

The endocannabinoid system (eCS) is represented by a group of neuromodulatory lipids and their receptors, notably the cannabinoid receptors 1 (CB1) and 2 (CB2). This system is present in mammalian tissues and, in particular, regulates the cardiovascular, nervous and immune systems. In the brain, the eCS is a key modulator of different neuronal aspects, including synaptic plasticity, cognition, anxiety, nociception and susceptibility to epileptic seizures (Khan et al., 2016). All these features also characterize the FXS patients' phenotype. Indeed, the lack of FMRP has been associated with impaired functioning of the eCB pathway in glutamatergic synapses, and this identifies the endocannabinoid signaling complex as a possible therapeutic target for FXS (Jung et al., 2012). Rimonabant, a selective antagonist of the CB1 receptor, has been the first drug targeting the eCS used to attenuate the FXS symptoms (Busquets-García et al., 2013). This drug was first developed for the treatment of obesity, but was withdrawn from the market because of its significant psychiatric side effects, such as depression, anxiety and suicidal thoughts. Nevertheless, the adverse effects only appear in patients that were given the highest administered doses. Notably, it was shown that the treatment with very low doses of rimonabant rescues synaptic plasticity in the hippocampus of *Fmr1*-KO mice and also learning and memory (Gomis-González et al., 2016). A new CB1 receptor neutral antagonist (NESS0327) was recently shown to have the same beneficial effects on *Fmr1*-KO mice behavior as rimonabant, supporting the CB1 receptor as a target to treat FXS (Gomis-González et al., 2016).

Deregulation of eCS could be involved in the physiopathology of ASD forms other than FXS. Indeed, 450 children born between 2006 and 2014 from mothers who, during their pregnancy, had

taken valproic acid (VPA), an anti-epileptic and mood stabilizing drug showed neurobehavioral dysfunctions. This suggested that VPA plays an important role in developing ASD (Inspection Générale des Affaires Sociales (IGAS), 2016) and subsequently led to the generation of an environmental model of ASD by exposing pregnant rodents to VPA (Williams and Hersch, 1997; Williams et al., 2001). Recently, some social deficits displayed by two VPA-induced ASD rat models have been corrected by treatment with anandamide, an endocannabinoid positively stimulating the eCS pathway (Servadio et al., 2016). These findings further confirm that the eCS may be an interesting and important target for ASD therapy by using both agonist or antagonist approaches.

## Serotonin Pathway

Hyperserotonemia was the first biomarker identified in patients affected by ASD. More recently, it has been shown that the levels of the amino acid tryptophan, the precursor of serotonin, is lower than normal in autistic brains, and that a diet poor in tryptophan worsens autistic symptoms (Boccutto et al., 2013). It was shown that polymorphisms in a gene encoding a 5-HT reuptake transporter protein cause lower synaptic serotonin availability and correlate with increased aggression and destructive behaviors (Hessl et al., 2008). Interestingly, decreased serotonin production was observed especially in young ASD children between 2 and 5 years of age, when the serotonin level should be at its maximal production (Chugani et al., 1999). Animal models in which genes involved in serotonin signaling have been inactivated display altered social interaction (Muller et al., 2016). Conversely, several mouse models of ASD, such as the 15q11-13 duplication and Smith-Laemli-Opitz syndrome models, to which we can also include the *Fmr1*-KO mouse, display altered 5-HT signaling (Muller et al., 2016). Indeed, it was shown that the stimulation of 5-HT<sub>7</sub> serotonin receptors in post-synaptic compartments reverses mGluR-LTD in hippocampal slices of FXS mouse brains, suggesting that 5-HT<sub>7</sub> receptor agonists might be envisaged as novel therapeutic tools for FXS (Costa et al., 2012). These same authors characterized two new molecules with very high binding affinity and selectivity for 5-HT<sub>7</sub> receptors and ability to rescue exaggerated mGluR-LTD that might be used as novel pharmacological tools for the therapy of FXS (Costa et al., 2015).

The growing body of evidence linking ASD to abnormalities in serotonin function caused the use of the selective serotonin re-uptake inhibitors (SSRIs: citalopram, escitalopram, fluoxetine, fluvoxamine, and sertraline) to target various symptoms of the disorders. Most studies resulted in significant improvements in global functioning and in symptoms associated with anxiety and repetitive behaviors with mild side effects (Kolevzon et al., 2006). Due to the commonalities between ASD and FXS, low-dose sertraline was used to treat young children (12–50 months) affected by FXS. This drug, considered to be one of the most potent inhibitors of serotonin re-uptake, gave significant benefits in behavioral and cognitive features, especially in language skills (Winarni et al., 2012). More recently, a double-blind control trial was performed in 57 FXS patients aged between 2 years and 5 years using another serotonin re-uptake inhibitor (SSRI

named Zolof), an anti-depressant typically used in the treatment of depression, obsessive-compulsive disorder, panic disorder. Despite disappointing primary endpoint results, this treatment demonstrated a positive effect on cognition, visual reception score improving social interaction and early expressive language development (Greiss Hess et al., 2016), strongly suggesting serotonin re-uptake as a promising target to improve the FXS phenotype. Some selective serotonin (5-HT) re-uptake inhibitors seem to act through oxytocin release. Further, the administration of fenfluramine, a serotonergic agonist, to healthy subjects increases plasma oxytocin levels (Marazziti et al., 2012). It is interesting to note that the oxytocin signaling has been proposed as a target to treat FXS (see below). Thus, a better exploration of this cross-talk could result in new therapeutic approaches for FXS and ASD.

## Oxytocin

Oxytocin is a neuropeptide that acts both as a hormone and as a neurotransmitter exerting pleiotropic effects in humans. It is well known to trigger labor, but also induces trust, empathy, and parental-infant relationships. It promotes social behavior and reduces stress and anxiety. In the last decade, it has been shown that intranasal administration of oxytocin is a potential treatment that improves social communication skills in various disorders. Some promising studies in animal models (Meyer-Lindenberg, 2008) paved the way for clinical trials focusing on the treatment of impaired social skills in a variety of conditions, including ASD and schizophrenia. Recent studies suggest that intranasal administration of oxytocin can ameliorate some symptoms of FXS, showing anxiolytic and pro-social qualities (Hall et al., 2012). Ben-Ari et al. (1989) shed light on the molecular mechanisms of the benefits of oxytocin treatment. Oxytocin plays a key role in regulating the effect of GABA on neuron activity. GABA is mostly known as an inhibitory neurotransmitter that acts on a receptor channel complex permeable to chloride anions. These anions flow through the channel according to their electrochemical gradient across the plasma membrane. It is noteworthy that the net value of this gradient changes along the development of the brain, depending on the expression of two major chloride co-transporters (KCC2 and NKCC1) that consequently modify the effects of GABA stimulation (Ben-Ari et al., 1989). A critical period for this shift occurs perinatally and the excitatory-to-inhibitory change of GABA effect is actually mediated by oxytocin receptors (Tyzio et al., 2006).

These authors further reported that the oxytocin-mediated GABA excitatory-inhibitory shift during delivery is abolished in the VPA-treated and *Fmr1*-KO mice, both rodent models of ASD. Consistently, blocking oxytocin signaling in naïve mothers resulted in the production of offspring with electrophysiological and behavioral autistic-like features (Tyzio et al., 2014). These authors also showed that during delivery, both *Fmr1*-KO and VPA-treated mice have elevated intracellular chloride levels in hippocampal neurons. These elevated chloride levels may explain the paradoxical effects of benzodiazapines and phenobarbital that occur through GABA modulation in patients with ASD. Interestingly, the maternal pretreatment with bumetanide, a diuretic belonging to the sulfamyl category that blocks the

chloride co-transporter NKCC1, restored electrophysiological and behavioral phenotypes in the offspring (Tyzio et al., 2014). Very recently, the same authors performed a clinical trial and remarkably showed that bumetanide improves the core symptoms of ASD and presents a favorable benefit/risk ratio particularly at 1.0 mg twice a day (Lemonnier et al., 2017). Collectively, these studies strongly indicate that the oxytocin pathway is involved in ASD physiopathology and that bumetanide is a promising treatment for various forms of ASD, including FXS.

## CONCLUDING REMARKS

The intense efforts to unravel the physiopathology of FXS appear to have produced some relevant pharmacological targets to treat this disorder. It is interesting to underline that most of the FXS deregulated pathways have been found to be unbalanced also in other forms of ASD or ID-associated diseases. This supports the relevance of these pathways in the physiopathology of ASD and/or intellectual disability. The success of preclinical treatments in mouse, rat or fly FXS models should be considered an exceptionally important result. However, we have learned from past clinical trials that to evaluate the effectiveness of therapies in humans, the design of clinical trials as well as the definition of disease-specific endpoints are of critical importance. Indeed, even on the basis of excellent pre-clinical results, these same preclinical targets have not been translated to therapies to improve behavior and cognition of FXS patients. It is clear that the trials could benefit from the analysis of previous trials results by performing, for instance, longer treatments (Berry-Kravis et al., 2016; Erickson et al., 2017). By further understanding the molecular deregulations in FXS, it should be possible to combine two (or more) drugs targeting different altered pathways, as proposed by the Willemsen laboratory (Zeidler et al., 2015), or treating patients at different ages with different targeted treatments, as we have recently proposed (Bardoni et al., 2017). The positive impact of metformin on FXS behavior troubles underlines the importance to focus on repositioning existing drugs to find new targeted treatments for FXS, as well as for other neurodevelopmental disorders. Lastly, the fact that some clinical trials worked only in small sets of patients (Berry-Kravis et al., 2016), suggests the importance of stratification of FXS patients on the basis of their multiple phenotypes for “*ad hoc*” therapies.

Furthermore, according to Budimirovic et al. (2017), 22 double-blind controlled clinical trials in FXS have been finalized between 2008 and 2015. The accurate analysis of these studies led the authors to the conclusion that the readouts employed to evaluate the outcome of treatments were in general of moderate/poor quality (Budimirovic et al., 2017). In this context, the search for specific and easily measurable biomarkers for FXS should be encouraged. Even if efforts are in progress concerning blood-based and neurophysiological measures (Ethridge et al., 2016; Ray et al., 2016; AlOlaby et al., 2017; Pellerin et al., 2017; Wang et al., 2017), it would be interesting to develop cell-based biomarkers improving analysis of FXS iPS cell lines, while parameters analyzed so far have

highlighted the great heterogeneity of these cells (for review see Khalifallah et al., 2017). Also in this case, more detailed studies could result into personalized treatments or treatments concerning subsets of patients. We can underline that only a few examples of FXS cell lines exist that can be used to investigate preclinical treatment *in cellulo* or screening with chemical libraries (Castets et al., 2005; Khalifallah et al., 2017). The availability of such tools could accelerate the definition of new pharmacological approaches identified by the dissection of altered pathways in FMRP-null brains. This dissection can be realized by the analysis of FMRP targets (mRNAs and proteins) and the FXS-translatome in different brain regions and/or neuron subtypes at different ages of neurodevelopment upon different conditions (e.g., stress and learning) or upon various stimuli.

All these considerations indicate that research on FXS has still some stimulating areas to investigate in order to define new treatments. In addition, the recent promising studies presented

here suggest the conclusion that treatments for all FXS patients will be available in a near future and will not remain only a dream for patients' families and researchers in the field.

## AUTHOR CONTRIBUTIONS

SC, BB and TM wrote the manuscript.

## ACKNOWLEDGMENTS

We thank Enzo Lalli and Maria Capovilla for critical reading of the manuscript. This study was supported by: INSERM; CNRS; CNRS LIA "NEOGENEX"; ANR-11-LABX-0028-01, Monaco Against Autism Foundation, ANR-12-BSV4-0020, and Fondation pour la Recherche Médicale (FRM) DEQ20140329490 to BB; FRAXA Foundation to TM. SC is recipient of an international PhD fellowship "Signalife- LabEx" Program.

## REFERENCES

- Abekhouk, S., and Bardoni, B. (2014). CYFIP family proteins between autism and intellectual disability: links with Fragile X syndrome. *Front. Cell. Neurosci.* 8:81. doi: 10.3389/fncel.2014.00081
- Abekhouk, S., Sahin, H. B., Grossi, M., Zongaro, S., Maurin, T., Madrigal, I., et al. (2017). New insights into the regulatory function of CYFIP1 in the context of WAVE- and FMRP-containing complexes. *Dis. Model. Mech.* 10, 463–474. doi: 10.1242/dmm.025809
- Adusei, D. C., Pacey, L. K., Chen, D., and Hampson, D. R. (2010). Early developmental alterations in GABAergic protein expression in Fragile X knockout mice. *Neuropharmacology* 59, 167–171. doi: 10.1016/j.neuropharm.2010.05.002
- AIOLaby, R. R., Sweha, S. R., Silva, M., Durbin-Johnson, B., Yrigollen, C. M., Pretto, D., et al. (2017). Molecular biomarkers predictive of sertraline treatment response in young children with Fragile X syndrome. *Brain Dev.* 39, 483–492. doi: 10.1016/j.braindev.2017.01.012
- Androschuk, A., Al-Jabri, B., and Bolduc, F. V. (2015). From learning to memory: what flies can tell us about intellectual disability treatment. *Front. Psychiatry* 6:85. doi: 10.3389/fpsy.2015.00085
- Bailey, D. B. Jr., Berry-Kravis, E., Wheeler, A., Raspa, M., Merrien, F., Ricart, J., et al. (2016). Mavoglurant in adolescents with Fragile X syndrome: analysis of Clinical Global Impression-Improvement source data from a double-blind therapeutic study followed by an open-label, long-term extension study. *J. Neurodev. Disord.* 8:1. doi: 10.1186/s11689-015-9134-5
- Bardoni, B., Capovilla, M., and Lalli, E. (2017). Modeling Fragile X syndrome in neurogenesis: an unexpected phenotype and a novel tool for future therapies. *Neurogenesis* 4:e1270384. doi: 10.1080/23262133.2016.1270384
- Bardoni, B., Davidovic, L., Bensaid, M., and Khandjian, E. W. (2006). The fragile X syndrome: exploring its molecular basis and seeking a treatment. *Expert Rev. Mol. Med.* 8, 1–16. doi: 10.1017/s1462399406010751
- Bardoni, B., Mandel, J. L., and Fisch, G. S. (2000). FMR1 gene and fragile X syndrome. *Am. J. Med. Genet.* 97, 153–163. doi: 10.1002/1096-8628(200022)97:2<153::aid-ajmg7>3.0.co;2-m
- Bassell, G. J., and Warren, S. T. (2008). Fragile X syndrome: loss of local mRNA regulation alters synaptic development and function. *Neuron* 60, 201–214. doi: 10.1016/j.neuron.2008.10.004
- Bear, M. F., Huber, K. M., and Warren, S. T. (2004). The mGluR theory of fragile X mental retardation. *Trends Neurosci.* 27, 370–377. doi: 10.1016/j.tins.2004.04.009
- Bedogni, F., Rossi, R. L., Galli, F., Cobolli Gigli, C., Gandaglia, A., Kilstrup-Nielsen, C., et al. (2014). Rett syndrome and the urge of novel approaches to study MeCP2 functions and mechanisms of action. *Neurosci. Biobehav. Rev.* 46, 187–201. doi: 10.1016/j.neubiorev.2014.01.011
- Ben-Ari, Y., Cherubini, E., Corradetti, R., and Gaiarsa, J. L. (1989). Giant synaptic potentials in immature rat CA3 hippocampal neurones. *J. Physiol.* 416, 303–325. doi: 10.1113/jphysiol.1989.sp017762
- Berry-Kravis, E., Des Portes, V., Hagerman, R., Jacquemont, S., Charles, P., Visootsak, J., et al. (2016). Mavoglurant in fragile X syndrome: results of two randomized, double-blind, placebo-controlled trials. *Sci. Transl. Med.* 8:321ra5. doi: 10.1126/scitranslmed.aab4109
- Berry-Kravis, E. M., Hessel, D., Rathmell, B., Zarevics, P., Cherubini, M., Walton-Bowen, K., et al. (2012). Effects of STX209 (arbaclofen) on neurobehavioral function in children and adults with fragile X syndrome: a randomized, controlled, phase 2 trial. *Sci. Transl. Med.* 4:152ra127. doi: 10.1126/scitranslmed.3004214
- Bhattacharya, A., Kaphzan, H., Alvarez-Dieppa, A. C., Murphy, J. P., Pierre, P., and Klann, E. (2012). Genetic removal of p70 S6 kinase 1 corrects molecular, synaptic, and behavioral phenotypes in fragile X syndrome mice. *Neuron* 76, 325–337. doi: 10.1016/j.neuron.2012.07.022
- Bienkowski, R. S., Banerjee, A., Rounds, J. C., Rha, J., Omotade, O. F., Gross, C., et al. (2017). The conserved, disease-associated RNA binding protein dNab2 interacts with the fragile X protein ortholog in drosophila neurons. *Cell Rep.* 20, 1372–1384. doi: 10.1016/j.celrep.2017.07.038
- Bilousova, T. V., Dansie, L., Ngo, M., Aye, J., Charles, J. R., Ethell, D. W., et al. (2009). Minocycline promotes dendritic spine maturation and improves behavioral performance in the fragile X mouse model. *J. Med. Genet.* 46, 94–102. doi: 10.1136/jmg.2008.061796
- Boccuto, L., Chen, C. F., Pittman, A. R., Skinner, C. D., McCartney, H. J., Jones, K., et al. (2013). Decreased tryptophan metabolism in patients with autism spectrum disorders. *Mol. Autism* 4:16. doi: 10.1186/2040-2392-4-16
- Braat, S., D'Hulst, C., Heulens, I., De Rubeis, S., Mientjes, E., Nelson, D. L., et al. (2015). The GABA<sub>A</sub> receptor is an FMRP target with therapeutic potential in fragile X syndrome. *Cell Cycle* 14, 2985–2995. doi: 10.4161/15384101.2014.989114
- Budimirovic, D. B., Berry-Kravis, E., Erickson, C. A., Hall, S. S., Hessel, D., Reiss, A. L., et al. (2017). Updated report on tools to measure outcomes of clinical trials in fragile X syndrome. *J. Neurodev. Disord.* 9:14. doi: 10.1186/s11689-017-9193-x
- Busquets-García, A., Gomis-González, M., Guegan, T., Augustin-Pavón, C., Pastor, A., Mato, S., et al. (2013). Targeting the endocannabinoid system in the treatment of Fragile X syndrome. *Nat. Med.* 19, 603–607. doi: 10.1038/nm.3127
- Castets, M., Schaeffer, C., Bechara, E., Schenck, A., Khandjian, E. W., Luche, S., et al. (2005). FMRP interferes with the Rac1 pathway and controls actin cytoskeleton dynamics in murine fibroblasts. *Hum. Mol. Genet.* 14, 835–844. doi: 10.1093/hmg/ddi077

- Castrén, M. L., and Castrén, E. (2014). BDNF in fragile X syndrome. *Neuropharmacology* 76, 729–736. doi: 10.1016/j.neuropharm.2013.05.018
- Chugani, D. C., Muzik, O., Behen, M., Rothermel, R., Janisse, J. J., Lee, J., et al. (1999). Developmental changes in brain serotonin synthesis capacity in autistic and nonautistic children. *Ann. Neurol.* 45, 287–295. doi: 10.1002/1531-8249(199903)45:3<287::aid-ana3>3.0.co;2-9
- Costa, L., Sardone, L. M., Lacivita, E., Leopoldo, M., and Ciranna, L. (2015). Novel agonists for serotonin 5-HT<sub>7</sub> receptors reverse metabotropic glutamate receptor-mediated long-term depression in the hippocampus of wild-type and Fmr1 KO mice, a model of Fragile X Syndrome. *Front. Behav. Neurosci.* 9:65. doi: 10.3389/fnbeh.2015.00065
- Costa, L., Spatuzza, M., D'Antoni, S., Bonaccorso, C. M., Trovato, C., Musumeci, S. A., et al. (2012). Activation of 5-HT<sub>7</sub> serotonin receptors reverses metabotropic glutamate receptor-mediated synaptic plasticity in wild-type and Fmr1 knockout mice, a model of fragile X syndrome. *Biol. Psychiatry* 72, 924–933. doi: 10.1016/j.biopsych.2012.06.008
- Costales, J., and Kolevzon, A. (2016). The therapeutic potential of insulin-like growth factor-1 in central nervous system disorders. *Neurosci. Biobehav. Rev.* 63, 207–222. doi: 10.1016/j.neubiorev.2016.01.001
- D'Antuono, M., Merlo, D., and Avoli, M. (2003). Involvement of cholinergic and gabaergic systems in the fragile X knockout mice. *Neuroscience* 119, 9–13. doi: 10.1016/s0306-4522(03)00103-9
- Davidovic, L., Jaglin, X. H., Lepagnol-Bestel, A. M., Tremblay, S., Simonneau, M., Bardoni, B., et al. (2007). The fragile X mental retardation protein is a molecular adaptor between the neurospecific KIF3C kinesin and dendritic RNA granules. *Hum. Mol. Genet.* 16, 3047–3058. doi: 10.1093/hmg/ddm263
- Davidovic, L., Navratil, V., Bonaccorso, C. M., Catania, M. V., Bardoni, B., and Dumas, M. E. (2011). A metabolomic and systems biology perspective on the brain of the fragile X syndrome mouse model. *Genome Res.* 21, 2190–2202. doi: 10.1101/gr.116764.110
- Deacon, R. M., Glass, L., Snape, M., Hurley, M. J., Altimiras, F. J., Biekofsky, R. R., et al. (2015). NNZ-2566, a novel analog of (1–3) IGF-1, as a potential therapeutic agent for fragile X syndrome. *Neuromolecular Med.* 17, 71–82. doi: 10.1007/s12017-015-8341-2
- Desai, N. S., Casimiro, T. M., Gruber, S. M., and Vanderklish, P. W. (2006). Early postnatal plasticity in neocortex of Fmr1 knockout mice. *J. Neurophysiol.* 96, 1734–1745. doi: 10.1152/jn.00221.2006
- D'Hulst, C., and Kooy, R. F. (2007). The GABA<sub>A</sub> receptor: a novel target for treatment of fragile X? *Trends Neurosci.* 30, 425–431. doi: 10.1016/j.tins.2007.06.003
- Dy, A. B. C., Tassone, F., Eldeeb, M., Salcedo-Arellano, M. J., Tartaglia, N., and Hagerman, R. (2017). Metformin as targeted treatment in fragile X syndrome. *Clin. Genet.* doi: 10.1111/cge.13039 [Epub ahead of print].
- Erickson, C. A., Davenport, M. H., Schaefer, T. L., Wink, L. K., Pedapati, E. V., Sweeney, J. A., et al. (2017). Fragile X targeted pharmacotherapy: lessons learned and future directions. *J. Neurodev. Dis.* 9:7. doi: 10.1186/s11689-017-9186-9
- Erickson, C. A., Ray, B., Maloney, B., Wink, L. K., Bowers, K., Schaefer, T. L., et al. (2014a). Impact of acamprosate on plasma amyloid- $\beta$  precursor protein in youth: a pilot analysis in fragile X syndrome-associated and idiopathic autism spectrum disorder suggests a pharmacodynamic protein marker. *J. Psychiatr. Res.* 59, 220–228. doi: 10.1016/j.jpsychires.2014.07.011
- Erickson, C. A., Veenstra-VanderWeele, J. M., Melmed, R. D., McCracken, J. T., Ginsberg, L. D., Sikich, L., et al. (2014b). STX209 (arbaclofen) for autism spectrum disorders: an 8-week open-label study. *J. Autism Dev. Disord.* 44, 958–964. doi: 10.1007/s10803-013-1963-z
- Ethridge, L. E., White, S. P., Mosconi, M. W., Wang, J., Byerly, M. J., and Sweeney, J. A. (2016). Reduced habituation of auditory evoked potentials indicate cortical hyper-excitability in Fragile X Syndrome. *Transl. Psychiatry* 6:e787. doi: 10.1038/tp.2016.48
- Ferron, L. (2016). Fragile X mental retardation protein controls ion channel expression and activity. *J. Physiol.* 594, 5861–5867. doi: 10.1113/JP270675
- Ganguly, K., Rejmak, E., Mikosz, M., Nikolaev, E., Knapska, E., and Kaczmarek, L. (2013). Matrix metalloproteinase (MMP) 9 transcription in mouse brain induced by fear learning. *J. Biol. Chem.* 288, 20978–20991. doi: 10.1074/jbc.M113.457903
- Gantois, I., Khoutorsky, A., Popic, J., Aguilar-Valles, A., Freemantle, E., Cao, R., et al. (2017). Metformin ameliorates core deficits in a mouse model of fragile X syndrome. *Nat. Med.* 23, 674–677. doi: 10.1038/nm.4335
- Gomis-González, M., Busquets-Garcia, A., Matute, C., Maldonado, R., Mato, S., and Ozaita, A. (2016). Possible therapeutic doses of cannabinoid type 1 receptor antagonist reverses key alterations in Fragile X syndrome mouse model. *Genes* 7:E56. doi: 10.3390/genes7090056
- Greiss Hess, L., Fitzpatrick, S. E., Nguyen, D. V., Chen, Y., Gaul, K. N., Schneider, A., et al. (2016). A randomized, double-blind, placebo-controlled trial of low-dose sertraline in young children with fragile X syndrome. *J. Dev. Behav. Ped.* 37, 619–628. doi: 10.1097/DBP.0000000000000334
- Gross, C., and Bassell, G. J. (2014). Neuron-specific regulation of class I PI3K catalytic subunits and their dysfunction in brain disorders. *Front. Mol. Neurosci.* 7:12. doi: 10.3389/fnmol.2014.00012
- Gross, C., and Bhattacharya, A. (2017). “Intracellular signaling network in fragile X syndrome: approaches to drug discovery and therapeutics,” in *Fragile X Syndrome—From Genetics to Targeted Treatments*, eds R. Willemsen and F. Kooy (Amsterdam: Elsevier), 498.
- Gross, C., Chang, C. W., Kelly, S. M., Bhattacharya, A., McBride, S. M., Danielson, S. W., et al. (2015a). Increased expression of the PI3K enhancer PIKE mediates deficits in synaptic plasticity and behavior in fragile X syndrome. *Cell Rep.* 11, 727–736. doi: 10.1016/j.celrep.2015.03.060
- Gross, C., Raj, N., Molinaro, G., Allen, A. G., Whyte, A. J., Gibson, J. R., et al. (2015b). Selective role of the catalytic PI3K subunit p110 $\beta$  in impaired higher order cognition in fragile X syndrome. *Cell Rep.* 11, 681–688. doi: 10.1016/j.celrep.2015.03.065
- Hagerman, R. J., Berry-Kravis, E., Kaufmann, W. E., Ono, M. Y., Tartaglia, N., Lachiewicz, A., et al. (2009). Advances in the treatment of fragile X syndrome. *Pediatrics* 123, 378–390. doi: 10.1542/peds.2008-0317
- Hall, S. S., Lightbody, A. A., McCarty, B. E., Parker, K. J., and Reiss, A. L. (2012). Effects of intranasal oxytocin on social anxiety in males with fragile X syndrome. *Psychoneuroendocrinology* 37, 509–518. doi: 10.1016/j.psyneuen.2011.07.020
- Hessl, D., Tassone, F., Cordeiro, L., Koldewyn, K., McCormick, C., Green, C., et al. (2008). Brief report: aggression and stereotypic behavior in males with fragile x syndrome—moderating secondary genes in a “single gene” disorder. *J. Autism Dev. Disord.* 38, 184–189. doi: 10.1007/s10803-007-0365-5
- Huber, K. M., Gallagher, S. M., Warren, S. T., and Bear, M. F. (2002). Altered synaptic plasticity in a mouse model of fragile X mental retardation. *Proc. Natl. Acad. Sci. U S A* 99, 7746–7750. doi: 10.1073/pnas.122205699
- Imbesi, M., Uz, T., Manev, R., Sharma, R. P., and Manev, H. (2008). Minocycline increases phosphorylation and membrane insertion of neuronal GluR1 receptors. *Neurosci. Lett.* 447, 134–137. doi: 10.1016/j.neulet.2008.10.006
- Inspection Générale des Affaires Sociales (IGAS). (2016). *Enquête Relative aux Spécialités Pharmaceutiques Contenant du Valproate de Sodium*. France: IGAS.
- Jung, K. M., Sepers, M., Henstridge, C. M., Lassalle, O., Neuhofer, D., Martin, H., et al. (2012). Uncoupling of the endocannabinoid signalling complex in a mouse model of fragile X syndrome. *Nat. Commun.* 3:1080. doi: 10.1038/ncomms2045
- Khalifallah, O., Jarjat, M., Davidovic, L., Nottet, N., Cestèle, S., Mantegazza, M., et al. (2017). Depletion of the fragile X mental retardation protein in embryonic stem cells alters the kinetics of neurogenesis. *Stem Cells* 35, 374–385. doi: 10.1002/stem.2505
- Khan, M. I., Sobocińska, A. A., Czarnecka, A. M., Król, M., Botta, B., and Szczylik, C. (2016). The therapeutic aspects of the endocannabinoid system (ECS) for cancer and their development: from nature to laboratory. *Curr. Pharm. Des.* 22, 1756–1766. doi: 10.2174/1381612822666151211094901
- Knapska, E., Liodyno, V., Kiryk, A., Mikosz, M., Górkiewicz, T., Michaluk, P., et al. (2013). Reward learning requires activity of matrix metalloproteinase-9 in the central amygdala. *J. Neurosci.* 33, 14591–14600. doi: 10.1523/JNEUROSCI.5239-12.2013

- Kolevzon, A., Mathewson, K. A., and Hollander, E. (2006). Selective serotonin reuptake inhibitors in autism: a review of efficacy and tolerability. *J. Clin. Psychiatry* 67, 407–414. doi: 10.4088/jcp.v67n0311
- Lauterborn, J. C., Rex, C. S., Kramár, E., Chen, L. Y., Pandeyarajan, V., Lynch, G., et al. (2007). Brain-derived neurotrophic factor rescues synaptic plasticity in a mouse model of fragile X syndrome. *J. Neurosci.* 27, 10685–10694. doi: 10.1523/JNEUROSCI.2624-07.2007
- Leigh, M. J., Nguyen, D. V., Mu, Y., Winarni, T. I., Schneider, A., Chechi, T., et al. (2013). A randomized double-blind, placebo-controlled trial of minocycline in children and adolescents with fragile X syndrome. *J. Dev. Behav. Pediatr.* 34, 147–155. doi: 10.1097/DBP.0b013e318287cd17
- Lemonnier, E., Villeneuve, N., Sonie, S., Serret, S., Rosier, A., Roue, M., et al. (2017). Effects of bumetanide on neurobehavioral function in children and adolescents with autism spectrum disorders. *Transl. Psychiatry* 7:e1124. doi: 10.1038/tp.2017.101
- Ligsay, A., Van Dijk, A., Nguyen, D. V., Lozano, R., Chen, Y., Bickel, E. S., et al. (2017). A randomized double-blind, placebo-controlled trial of ganaxolone in children and adolescents with fragile X syndrome. *J. Neurodev. Disord.* 9:26. doi: 10.1186/s11689-017-9207-8
- Marazziti, D., Baroni, S., Giannaccini, G., Betti, L., Massimetti, G., Carmassi, C., et al. (2012). A link between oxytocin and serotonin in humans: supporting evidence from peripheral markers. *Eur. Neuropsychopharmacol.* 22, 578–583. doi: 10.1016/j.euroneuro.2011.12.010
- Maurin, T., Melko, M., Abekhouk, S., Khalfallah, O., Davidovic, L., Jarjat, M., et al. (2015). The FMRP/GRK4 mRNA interaction uncovers a new mode of binding of the Fragile X mental retardation protein in cerebellum. *Nucleic Acids Res.* 43, 8540–8550. doi: 10.1093/nar/gkv801
- Maurin, T., Zongaro, S., and Bardoni, B. (2014). Fragile X Syndrome: from molecular pathology to therapy. *Neurosci. Biobehav. Rev.* 46, 242–255. doi: 10.1016/j.neubiorev.2014.01.006
- Menon, R. P., Gibson, T. J., and Pastore, A. (2004). The C terminus of fragile X mental retardation protein interacts with the multi-domain Ran-binding protein in the microtubule-organising centre. *J. Mol. Biol.* 343, 43–53. doi: 10.1016/j.jmb.2004.08.024
- Meyer-Lindenberg, A. (2008). Impact of prosocial neuropeptides on human brain function. *Prog. Brain Res.* 170, 463–470. doi: 10.1016/S0079-6123(08)00436-6
- Monyak, R. E., Emerson, D., Schoenfeld, B. P., Zheng, X., Chambers, D. B., Rosenfelt, C., et al. (2017). Insulin signaling misregulation underlies circadian and cognitive deficits in a *Drosophila* Fragile X model. *Mol. Psychiatry* 22, 1140–1148. doi: 10.1038/mp.2016.51
- Muller, C. L., Anacker, A. M., and Veenstra-VanderWeele, J. (2016). The serotonin system in autism spectrum disorder: from biomarker to animal models. *Neuroscience* 321, 24–41. doi: 10.1016/j.neuroscience.2015.11.010
- Osterweil, E. K., Chuang, S. C., Chubykin, A. A., Sidorov, M., Bianchi, R., Wong, R. K. S., et al. (2013). Lovastatin corrects excess protein synthesis and prevents epileptogenesis in a mouse model of Fragile X syndrome. *Neuron* 77, 243–250. doi: 10.1016/j.neuron.2012.01.034
- Paribello, C., Tao, L., Folino, A., Berry-Kravis, E., Tranfaglia, M., Ethell, I. M., et al. (2010). Open-label add-on treatment trial of minocycline in fragile X syndrome. *BMC Neurol.* 10:91. doi: 10.1186/1471-2377-10-91
- Pellerin, D., Lortie, A., and Corbin, F. (2017). Platelets as a surrogate disease model of neurodevelopmental disorders: insights from Fragile X syndrome. *Platelets* doi: 10.1080/09537104.2017.1317733 [Epub ahead of print].
- Prilutsky, D., Kho, A. T., Palmer, N. P., Bhakar, A. L., Smedemark-Margulies, N., Kong, S. W., et al. (2015). Gene expression analysis in Fmr1KO mice identifies an immunological signature in brain tissue and mGluR5-related signaling in primary neuronal cultures. *Mol. Autism* 6:66. doi: 10.1186/s13229-015-0061-9
- Quiroz, J. A., Tamburri, P., Deptula, D., Banken, L., Beyer, U., Rabbia, M., et al. (2016). Efficacy and safety of basimglurant as adjunctive therapy for major depression: a randomized clinical trial. *JAMA Psychiatry* 73, 675–684. doi: 10.1001/jamapsychiatry.2016.0838
- Raspa, M., Bailey, D. B., Bishop, E., Holiday, D., and Olmsted, M. (2010). Obesity, food selectivity, and physical activity in individuals with fragile X syndrome. *Am. J. Intellect. Dev. Disabil.* 115, 482–495. doi: 10.1352/1944-7558-115.6.482
- Ray, B., Sokol, D. K., Maloney, B., and Lahiri, D. K. (2016). Finding novel distinctions between the sAPP $\alpha$ -mediated anabolic biochemical pathways in autism spectrum disorder and Fragile X syndrome plasma and brain tissue. *Sci. Rep.* 6:26052. doi: 10.1038/srep26052
- Reinhard, S. M., Razak, K., and Ethell, I. M. (2015). A delicate balance: role of MMP-9 in brain development and pathophysiology of neurodevelopmental disorders. *Front. Cell. Neurosci.* 9:280. doi: 10.3389/fncel.2015.00280
- Rotschaefer, S. E., Trujillo, M. S., Dansie, L. E., Ethell, I. M., and Razak, K. A. (2012). Minocycline treatment reverses ultrasonic vocalization production deficit in a mouse model of Fragile X Syndrome. *Brain Res.* 1439, 7–14. doi: 10.1016/j.brainres.2011.12.041
- Schneider, A., Leigh, M. J., Adams, P., Nanakul, R., Chechi, T., Olichney, J., et al. (2013). Electrochemical changes associated with minocycline treatment in fragile X syndrome. *J. Psychopharmacol.* 27, 956–963. doi: 10.1177/0269881113494105
- Scotto-Lomassese, S., Nissant, A., Mota, T., Néant-Féry, M., Oostra, B. A., Greer, C. A., et al. (2011). Fragile X mental retardation protein regulates new neuron differentiation in the adult olfactory bulb. *J. Neurosci.* 31, 2205–2215. doi: 10.1523/jneurosci.5514-10.2011
- Seese, R. R., Babayan, A. H., Katz, A. M., Cox, C. D., Lauterborn, J. C., Lynch, G., et al. (2012). LTP induction translocates cortactin at distant synapses in wild type but not Fmr1 knock-out mice. *J. Neurosci.* 32, 7403–7413. doi: 10.1523/jneurosci.0968-12.2012
- Servadio, M., Melancia, F., Manduca, A., di Masi, A., Schiavi, S., Cartocci, V., et al. (2016). Targeting anandamide metabolism rescues core and associated autistic-like symptoms in rats prenatally exposed to valproic acid. *Transl. Psychiatry* 6:e902. doi: 10.1038/tp.2016.182
- Sharma, N. R., Mani, P., Nandwani, N., Mishra, R., Rana, A., and Sarkar, D. P. (2010). Reciprocal regulation of AKT and MAP kinase dictates virus-host cell fusion. *J. Virol.* 84, 4366–4382. doi: 10.1128/jvi.01940-09
- Sidhu, H., Dansie, L. E., Hickmott, P. W., Ethell, D. W., and Ethell, I. M. (2014). Genetic removal of matrix metalloproteinase 9 rescues the symptoms of fragile X syndrome in a mouse model. *J. Neurosci.* 34, 9867–9879. doi: 10.1523/jneurosci.1162-14.2014
- Suvrathan, A., and Chattarji, S. (2011). Fragile X syndrome and the amygdala. *Curr. Opin. Neurobiol.* 21, 509–515. doi: 10.1016/j.conb.2011.04.005
- Tian, M., Zeng, Y., Hu, Y., Yuan, X., Liu, S., Li, J., et al. (2015). 7, 8-Dihydroxyflavone induces synapse expression of AMPA GluA1 and ameliorates cognitive and spine abnormalities in a mouse model of fragile X syndrome. *Neuropharmacology* 89, 43–53. doi: 10.1016/j.neuropharm.2014.09.006
- Tounian, P., Frelut, M. L., Parlier, G., Abounaufal, C., Aymard, N., Veinberg, F., et al. (1999). Weight loss and changes in energy metabolism in massively obese adolescents. *Int. J. Obes. Relat. Metab. Disord.* 23, 830–837. doi: 10.1038/sj.ijo.0800959
- Tyzio, R., Cossart, R., Khalilov, I., Minlebaev, M., Hübner, C. A., Represa, A., et al. (2006). Maternal oxytocin triggers a transient inhibitory switch in GABA signaling in the fetal brain during delivery. *Science* 314, 1788–1792. doi: 10.1126/science.1133212
- Tyzio, R., Nardou, R., Ferrari, D. C., Tsintsadze, T., Shahrokhi, A., Eftekhari, S., et al. (2014). Oxytocin-mediated GABA inhibition during delivery attenuates autism pathogenesis in rodent offspring. *Science* 343, 675–679. doi: 10.1126/science.1247190
- Vahdatpour, C., Dyer, A. H., and Tropea, D. (2016). Insulin-like growth factor 1 and related compounds in the treatment of childhood-onset neurodevelopmental disorders. *Front. Neurosci.* 10:450. doi: 10.3389/fnins.2016.00450
- Viollet, B., Guigas, B., Sanz Garcia, N., Leclerc, J., Foretz, M., and Andreelli, F. (2012). Cellular and molecular mechanisms of metformin: an overview. *Clin. Sci.* 122, 253–270. doi: 10.1042/cs20110386
- Wang, J., Ethridge, L. E., Mosconi, M. W., White, S. P., Binder, D. K., Pedapati, E. V., et al. (2017). A resting EEG study of neocortical hyperexcitability and altered functional connectivity in fragile X syndrome. *J. Neurodev. Disord.* 9:11. doi: 10.1186/s11689-017-9191-z
- Wei, H., Dobkin, C., Sheikh, A. M., Malik, M., Brown, W. T., and Li, X. (2012). The therapeutic effect of memantine through the stimulation of synapse formation and dendritic spine maturation in autism and fragile X syndrome. *PLoS One* 7:e36981. doi: 10.1371/journal.pone.0036981
- Westmark, C. J., Sokol, D. K., Maloney, B., and Lahiri, D. K. (2016). Novel roles of amyloid- $\beta$  precursor protein metabolites in fragile X syndrome and autism. *Mol. Psychiatry* 21, 1333–1341. doi: 10.1038/mp.2016.134

- Williams, P. G., and Hersch, J. H. (1997). A male with fetal valproate syndrome and autism. *Dev. Med. Child Neurol.* 39, 632–634. doi: 10.1111/j.1469-8749.1997.tb07500.x
- Williams, G., King, J., Cunningham, M., Stephan, M., Kerr, B., and Hersch, J. H. (2001). Fetal valproate syndrome and autism: additional evidence and association. *Dev. Med. Child Neurol.* 43, 202–206. doi: 10.1111/j.1469-8749.2001.tb00188.x
- Winarni, T. I., Schneider, A., Borodyanskara, M., and Hagerman, R. J. (2012). Early intervention combined with targeted treatment promotes cognitive and behavioral improvements in young children with fragile x syndrome. *Case Rep. Genet.* 2012:280813. doi: 10.1155/2012/280813
- Wrigley, S., Arafa, D., and Tropea, D. (2017). Insulin-like growth factor 1: at the crossroads of brain development and aging. *Front. Cell. Neurosci.* 11:14. doi: 10.3389/fncel.2017.00014
- Yabluchanskiy, A., Ma, Y., Iyer, R. P., Hall, M. E., and Lindsey, M. (2013). Matrix Metalloproteinase-9: many shades of function in cardiovascular disease. *Physiology* 28, 391–403. doi: 10.1152/physiol.00029.2013
- Youssef, E. A., Berry-Kravis, E., Czech, C., Hagerman, R. J., Hessl, D., Wong, C. Y., et al. (2017). Effect of the mGluR5-NAM basimglurant on behavior in adolescents and adults with fragile X syndrome in a randomized, double-blind, placebo-controlled trial: fragx phase 2 results. *Neuropsychopharmacology* doi: 10.1038/npp.2017.177 [Epub ahead of print].
- Zeidler, S., Hukema, R. K., and Willemsen, R. (2015). The quest for targeted therapy in fragile X syndrome. *Expert Opin. Ther. Targets* 19, 1277–1281. doi: 10.1517/14728222.2015.1079176

**Conflict of Interest Statement:** The authors declare that the research was conducted in the absence of any commercial or financial relationships that could be construed as a potential conflict of interest.

Copyright © 2017 Castagnola, Bardoni and Maurin. This is an open-access article distributed under the terms of the Creative Commons Attribution License (CC BY). The use, distribution or reproduction in other forums is permitted, provided the original author(s) or licensor are credited and that the original publication in this journal is cited, in accordance with accepted academic practice. No use, distribution or reproduction is permitted which does not comply with these terms.

# Publication 2

ARTICLE

DOI: 10.1038/s41467-018-03222-y

OPEN

# Sumoylation regulates FMRP-mediated dendritic spine elimination and maturation

Anouar Khayachi<sup>1</sup>, Carole Gwizdek<sup>1</sup>, Gwénola Poupon<sup>1</sup>, Damien Alcor<sup>2</sup>, Magda Chafai<sup>1</sup>, Frédéric Cassé<sup>1</sup>, Thomas Maurin<sup>1</sup>, Marta Prieto<sup>1</sup>, Alessandra Folci<sup>1</sup>, Fabienne De Graeve<sup>3</sup>, Sara Castagnola<sup>1</sup>, Romain Gautier<sup>1</sup>, Lenka Schorova<sup>1</sup>, Céline Lorio<sup>1</sup>, Marie Pronot<sup>1</sup>, Florence Besse<sup>3</sup>, Frédéric Brau<sup>1</sup>, Emmanuel Deval<sup>1</sup>, Barbara Bardoni <sup>4</sup> & Stéphane Martin <sup>4</sup>

Fragile X syndrome (FXS) is the most frequent inherited cause of intellectual disability and the best-studied monogenic cause of autism. FXS results from the functional absence of the fragile X mental retardation protein (FMRP) leading to abnormal pruning and consequently to synaptic communication defects. Here we show that FMRP is a substrate of the small ubiquitin-like modifier (SUMO) pathway in the brain and identify its active SUMO sites. We unravel the functional consequences of FMRP sumoylation in neurons by combining molecular replacement strategy, biochemical reconstitution assays with advanced live-cell imaging. We first demonstrate that FMRP sumoylation is promoted by activation of metabotropic glutamate receptors. We then show that this increase in sumoylation controls the homomerization of FMRP within dendritic mRNA granules which, in turn, regulates spine elimination and maturation. Altogether, our findings reveal the sumoylation of FMRP as a critical activity-dependent regulatory mechanism of FMRP-mediated neuronal function.

<sup>1</sup>Université Côte d'Azur, CNRS, IPMC, 06560 Valbonne, France. <sup>2</sup>Université Côte d'Azur, INSERM, C3M, 06200 Nice, France. <sup>3</sup>Université Côte d'Azur, CNRS, INSERM, iBV, 06108 Nice, France. <sup>4</sup>Université Côte d'Azur, INSERM, CNRS, IPMC, 06560 Valbonne, France. These authors contributed equally: Anouar Khayachi and Carole Gwizdek. Correspondence and requests for materials should be addressed to S.M. (email: [martin@ipmc.cnrs.fr](mailto:martin@ipmc.cnrs.fr))

In neurons, messenger RNA (mRNA) targeting to synapses and local synthesis of synaptic proteins are tightly regulated. Indeed, dysregulation of such processes leads to structural synaptic abnormalities and consequently to neurological disorders<sup>1</sup> classified as synaptopathies<sup>2</sup>. Among them, the fragile X syndrome (FXS) is the most frequent form of inherited intellectual disability and a leading monogenic cause of autism with the prevalence of 1:4000 males and 1:7000 females. FXS results from mutations within the *FMR1* gene causing the loss of function of the RNA-binding protein FMRP. Localization studies revealed that FMRP is highly expressed in the central nervous system. FMRP binds a large subset of mRNAs in the mammalian brain and is a key component of RNA granules. These granules transport mRNA along axons and dendrites and are targeted to the base of active synapses to regulate local translation in an activity-dependent manner<sup>3–5</sup>. Therefore, the transport and the subsequent regulation of local translation are critical processes to brain development as they play essential roles in stabilizing and maturing synapses<sup>3,4</sup>. According to the role of FMRP in regulating translation at synapses, the loss of FMRP function in FXS leads to a pathological hyperabundance of long thin immature dendritic protrusions called filopodia<sup>6,7</sup>. These structural defects result from an abnormal post-synaptic maturation and/or a failure in the synapse elimination process<sup>8</sup>. An increased number of immature spines associated with severe changes in synaptic transmission and plasticity as well as in social and cognitive behaviors have also been reported in *Fmr1* knockout (*Fmr1*<sup>−/y</sup>) mouse models for FXS<sup>4,9,10</sup>.

The majority of FMRP-containing mRNA granules localizes at the base of dendritic spines<sup>3,4</sup>. Neuronal activation leads to the release of mRNAs from dendritic granules and their local translation at synapses (for a review, see ref. 5). Importantly, this activity-dependent process requires a tight spatiotemporal regulation involving many protein–protein interactions. Such a regulation is mainly governed by post-translational modifications (PTMs). Previous reports have shown that FMRP function is regulated by phosphorylation, which inhibits translation of its associated mRNAs, whereas dephosphorylation of FMRP promotes their translation<sup>11,12</sup>. Activation of metabotropic glutamate receptor 5 (mGlu5R) induces dephosphorylation of FMRP and its subsequent ubiquitination, which ultimately leads to FMRP degradation via the ubiquitin–proteasome pathway<sup>13,14</sup>. Thus, a deeper comprehension of the activity-dependent molecular mechanisms controlling FMRP is absolutely critical to understanding the functional regulation of FMRP-mediated mRNA transport and local protein synthesis in physiological and pathological conditions, including FXS.

Sumoylation is a PTM involved in many cellular signaling pathways. It consists in the covalent enzymatic conjugation of the small ubiquitin-like modifier (SUMO) protein to specific lysine residues of substrate proteins<sup>15,16</sup>. The sumoylation process requires a dedicated enzymatic pathway<sup>17–19</sup>. SUMO paralogs (~100 amino acids; ~11 kDa) are conjugated to its substrates via the action of the E2-conjugating enzyme Ubc9. Sumoylation is a reversible process due to the activity of specific desumoylation enzymes called Sentrin-proteases (SENPs<sup>20</sup>). At the molecular level, sumoylation can modulate the dynamics of multi-protein complexes by preventing protein–protein interactions and/or by providing new binding sites for novel interactors<sup>21,22</sup>.

Sumoylation regulates a wide range of neurodevelopmental processes<sup>18,19,23</sup>. For instance, our group has demonstrated the spatiotemporal regulation of the SUMO system in the developing rat brain<sup>24</sup> and that sumoylation is regulated by neuronal activity<sup>25</sup> and the activation of mGlu5R<sup>26</sup>. Sumoylation also influences various aspects of the neuronal function including

neurotransmitter release<sup>27,28</sup>, spinogenesis<sup>29,30</sup>, and synaptic communication<sup>31–33</sup>.

Here, we report that FMRP is a novel sumoylation substrate in neurons. We demonstrate that FMRP sumoylation is absolutely essential to maintaining the shape of mRNA granules in dendrites and to controlling both the spine density and maturation. We identify the active SUMO sites on FMRP and show that activation of mGlu5R rapidly induces FMRP sumoylation triggering the dissociation of FMRP from dendritic RNA granules to allow for local translation. Altogether, our findings shed light on sumoylation as an essential activity-dependent mechanism that tunes spine elimination and maturation in the mammalian brain.

## Results

**FMRP is sumoylated in vivo.** Given the critical importance of FMRP in brain development and maturation, it is of particular interest to understand the molecular mechanisms regulating FMRP function. Thus, we investigated whether FMRP is subjected to sumoylation. To this end, we performed immunoblot analyses and control assays using several commercial as well as in-house anti-FMRP and anti-SUMO1 antibodies on rodent brain homogenates (Fig. 1; Supplementary Fig. 1). We first analyzed rat brain homogenates in absence or presence of NEM (*N*-ethyl maleimide), which protects proteins from desumoylation during the lysis process<sup>31</sup> (Fig. 1a; Supplementary Fig. 1f). FMRP is detected as isoforms ranging from 70 to 90 kDa. Interestingly, we found a higher molecular weight band at ~120 kDa that was detected only in the presence of NEM (Fig. 1a, total lane). The densitometric analysis of the ratio between the sumoylated form of FMRP and the total level of FMRP in NEM-treated input lanes revealed that there is about 4% of sumoylated FMRP in all the conditions tested (Supplementary Fig. 1c). We confirmed the upper band to be the sumoylated form of FMRP by immunoprecipitation experiments with specific anti-FMRP antibodies and anti-SUMO1 immunoblot (Fig. 1b) or with the converse experiment using anti-SUMO1 immunoprecipitation and anti-FMRP immunoblot (Fig. 1c). We also validated the sumoylation of FMRP in wild-type (WT) mouse brain homogenates (Fig. 1d). Accordingly, we were also able to co-immunoprecipitate the sole SUMO-conjugating enzyme Ubc9 from mouse brain homogenates using anti-FMRP antibodies (Fig. 1e). We further validated the sumoylation of FMRP in vivo using several combinations of FMRP/SUMO1 antibodies (Supplementary Fig. 1d, e, g–j) or in cultured neurons (Supplementary Fig. 1k–n). Immunolabeling experiments (Fig. 1f) showed that FMRP partially co-localizes with Ubc9 and SUMO1 in dendrites of mouse hippocampal neurons, providing further evidence of the interplay between FMRP and the SUMO pathway.

Sumoylation consists in the covalent binding of the SUMO moiety to a lysine residue of the consensus sequence on the substrate protein ( $\Psi$ KxD/E, where  $\Psi$  is a large hydrophobic residue, K is the target lysine, x can be any residue, and D/E are aspartate or glutamate<sup>34</sup>). To identify lysine residues in FMRP potentially targeted by the sumoylation system, we used SUMO-prediction softwares to analyze the primary sequence of FMRP and then alignment tools to assess whether these potential sites are evolutionarily conserved across species (Fig. 1g). We identified three conserved residues, two proximal (K88, K130) and one distal (K614) lysines as putative targets of the SUMO system. To validate whether these lysine residues could be sumoylated, we performed site-directed mutagenesis combined with bacterial sumoylation assays<sup>31,35</sup> (Fig. 1h, i). We demonstrated that FMRP sumoylation occurs at these residues (K88, K130, and K614) and showed that their mutation into arginine residues (K-to-R mutation) abolishes the sumoylation of FMRP (Fig. 1h, i). We



**FMRP sumoylation participates in dendritic spine regulation.** FMRP is essential to proper spine stabilization and maturation<sup>3,4</sup>. In FXS patients, the lack of functional FMRP leads to an immature neuronal morphology with a characteristic excess of abnormally long and thin filopodia<sup>36</sup>. Similar morphological defects are also present in *Fmr1*<sup>-/-</sup> mouse brains<sup>37</sup>. Thus, we hypothesized that FMRP sumoylation could be critical in maintaining the density and the maturation of dendritic spines. To address this point, we used attenuated Sindbis particles<sup>38–40</sup> to express either free green fluorescent protein (GFP), the WT GFP-FMRP, the N-terminal K88,130R, C-terminal K614R or non-sumoylatable K88,130,614R GFP-FMRP mutants in cultured *Fmr1*<sup>-/-</sup> neurons at 17 days in vitro (17 DIV). We then analyzed and compared the morphology of dendritic spines 24 h post transduction (Fig. 2a, b). In GFP-expressing *Fmr1*<sup>-/-</sup> neurons, ~60% of protrusions showed an immature phenotype (see Methods for the spine characterization; Fig. 2a, b). Conversely, the expression of either FMRP WT or the K614R GFP-FMRP mutant, which behaves as the WT, promoted spine maturation (Fig. 2a, b). In stark contrast, expressing either the N-terminal K88,130R or the non-sumoylatable K88,130,614R GFP-FMRP mutant failed to promote spine maturation (Fig. 2a, b).

The excess of dendritic protrusions in neurons is a hallmark of FXS<sup>6,7</sup>. Interestingly, the density of the protrusions was considerably decreased upon the expression of the WT or K614R mutant form of GFP-FMRP (Fig. 2c; GFP control, 7.22 ± 0.16 protrusions per 10 μm; GFP-FMRP WT, 5.34 ± 0.13 protrusions per 10 μm; GFP-FMRP-K614R, 5.39 ± 0.13 protrusions per 10 μm), whereas expressing either the N-terminal K130R, the K88,130R GFP-FMRP mutants, or the non-sumoylatable GFP-FMRP-K88,130,614R did not affect the spine density with measured values almost identical to control neurons expressing free GFP (Fig. 2c). Furthermore, re-expressing WT GFP-FMRP in *Fmr1*<sup>-/-</sup> neurons not only affected the spine number but also drastically reduced the mean length of immature spines from ~3.7 μm to <2.6 μm (Fig. 2d).

To individually assess the role of the N-terminal lysine residue, we quantified the morphological changes occurring in *Fmr1*<sup>-/-</sup> neurons expressing GFP-FMRP with a single mutated lysine residue (K88R or K130R; Supplementary Fig. 2). While the expression of both mutants promoted spine maturation similarly to GFP-FMRP WT (Supplementary Fig. 2b, d), the K130R mutant failed to reduce the density of the protrusions (Supplementary Fig. 2c; GFP control, 7.22 ± 0.16 protrusions per 10 μm; WT, 5.34 ± 0.13 protrusions per 10 μm; K130R, 6.48 ± 0.15 protrusions per 10 μm) indicating that the integrity of the K130 residue is essential to maintain spine density. Altogether, the data above

indicate that the integrity of both N-terminal lysine residues is critical for the regulation of spine density and maturation since the expression of the K-to-R mutant forms failed to restore the density and the maturity of dendritic spines in *Fmr1*<sup>-/-</sup> neurons. Our initial findings therefore support the role of the N-terminal sumoylation of FMRP in the regulation of spine elimination and maturation events.

To start assessing the functional effect of FMRP sumoylation, we compared synaptic transmission by measuring spontaneous miniature excitatory post-synaptic currents (mEPSCs) in *Fmr1*<sup>-/-</sup> neurons expressing either GFP-FMRP WT or its non-sumoylatable K88,130,614R mutant (Supplementary Fig. 3). The comparison of cumulative distributions indicated that the amplitude of mEPSCs (from 20 to 40 pA) was significantly increased in neurons expressing the mutant form of GFP-FMRP (Supplementary Fig. 3a, b). Moreover, intervals between mEPSC events (between 300 ms and 1 s) were slightly but significantly increased upon expression of GFP-FMRP-K88,130,614R when compared to GFP-FMRP WT indicating that the mEPSC frequency is decreased in mutant-expressing cells (Supplementary Fig. 3a, c). Data comparing mEPSC properties in WT and *Fmr1*<sup>-/-</sup> brain slices have been described in the literature with either a decrease, an increase or no changes in their amplitudes or frequencies, depending on the brain area recorded, the age of the animals, and/or the associated genetic background<sup>41–43</sup>. To our knowledge, there are no available data on mEPSCs recorded from FMRP WT-expressing *Fmr1*<sup>-/-</sup> cultured hippocampal neurons and the results from Supplementary fig. 3 indicate that restoring the expression of FMRP in *Fmr1*<sup>-/-</sup> neurons leads to changes in basal synaptic transmission, occurring most probably via both pre- and post-synaptic modifications. Additional experiments are now needed to precisely define the associated mechanisms and to address the electrophysiological consequences of FMRP sumoylation in synaptic plasticity in vivo.

**Preventing FMRP sumoylation alters the size of mRNA granules.** Since FMRP is an RNA-binding protein, we also examined whether the mutation of the sumoylation sites interferes with the RNA-binding capacity of FMRP by performing cross-linking and immunoprecipitation (CLIP) assays (Fig. 2e, f). FMRP-CLIPed mRNAs from *Fmr1*<sup>-/-</sup> neurons expressing either the WT or K88,130,614R forms of GFP-FMRP were analyzed by quantitative PCR to compare the abundance of some known FMRP target mRNAs (Fig. 2e). Our data showed that either forms of GFP-FMRP are able to bind target RNAs to similar extent (Fig. 2f).

**Fig. 1** FMRP is sumoylated in vivo in the rat and mouse brain and the SUMO system targets the conserved residues K88, 130, and 614 of FMRP. **a** Representative immunoblot anti-FMRP (Ab#056) of P7 post-nuclear rat brain extracts prepared or not in the presence of the cysteine protease inhibitor NEM to prevent desumoylation. **b** Immunoblot anti-SUMO1 of NEM-treated P7 post-nuclear rat brain extracts subjected to immunoprecipitation with FMRP (Ab#056) antibody or control IgG. **c** Converse immunoblot with anti-FMRP (Ab#056) antibody of NEM-treated P7 post-nuclear rat brain extracts subjected to immunoprecipitation with SUMO1 antibody or control IgG. **d** Immunoblot anti-SUMO1 of NEM-treated P1 post-nuclear mouse brain extracts subjected to immunoprecipitation with FMRP (Ab#056) antibody or control IgG. \*Non-specific band. **e** Immunoblot of post-nuclear mouse brain extracts (input) subjected to immunoprecipitation with FMRP antibody or control IgG and probed with anti-Ubc9 antibody. **f** Co-localization assays performed on cultured mouse neurons (20 DIV) with antibodies directed against Ubc9, FMRP (Ab#4317), SUMO1. Bar, 2 μm. Degree of co-localization (Manders' coefficient) between FMRP and Ubc9 or SUMO1. *N* = 3 independent primary cultures with 60 dendrites analyzed for each condition. **g** Sequence alignments showing the evolutionary conservation of the potential SUMO-targeted lysine residues (stars) within the consensus sumoylation sites of FMRP. **h, i** Bacterial sumoylation assay. Representative immunoblots of purified fractions of N- and C-terminal WT or mutated parts of His-FMRP in a recombinant bacterial system and probed with anti-FMRP (**h**, Ab#1C3) or (**i**, #17722) and anti-SUMO1 antibodies as indicated. **j** COS7 sumoylation assay. Immunoblots with anti-FMRP (Ab#056) antibody of full-length WT or lysine-mutated FMRP expressed in COS7 cells with mcherry-SUMO1 WT or mutated (ΔGG) to prevent its conjugation. **k** Original X-ray structures fitted of three human N-terminal FMRP (PDB: 4OVA in green, 4QVZ in light green, 4QW2 in dark green) shown in cartoon representation. K88 and K130 are shown in sphere representation in red and blue, respectively. **l** Original model of FMRP (PDB: 4OVA) and SUMO1 (PDB: 4WJQ) structural links in cartoon and surface representation (with transparency), respectively, in green and light blue. Lysine residues 88 and 130 of FMRP are shown in sphere representation in red and blue, respectively

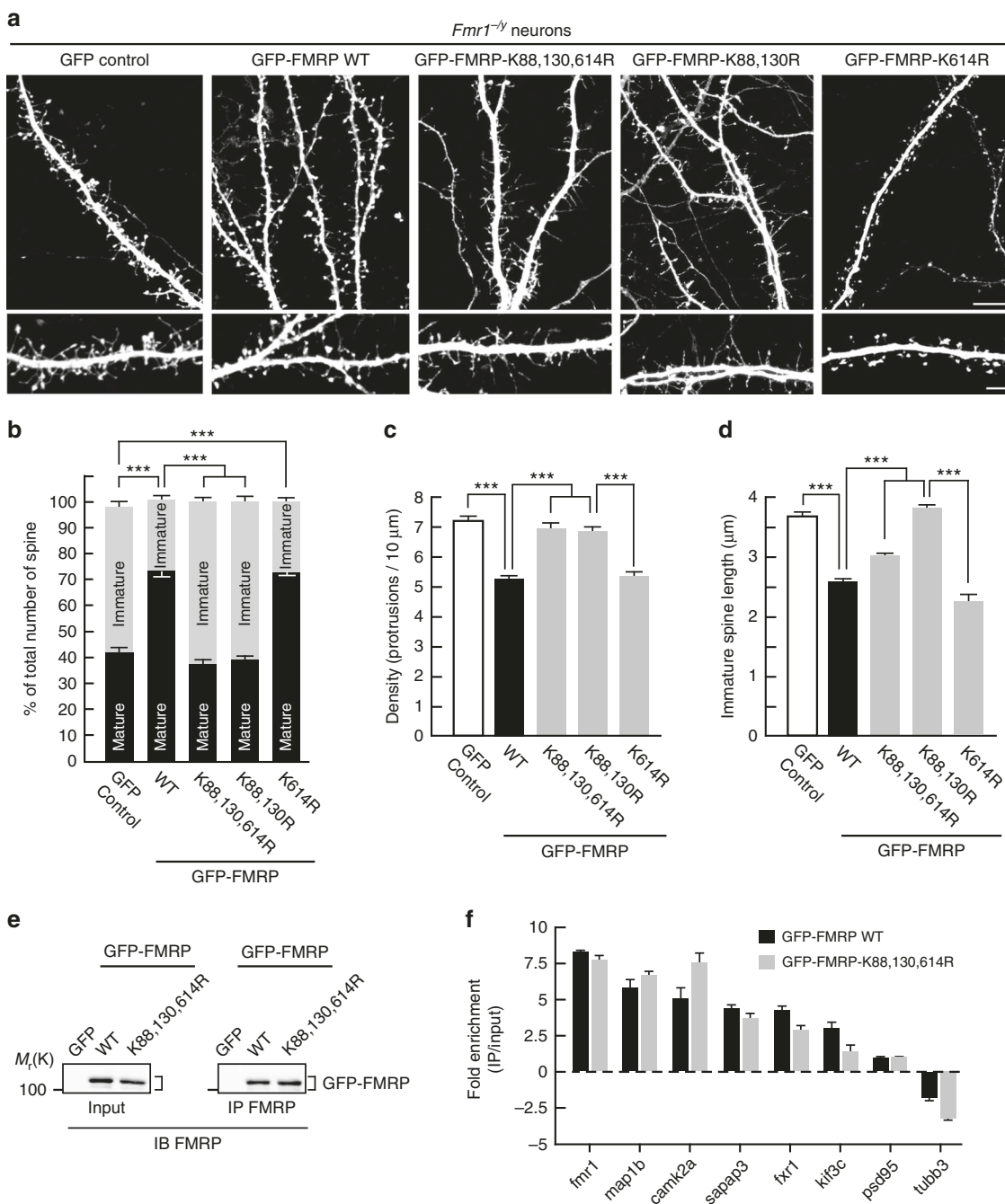


**Fig. 2** The N-terminal sumoylation of FMRP is involved in the regulation of the spine density and maturation. **a** Representative confocal images of dendrites from transduced *Fmr1*<sup>-/-</sup> neurons expressing free GFP, the WT or the non-sumoylatable K88,130,614R, K88,130R, or K614R forms of GFP-FMRP for 24 h. Bar, 10 μm. Enlargements of dendrites are also shown. Bar, 5 μm. Histograms show the relative proportion of mature and immature dendritic spines **b** and the density of the protrusions **c** in GFP, in WT, and mutated GFP-FMRP-expressing cells as shown in **a**. **d** Histograms of immature spine length measured from *Fmr1*<sup>-/-</sup> neurons expressing the indicated constructs. Data shown in **b–d** are the mean ± s.e.m. and statistical significance determined by a one-way analysis of variance (ANOVA) with a Bonferonni post-test. *N* = ~4500 protrusions per condition from four independent experiments. \*\*\**p* < 0.001. **e, f** CLIP analysis from transduced *Fmr1*<sup>-/-</sup> cortical neurons expressing the WT or the K88,130,614R form of GFP-FMRP revealed that they bind the same RNA repertoire. **e** Representative immunoblots anti-FMRP of the indicated neuronal extracts subjected or not (Input) to immunoprecipitation (IP) with FMRP antibodies. GFP-expressing *Fmr1*<sup>-/-</sup> neurons were used as a negative control. **f** Enrichment (CLIPed/Input) of a set of FMRP-target RNA fragments in the indicated conditions. Several known RNA targets of FMRP (*fmr1*, *map1b*, *camk2a*, *sapap3*, *fxr1*, *kif3c*, and *psd95*) as well as a non-targeted RNA (*tubb3*) were detected by quantitative PCR. Fold enrichment were calculated as described in the Methods section and did not show any statistical differences

Since preventing FMRP sumoylation with the K-to-R mutations does not affect the ability of FMRP to interact with its target RNAs, we hypothesized that FMRP sumoylation is involved in the transport of mRNAs along dendrites. To this purpose, we first examined the FMRP-containing granules along dendrites. We

transfected *Fmr1*<sup>-/-</sup> neurons to express either the WT or K88,130R form of GFP-FMRP and performed smFISH experiments using Stellaris probes complementary to three known FMRP mRNA targets: GFP (for GFP-FMRP), PSD-95<sup>44</sup>, and CaMKII mRNAs (Fig. 3a–c). Interestingly, the fluorescence of all

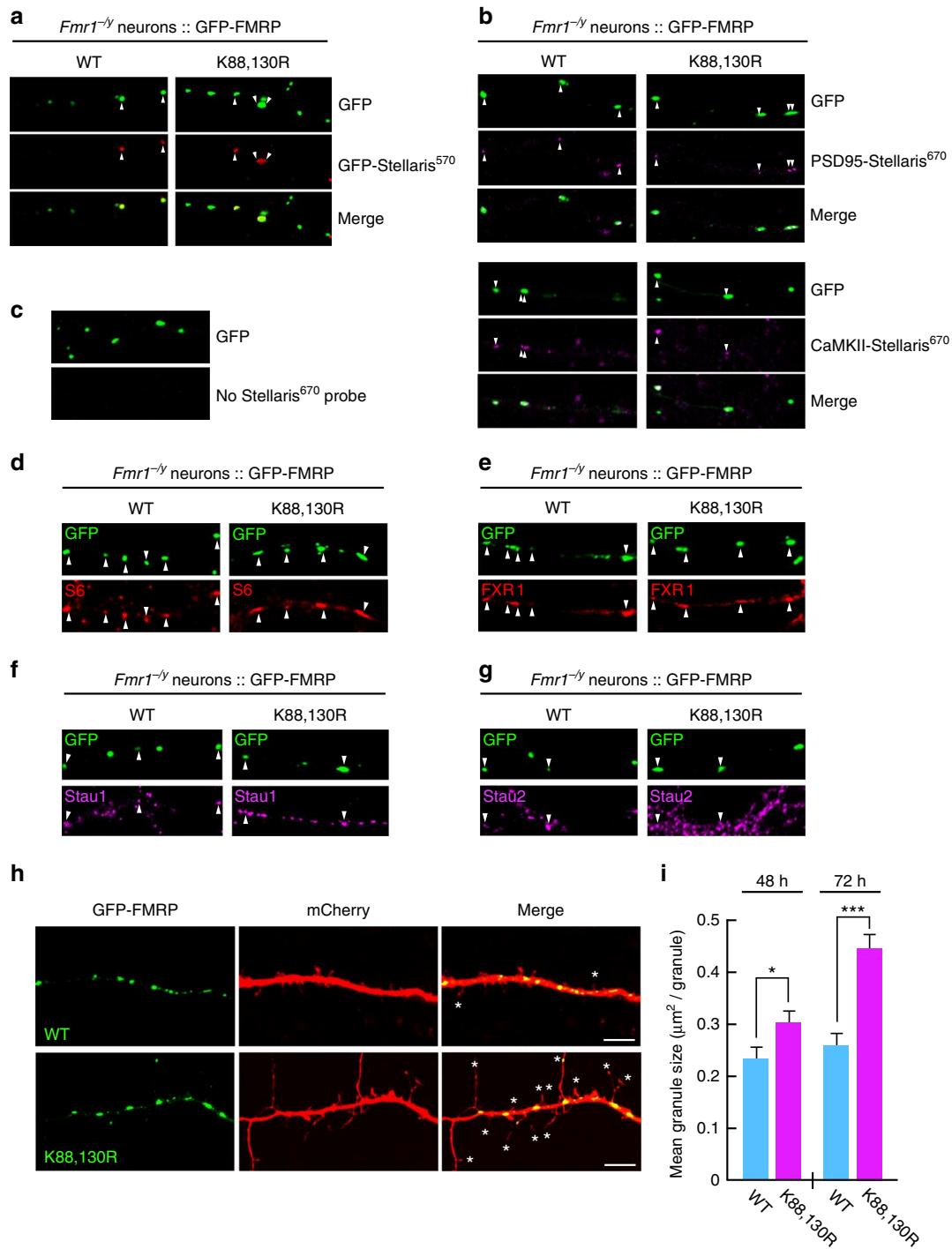


**Fig. 3** Preventing FMRP sumoylation drastically impacts on the size of dendritic FMRP-containing mRNA granules. **a–c** Representative images of WT and K88,130R GFP-FMRP-expressing *Fmr1*<sup>-/-</sup> dendrites were hybridized with GFP **a**, PSD-95 **b**, or CaMKII mRNA **b**, using Stellaris probes. Arrowheads show the co-localization between the indicated Stellaris signals and the GFP-FMRP granules. **c** GFP-FMRP-transfected neurons with no Stellaris probes were used as FISH controls. **d–g** Co-localization assays performed on WT and K88,130R GFP-FMRP-expressing *Fmr1*<sup>-/-</sup> neurons with antibodies directed against the S6 ribosomal protein **d**, FXR1 **e**, and the RNA-binding proteins Stau1 **f** and Stau2 **g**. Arrowheads indicate the co-localization with the GFP-FMRP positive mRNA granules. **h** Representative confocal images of dendrites from co-transfected *Fmr1*<sup>-/-</sup> neurons co-expressing free mCherry with either the WT or the K88,130R form of GFP-FMRP for 72 h. Bar, 5  $\mu\text{m}$ . **i** Histograms show the mean size of dendritic GFP-FMRP granules after 48 and 72 h of expression.  $N = 190$ –460 granules per condition from three to four separate experiments. Data shown in **i** are the mean  $\pm$  s.e.m. and statistical significance was determined using unpaired *t* test. \* $p < 0.05$ ; \*\*\* $p < 0.0001$

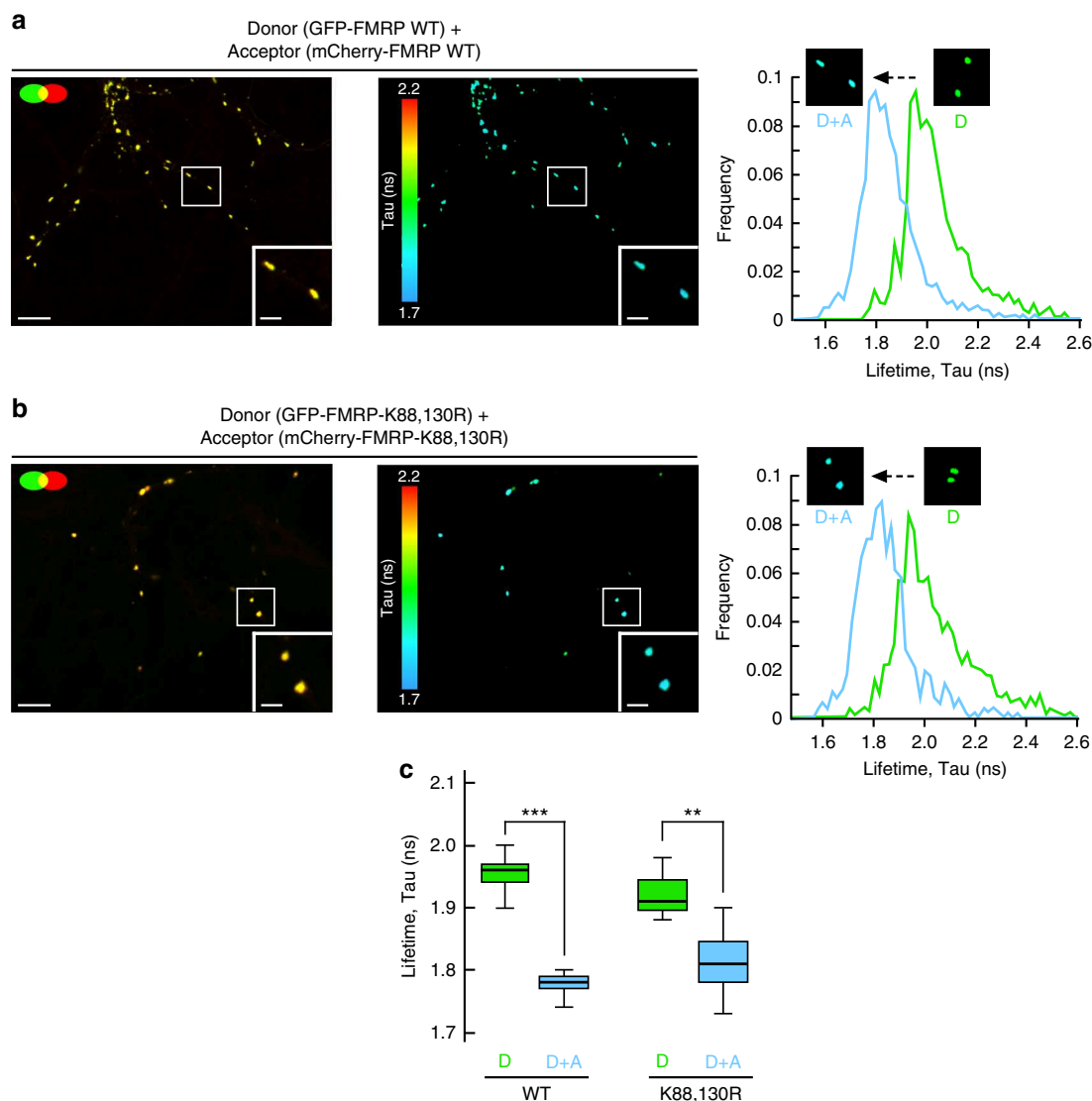


**Fig. 4** Preventing the N-terminal sumoylation of FMRP by the K88,130R mutation does not alter the homomeric FMRP-FMRP interaction within dendritic mRNA granules. **a, b** Analysis of GFP-FMRP/mCherry-FMRP interaction within dendritic mRNA granules by fluorescence lifetime imaging (FLIM). Representative confocal images showing the co-localization of the WT **a** or the K88,130R **b** forms of GFP-FMRP and mCherry-FMRP (left images) in dendritic granules; bar, 4  $\mu\text{m}$ . FLIM images of the same field are shown on the right images **a, b** where fluorescence lifetime is represented using a pseudo-color scale ranging from 1.7 to 2.2 ns. Insets show representative clusters for each condition; bar, 1  $\mu\text{m}$ . The third row represents the distribution histograms of GFP-FMRP fluorescence lifetime of the donor (D) alone in green and the donor + acceptor (D + A) in blue. FLIM images corresponding to the donor alone condition are displayed in Supplementary Fig. 3b. **c** Box and whiskers plots show the variation of the lifetime determined from FLIM curves. This representation displays upper and lower quartiles, maximum and minimum values in addition to median.  $N = 114\text{--}189$  granules per condition from three separate experiments. Statistical significance in **c** was determined by a non-parametric Mann-Whitney test.  $**p < 0.01$ ;  $***p < 0.0001$

three probe sets was detectable in GFP-positive granules from secondary dendrites containing either the WT or mutant K88,130R form of GFP-FMRP (Fig. 3a–c). Together with the CLIP experiments (Fig. 2e, f), this reveals that both WT and K88,130R GFP-FMRP-containing granules can travel along dendrites, carrying their mRNA cargoes.

We further characterized these mRNA granules using co-localization assays to investigate whether known components of such granules<sup>45,46</sup> are also present in WT and K88,130R-GFP-FMRP positive granules. As clearly depicted in Fig. 3d–g, both the WT and K88,130R GFP-FMRP granules co-localize with the ribosomal protein S6 (Fig. 3d) and the RNA-binding proteins FXR1 (Fig. 3e), Staufen 1 (Fig. 3f), and Staufen 2 (Fig. 3g), indicating that these granules contain not only some of the target

mRNAs of FMRP (Fig. 3a–c) but also several described components of such dendritic mRNA granules<sup>45,46</sup>.

We then measured the surface of dendritic GFP-FMRP-positive mRNA granules at different time points post transfection (Fig. 3h, i). Interestingly, the expression of the K88,130R GFP-FMRP for 48 h significantly increased the size of FMRP-containing granules compared to the WT GFP-FMRP-positive granules (Fig. 3i; WT 48 h,  $0.236 \pm 0.017 \mu\text{m}^2$ ; K88,130R 48 h,  $0.305 \pm 0.020 \mu\text{m}^2$ ). The difference in granule size between the WT and the K88,130R form of GFP-FMRP was further enhanced after 72 h of transfection (Fig. 3i; WT 72 h,  $0.265 \pm 0.020 \mu\text{m}^2$ ; K88,130R 72 h,  $0.440 \pm 0.030 \mu\text{m}^2$ ). All these data reveal that the expression of GFP-FMRP K88,130R results in larger FMRP-containing dendritic mRNA granules suggesting that FMRP

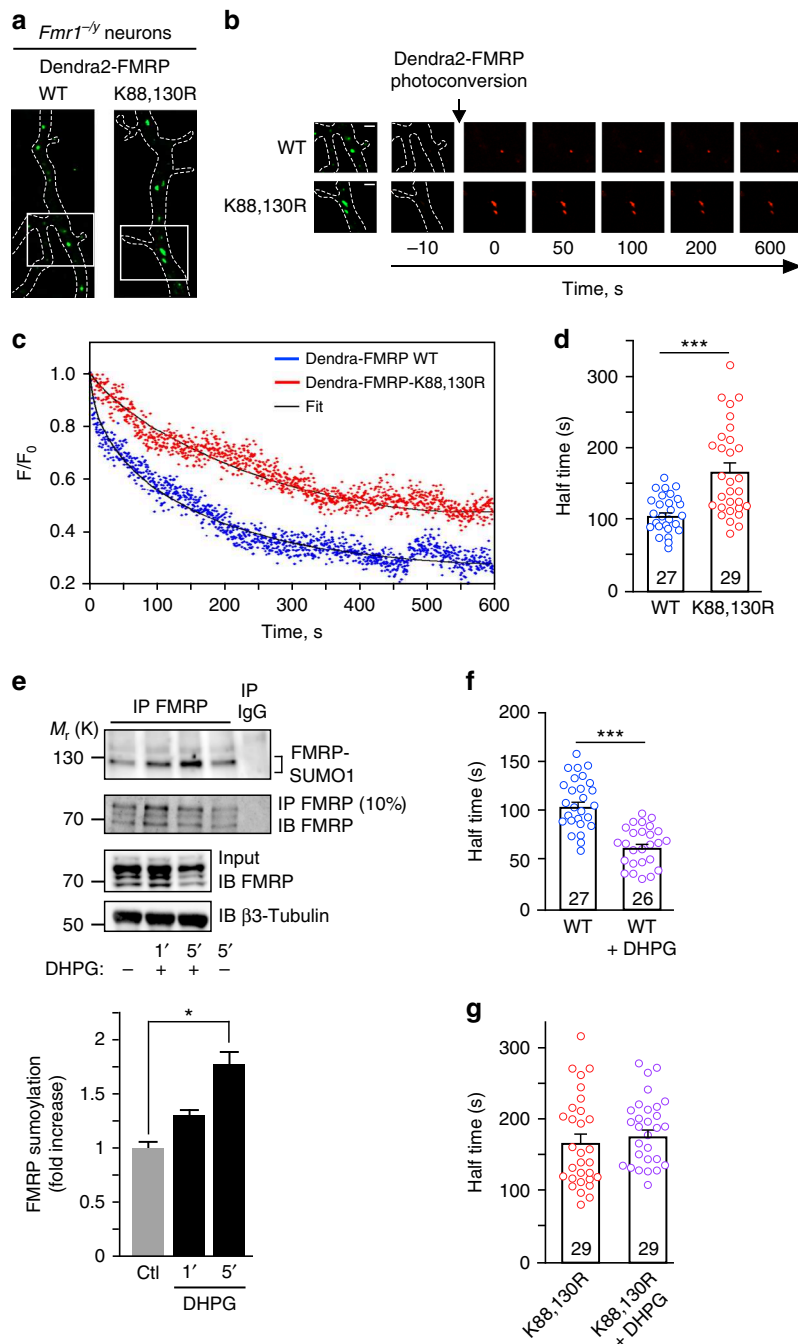


**Fig. 5** Activation of mGlu5 receptors promotes FMRP sumoylation and leads to the release of FMRP from dendritic mRNA granules. **a** Images of transfected *Fmr1*<sup>-/-</sup> dendrites expressing the WT or the non-sumoylatable K88,130R forms of GFP-FMRP before Dendra2-FMRP photoconversion are shown. **b** Time lapse series of confocal images of photoconverted Dendra2-FMRP red fluorescence in dendritic granules in basal unstimulated conditions. Enlargement of dendritic granules from the boxed area in **a** is also shown on the left. The decrease in red photoconverted Dendra2-FMRP fluorescence was then monitored over time. Scale bar, 1  $\mu$ m. **c** Representative sample recording traces of normalized fluorescence from photoconverted WT or mutated Dendra2-FMRP in individual granules in basal unstimulated conditions. The thin traces (black) represent the corresponding fits. **d** Histograms with scatter plots of computed half-time of photoconverted WT and K88,130R Dendra2-FMRP fluorescence diffusion in granules in basal conditions. The number of photoconverted granules is indicated on the bars. **e** Immunoprecipitation of FMRP (Ab#046) and immunoblotting for SUMO1. Control for the immunoprecipitated FMRP fractions is also depicted. Input lanes for FMRP and  $\beta$ -tubulin are also shown. Quantification for DHPG-induced endogenous FMRP sumoylation in neurons over time is also indicated. The data are from three separate experiments and show the mean  $\pm$  s.e.m. \* $p = 0.0213$ . **f** Histograms with scatter plots of half-time of photoconverted Dendra2-FMRP WT fluorescence diffusion in granules from *Fmr1*<sup>-/-</sup> neurons stimulated with DHPG. The number of photoconverted granules is indicated on the bars and the histogram/scatter plot in absence of stimulation is taken from **d**. **g** Histograms with scatter plots of half-time of photoconverted Dendra2-FMRP-K88,130R fluorescence diffusion in granules in basal and DHPG-stimulated conditions. The histogram/scatter plot in absence of stimulation is taken from **d**. The number of photoconverted granules is indicated on the bars. Data shown in **d-f** and **g** are the mean  $\pm$  s.e.m. Statistical significance in **d**, **f**, and **g** was determined using a non-parametric Mann-Whitney test. Statistical significance in **e** was determined by an ANOVA with a Bonferroni post-test. \* $p < 0.05$ ; \*\*\* $p < 0.0001$

sumoylation could participate in the regulation of FMRP interactions within these granules.

FMRP has been reported to form homodimers via its N-terminal 1–134 domain<sup>47</sup>, where the sumoylatable K88 and K130 residues are localized. Thus, to assess whether the difference in granule size measured in Fig. 3i results from abnormal interaction properties of FMRP homodimers directly inside dendritic granules, we performed fluorescence lifetime imaging microscopy (FLIM) experiments on neurons co-expressing WT or K88,130R GFP-FMRP with their respective WT or K88,130R mCherry-tagged constructs (Fig. 4; Supplementary Fig. 4). We observed a clear co-localization of the mCherry/GFP-FMRP constructs in dendritic granules confirming the incorporation of the proteins into granules (Fig. 4a, b). The energy transfer known as fluorescence resonance energy transfer from donor green fluorescent protein (GFP) toward the acceptor mCherry is

quantified by the reduction of the donor fluorescence lifetime (Fig. 4c). We measured a significant reduction of the donor GFP-FMRP fluorescence lifetime in presence of mCherry-FMRP indicating that FMRP/FMRP interaction occurs in dendritic granules. Interestingly, we also found that this homomeric interaction is not affected by the K88,130R mutations (Fig. 4c).

**Sumoylation triggers FMRP dissociation from mRNA granules.** Our results so far indicate that preventing FMRP sumoylation directly impacts on the morphology of mRNA granules in dendrites (Fig. 3h, i) without altering the intrinsic FMRP/FMRP interacting properties within the granules (Fig. 4). Therefore, we investigated whether the absence of FMRP sumoylation affects the dissociation of FMRP from dendritic granules. To assess the diffusion properties of FMRP in dendritic granules, we performed

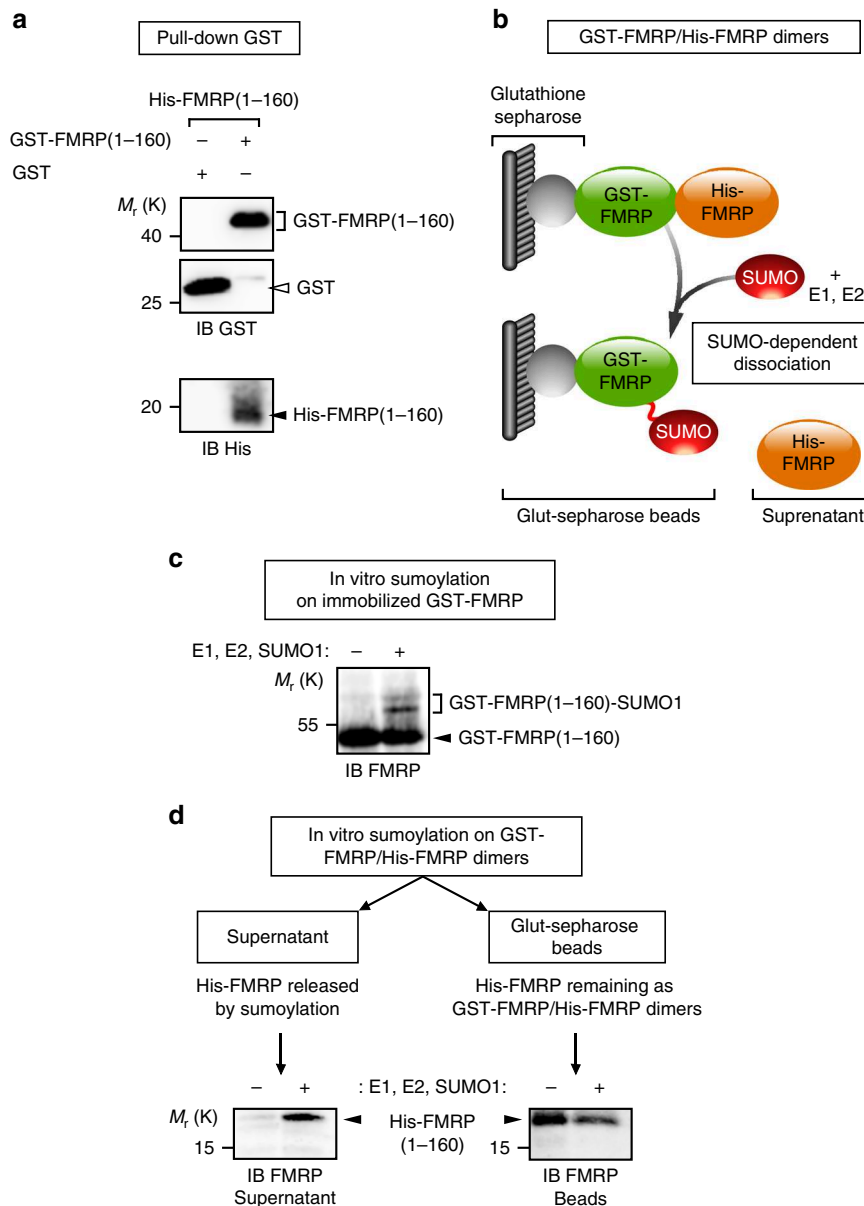


**Fig. 6** The N-terminal sumoylation of FMRP dissociates FMRP homomers. **a** GST pull-down of purified His-FMRP (1–160 aa) with the N-terminal (1–160 amino acids) domain of FMRP fused to the GST protein. Free GST is used as a negative control. **b** Schematic diagram of the SUMO-dependent dissociation assay showing the release into the supernatant of His-FMRP from the immobilized sumoylated GST-FMRP fraction. **c** In vitro sumoylation assay on immobilized GST-FMRP (1–160 aa). **d** In vitro sumoylation assay on GST-FMRP/His-FMRP dimers. Representative immunoblots anti-FMRP (Ab#2F5-1) following the SUMO-dependent dissociation of His-FMRP

live-time restricted photoconversion experiments<sup>48</sup> in *Fmr1*<sup>-/-</sup> neurons expressing the photoswitchable WT or K88,130R Dendra2-FMRP constructs (Fig. 5a, b). Dendra2 is a green-to-red photoactivatable fluorescent protein that allows the real-time tracking of a photoconverted protein<sup>49,50</sup>. We measured and compared the half-times of the decrease in red photoconverted fluorescence, which corresponds to the real-time diffusion of WT and K88,130R Dendra2-FMRP out of dendritic granules (Fig. 5b–d). In basal conditions, the mean half-time of Dendra2-FMRP WT fluorescence dissociation from dendritic granules was significantly shorter than the value measured for the Dendra2-FMRP K88,130R mutant (Fig. 5d; half-time WT = 101.8 ± 4.5 s vs half-time K88,130R = 165.3 ± 12.1 s) indicating that the dissociation of WT FMRP from the granules is much faster than for

the K88,130R mutant. These data strongly support the involvement of FMRP sumoylation in controlling the dissociation of the protein from dendritic mRNA granules.

Activation of mGlu5R regulates FMRP-mediated mRNA transport<sup>51,52</sup> and also modulates its phosphorylation and ubiquitination<sup>13,14</sup>. Interestingly, we previously showed that activation of these receptors also evokes sumoylation in cultured neurons<sup>26</sup>. This prompted us to assess whether the application of the mGluR agonist DHPG triggers FMRP sumoylation in neurons (Fig. 5e). We first confirmed that the activation of mGlu5R with DHPG is effective in our neuronal cultures and evokes an intracellular calcium increase (Supplementary Fig. 5). Then, FMRP-immunoprecipitates were probed with specific anti-SUMO1 antibodies and revealed that the sumoylation of FMRP

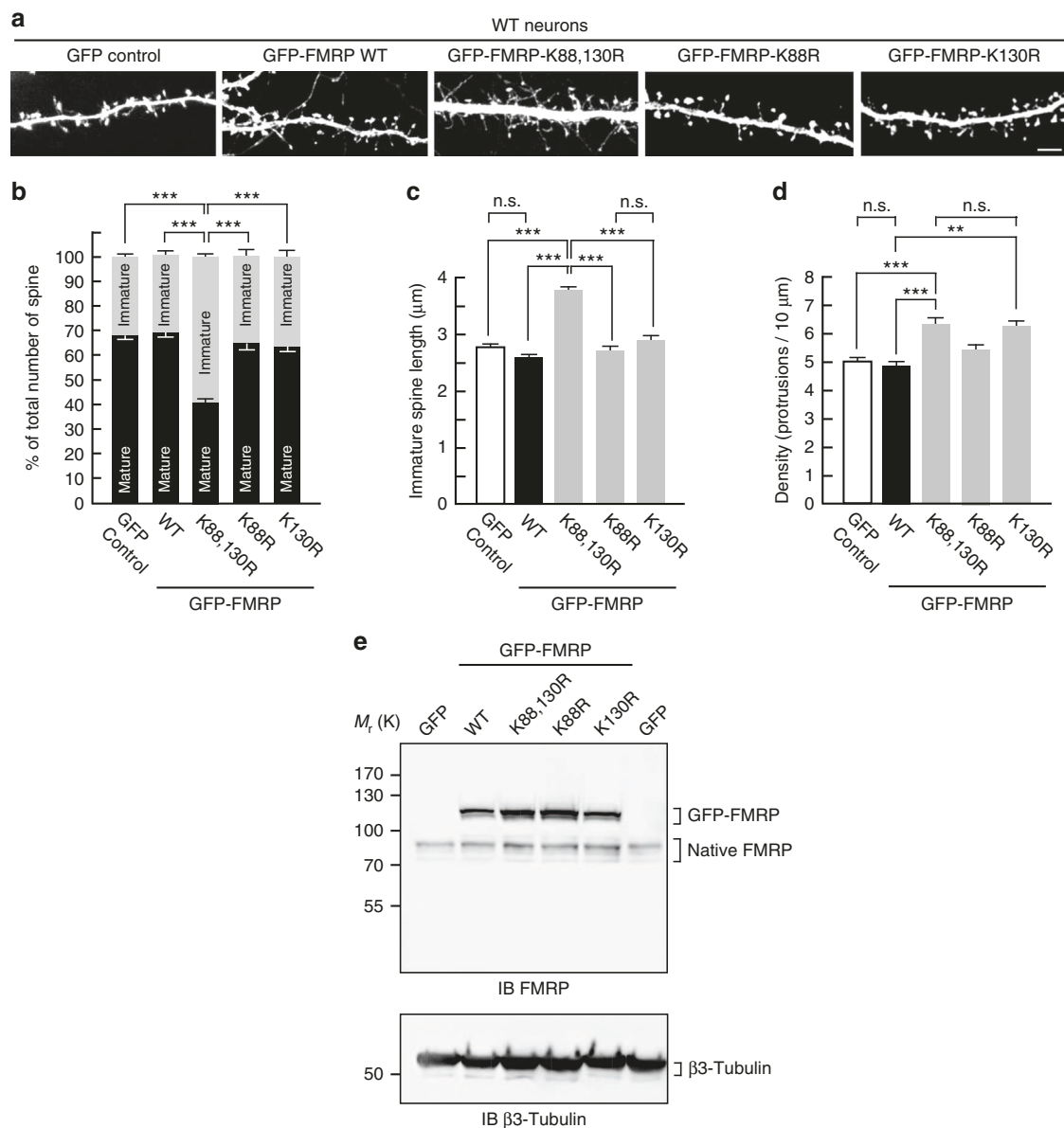


**Fig. 7** Spine density and maturation processes are intrinsically linked to the ability of FMRP to be sumoylated. **a** Representative confocal images of dendrites from transduced WT neurons expressing free GFP, the WT, K88R, K130R, or K88,130R mutant forms of GFP-FMRP for 30 h. Bar, 5 μm. Histograms show the relative proportion of mature and immature spines **b** and the density of the protrusions **d** in the indicated conditions shown in **a**. **c** Histograms of immature spine length measured from WT neurons expressing the indicated constructs. **e** Relative protein expression levels of the WT and mutant forms of GFP-FMRP in WT transduced neurons as in **a** showing an approximate threefold increase in the levels of exogenous GFP-FMRP expression. Data shown in **b–d** are the mean ± s.e.m. Statistical significance in **b–d** was determined by a one-way analysis of variance (ANOVA) with a Bonferroni post-test. *N* = ~3000 spines per condition from four independent experiments. \*\*\**p* < 0.001; n.s. not significant

is low in basal unstimulated conditions but rapidly increases after 1 and 5 min of DHPG treatment (DHPG 1 min,  $1.28 \pm 0.12$  fold/control; DHPG 5 min,  $1.73 \pm 0.2$  fold/control; Fig. 5e) indicating that FMRP sumoylation is rapidly triggered by the mGlu5R activation.

These results led us to hypothesize that the activity-dependent sumoylation of FMRP controls FMRP dissociation from dendritic mRNA granules. To address this point, we pharmacologically stimulated mGlu5R in *Fmr1*<sup>-/-</sup> neurons expressing either Dendra2-FMRP WT or K88,130R and measured the dissociation properties of FMRP from dendritic granules using the photo-conversion assay (Fig. 5f, g). Interestingly, mGlu5R stimulation enhanced the exit rate of the red photoconverted Dendra2-FMRP WT fluorescence from granules by ~40% (Fig. 5f). By contrast, mGlu5R activation had no effect on the dissociation of Dendra2-FMRP-K88,130R positive granules (Fig. 5g). These findings strongly support that the mGlu5R-dependent sumoylation of FMRP regulates the dissociation of FMRP from dendritic mRNA granules.

### Sumoylation regulates homomeric FMRP–FMRP interaction.

Our data demonstrate that FMRP sumoylation controls FMRP release from dendritic granules. To further assess the role of sumoylation in the regulation of FMRP–FMRP interaction, we combined pull-down assays with in vitro SUMO reactions and analyzed the impact of sumoylation on the dissociation of FMRP homomers (Fig. 6).

We purified GST- and His-tagged FMRP (1–160 aa) fusion proteins and found that GST-FMRP (1–160) specifically interacts with His-FMRP (1–160 aa) and forms N-terminal FMRP homodimers in vitro (Fig. 6a). We then performed an in vitro sumoylation assay<sup>31</sup> on purified FMRP (1–160 aa) dimers to assess whether sumoylation promotes their dissociation (Fig. 6b–d). First, we verified that the immobilization of GST-FMRP (1–160 aa) on the glutathione matrix did not prevent the in vitro sumoylation of the protein (Fig. 6c). Incubation of immobilized GST-FMRP (1–160 aa) with the sumoylation reaction mix gave rise to higher molecular weight bands corresponding to the sumoylated forms of GST-FMRP (1–160 aa). These bands were absent in control conditions (Fig. 6c).

Next, we performed in vitro sumoylation assays on immobilized GST-FMRP–His-FMRP dimers (Fig. 6d). The pool of His-FMRP (1–160 aa) released by sumoylation was separated from the remaining immobilized dimers by centrifugation of the glutathione beads. Proteins either in the supernatant or bound to the beads were both analyzed by immunoblotting with anti-FMRP antibodies. As seen in Fig. 6d, the release of His-FMRP

(1–160 aa) from the immobilized dimers was only promoted upon sumoylation with the concurrent decrease of the remaining His-FMRP (1–160 aa) in the pelleted FMRP fraction. This particular set of data demonstrates that sumoylation promotes the dissociation of FMRP–FMRP dimers.

### SUMO-deficient FMRP-expressing WT neurons show FXS phenotype.

Collectively, our data clearly demonstrate that sumoylation of the N-terminal part of FMRP is essential to allow for the dissociation of the protein from dendritic mRNA granules and to promote spine elimination and maturation. To confirm the key involvement of FMRP sumoylation in neuronal maturation events, we hypothesized that the expression of the non-sumoylatable FMRP mutant could reverse the spine density and maturation of WT neurons. Thus, we expressed either the WT or the K88,130R mutant form of GFP-FMRP into WT mouse neurons (Fig. 7). WT neurons expressing GFP-FMRP-K88,130R resembled the GFP-expressing *Fmr1*<sup>-/-</sup> neurons (Fig. 2) with >67% of protrusions characterized by an immature phenotype (Fig. 7a, b). Similarly, the length of dendritic spines in WT neurons expressing GFP-FMRP-K88,130R was also significantly increased (Fig. 7c; K88,130R,  $3.77 \pm 0.08$  μm) comparable to the values measured in *Fmr1*<sup>-/-</sup> neurons (Fig. 2d).

Importantly, the density of dendritic spines was dramatically increased upon the expression of the K88,130R mutant (Fig. 7a, d; GFP control,  $5.03 \pm 0.17$  protrusions per 10 μm; K88,130R,  $6.33 \pm 0.24$  protrusions per 10 μm), comparable to the values obtained in *Fmr1*<sup>-/-</sup> neurons (Fig. 2c). Interestingly, the expression of the single K130R mutant in WT mouse neurons also leads to a significant increase in the density of the protrusions (Fig. 7a, d; GFP control,  $5.03 \pm 0.17$  protrusions per 10 μm; K130R,  $6.29 \pm 0.41$  protrusions per 10 μm) without altering the maturity of dendritic spines (Fig. 7b, c). As expected, expressing the WT form of GFP-FMRP in WT neurons did not affect any of the spine characteristics confirming the essential role of FMRP sumoylation in spine elimination and maturation processes.

### Discussion

Here, we report for the first time that FMRP is a sumoylation target in vivo. We identify three sumoylatable residues, two of which lay within the N-terminal domain of FMRP and are the active SUMO sites. We further find that the activation of metabotropic mGlu5R promotes the sumoylation of FMRP and rapidly leads to the dissociation of FMRP from dendritic mRNA granules allowing for the regulation of spine elimination and maturation (Fig. 8). Thus, our work uncovers a novel activity-

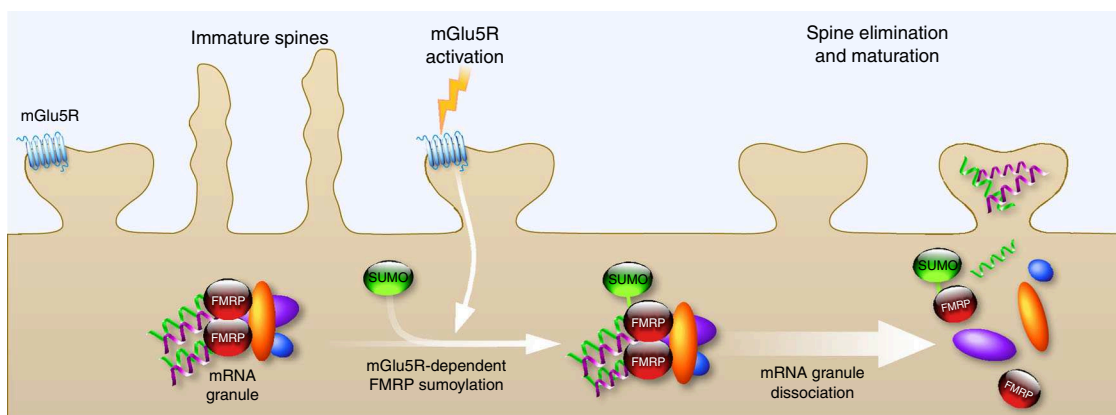


**Fig. 8** Schematic model for the mGlu5R-dependent regulation of FMRP function via the sumoylation process. The activity-dependent sumoylation of FMRP is a key step to dissociate FMRP from dendritic mRNA granules and consequently to regulate spine elimination and maturation

dependent role of sumoylation in the regulation of FMRP neuronal function.

We provide the first evidence that FMRP sumoylation is required for spine elimination and proper maturation. The initial step of spine formation is the emergence of immature long thin protrusions, which are later on eliminated or matured with enlargement of spine head<sup>8</sup>. A tight balance between these processes is thus required for the development of a functional neuronal network. This is in line with our data showing a decrease in the density of protrusions when expressing FMRP in *Fmr1*<sup>-/-</sup> neurons, and an increased density in WT neurons expressing the SUMO-deficient form of FMRP. Such compensatory and deleterious effects support the idea that immature spines are over-produced and/or less efficiently eliminated when FMRP sumoylation is perturbed.

In correlation with our findings, the role of sumoylation at the post-synaptic compartment has already been described for several proteins<sup>19</sup>. For instance, sumoylation of the scaffolding calcium/calmodulin-dependent serine protein kinase (CASK) reduces CASK interaction with protein 4.1, a protein that connects spectrin to the actin cytoskeleton in dendritic spines. Mimicking CASK sumoylation dramatically impairs spine formation<sup>53</sup>. According to the importance of sumoylation in the post-synaptic formation and maturation, our findings demonstrate a role of sumoylation in spine elimination and maturation by tuning FMRP dimerization within dendritic mRNA granules. Altogether, these data shed light on the role of sumoylation as a critical molecular regulator in neuronal development and maturation.

Interestingly, we demonstrate that the sumoylation of FMRP is triggered upon mGlu5R activation. mGlu5R has been previously reported to differentially regulate FMRP function depending on its subcellular localization. For instance, a direct involvement of FMRP was shown in targeting and transport of several mRNAs from the soma along dendrites upon mGlu5R activation<sup>52</sup>. Furthermore, the repression of mRNA translation exerted by FMRP in dendrites is counteracted by the activation of mGlu5R<sup>51</sup>. Here, we unravel a novel activity-dependent regulation of the FMRP function. We show that mGlu5R-induced sumoylation of FMRP drives its own dissociation from dendritic mRNA granules to regulate both spine elimination and maturation.

It has been previously described that FMRP is a target of mGluR-dependent PTMs<sup>11,13,14,54,55</sup>. Activation of mGluRs in neurons induces a rapid dephosphorylation of FMRP C-terminal region as a result of an enhanced protein phosphatase 2A (PP2A) activity<sup>11</sup>. Conversely, mGluR activation that lasts longer than 5 min results in an mTOR-mediated PP2A suppression followed by rapid rephosphorylation of FMRP C-terminus by the ribosomal protein S6 kinase (S6K1)<sup>11,55</sup>. Accordingly to the role of phosphorylation in controlling FMRP function, the lack of S6K1-dependent FMRP phosphorylation mimics FMRP loss of function and leads to an increased expression of the FMRP target mRNA SAPAP3<sup>55</sup>. In addition, Nalavadi et al.<sup>14</sup> described a rapid ubiquitination of the C-terminal part of FMRP upon stimulation with the mGlu5R agonist DHPG in rat cultured neurons. FMRP ubiquitination promotes a proteasome-mediated FMRP degradation, which in turn controls FMRP levels at the synapse. Interestingly, these authors showed that FMRP ubiquitination requires a prior FMRP-dephosphorylation carried by PP2A. Taken together, these pieces of evidence suggest a crosstalk between various PTMs in the regulation of FMRP function. Here, we demonstrate that mGlu5R activation triggers a rapid sumoylation of FMRP. This event promotes the release of FMRP from transport mRNA granules. Thus, the present study adds another level of complexity to the post-translational regulation of FMRP and advances our understanding of the activity-dependent control of FMRP function in neurons. It will therefore be of future

interest to examine whether the interplay between these PTMs could take place to orchestrate the mGlu5R-dependent regulation of FMRP.

The present study shows that the activation of mGlu5R directly promotes FMRP sumoylation, regulating its neuronal function in spine elimination and maturation. Our work therefore raises the intriguing possibility that the impairment of FMRP sumoylation could contribute to FXS pathophysiology. Recent publications have reported missense point mutations within the *FMR1* gene in patients affected by FXS. Importantly, these mutations lead to amino-acid changes close to the SUMO active sites of FMRP (F126S<sup>56</sup> and R138Q<sup>57</sup>). Similarly to our data on the K88,130R FMRP mutant, the FXS R138Q mutation does not modify the expression of FMRP nor its RNA-binding properties, indicating that the pathogenicity is caused independently of the FMRP expression level and the ability of FMRP to bind mRNAs<sup>58</sup>. To date, no data have been reported regarding the functional impairment due to the F126S mutation. Our data report that the reintroduction of the FMRP WT but not the K88,130R mutant in *Fmr1*<sup>-/-</sup> neurons promotes spine maturation and elimination demonstrating that FMRP sumoylation is critical for these processes. Therefore, an interesting possible explanation could be that the F126S and R138Q FXS mutations, which are very close to the active K130-SUMO site, would directly impact on the mGlu5R-dependent regulation of FMRP sumoylation and consequently, on post-synaptic FMRP-driven regulatory events. Future work will have to be performed aiming at understanding the effect of these FXS mutations on FMRP sumoylation. These next exciting steps will allow assessing whether FMRP sumoylation defects participate in the pathophysiology of FXS patients, raising the possibility to identify new targets and potentially develop novel therapeutic approaches.

## Methods

**Constructs.** GFP-FMRP was obtained by subcloning the isoform 1 of the human *FMR1* sequence into the EcoRI/PstI site of the mammalian expression vector pEGFP-C2 (Clontech). GFP-Dendra2-/GST-/His-FMRP mutant constructs were all made by site-directed mutagenesis using the Quick-change mutagenesis solution (Agilent). pSinRep5 constructs used to produce Sindbis particles were generated using the Gateway recombination technology (Invitrogen). All constructs were then entirely sequenced.

**Building model for FMRP-SUMO1.** Three X-ray structures of human FMRP are available in Protein Data Bank (PDB, <http://www.rcsb.org>; PDB ID: 4OVA residues 1–209 at 3.0 Å resolution<sup>59</sup>, 4QVZ residues 1–213 at 3.2 Å resolution, and 4QW2 residues 1–213 with the mutation R138Q at 3.0 Å resolution<sup>60</sup>). The solvent ASA values for each residue have been calculated using Naccess tool<sup>61</sup> on all monomers of each PDB files (4 for 4OVA, 2 for 4QVZ, and 2 for 4QW2). We calculated the average values for K88 and K130 for each structure. The classical parameters used are 1.4 for the radius of the “solvent” sphere and 25% for the threshold that determines if a residue is considered as buried or exposed. We utilized the X-ray structures of human FMRP PDB ID: 4OVA residues 1–209 at 3.0 Å resolution<sup>59</sup> and of human SUMO1 PDB ID: 4WJQ at 1.35 Å resolution<sup>62</sup>. To build models of FMRP modified with the SUMO1 protein, we first verified the shape compatibility and then used the Pymol software to manipulate the structures, make and visualize the FMRP-SUMO1 models.

**Mouse lines and rat strain.** All animals (3–10-month-old pregnant female Wistar rats from Janvier, St Berthevin, France; 3–10 month-old female C57BL/6 WT and *Fmr1* knockout (*Fmr1*<sup>-/-</sup>) mice<sup>10</sup>) were handled in our facility in accordance with the European Council Guidelines for the Care and Use of Laboratory animals and approved by the Animal Care and Ethics Committee (Comité Institutionnel d’Éthique Pour l’Animal de Laboratoire N°28, Nice, France; project reference NCE/2012-63). All animals had free access to water and food. The light cycle was controlled as 12 h light and dark cycle and the temperature was maintained at 23 ± 1 °C. Protocols to prepare primary neuronal cultures from mouse embryos at E15.5 or at E18 for rats were also approved by the Animal Care and Ethics Committee (Comité Institutionnel d’Éthique Pour l’Animal de Laboratoire N°28, Nice, France; project reference NCE/2012-63). All mice were maintained on a C57BL/6 genetic background, whereas Wistar rats were exclusively from a commercial source (Janvier). The *Fmr1* knockout (*Fmr1*<sup>-/-</sup>) mouse line<sup>10</sup> was maintained on a C57BL/6 background.

**Mouse and rat brain lysate preparation.** Brain lysates were prepared as previously described<sup>26</sup> from post-natal P1–3 mouse or P5–7 rat brains. Briefly, freshly dissected brains were transferred in 5 volumes (w/v) of ice-cold sucrose buffer (10 mM Tris-HCl, pH 7.4, 0.32 M sucrose) supplemented with a protease inhibitor cocktail (Sigma, 1/100), Pefabloc 0.5 mM (Roche), MG132 100  $\mu$ M (Enzo), ALLN 100  $\mu$ M (Sigma), and 20 mM freshly prepared NEM (Sigma), and homogenized at 4 °C using a Teflon-glass potter and a motor-driven pestle at 500 rpm. Nuclear fraction and cell debris were pelleted by centrifugation at 1000 $\times$ g for 10 min. The post-nuclear S1 fraction (supernatant) was collected and protein concentration measured using the BCA protein assay (Bio-Rad).

**Primary neuronal cultures.** Hippocampal and cortical neurons were prepared from embryonic (E18) pregnant Wistar rats as previously described<sup>26</sup> or from WT or *Fmr1*<sup>-/-</sup> E15.5 pregnant C57BL/6 mice. Briefly, neurons were plated in Neurobasal medium (Invitrogen, France) supplemented with 2% B27 (Invitrogen), 0.5 mM glutamine and penicillin/streptomycin (Ozyme) on 60-mm dishes or 24-mm glass coverslips (VWR) pre-coated with poly-L-lysine (0.5 mg mL<sup>-1</sup>; Sigma). Neurons (800,000 cells per 60-mm dish or 110,000 cells per coverslip) were then fed once a week with neurobasal medium supplemented with 2% B27 and penicillin/streptomycin for a maximum of 3 weeks.

**Cell transfection.** COS7 cells and primary neurons (14–16 DIV) were transfected using Lipofectamine 2000 (Invitrogen) according to the manufacturer's instructions and used 48–72 h post transfection.

**Sindbis virus production and neuronal transduction.** Attenuated Sindbis viral particles (SINrep(nsP2S726)) were prepared and used as previously described<sup>38–40</sup>. Briefly, cRNAs were generated from the pSINrep5 plasmid containing the sequence coding for WT or mutated GFP-FMRP constructs and from the defective helper (pDH-BB) plasmid using the Mmessage Mmachine SP6 solution (Ambion). cRNAs were then mixed and electroporated into BHK21 cells. Pseudovirions present in the culture medium were collected 48 h after electroporation and concentrated using ultracentrifugation on SW41Ti. Aliquots of resuspended Sindbis particles were then stored at -80 °C until use. Neurons were transduced at a multiplicity of infection (MOI) of 0.1–2 and returned to the incubator at 37 °C under 5% CO<sub>2</sub> for 24–30 h depending on their subsequent utilization.

**Bacterial sumoylation assay in *Escherichia coli*.** Bacterial sumoylation assays were performed as previously described<sup>31,35</sup>. Briefly, competent *E. coli* BL21(DE3) cells (Invitrogen, France) expressing pE1-E2SUMO1 were transformed with 1  $\mu$ g of pET-expression plasmid (Novagen) to express the WT or non-sumoylatable forms of His-tagged FMRP were selected on LB-Agar plates containing chloramphenicol (50  $\mu$ g mL<sup>-1</sup>) and ampicillin (50  $\mu$ g mL<sup>-1</sup>). A 10 mL preculture was then used to inoculate 50 mL of LB containing chloramphenicol and ampicillin. After incubation under shaking at 37 °C until OD<sub>600</sub> reaches 0.7, cells were cooled down to 20 °C and isopropyl- $\beta$ -D-thiogalactopyranoside (IPTG) was added at a concentration of 1 mM. After 4 h at 20 °C, bacteria were pelleted by centrifugation at 4 °C at 7000 $\times$ g and kept at -80 °C until use. Pellets were resuspended in 1 mL lysis buffer (25 mM Tris pH 8, 300 mM KCl, 1 mM EDTA, 20% glycerol, 5% ethanol, 0.5% NP40, 0.5 M urea, 1 mM DTT) supplemented with proteases inhibitors (leupeptine 1  $\mu$ g mL<sup>-1</sup>, Pepstatine 1  $\mu$ g mL<sup>-1</sup>, Aprotinin 1  $\mu$ g mL<sup>-1</sup>, Pefabloc 0.5 mM, and freshly prepared NEM 20 mM), and incubated under rotation for 30 min at 4 °C in the presence of 5 mg mL<sup>-1</sup> lysozyme. Bacterial cytoplasmic membranes were then solubilised by addition of 1 mg mL<sup>-1</sup> sodium deoxycholate and released DNA digested by incubation with 50  $\mu$ g mL<sup>-1</sup> of DNase I and 10 mM MgCl<sub>2</sub> for 30 min at 4 °C. Cellular debris were pelleted by centrifugation at 20,000 $\times$ g for 15 min at 4 °C and supernatants were incubated with 40  $\mu$ L of nickel agarose beads (Qiagen) for 2 h at 4 °C under gentle rotation. After three washes (25 mM Tris pH 8, 50 mM KCl, 1 mM EDTA, 20% glycerol, 0.1% Triton X-100, 0.5 M urea, 1 mM DTT), purified proteins were eluted in 200  $\mu$ L of  $\beta$ ME-reducing sample buffer for 5 min at 95 °C.

**COS7 sumoylation assay.** Mycoplasma-free COS7 cells (ATCC reference CRL-1651, Molsheim, France) at 60% of confluence in six-well plates were co-transfected using 1  $\mu$ g of the eukaryotic expression vector pTL1-FMRP plasmid<sup>63</sup> or its derived non-sumoylatable mutants with 0.5  $\mu$ g of mCherry or mCherry-SUMO1 plasmids<sup>26</sup> and 0.5  $\mu$ g of plasmid coding for Flag-Ubc9 using Lipofectamine 2000 (Invitrogen) according to the manufacturer's instructions. After 48 h of expression, cells were washed once in PBS containing 20 mM NEM and reduced for 5 min at 95 °C in  $\beta$ ME-containing sample buffer.

**CLIP analysis.** To isolate neuronal mRNAs associated with WT and SUMO-deficient GFP-FMRP mutant, UV cross-linking, and FMRP immunoprecipitations were performed on 20 DIV *Fmr1*<sup>-/-</sup> neurons transduced (MOI of 3) at day 19 to express free GFP, the WT, or the non-sumoylatable K88,130,614R form of GFP-FMRP. RNAs and proteins were cross-linked through three rounds of UV irradiation (400 mJ each; 254 nm). Cells were then scraped in ice-cold PBS, collected by centrifugation, and lysed in NP40 buffer as described in ref.<sup>64</sup> For each assay, 5  $\mu$ g of affinity-purified rabbit anti-FMRP antibody (Ab#056) was used to

immunoprecipitate 1 mg of neuronal extracts and 2% of the lysate was used for assessment of relative RNA expression in the input material. IPs were then carried out at 4 °C for 4 h and 2% of the homogenate and 10% of the immunoprecipitates were saved to check for the IP quality using anti-FMRP immunoblots. After three washes in lysis buffer (50 mM HEPES, pH 7.4, 150 mM NaCl, 0.5% NP40, 10 mM EDTA, 1 mM NaF, 0.5 mM DTT, protease and phosphatase inhibitors (Pierce), proteins were digested with proteinase K (1  $\mu$ g mL<sup>-1</sup>) for 30 min at 56 °C. IP and input RNAs were purified through two successive rounds of phenol/chloroform extraction, then reverse transcribed using a mix of Oligo dT and random primers and Superscript II enzyme (Invitrogen) according to the manufacturer's protocol. RT reactions were diluted two times and 1  $\mu$ L of diluted material was used for qPCR analysis. Relative enrichment of the amplified RNA in the IP vs the input in each condition was calculated with the 2<sup>- $\Delta\Delta$ Ct</sup> (Ct<sub>IP</sub>-Ct<sub>input</sub>).

Oligonucleotides (5'-3') used in RNA work was as follows:

*Fmr1*\_F: GAACAAAAGACAGCATCGCT; *Fmr1*\_R: CCAATTTGTCGCAACTGCTC; *Camk2a*\_F: TATCCGCATCACTCAGTAC; *Camk2a*\_R: GAAGTGGACGATCTGCCATTT; *Sapap3*\_F: ACCATGTAACCCCGGCTG; *Sapap3*\_R: CCTTGATGTCAGGATCCCC; *Fxr1*\_F: GTGCAGGTCCCGAGGT; *Fxr1*\_R: GGTGGTGGTAATCGGACTTC; *Kif3c*\_F: GGTCCCATCCAGATACAGA; *Kif3c*\_R: CCAGAAAGCTGCAAACCTC; *Tubb3*\_F: CGAGACTGCTACGACAG; *Tubb3*\_R: CATTGAGCTGACAGGGAAT; *PP2a*\_F: GTCAAGAGCCTCTGCGAGAA; *PP2a*\_R: GCCCATGTACATCTCCACAG;  $\beta$ -*actin*\_F: ACGGCCAGTCACTATTG;  $\beta$ -*actin*\_R: CACAGATTCCATACCCAAGA; *PSD95*\_F: GGCGGAGAGAACTGTCC; *PSD95*\_R: AGAATTGGCCTTGAGGGAGGA; *Map1b*\_F: TCCGATCGTGGACACAAACCTG; *Map1b*\_R: AGCACCAGCAGTTTATGGCGGG.

**Immunoprecipitation.** Proteins from rodent brain lysates or cultured neurons were solubilized for 1 h at 4 °C under gentle rotation in lysis buffer (10 mM Tris-HCl, pH 7.5, 10 mM EDTA, 150 mM NaCl, 1% Triton X-100, 0.1% SDS) supplemented with a protease inhibitor cocktail (Sigma, 1/100), Pefabloc 0.5 mM (Roche), MG132 100  $\mu$ M (Enzo), ALLN 100  $\mu$ M (Sigma), and 20 mM freshly prepared NEM (Sigma). Then, NaCl concentration was raised to 400 mM and lysates were sonicated for 10 s, further incubated for 30 min at 4 °C and clarified (for primary neuronal extracts) or not (for brain homogenates) at 20,000 $\times$ g at 4 °C for 15 min. Supernatants were diluted 2.5-fold with lysis buffer devoid of NaCl and pre-cleared for 1 h with a 50/50 mix of untreated and pre-blocked protein G-sepharose beads (Sigma) with a blocking buffer (PBS containing 5 mg mL<sup>-1</sup> BSA, 5 mg mL<sup>-1</sup> Dextran (40 kDa), 1 mg mL<sup>-1</sup> gelatin, yeast t-RNA 0.1 mg mL<sup>-1</sup>, and glycogen 0.1 mg mL<sup>-1</sup>) for 1 h at 4 °C. Proteins (800  $\mu$ g) from pre-cleared lysates were incubated with either 8  $\mu$ g of mouse monoclonal anti-SUMO1 antibody (Ab#D11, Santa-Cruz), 4  $\mu$ g of custom rabbit anti-FMRP (Ab#056, Supplementary Fig. 1), or 12  $\mu$ g commercially available rabbit anti-FMRP (#Ab17722, Abcam; Supplementary Fig. 1) antibodies (or their corresponding IgGs as IP control) for 1 h at 4 °C and then overnight at 4 °C with 30  $\mu$ L of pre-blocked protein G-sepharose beads (Sigma). Precipitates were washed three times with 1 mL lysis buffer and proteins were eluted by boiling the beads 5 min in  $\beta$ ME-reducing sample buffer before SDS-PAGE.

**Immunoblotting.** Protein extracts were resolved by SDS-PAGE, transferred onto nitrocellulose membrane (Hybond-C Extra, Amersham or BioTraceNT, PALL), immunoblotted with the indicated concentration of primary antibodies and revealed using the appropriate horseradish peroxidase (HRP)-conjugated secondary antibodies (GE healthcare) or True Blot (Rockland, Tebu-Bio). Proteins were then identified using Immobilon Western (Millipore) or Western Lightning Ultra (Perkin Helmer) chemiluminescent solutions and images acquired on a Fusion FX7 system (Vilber Lourmat). Full-size blots for cropped gels can be found in Supplementary figures 6, 7.

**Immunocytochemistry.** Neurons (18–21 DIV) were fixed in phosphate-buffered saline (PBS) containing 3.7% formaldehyde and 5% sucrose for 1 h at room temperature (RT). Neurons were then permeabilized for 20 min in PBS containing 0.1% Triton X-100 and 10% horse serum (HS) at RT and immunostained with either a rabbit monoclonal anti-S6 (1/200; Cell Signaling), a goat anti-Staufen1 (1/100; Santa-Cruz), a goat anti-Staufen2 (1/100; Santa-Cruz), a rabbit anti-FXR1 (1/100<sup>65</sup>), a mouse monoclonal anti-Ubc9 (1/50; BD Bioscience, France), a mouse anti-SUMO1 (1/50; Ab#D11, Santa-Cruz; 1/50 Ab#2F5-1, DSHB) or rabbit anti-FMRP (1/200; Custom Ab#056 or 1/50; Ab#4317s, Cell Signaling) antibodies in PBS containing 0.05% Triton X-100 and 5% HS. Cells were washed three times in PBS and incubated with the appropriate secondary antibodies (1/400) conjugated to Alexa488 or Alexa594, and mounted with Mowiol (Sigma) until confocal examination.

**Ratiometric calcium imaging.** Mouse cortical/hippocampal neurons (19–23 DIV) were loaded in neurobasal containing 20  $\mu$ M Fura-2AM (Invitrogen) for 30 min. After two washes in physiological 1.6 mM calcium-containing buffer (139 mM NaCl, 1.25 mM glucose, 15 mM Na<sub>2</sub>HPO<sub>4</sub>, 1.8 mM MgSO<sub>4</sub>, 1.6 mM CaCl<sub>2</sub>, 3 mM

KCl, 10 mM HEPES), Fura-2AM-loaded neurons were imaged at 37 °C on an inverted AxioObserver microscope (Carl Zeiss) equipped with a 300 W Xenon lamp (Suttler instruments) and a Fluor 40× (numerical aperture (NA) 1.4) oil immersion objective. Fura-2AM was sequentially excited at 340 and 380 nm and the emission monitored at 510 nm. Images were acquired with a cascade 512 EMCCD camera every 2 s and digitized using Metafluor software (Roper scientific). The intracellular calcium concentration was estimated by measuring the F340/380 nm ratio of fluorescence. Neurons were treated for 40 s with 100 μM DHPG in 1.6 mM calcium-containing buffer.

**GFP-FMRP-associated granules analysis.** *Fmr1*<sup>-/-</sup> neurons were co-transfected to express mCherry with the WT or the non-sumoylatable mutant form of GFP-FMRP either for 48 or 72 h. Cells were then rinse twice in PBS and fixed in PBS containing 3.7% formaldehyde and 5% sucrose for 1 h at RT and mounted with Mowiol until use.

**smFISH assays.** smFISH assays were performed as described previously in ref. 44. Briefly, *Fmr1*<sup>-/-</sup> neurons grown on glass coverslips were transfected as above at 12 DIV to express the WT or the K88,130R mutant form of GFP-FMRP for 48–60 h. Cells were then fixed in PBS containing 4% formaldehyde for 10 min at RT. smFISH assays were performed as described previously in ref. 44 with the following modified prehybridization buffer: formamide (10%, NaCl 68.5 mM, KCl 1.35 mM, KH<sub>2</sub>PO<sub>4</sub> 1 mM, Na<sub>2</sub>HPO<sub>4</sub> 5 mM, SSC 2× (Euromedex), dextran sulfate 10% (Sigma), ribonucleoside vanadyl complexes 10 mM (Sigma), BSA 2 mg mL<sup>-1</sup>, salmon sperm DNA 0.67 mg mL<sup>-1</sup> (Sigma), yeast tRNA 0.67 mg mL<sup>-1</sup> (Sigma). Neurons were incubated overnight at 37 °C in the presence of GFP Quasar 570-labeled, PSD-95 or CamKII Quasar 670-labeled Stellaris probes (12.5 picomoles in 100 μL of prehybridization buffer), washed 2 times with pre-warmed 10% formamide in 2× SSC for 20 min at 37 °C, three times 1 min with 2× SSC, and twice for 5 min with 2× SSC under mild agitation prior to coverslip mounting in Vectashield (Clinisciences).

GFP Stellaris probes (used to detect GFP-FMRP mRNA) labeled with Quasar 570 dye were (5′–3′) as follows: tctctgccttctgctaccat, atggccaccaccctggtaa, gtcgcccctcagctcgaacca, cgctgaactgtggccgttt, tgcctcgcctcctcgcgga, ggtcagcttccgtaggtgg, cgggtgctcagatgaactc, ggccagggcagggcagctt, taggtcaggtggtcagcg, tagcggctgaagcactgcac, gctgctctcagtggtcgg, gcatggcggactgaagaag, cgctcctggactgacctc, gctgcttgaagaagatg, tgcggcgggtctgtgatt, ggtgctcctcgaactca, ttcagctcagctcgggttac, gtcctcctgaagctcagtc, agctgtgccccagatgtt, gttgctgtttagttagtact, ttgtcggcatgatagac, caccttgatcggcttctt, atgttggggactgtgaa, gactgacagctgcctctct, tggctctggttagtggctg, agccagggcggctcggat, caggtagtggttgcgggca, ttgctcagggcggactgggt, atctcggctctgtgggt, cgaactcagcaggacatg, agatgattccggcggcgg, ctgtcagactcgtcctagc.

PSD-95 Stellaris probes, labeled with Quasar 670 dye were (5′–3′) as follows: ctctatgatcttcagctg, tagccctttgataagctt, tgcagctgtaagccaagtc, ctattatcaggatggtg, ccttcgatgatctgtgtac, aggatctgttccatgctg, tcatgatgacatcctcag, atagtgttctcaggcgtg, ccacttttagtcaacaacg, catagctcactcaggtag, taggagttgtgatctg, tagctctgactgactc, tcaacacaggtgaccgacag, tggctgactggcattg, tactgagcagatcgtgac, cgaactcgtactactctt, ataagctgttcccgaagatc, tgatataagaaccccgctt, ttgtcgtgtaaaacagggc, tcaagaacccagctcctt, gctggcgtcaattacatgaa, catcgttctactgacag, ttgctgggaatgaagcaaa, tctcatagctcagaaccgag, aagatgatgatggggcag, agaagatcatcgttggcagc, aaactgtcggggaactcgg, tctgatgagggacagggat, tatctatattcccgttag, cgggagagacaaagtggta, tgaatgtccttccatttt, cagcctcaatgaactgtg, tagaggtgctgtgtgactg, gactgtgtaagacatcaag, ggatgaagatggcagtaggg, cgttatgatctcagcagc.

CaMKII Stellaris probes, labeled with Quasar 670 dye were (5′–3′) as follows: tactctctgtaactcgggt, taactctggcagcactatc, ctcaacaagcggcagatg, tcatggagtcgagcagatatt, accagtaacagatcgaaga, gccacaatgtctcaaacag, ggatcagctcactgtaatt, tccaagatcctggtgata, catctggtgacagtgtagca, ttacagcagcggccttgg, taccagctgctgctgca, ctctcagcacttctgggg, aggtccacgggtctccgta, agatatacaggtgacgca, ctggtctcactcccagaagc, ctgtgatcgtggtacagg, gatgggaatcattagcacc, ggtgacgggttcccattctg, tgcagatcctgcttct, ggttgatgctcagatctt, tcagcggcgtgtagcgtt, agatccatgggtgctgaga, tctcgtgctgctgacgag, ctccggagaagtctcgtg, gtcctcagaagattcct, tctctcctcaatggtg, ttctgtttgcgacttgg, gctgctctgacttggata, cactgtctatggctcgtg, ctctgctgtaggactcaaa, ctgctcattccagggtcagc, cccagggcctctggttcaaa, gaactgatgaagtcagggc, gggaccacaggttttcaaaa, tgactcgtcaccatcaggt, atcggatataagggcagc, gctgctcaggtactgag, cagacgggtctcctcga, atctgtggaagtgagcagc, cgagtacataggtggcaatg, aaatacaggaagttggct, agatgtcgttaaacgcaaa, acagcattcacaagaagc, tatarctcagatgagggca, ctgagcctatgaagaagc, ggattgtagatcctcagctg, catggagctgcatgag, ttgagcaggtgcttcaaa.

**Analysis of spine morphology.** *Fmr1*<sup>-/-</sup> or WT neurons were transduced at 18 DIV with Sindbis virus (MOI of 1) expressing free GFP, the WT or mutated forms of GFP-FMRP for either 24 h (*Fmr1*<sup>-/-</sup> neurons), or 30 h (WT neurons) before use.

Cells were then fixed using PBS containing 3.7% formaldehyde and 5% sucrose for 1 h at RT and mounted in Mowiol before confocal examination.

**Confocal imaging.** For fixed cells, confocal images (1024 × 1024) were acquired with a ×63 oil immersion lens (numerical aperture NA 1.4) on an inverted TCS-SP5 confocal microscope (Leica Microsystems, Nanterre, France). Z-series of 6–8 images of randomly selected secondary dendrites were compressed into two dimensions using the maximum projection of the LASAF acquisition software (Leica). Manders' co-localization parameters were computed using the JaCoP plug-in from the ImageJ software<sup>66</sup> when required.

For GFP-FMRP-containing granule measurements, two Z-series were acquired. The first was acquired at low laser intensity to clearly identify large granules without any pixel saturation and the second series was recorded at a higher laser intensity to detect smaller granules. These two Z-series were then averaged and compressed into two dimensions by a maximal projection. Measurements of the surface of GFP-FMRP-containing granules along dendrites were determined automatically using a home-made ImageJ macro program. Briefly, granules and dendrites were segmented in each image, and the length of the dendritic tree was measured after a step of skeletonization. The data were then imported in GraphPad Prism software for statistical analysis.

For dendritic spine imaging, Z-series of six to eight images of secondary dendrites from GFP-expressing neurons were compressed into two dimensions by a maximal projection using the LASAF software. About 3000–4500 spines were analyzed per condition (two to four dendrites per neuron and from 20 to 30 neurons per condition from four independent experiments, which were done blind for two of them). At the time of acquisition, laser power was adjusted so that all spines were below the saturation threshold. To analyze dendritic protrusions, projection images were imported into NeuronStudio software<sup>67</sup>, which allows for the automated detection of immature and mature dendritic spines. The length of individual spines was automatically measured and data were imported in GraphPad Prism software for statistical analysis. Mature spines were characterized by a head diameter ranging from 0.3 to 1 μm and a spine length between 0.4 and 3 μm. Immature spines corresponded to protrusions with a head diameter below 0.3 μm and a spine length ranging from 0.5 to 6 μm.

**Fluorescence lifetime imaging experiments.** *Fmr1*<sup>-/-</sup> neurons co-expressing mCherry with the WT or the non-sumoylatable mutant form of GFP-FMRP for 72 h were fixed in PBS containing 3.7% formaldehyde and 5% sucrose for 1 h at RT and mounted using Mowiol. FLIM was then performed on a Nikon A1R confocal laser-scanning microscope equipped with time-correlated single-photon counting electronics (PicoHarp 300; PicoQuant). Excitation was obtained using a pulsed laser LDH-D-C-485 (PicoQuant) at a repetition rate of 40 MHz allowing the acquisition of the full intensity decay. Fluorescence emission was collected by a hybrid photomultiplier detector (PicoQuant) through a 60 × λS, NA 1.4, oil objective (Nikon Instruments) and band-pass filter (520/35). The following parameters were kept constant for all acquisition: pixel size (70 nm, 512 × 512), pixel dwell time (4.8 μs), and acquisition time (5 min per image). So as to limit pile-up and to accumulate enough photons within the 5 min acquisition time, laser excitation power was adjusted to obtain a count rate between 0.4 and 2 MHz<sup>68</sup>. In these conditions, there was no measurable photobleaching. Each field of view was also acquired in conventional confocal mode. EGFP and mCherry channels were, respectively, acquired using the 488-nm excitation with the 525/50-nm band-pass detection and the 561-nm excitation with the 595/50-nm band-pass detection.

Fluorescence lifetime was measured by fitting the intensity decays with a monoexponential decay model reconvolved with experimental IRF (instrument response function) using the software SymPhoTime (PicoQuant). Intensity decays were fitted pixel by pixel to provide FLIM images and calculated lifetimes represented using a pseudo-color scale ranging from 1.7 to 2.2 ns. To improve robustness of the fit, IRF parameters were fixed as the IRF is expected to be invariant over the acquisition field. The robustness of the fit was assessed by the calculated standard weighted least square ( $\chi^2$ ) and the residual<sup>69</sup>. Values of the reduced  $\chi^2$  should be close to 1 and residue should be randomly distributed around zero. The average lifetime of the FLIM image (Tau, ns) was determined from the barycentre of the frequency histogram associated with the FLIM image. To calculate the fluorescence lifetime of individual granules, the intensity decay resulting from all the photons of the granule was fitted using a monoexponential model reconvolved with IRF.

To get enough photons at each pixel for an accurate intensity decay fit, only granules with >10,000 photons (integrated number of photons over the decay) were analyzed, with a minimum pixel threshold of 500 counts for background rejection. To reach 10,000 photons per granules and to reject granules, which were largely out of focus, only granules >0.35 μm<sup>2</sup> were analyzed (segmentation using ImageJ). To avoid pulse pile-up and to collect photons fast enough to meet the above criteria, count rate was kept between 0.4 and 4 MHz. Clusters with higher count rate were excluded from the analysis. In those conditions, the fluorescent lifetime was invariant.

**Dendra2-FMRP-containing granule photoconversion experiments.** Experiments were performed as previously described<sup>26,48</sup>. Briefly, live *Fmr1*<sup>-/-</sup> neurons

expressing the WT or mutated Dendra2-FMRP from were kept in Earle's buffer (25 mM HEPES-Tris, pH 7.4, 140 mM NaCl, 5 mM KCl, 1.8 mM CaCl<sub>2</sub>, 0.8 mM MgCl<sub>2</sub>, 0.9 g L<sup>-1</sup> glucose) on the heated stage (set at 37 °C) of a Nikon Ti inverted microscope and imaged using an ultraviolet spinning disk confocal system (Perkin Elmer, France). Cells were then stimulated or not with 50 μM DHPG in Earle's buffer. After a 10-min incubation time in either control or DHPG solution, Dendra2-FMRP-granules were photoconverted through a ×100/ NA 1.4 oil immersion objective for 30 ms using 405-nm laser light (50 mW, 15%). The red photoconverted Dendra2-FMRP was excited using a 561-nm laser light (50 mW, 17%) and two-dimensional-time series (2 Hz) were collected for 10 min. The decrease in red fluorescence from the Dendra2-FMRP photoconverted granules was measured over time using Volocity 6.3 software and data expressed as the percentage of the initial red photoconverted fluorescence ( $F/F_0$ ). Curves were fitted using a monoexponential decay equation and data analyzed using GraphPad Prism.

**GST- and His-FMRP production and purification.** GST- or His-FMRP (1–160) proteins were produced in *E. coli* BL21(DE3) cells (Invitrogen, France). A single colony was picked and used to inoculate 25 mL of LB broth supplemented with 50 μg mL<sup>-1</sup> ampicillin. This was used to inoculate 500 mL of LB and was shaken at 37 °C until OD<sub>600</sub> reached 0.8. Cells were then transferred at 20 °C and protein synthesis induced by addition of 1 mM IPTG (Sigma, France). After 4 h at 20 °C, cells were pelleted by centrifugation at 7000×g for 5 min and then gently resuspended in ice-cold PBS and frozen at -80 °C until use. Pellets were then resuspended in 5 mL lysis buffer (25 mM Tris-HCl pH 8, 300 mM KCl, 1 mM EDTA, 20% glycerol, 5% ETOH, 0.5% NP40, 0.5 M urea) supplemented with 1% protease inhibitor cocktail (Sigma-Aldrich, France). Cells were disrupted by incubation with 1% lysozyme (Sigma, France) for 30 min at 4 °C followed by another 30 min in the presence of 0.1% deoxycholic acid, 10 mM MgCl<sub>2</sub> and 200 ng μL<sup>-1</sup> DNase. Lysates were then clarified by centrifugation at 10,000×g for 15 min. GST- or His-tagged proteins were purified using either glutathione gel (GE Healthcare) for GST- and GST-FMRP or Nickel resin (Qiagen) for His-fusion proteins. Proteins were then concentrated on Amicon 3-kDa cutoff filters (Millipore) by centrifugation and resuspended in PBS. Concentrations of purified proteins were determined using the BCA protein assay (Bio-Rad) and protein quality assessed by SDS-PAGE and Coomassie Blue protein staining (Clinisciences).

**GST-FMRP/His-FMRP dimerization.** GST- (control) or GST-FMRP (1–160) fusion proteins (1 μg) were incubated with an excess of 2 μg His-FMRP (1–160) for 2 h at 4 °C in dimerization buffer (50 mM Tris-HCl pH 8, 150 mM NaCl, 2.5 mM MgCl<sub>2</sub>, 0.5% NP40, 0.5 mM DTT, 1% protease inhibitor cocktail) to allow for GST-FMRP/His-FMRP dimerization. Then, 50 μL of glutathione beads (GE Healthcare) were added to the dimerization mix and incubated at 4 °C for 2 h. After five washes in dimerization buffer at 4 °C, immobilized GST-FMRP (1–160)—His-FMRP (1–160) dimers were processed for in vitro sumoylation assays.

**In vitro SUMO assays.** Immobilized GST-FMRP/His-FMRP dimers were incubated with 0.15 μg of E1-activating complex (Enzo Life science), 0.1 μg of E2 Ubc9 (Enzo Life science), 3 μg of SUMO1-GG in 20 μL of in vitro SUMO reaction mix (20 mM HEPES pH 7.3, 110 mM KOAc, 2 mM Mg(OAc)<sub>2</sub>, 0.5 mM EGTA, 1 mM DTT 0.05% Tween 20, 0.2 mg mL<sup>-1</sup> ovalbumin) including the ATP regenerating system (20 mM ATP, 10 mM creatine phosphate, 3.5 U mL<sup>-1</sup> of creatine kinase, and 0.6 U mL<sup>-1</sup> of inorganic pyrophosphatase (Sigma-Aldrich) for 2 h at 30 °C). After centrifugation for 5 min at 3000×g at 4 °C, the supernatant containing the released His-FMRP (1–160) and the pellet containing the remaining immobilized GST-FMRP/His-FMRP dimers were denatured at 95 °C for 10 min in 5× Laemmli buffer containing 7.5% β-mercaptoethanol and analyzed by immunoblotting with FMRP #2F5-1 antibodies.

**Electrophysiological recordings.** Patch clamp experiments were carried out at RT (22–25 °C) on mixed cultured cortical/hippocampal neurons obtained from *FMRP*<sup>-/-</sup> mice (four different cultures). *FMRP*<sup>-/-</sup> neurons (18 DIV) were transfected for 24–26 h with attenuated Sindbis virus to express GFP-FMRP WT or the non-sumoylatable GFP-FMRP-K88,130,614R. Patch pipettes displayed a resistance of 4–7 MΩ and filled with a solution containing (in mM): 2 Na<sub>2</sub>-ATP, 130 CsMeSO<sub>4</sub>, 5 CsCl, 2.5 MgCl<sub>2</sub>, 1 Na-GTP, 5 EGTA, and 10 HEPES (pH adjusted to 7.2 with CsOH). The extracellular bathing solution contained (in mM): 145 NaCl, 5 KCl, 2 CaCl<sub>2</sub>, 2 MgCl<sub>2</sub>, 10 HEPES, 10 glucose, 0.02 bicuculline, and 0.00025 TTX (pH adjusted to 7.4 with NaOH). We used the whole-cell configuration to record mEPSCs from GFP-positive neurons that were voltage-clamped at -70 mV, i.e., the estimated reversal potential for chloride. mEPSCs were recorded for 10 min, starting 1–2 min after the whole-cell mode was achieved and series resistances were monitored every 50 s by injecting a 5 mV hyperpolarizing current for 10 ms. Data were sampled at 20 kHz, low-pass filtered at 5 kHz (Axopatch 200B Molecular Devices), digitalized (Digidata 1440, Molecular Devices) and recorded using Clampex software (pClamp 10, Molecular Devices). Analysis of series resistances and mEPSCs were performed offline using Clampfit software (pClamp 10, Molecular Devices). mEPSCs were analyzed over periods of 200 s for which series resistances were stable, i.e., did not vary for >25%.

**Data and statistical analysis.** Statistical analyses were calculated using GraphPad Prism (GraphPad software, Inc). All data are expressed as mean ± s.e.m. Unpaired *t* test (Fig. 3i) or non-parametric Mann-Whitney test (Figs. 4c and 5d, f, g) were used to compare medians of two data sets. For spine morphogenesis experiments, values represent means ± s.e.m. Statistical significance for multiple comparison data sets was computed using a one-way analysis of variance with a Bonferroni post-test (Figs. 2b–d, 5e, 7b–d, and Supplementary Fig. 2b–d). Normality for all groups was verified using the Shapiro–Wilk test. According to the Levene variance test, variances were homogenous for the percentage of immature and mature spines (Figs. 2b–d, 7b–d, and Supplementary Fig. 2b–d). For FLIM, data distributions were represented as box and whiskers plots displaying upper and lower quartiles, and maximum and minimum values in addition to median. For electrophysiological data, distributions were analyzed by a Kolmogorov–Smirnov test (Supplementary Fig. 3b, c). \**p* < 0.05 was considered significant.

**Data availability.** All relevant data are available from the corresponding author upon reasonable request.

Received: 25 July 2017 Accepted: 28 January 2018

Published online: 22 February 2018

## References

1. Penzes, P., Cahill, M. E., Jones, K. A., VanLeeuwen, J. E. & Woolfrey, K. M. Dendritic spine pathology in neuropsychiatric disorders. *Nat. Neurosci.* **14**, 285–293 (2011).
2. Grant, S. G. Synaptopathies: diseases of the synaptome. *Curr. Opin. Neurobiol.* **22**, 522–529 (2012).
3. Bassell, G. J. Fragile balance: RNA editing tunes the synapse. *Nat. Neurosci.* **14**, 1492–1494 (2011).
4. Darnell, J. C. & Klann, E. The translation of translational control by FMRP: therapeutic targets for FXS. *Nat. Neurosci.* **16**, 1530–1536 (2013).
5. Maurin, T., Zongaro, S. & Bardoni, B. Fragile X syndrome: from molecular pathology to therapy. *Neurosci. Biobehav. Rev.* **46**, 242–255 (2014).
6. Grossman, A. W., Elisseou, N. M., McKinney, B. C. & Greenough, W. T. Hippocampal pyramidal cells in adult *Fmr1* knockout mice exhibit an immature-appearing profile of dendritic spines. *Brain Res.* **1084**, 158–164 (2006).
7. Patel, A. B., Loerwald, K. W., Huber, K. M. & Gibson, J. R. Postsynaptic FMRP promotes the pruning of cell-to-cell connections among pyramidal neurons in the L5A neocortical network. *J. Neurosci.* **34**, 3413–3418 (2014).
8. Yan, Z., Kim, E., Datta, D., Lewis, D. A. & Soderling, S. H. Synaptic actin dysregulation, a convergent mechanism of mental disorders? *J. Neurosci.* **36**, 11411–11417 (2016).
9. Bakker, C. E. *Fmr1* knockout mice: a model to study fragile X mental retardation. The Dutch-Belgian Fragile X Consortium. *Cell* **78**, 23–33 (1994).
10. Mientjes, E. J. et al. The generation of a conditional *Fmr1* knock out mouse model to study *Fmrp* function in vivo. *Neurobiol. Dis.* **21**, 549–555 (2006).
11. Narayanan, U. et al. FMRP phosphorylation reveals an immediate-early signaling pathway triggered by group I mGluR and mediated by PP2A. *J. Neurosci.* **27**, 14349–14357 (2007).
12. Niere, F., Wilkerson, J. R. & Huber, K. M. Evidence for a fragile X mental retardation protein-mediated translational switch in metabotropic glutamate receptor-triggered Arc translation and long-term depression. *J. Neurosci.* **32**, 5924–5936 (2012).
13. Hou, L. et al. Dynamic translational and proteasomal regulation of fragile X mental retardation protein controls mGluR-dependent long-term depression. *Neuron* **51**, 441–454 (2006).
14. Nalavadi, V. C., Muddashetty, R. S., Gross, C. & Bassell, G. J. Dephosphorylation-induced ubiquitination and degradation of FMRP in dendrites: a role in immediate early mGluR-stimulated translation. *J. Neurosci.* **32**, 2582–2587 (2012).
15. Matunis, M. J., Coutavas, E. & Blobel, G. A novel ubiquitin-like modification modulates the partitioning of the Ran-GTPase-activating protein RanGAP1 between the cytosol and the nuclear pore complex. *J. Cell Biol.* **135**, 1457–1470 (1996).
16. Mahajan, R., Delphin, C., Guan, T., Gerace, L. & Melchior, F. A small ubiquitin-related polypeptide involved in targeting RanGAP1 to nuclear pore complex protein RanBP2. *Cell* **88**, 97–107 (1997).
17. Flotho, A. & Melchior, F. Sumoylation: a regulatory protein modification in health and disease. *Annu. Rev. Biochem.* **82**, 357–385 (2013).
18. Henley, J. M., Craig, T. J. & Wilkinson, K. A. Neuronal SUMOylation: mechanisms, physiology, and roles in neuronal dysfunction. *Physiol. Rev.* **94**, 1249–1285 (2014).
19. Schorova, L. & Martin, S. Sumoylation in synaptic function and dysfunction. *Front. Synaptic Neurosci.* **8**, 9 (2016).

20. Hickey, C. M., Wilson, N. R. & Hochstrasser, M. Function and regulation of SUMO proteases. *Nat. Rev. Mol. Cell Biol.* **13**, 755–766 (2012).
21. Kerscher, O. SUMO junction-what's your function? New insights through SUMO-interacting motifs. *EMBO Rep.* **8**, 550–555 (2007).
22. Meulmeester, E. & Melchior, F. Cell biology: SUMO. *Nature* **452**, 709–711 (2008).
23. Gwizdek, C., Casse, F. & Martin, S. Protein sumoylation in brain development, neuronal morphology and spinogenesis. *Neuromol. Med.* **15**, 677–691 (2013).
24. Loriol, C., Parisot, J., Poupon, G., Gwizdek, C. & Martin, S. Developmental regulation and spatiotemporal redistribution of the sumoylation machinery in the rat central nervous system. *PLoS ONE* **7**, e33757 (2012).
25. Loriol, C., Khayachi, A., Poupon, G., Gwizdek, C. & Martin, S. Activity-dependent regulation of the sumoylation machinery in rat hippocampal neurons. *Biol. Cell* **105**, 30–45 (2013).
26. Loriol, C. et al. mGlu5 receptors regulate synaptic sumoylation via a transient PKC-dependent diffusional trapping of Ubc9 into spines. *Nat. Commun.* **5**, 5113 (2014).
27. Girach, F., Craig, T. J., Rocca, D. L. & Henley, J. M. RIM1 $\alpha$  SUMOylation is required for fast synaptic vesicle exocytosis. *Cell Rep.* **5**, 1294–1301 (2013).
28. Craig, T. J., Anderson, D., Evans, A. J., Girach, F. & Henley, J. M. SUMOylation of Syntaxin1A regulates presynaptic endocytosis. *Sci. Rep.* **5**, 17669 (2015).
29. Shalizi, A. et al. A calcium-regulated MEF2 sumoylation switch controls postsynaptic differentiation. *Science* **311**, 1012–1017 (2006).
30. Shalizi, A. et al. PIASx is a MEF2 SUMO E3 ligase that promotes postsynaptic dendritic morphogenesis. *J. Neurosci.* **27**, 10037–10046 (2007).
31. Martin, S., Nishimune, A., Mellor, J. R. & Henley, J. M. SUMOylation regulates kainate-receptor-mediated synaptic transmission. *Nature* **447**, 321–325 (2007).
32. Chamberlain, S. E. et al. SUMOylation and phosphorylation of GluK2 regulate kainate receptor trafficking and synaptic plasticity. *Nat. Neurosci.* **15**, 845–852 (2012).
33. Craig, T. J. et al. Homeostatic synaptic scaling is regulated by protein SUMOylation. *J. Biol. Chem.* **287**, 22781–22788 (2012).
34. Sampson, D. A., Wang, M. & Matunis, M. J. The small ubiquitin-like modifier-1 (SUMO-1) consensus sequence mediates Ubc9 binding and is essential for SUMO-1 modification. *J. Biol. Chem.* **276**, 21664–21669 (2001).
35. Uchimura, Y., Nakao, M. & Saitoh, H. Generation of SUMO-1 modified proteins in *E. coli*: towards understanding the biochemistry/structural biology of the SUMO-1 pathway. *FEBS Lett.* **564**, 85–90 (2004).
36. Comery, T. A. et al. Abnormal dendritic spines in fragile X knockout mice: maturation and pruning deficits. *Proc. Natl Acad. Sci. USA* **94**, 5401–5404 (1997).
37. Zeier, Z. et al. Fragile X mental retardation protein replacement restores hippocampal synaptic function in a mouse model of fragile X syndrome. *Gene Ther.* **16**, 1122–1129 (2009).
38. Martin, S., Bouschet, T., Jenkins, E. L., Nishimune, A. & Henley, J. M. Bidirectional regulation of kainate receptor surface expression in hippocampal neurons. *J. Biol. Chem.* **283**, 36435–36440 (2008).
39. Xiong, H. et al. mTOR is essential for corticosteroid effects on hippocampal AMPA receptor function and fear memory. *Learn. Mem.* **22**, 577–583 (2015).
40. Xiong, H. et al. Interactions between N-ethylmaleimide-sensitive factor and GluA2 contribute to effects of glucocorticoid hormones on AMPA receptor function in the rodent hippocampus. *Hippocampus* **26**, 848–856 (2016).
41. Suvrathan, A., Hoeffler, C. A., Wong, H., Klann, E. & Chattarji, S. Characterization and reversal of synaptic defects in the amygdala in a mouse model of fragile X syndrome. *Proc. Natl Acad. Sci. USA* **107**, 11591–11596 (2010).
42. Scharkowski, F., Frotscher, M., Lutz, D., Korte, M., & Michaelsen-Preusse, K. Altered connectivity and synapse maturation of the hippocampal mossy fiber pathway in a mouse model of the fragile X syndrome. *Cereb. Cortex* <https://doi.org/10.1093/cercor/bhw408> (2017).
43. Gocel, J. & Larson, J. Synaptic NMDA receptor-mediated currents in anterior piriform cortex are reduced in the adult fragile X mouse. *Neuroscience* **221**, 170–181 (2012).
44. Ifrim, M. F., Williams, K. R. & Bassell, G. J. Single-molecule imaging of PSD-95 mRNA translation in dendrites and its dysregulation in a mouse model of fragile X syndrome. *J. Neurosci.* **35**, 7116–7130 (2015).
45. Kanai, Y., Dohmae, N. & Hirokawa, N. Kinesin transports RNA: isolation and characterization of an RNA-transporting granule. *Neuron* **43**, 513–525 (2004).
46. Elvira, G. et al. Characterization of an RNA granule from developing brain. *Mol. Cell. Proteom.* **5**, 635–651 (2006).
47. Adinolfi, S. et al. The N-terminus of the fragile X mental retardation protein contains a novel domain involved in dimerization and RNA binding. *Biochemistry* **42**, 10437–10444 (2003).
48. Casse, F. & Martin, S. Tracking the activity-dependent diffusion of synaptic proteins using restricted photoconversion of Dendra2. *Front. Cell. Neurosci.* **9**, 367 (2015).
49. Gurskaya, N. G. et al. Engineering of a monomeric green-to-red photoactivatable fluorescent protein induced by blue light. *Nat. Biotechnol.* **24**, 461–465 (2006).
50. Chudakov, D. M., Lukyanov, S. & Lukyanov, K. A. Tracking intracellular protein movements using photoswitchable fluorescent proteins PS-CFP2 and Dendra2. *Nat. Protoc.* **2**, 2024–2032 (2007).
51. Antar, L. N., Afroz, R., Dichtenberg, J. B., Carroll, R. C. & Bassell, G. J. Metabotropic glutamate receptor activation regulates fragile X mental retardation protein and FMR1 mRNA localization differentially in dendrites and at synapses. *J. Neurosci.* **24**, 2648–2655 (2004).
52. Dichtenberg, J. B., Swanger, S. A., Antar, L. N., Singer, R. H. & Bassell, G. J. A direct role for FMRP in activity-dependent dendritic mRNA transport links filopodial-spine morphogenesis to fragile X syndrome. *Dev. Cell* **14**, 926–939 (2008).
53. Chao, H. W., Hong, C. J., Huang, T. N., Lin, Y. L. & Hsueh, Y. P. SUMOylation of the MAGUK protein CASK regulates dendritic spinogenesis. *J. Cell. Biol.* **182**, 141–155 (2008).
54. Ceman, S. et al. Phosphorylation influences the translation state of FMRP-associated polyribosomes. *Hum. Mol. Genet.* **12**, 3295–3305 (2003).
55. Narayanan, U. et al. S6K1 phosphorylates and regulates fragile X mental retardation protein (FMRP) with the neuronal protein synthesis-dependent mammalian target of rapamycin (mTOR) signaling cascade. *J. Biol. Chem.* **283**, 18478–18482 (2008).
56. Quartier, A. et al. Intragenic FMR1 disease-causing variants: a significant mutational mechanism leading to fragile-X syndrome. *Eur. J. Hum. Genet.* **25**, 423–431 (2017).
57. Myrick, L. K. et al. Fragile X syndrome due to a missense mutation. *Eur. J. Hum. Genet.* **22**, 1185–1189 (2014).
58. Myrick, L. K. et al. Independent role for presynaptic FMRP revealed by an FMR1 missense mutation associated with intellectual disability and seizures. *Proc. Natl Acad. Sci. USA* **112**, 949–956 (2015).
59. Hu, Y. et al. The amino-terminal structure of human fragile X mental retardation protein obtained using precipitant-immobilized imprinted polymers. *Nat. Commun.* **6**, 6634 (2015).
60. Myrick, L. K., Hashimoto, H., Cheng, X. & Warren, S. T. Human FMRP contains an integral tandem Agenet (Tudor) and KH motif in the amino terminal domain. *Hum. Mol. Genet.* **24**, 1733–1740 (2015).
61. Richmond, T. J. Solvent accessible surface area and excluded volume in proteins. Analytical equations for overlapping spheres and implications for the hydrophobic effect. *J. Mol. Biol.* **178**, 63–89 (1984).
62. Cappadocia, L. et al. Structural and functional characterization of the phosphorylation-dependent interaction between PML and SUMO1. *Structure* **23**, 126–138 (2015).
63. Sittler, A., Devys, D., Weber, C. & Mandel, J. L. Alternative splicing of exon 14 determines nuclear or cytoplasmic localisation of fmr1 protein isoforms. *Hum. Mol. Genet.* **5**, 95–102 (1996).
64. Hafner, M. et al. Transcriptome-wide identification of RNA-binding protein and microRNA target sites by PAR-CLIP. *Cell* **141**, 129–141 (2010).
65. Khandjian, E. W. et al. Novel isoforms of the fragile X related protein FXR1P are expressed during myogenesis. *Hum. Mol. Genet.* **7**, 2121–2128 (1998).
66. Bolte, S. & Cordelières, F. P. A guided tour into subcellular colocalization analysis in light microscopy. *J. Microsc.* **224**, 213–232 (2006).
67. Rodriguez, A., Ehlenberger, D. B., Dickstein, D. L., Hof, P. R. & Wearne, S. L. Automated three-dimensional detection and shape classification of dendritic spines from fluorescence microscopy images. *PLoS ONE* **3**, e1997 (2008).
68. Becker, W. et al. Fluorescence lifetime imaging by time-correlated single-photon counting. *Microsc. Res. Tech.* **63**, 58–66 (2004).
69. Lakowicz, J. R. Principles of frequency-domain fluorescence spectroscopy and applications to cell membranes. *Subcell. Biochem.* **13**, 89–126 (1988).

## Acknowledgements

We thank J. Henley, F. Melchior, G. Bossis, Y. Uchimura, and H. Saitoh for sharing DNA plasmids and H. Leonhardt for the generous gift of mCherry antibodies. We gratefully acknowledge R. Willemsen (Rotterdam, NL) for the gift of *Fmr1*<sup>-/-</sup> mice. We also thank L. Davidovic and S. Zongaro for helpful discussion in the initial step of the work and F. Aguila for excellent artwork. We gratefully acknowledge the “Fondation pour la Recherche Médicale” (Equipe labellisée #DEQ20111223747 to S.M.; #DEQ20140329490 to B.B.; #DEQ20110421309 to E.D.), the “Agence Nationale de la Recherche” (ANR-15-CE16-0015-01 to S.M., ANR-12-BSV4-0020, ANR-12-SVSE8-0022, and ANR-15-CE16-0015-02 to B.B., ANR-13-BVS4-0009 to E.D.), the FRAXA foundation to T.M., the French Muscular Dystrophy Association AFM-Téléthon to E.D., the “Jérôme Lejeune” (S.M. and B.B.), and “Bettencourt-Schueller” (S.M.) foundations for financial support. We also thank the French Government for the “Investments for the Future” LabEx “SIGNALIFE” (ANR-11-LABX-0028-01), LabEx “ICST” (ANR-11-LABX-0015-01), the CNRS LIA “Neogenex” and the CG06 (AAP santé), GIS IBIISA (AO 2014) and Région PACA for the Microscopy and Imaging Côte d’Azur (MICA) platform funding. M.P., L.S., and S.C. are fellows from the international PhD “Signalife” LabEx program.

## Author contributions

A.K. performed the majority of fixed granule work and all the neuronal architecture imaging experiments and some biochemistry. C.G. performed most of the molecular cloning, bacterial sumoylation assays, some of the bioinformatic analyses, and some of the endogenous SUMO-protein work. A.K., C.L., F.C., L.S., A.F., M.P., M.Pro., and G.P. prepared neuronal cultures and biochemical tools. M.C. and E.D. performed and analyzed electrophysiology experiments. G.P. prepared viral particles and achieved the FMRP dimerization/sumoylation experiments. T.M. and A.K. performed and analyzed CLIP experiments. S.C. and T.M. performed calcium imaging. F.D.G. and F.B. performed and analyzed smFISH experiments. R.G. performed FMRP structural analysis with help from C.G., F.C., and S.M. performed live-cell imaging experiments. F.Br. provided computational tools to analyze imaging data. D.A. performed and analyzed FLIM experiments. B. B. provided some FMRP coding complementary DNAs and antibodies as well as input for the mRNA work. A.K., C.G., and S.M. contributed to hypothesis development, experimental design, and data interpretation. S.M. provided the overall supervision, the funding, and wrote the article. All authors discussed the data and commented on the manuscript.

## Additional information

**Supplementary Information** accompanies this paper at <https://doi.org/10.1038/s41467-018-03222-y>.

**Competing interests:** The authors declare no competing financial interests.

**Reprints and permission** information is available online at <http://npg.nature.com/reprintsandpermissions/>

**Publisher's note:** Springer Nature remains neutral with regard to jurisdictional claims in published maps and institutional affiliations.



**Open Access** This article is licensed under a Creative Commons Attribution 4.0 International License, which permits use, sharing, adaptation, distribution and reproduction in any medium or format, as long as you give appropriate credit to the original author(s) and the source, provide a link to the Creative Commons license, and indicate if changes were made. The images or other third party material in this article are included in the article's Creative Commons license, unless indicated otherwise in a credit line to the material. If material is not included in the article's Creative Commons license and your intended use is not permitted by statutory regulation or exceeds the permitted use, you will need to obtain permission directly from the copyright holder. To view a copy of this license, visit <http://creativecommons.org/licenses/by/4.0/>.

© The Author(s) 2018

# Publication 3

# HITS-CLIP in various brain areas reveals new targets and new modalities of RNA binding by fragile X mental retardation protein

Thomas Maurin<sup>1,2,\*</sup>, Kevin Lebrigand<sup>1,†</sup>, Sara Castagnola<sup>1,2</sup>, Agnès Paquet<sup>1</sup>, Marielle Jarjat<sup>1,2</sup>, Alexandra Popa<sup>3</sup>, Mauro Grossi<sup>1,2</sup>, Florence Rage<sup>4</sup> and Barbara Bardoni<sup>2,5,\*</sup>

<sup>1</sup>Université Côte d'Azur, CNRS, IPMC, 06560 Valbonne, France, <sup>2</sup>CNRS LIA « Neogenex », 06560 Valbonne, France, <sup>3</sup>Research Center for Molecular Medicine of the Austrian Academy of Sciences, A-1090 Vienna, Austria, <sup>4</sup>CNRS, Institut de Génétique Moléculaire, 34293 Montpellier, France and <sup>5</sup>Université Côte d'Azur, INSERM, CNRS, IPMC, 06560 Valbonne, France

Received February 15, 2018; Revised March 23, 2018; Editorial Decision March 27, 2018; Accepted March 29, 2018

## ABSTRACT

Fragile X syndrome (FXS), the most common form of inherited intellectual disability, is due to the functional deficiency of the fragile X mental retardation protein (FMRP), an RNA-binding protein involved in translational regulation of many messenger RNAs, playing key roles in synaptic morphology and plasticity. To date, no effective treatment for FXS is available. We searched for FMRP targets by HITS-CLIP during early development of multiple mouse brain regions (hippocampus, cortex and cerebellum) at a time of brain development when FMRP is most highly expressed and synaptogenesis reaches a peak. We identified the largest dataset of mRNA targets of FMRP available in brain and we defined their cellular origin. We confirmed the G-quadruplex containing structure as an enriched motif in FMRP RNA targets. In addition to four less represented motifs, our study points out that, in the brain, CTGKA is the prominent motif bound by FMRP, which recognizes it when not engaged in Watson-Crick pairing. All of these motifs negatively modulated the expression level of a reporter protein. While the repertoire of FMRP RNA targets in cerebellum is quite divergent, the ones of cortex and hippocampus are vastly overlapping. In these two brain regions, the *Phosphodiesterase 2a* (*Pde2a*) mRNA is a prominent target of FMRP, which modulates its translation and intracellular transport. This enzyme regulates the homeostasis of cAMP and

cGMP and represents a novel and attractive therapeutic target to treat FXS.

## INTRODUCTION

Fragile X mental retardation protein (FMRP) is an RNA binding protein (RBP) encoded by the fragile X mental retardation 1 (*FMR1*) gene whose silencing causes the fragile X syndrome (FXS), the most common form of intellectual disability and a leading genetic cause of autism. FMRP is involved in different steps of RNA metabolism, ranging from nuclear export to transport of mRNA along neurites and translational control in the soma as well as at synapses (1). FMRP deficiency impacts the size of brain regions, synaptogenesis and alters the morphology of dendritic spines as well as some forms of synaptic plasticity (2,3). To date, no specific and effective therapy is available for FXS. Current clinical approaches are focused on behavioral therapy and off-label medications that only mitigate a limited set of symptoms, such as hyperactivity, seizures or anxiety (4). Recent clinical trials based on antagonist of metabotropic glutamate Receptor 5 (mGlu5) and antagonist of GABA-B receptor were discontinued (5,6). The understanding of the physiopathology of FXS and the development of a specific therapy are intimately linked to the understanding of FMRP function and then to the identification of FMRP mRNA targets. For this reason, the search for molecular interactors (proteins and mRNAs) of FMRP has been very active (1). By using high-throughput sequencing-crosslinking immunoprecipitation (HITS-CLIP) on mRNAs associated with polyribosomes in whole brains of 11–25 day-old mice, 842 mRNAs were identified as targets of FMRP, likely during their

\*To whom correspondence should be addressed. Tel: +33 493 957 766; Fax: +33 493 957 708; Email: bardoni@ipmc.cnrs.fr  
Correspondence may also be addressed to Thomas Maurin. Tel: +33 493 957 762; Fax: +33 493 957 708; Email: maurin@ipmc.cnrs.fr  
†The authors wish it to be known that, in their opinion, the first two authors should be regarded as Joint First Authors.

translation (7). A phospho-activatable ribonucleoside CLIP (PAR-CLIP) analysis was also performed in a non-neuronal cell line (HEK) co-expressing FMRP endogenously and its inducible flag-tagged form that was immunoprecipitated together with 6,000 mRNAs (8). More recently, a CLIP study using microarray performed in 8-day *in vitro* cultured neurons resulted in the identification of one predominant mRNA target of FMRP (9). Nevertheless, it is not clear if most of these targets have a critical role in the physiopathology of FXS and in which cells they interact with FMRP.

Here, we used HITS-CLIP to identify FMRP targets at an early mouse developmental stage [postnatal day (PND) 13], when FMRP is most highly expressed (10,11) and synaptogenesis peaks (12). Our analysis resulted in the identification of the largest set of brain mRNA targets of FMRP to date. This allowed us to dissect the role of FMRP in different brain regions and cell types. On the basis of these findings we were able to identify a predominant motif bound by FMRP in brain and a prominent mRNA target that is a promising druggable pathway for this disorder.

## MATERIALS AND METHODS

### HITS-CLIP (high-throughput sequencing of RNA isolated by crosslinking immunoprecipitation)

The protocol was optimized following previously described published methods (13–16). Briefly, to isolate mRNAs associated with FMRP *in vivo*, UV-crosslinking and immunoprecipitations were performed on 100 mg of tissues grinded in liquid nitrogen. Powders were spread onto 60 mm dishes floating onto liquid nitrogen. RNAs and protein were crosslinked through three rounds of 254 nm UV irradiation (400 mJ each). IP was carried out as described previously with minor modifications (13–16). Crosslinked material was lysed in NP40 buffer [50 mM Hepes pH 7.6, 150 mM NaCl, 0.5% NP40, 1 mM NaF, 0.5 mM Dithiothreitol (DTT), proteases/phosphatases inhibitors (Pierce), RNaseOut (1:1000)] as described in Spitzer *et al.* (15). Debris were removed by centrifugation (10 min, 20 000 g, 4°C) and supernatants were incubated with RNaseI (0.01 u/μl; Ambion) for 15 min at 22°C. RNase digestion was stopped by the addition of SUPERase In RNase inhibitor (0.2 u/μl). For each assay, 15 μl of Rb11 polyclonal anti-FMRP antibody were bound to 50 μl of protein A dynabeads (Invitrogen) for each mg of protein lysate in the input. Salt concentration in the lysates was adjusted to 400 mM for 5 min then brought back to 150 mM. IP was carried out at 4°C for 4 h and ~2% of the input lysate and 10% of the immunoprecipitated material were saved for western blot analysis to check IP quality. Beads were washed once in NP40 buffer, washed once in high salt buffer (50 mM Hepes pH 7.6, 0.1% sodium dodecyl sulphate, 1 M NaCl, 1 mM ethylenediaminetetraacetic acid, 1% NP40) then twice again in NP40 buffer. Co-precipitated RNAs were dephosphorylated in PNK buffer (50 mM Tris pH 8, 100 mM NaCl, 10 mM MgCl<sub>2</sub>, 1 mM DTT) without ATP, then DTT was adjusted to 5mM and RNAs were labeled with gamma-<sup>32</sup>P-ATP and T4 Polynucleotide Kinase (PNK) (NEB). Beads were washed 5 times in PNK buffer without DTT complemented with 0.2% Tween 20. IP materials were resuspended in LDS (Invitrogen), heat-denatured

for 10 min at 70°C and separated on NuPage 4–12% gel, run in 3-(N-morpholino)propanesulfonic acid (MOPS) buffer. Ribonucleoprotein complex were transferred to nitrocellulose membrane with NuPage neutral transfer buffer (Invitrogen), washed with RNase free water (Ambion) and exposed to phosphorimager screens over night at –20°C. The area containing the specific radioactive signal corresponding to FMRP ribonucleoprotein complexes (100 to 130 kDa) was cut out of the membrane, sliced and digested with proteinase K (1 mg/ml) for 30 min at 56°C (Ambion) then urea concentration was adjusted to 3 M and the samples were further incubated for 10 min at 56°C (16). After purification, RNAs were cloned with the CleanTag Ligation Kit for Small RNA Library Prep (Trilink; adapter diluted <sup>1</sup>/<sub>4</sub>) according to the manufacturer's instructions, reverse transcribed with superscript II (Invitrogen) and amplified through 16–20 cycles of polymerase chain reaction (PCR) (NEB next).

### CLIP sequencing

CLIP samples have been sequenced on Ion torrent Proton and SOLiD WildFire. Due to the RNase digestion, fragments should fit the FMRP footprint and may contain adapter sequences at the 3' end of the reads. Using cutadapt (v1.2.1), reads were trimmed for the 5' adapter sequence present due to the Proton library construction protocol used (–front = TTCTACAGTCCGACGATC). Cutadapt was also used to trim for potential 3' adapter sequence (–adapter = TGGAATTCTCGGGTGCCAAGG, for Proton and –adapter = 33020103 for SOLiD reads). Trimmed reads with a length under 20 nt were discarded from further analysis to avoid ambiguous mapping. Remaining reads were aligned with bowtie (version 0.12.7) directly to refseq transcriptome (release 20161019) with ‘–best –strata –norc’. Custom Java class, based on Picard Java API, was used to discard reads mapping to more than one unique gene. Alignment files were filtered to discard PCR duplicates by keeping only one read per alignment start position taking into account possible stretch of soft clipped bases at the start of the reads. Resulting reads are called fragments and represent the total signal of CLIP experiments aiming at the detection of the FMRP binding sites. The CLIP signal per sample is presented in Supplementary Table S1. Results of the various filtering steps are presented in Supplementary Table S2.

### Peak calling and motif detection

FMRP binding sites were identified with Pyicoclip from Pyicoteo Tools Suite (17), that was applied independently for all the samples. Bam files with no multi gene hit reads filtered for PCR duplicates were converted to Bed file with bedtools2 BamToBed and then provided to pyicoclip for peak calling on the whole mouse transcriptome described in refseq (release 19 October 2016). We started from the unfiltered list of peaks detected by pyicoclip, processed the file to filter peaks with <2 fragments counts and removed the peaks present in mir, RNU, Sno Rny, mitochondrial and riken sequences. Given the large amount of splice variants described in refseq for each gene we generated a method to

remove peaks called in different splice variants of the same gene and identifying the same genomic region using a custom perl script. We finally called a total of 18.124 peaks across all samples. We gathered all peaks in a unique file and removed peaks identifying the same genomic region with the same custom perl script previously used. We finally identified a total of 18.124 peaks (8962, 5082, 4080 peaks for CB, HC and CX, respectively) that we used to feed to the motif detection software DREME (Meme release 4.10.1) using ‘–norc –m 5’ parameter in order to identify enriched motifs within our sets of peaks. Genebank annotations were used to annotate the coding sequence (cds) and the untranslated regions for each mRNA to map G-4 regions and FMRP binding sites.

### Motifs fold analysis

*In vivo* DMS-mediated RT stop scores were computed as previously described (18) for each base of transcripts. We then mapped the 14.376 peaks (FMRP binding sites) and computed unpairing scores for motifs contained in FMRP binding sites or for the same motif in the same transcript outside of an FMRP binding site. Only transcripts for which we detected 100% base coverage for all motifs in a given transcript in the DMS\_vitro\_95C condition were processed for folding analysis in the three replicates of mESC\_DMS\_vivo conditions.

### Codon analysis

Codon composition of FMRP binding site in the cds regions was analyzed according to the following formula  $\text{PauseScore} = (\text{Reads}_{\text{codon/orf}} / \text{Reads}_{\text{ORF}}) / (\text{Nbr}_{\text{codon/ORF}} / \text{Length}_{\text{ORF}})$ . In which  $\text{Reads}_{\text{codon/orf}}$  = number of reads covering a given codon for a given ORF,  $\text{Reads}_{\text{ORF}}$  = number of reads covering the ORF,  $\text{Nbr}_{\text{codon/ORF}}$ : number of a given codon in a given ORF and  $\text{Length}_{\text{ORF}}$ : the length of the ORF.

### G-quadruplex (G-4) mapping

Presence of a G-4 structure in the various RNAs was assessed by reverse transcriptase-mediated primer extension based on a previously described protocol (19) with some modifications. The DNA sequence of interest was PCR amplified and subcloned into pGEM-T easy vector. The insertion was verified by sequencing and the sequence of interest was PCR amplified with the following primers (T7invitroT; 5'-GACTGACTTAATACGACTCACTATA GGG-3'; M13Rev; 5'-CACACAGGAAACAGCTATGA C -3'). Electropherograms were generated and analyzed with the QuShape software (20).

### Single cell dataset analysis

Mouse cortex and hippocampus single cell RNAseq data from Zeisel *et al.* (21) was downloaded from their website (<http://linnarssonlab.org/cortex/>) and analyzed using the R package Seurat. Raw RNA molecule counts (i.e. unique molecule identifier counts, UMI) were downloaded from <http://linnarssonlab.org/cortex/>. Count data were normalized to the median count, then log2 transformed. For each

organ, among all FMRP targets identified, the most variable genes between all cell types were selected using a coefficient of variation cut-off of 0.7 and an average expression value >0.2. This resulted in the selection of 74 FMRP target genes for hippocampus and 58 FMRP target genes for cortex. These genes were then used as input for unsupervised hierarchical analysis. Hierarchical clustering and heatmaps of gene expression were generated using the R package pheatmap. Selected genes were clustered using the Ward.D clustering method and the Pearson correlation as distance. Cells were ordered by cell types using the level 1 classification provided with the original data. For each cell type, a list of genes differentially expressed was determined using the FindMarkers function from the R package Seurat, with parameters *thresh.use* = 1 and *min.pct* = 0.25. For each cell type, the 30 genes with highest *P*-values were used for enrichment analysis. Enrichment in FMRP targets by cell types was assessed using hypergeometric test. All *P*-values were adjusted for multiple testing using the Benjamini–Hochberg correction.

### RT-qPCR

quantitative PCR (qPCR) was performed on a Light Cycler 480 (Roche) with MasterMix SYBRGreen (Roche) following the manufacturer's instructions and according to the MIQE guidelines (22). Primer sequences are reported in Supplementary Table S3.

### Synaptosomes purification

Synaptosomes fractions were prepared by centrifugation on sucrose density gradients. Mouse PND13 cortices were homogenized in sucrose buffer (0.32 M sucrose, 10 mM Tris–HCl, pH 7.4) in a 7× weight/volume ratio. The homogenates were centrifuged at 1000 g for 5 min at 4°C. The supernatants were brought to a final volume of 2 ml with sucrose buffer and carefully placed on sucrose-percoll 2–6–10–20% non-continuous density gradients. The gradients were ultracentrifuged at 18 000 rpm for 10 min at 4°C with slow brake, and the crude synaptosomal fractions, placed between 10 and 20% sucrose-percoll, were carefully recovered with a glass pipette pre-coated with sucrose buffer. The crude synaptosomal fractions were diluted to 10 ml with Hepes buffer (140 mM NaCl, 3 mM KCl, 1.2 mM MgSO<sub>4</sub>, 1.2 mM CaCl<sub>2</sub>, 1 mM NaH<sub>2</sub>PO<sub>4</sub>, 5 mM NaHCO<sub>3</sub>, 10 mM glucose, 5 mM Hepes, pH 7.4 at 37°C) and centrifuged at 10 000 g for 30 min at 4°C with full brake. The pellets were resuspended in NP40 lysis buffer (1 M Tris–HCl, 3 M NaCl, 12 mM MgCl<sub>2</sub>, 0,1 M DTT, 1% NP40), centrifuged full speed for 10 min at 4°C and then resuspended in sodium dodecyl sulphate-polyacrylamide gel electrophoresis (SDS-PAGE) buffer.

### Polyribosome fractionation

Polyribosome fractionation was performed as described previously (23) on 20–50% (w/w) continuous sucrose gradients. Fractions were separated on a BR-188 Density Gradient Fractionation System (Brandel). Fold changes in *Tbp* and *Pde2a* mRNA levels were assessed by RT-qPCR and

were calculated for individual fraction 8 to 14 according to the  $2^{-\partial Cp}$  formula for which  $\partial Cp$  is ( $Cp_{gene_x}$  KO fraction<sub>n</sub> –  $Cp_{gene_x}$  WT fraction<sub>n</sub>). Results from fractions 6 to 8 (Light), 9 to 11 (Medium) and 12–14 (Heavy) were pooled and analyzed together.

### Protein extraction and western blot analysis

Immunoblot was performed as follows: cells or grinded tissues were homogenized in NP40 buffer, debris were removed by centrifugation (20 000 g, 10 min, 4°C). Protein content in the supernatant was measured using the Bradford assay (Biorad) and samples were separated on NuPage bis-tris 4–12% gels in MOPS buffer. Separated proteins were transferred to nitrocellulose membranes (Biorad). Membranes were blocked with phosphate-buffered saline-Tween (0.05%) and milk (5%). Primary antibodies were incubated overnight. Antibody Rb11 was generated by immunization of rabbits with a truncated FMRP protein corresponding to its C-terminal region, as previously described (10). Rb11 was used at the dilution of 1:500 for Western blot. Monoclonal 1C3 anti-FMRP antibody (24) was used at the dilution 1:1000; mouse polyclonal anti-FMRP 1R was used at the dilution 1:1000 (11). Anti PDE2A (Fabgennix, # PD2A-101AP), PSD95 (Millipore, AB9708), Anti-rpS6 (Cell signaling Technology, 54D2) anti  $\beta$ -Actin (Sigma, clone AC-74).

### Cloning of cDNA fragments corresponding to FMRP binding sites

We cloned fragments bound by FMRP. These fragments were cloned by PCR from mouse genomic DNA and inserted in the PmeI site of pSi-check2 (Promega). The sequences of the various constructs were verified by Sanger sequencing on an Applied Biosystems 3130XL and are provided in Supplementary Table S3.

### Luciferase assays

STEK cells, expressing or not FMRP were seeded in 96-wells plates (20 000 cells/well) and were immediately transfected with pSi-check2-derived constructs using Lipofectamine 2000 (Invitrogen) following the manufacturer's instructions. Renilla and firefly activities were measured with the Dual-glo luciferase assay (Promega) using the Glomax 96-wells plate luminometer (Promega).

### Probes, smFISH and image analysis

smFISH primary probes and FLAPs (secondary fluorescent probes) were produced and purchased from Integrated DNA Technologies (IDT) as described (25). Three-dimensional image stacks were captured on a wide-field microscope (Zeiss Axioimager Z1/Apotome) equipped with a 63 $\times$  objective and a CCD camera (AxioCam MRm 4), controlled with Metamorph (Molecular Devices). Spots in the Cy3 channels were detected in 3D stacks with Imaris (Bit-plane) and categorized as being labeled. Spots were split into different branching surfaces drawn by Imaris software (filament) or into cell bodies surfaces.

### Statistical analysis

Results are expressed as mean $\pm$ SEM. All statistical analyses were based on biological replicates. Appropriate statistical tests used for each experiment are described in the corresponding figure legends or in the 'Materials and Methods' section for HITS-CLIP. All statistical analyses were carried out using the GraphPad Prism Version 6.0e.

## RESULTS

### FMRP target RNAs in different mouse brain areas

We purified a new polyclonal antibody, Rb#11 and showed that it efficiently pulls down FMRP and recognizes FMRP in Western blot (Supplementary Figure S1A and B). We then set up the CLIP conditions adapting a procedure from previous HITS-CLIP, PAR-CLIP and iCLIP assays (8,13,16). Specific brain regions (cortex, hippocampus and cerebellum) from Post Natal Day (PND) 13 male mice were grinded in liquid nitrogen into fine powder, UV crosslinked (lanes Ab- and XL), and proteins solubilized in NP40 buffer (Figure 1A). After RNaseI treatment, FMRP was immunoprecipitated and bound RNAs were radioactively labeled. Ribonucleoprotein complexes (RNPs) were separated by SDS-PAGE and transferred to a nitrocellulose membrane. Radiolabeled RNPs were detected by autoradiography (Figure 1A, upper panel). The same membrane was subsequently analyzed by Western blot to detect FMRP (Figure 1A, bottom panel). We observed that an increased amount of FMRP/fragmented RNA complex is immunoprecipitated after cross-link (XL), compared to the no XL (XL-) condition (Figure 1A)—an example using immunoprecipitated FMRP from cortex is shown), while no FMRP and FMRP-containing RNPs were detected in the control lane Ab- (without antibody). We selected a set of previously described target mRNAs of FMRP (*Grin2a*, *Map1b* and *Ppp2ca*) and some control RNAs (*Gapdh* and *Tbp*). In the absence of RNase treatment, we analyzed their relative enrichment by RT-qPCR in immunoprecipitated mRNAs from wild-type (WT) and compared them with immunoprecipitated mRNAs from *Fmr1*-KO cortices (Figure 1B), confirming the specificity of co-immunoprecipitated target mRNAs of FMRP. We then performed HITS-CLIP, sequenced co-immunoprecipitated cross-linked fragments. The size distribution of the mapped reads was consistent with a protection from RNase degradation since we could observe reads longer than 40 nt (see an example Supplementary Figure S1C). We repeated this assay twice for cerebellum, three times for cortex and four times for hippocampus. The correlation in the fragment counts per gene from replicate experiments showed the robustness of the experimental protocol (Supplementary Figure S1D). We mapped 712 000 unique reads to the latest ref seq assembly (NCBI ftp web server ref10/2016). We used pyico clip (17) to identify FMRP binding sites, referred thereafter as peaks, resulting in the identification of 14 376 peaks corresponding to 4.174 RNA targets (Supplementary Table S1). A total of 288 of our hits overlap with deregulated synaptic proteins identified in the cortex of young *Fmr1*-null mice (26) (Figure 1C). Approximately one-fourth of the FMRP targets we identified were previously described as distantly

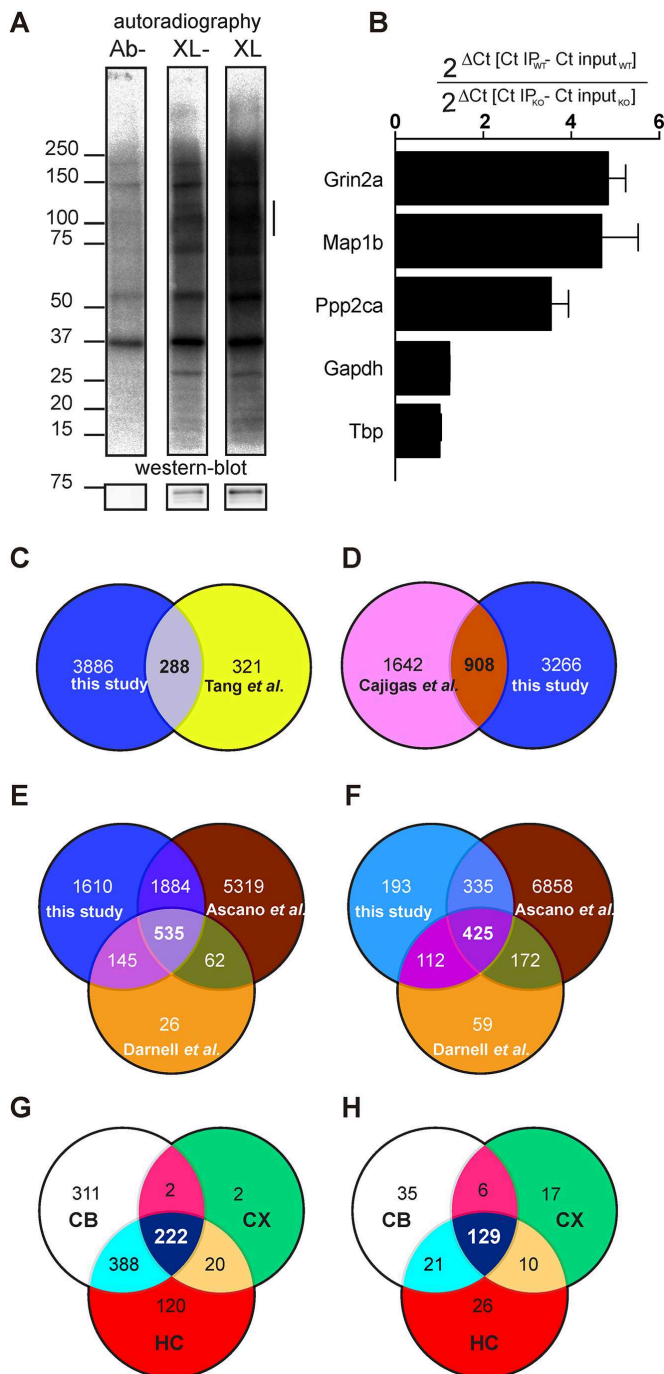


**Figure 1.** Identification of mRNA targets of FMRP. (A) Upper panel: autoradiography of immunoprecipitated UV-crosslinked RNPs from 13 PND male mouse brain cortex extracts after separation on a SDS-PAGE gel and then transferred onto a nitrocellulose membrane. Ab-: immunoprecipitation in the absence of the polyclonal anti-FMRP antibody Rb#11; XL-: Immunoprecipitation in the presence of Rb#11, but without UV-crosslink; XL: Immunoprecipitation in the presence of both Rb#11 and UV cross-link. Bottom panel: the presence of FMRP on the nitrocellulose membrane was revealed by immunoblot using the monoclonal anti-FMRP IR antibody. On the left, the apparent molecular weights (kDa) of proteins and RNPs are indicated. On the right, the presence of RNPs coimmunoprecipitated with FMRP in a dose-dependent manner but absent in the control lane (Ab-) is indicated by a vertical line. (B) Levels of RNA targets co-immunoprecipitated with FMRP were measured by qRT-PCR. *Grin2a*, *Map1b*, *Ppp2ca*, were the positive controls of this CLIP and

transported RNAs in hippocampus neuropils of rats (Figure 1D) (27), which is consistent with the role of FMRP in RNA transport in specialized cells. Our target mRNA repertoire clearly shows some similarity with datasets obtained by other groups (Figure 1E and Supplementary Table S1) as it shares 680 hits with the list of FMRP target mRNAs associated with brain polyribosomes (13) and 2419 hits with the FMRP target list in Human Embryonic Kidney (HEK) 293 cells (8) (Figure 1E). Taking in consideration only those having at least 50 fragments (counts) co-immunoprecipitated with FMRP, we found a total of 1065 targets (Supplementary Table S4 and Figure 1F), among them 872 are overlapping with previous studies (Figure 1F) (8,13). Considering our most stringent analysis, we identified 192 new RNA targets of FMRP. Further strengthening the interest of a tissue-specific CLIP approach, 80 these new targets were found specifically in the cerebellum and 36 in the hippocampus. To identify signaling pathways regulated by FMRP in the brain, we performed Gene Ontology analysis of its target RNAs in the cortex, hippocampus and cerebellum using Ingenuity Pathway Analysis (IPA) by considering the most restricted number of targets (Supplementary Table S5). Even if most of these mRNAs are common to the various brain areas (Figure 1G), specific pathways are regulated in each brain region (Figure 1H and Supplementary Table S5). We also took advantage of the recent publication of single-cell transcriptomic datasets and compared our dataset with the recent single cell transcriptomic analysis in the somatosensory cortex and the hippocampus (21) and observed that FMRP target RNAs are mostly expressed in neuronal cells (interneurons and pyramidal cells) in the cortex and the hippocampus (Supplementary Figure S2A and B). Cumulative Distribution analysis shows that mRNA targets carrying a G-4 forming motif, or encoded by autism-related genes (autismdb; <https://gene.sfari.org/autdb/Welcome.do>) are amongst the best targets of FMRP (Figure 2A and Supplementary Table S1). Target mRNAs harboring at least one peak are also enriched in the immuno-precipitated material compared to those devoid of any FMRP binding site (Figure 2A).

showed a significant enrichment according to one sample *t*-test. *Gapdh* and *Tbp*, two RNA that are not targeted by FMRP were used as negative controls. (C-E) Schematic representation of the shared identified FMRP targets between our HITS-CLIP dataset and (C) proteins that were previously described to be differentially localized in cortical synaptosomes between WT and *Fmr1*-KO mice and (D) mRNAs localized at the neuropil of rat CA1. (E) FMRP targets previously identified by CLIP analysis using polyribosome-associated RNAs and RNAs obtained by HEK-293 cells expressing an inducible and tagged FMRP. (F) Schematic representation of the shared identified FMRP targets between our HITS-CLIP restricted (only 50 counts) dataset and FMRP targets previously identified by CLIP analysis using polyribosome-associated RNAs and RNAs obtained by HEK-293 cells expressing an inducible and tagged FMRP. (G) Schematic representation of shared FMRP targets (restricted dataset) in the cortex (CX), hippocampus (HC) and cerebellum (CB). (H) Schematic representation of shared regulated pathways identified by Ingenuity Pathways analysis of FMRP targets in the cortex (CX), hippocampus (HC) and cerebellum (CB). See Supplementary Table S5 for details.



### Motifs bound by FMRP

Consistent with previous studies we found that FMRP mostly binds cds regions of mRNA (59–68% of our identified FMRP binding sites) and 25–37% of FMRP binding sites are present in the 3'UTRs (Supplementary Figure S3A). Interestingly, one of the peaks overlaps with the *Fmr1* G-4-forming structure, a site that has been described previously as bound by FMRP (19). We thus analyzed the folding of the peaks sequences with RNA fold (28) and identified 208 peaks overlapping strong RT-stop regions described in Guo *et al.*, (18). We could also identify 149 G-4-forming structures, according to RNAfold (28), that are strikingly enriched in the CLIPed RNA (Figure 2A). These RNA structures were predominantly located in cds sequences (49.7%) of FMRP target mRNA, but G-4 are strikingly more abundant in 5'UTR compared to the other motifs we identified (23.5 versus 4.5–13%) (Supplementary Figure S3B). We validated *in vitro* the presence of G-4 forming structure in three of them (*Calm1*, *Pcdh9* and *Map2*) by fluorescent primer extension (Figure 2B).

We studied the peak sequences of the three analyzed tissues with DREME (29) and we identified a consensus CTGKA-based motif (Figure 2C), and other less prominent motifs (Figure 2C). Taking advantage of the recent structure-seq dataset in mouse embryonic stem cells (18) we could assess whether the motifs that we identified were engaged in Watson-crick pairing *in vivo*. Our analysis clearly shows that the CTGKA, the GWRGA and the TAY motifs present in FMRP binding sites are more accessible to DMS modification *in vivo* (Figure 2D) and *in vitro* (not shown) than the unbound cognate motifs present in the same transcripts. This shows that FMRP recognizes motifs that are presented in single stranded regions or loop sequences of stem loop structures, suggesting a combinatorial RNA binding modality by FMRP through both structure and sequence recognition (Figure 2D).

It was proposed that FMRP could stall ribosomes onto mRNA thereby reducing the translation of its targets (13). We reasoned that FMRP could achieve such an effect by binding to specific mRNA regions that contain sequences or structures that slow down ribosome progression. We computed a ribosome pause score based on the read coverage of each codon, normalized to its frequency in the ORF also considering the expression and length of the ORF. Our approach therefore computes FMRP binding on codons based on the context sequence and expression of the different ORFs. Our results show that while GC rich codons are underrepresented from these sequences the GAC codon is strikingly enriched in FMRP binding sites (Figure 2E). This latter observation is consistent with a recent report (30). However, to our knowledge, the GAC codon has not been shown to interfere with ribosome elongation speed.

### *Pde2a* mRNA is a prominent target of FMRP

We tested by RT-qPCR the enrichment of prominent CLIPed RNAs (*Pde2a*, *Cacna1a*, *Atp2b2*, *Grm4*, *Grik5*, *Shank1* and *Mef2c*) in addition to four positive controls (*Grin2a*, *Map1b*, *Ppp2ca* and *Sapap3*: RNAs that have been previously indicated as targets of FMRP) and three negative controls (*P0*, *Gapdh* and *Tbp*) (Figure 3) and we con-

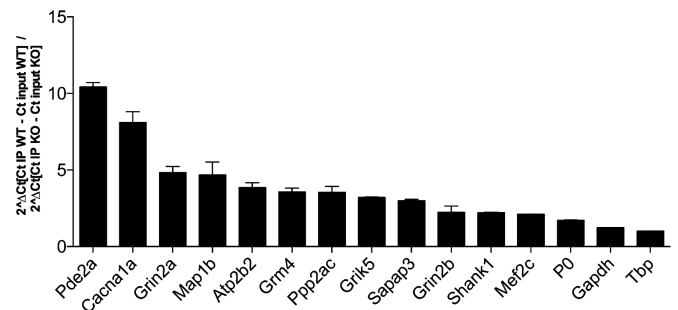


**Figure 3.** Validation of target mRNAs of FMRP. FMRP was immunoprecipitated from two independent UV-crosslinked assays. FMRP-associated RNAs were quantified by RT-qPCR. All RNAs except *P0*, *Gapdh* and *Tbp* (these mRNAs are not a target of FMRP) showed a significant enrichment according to one sample *t*-test.

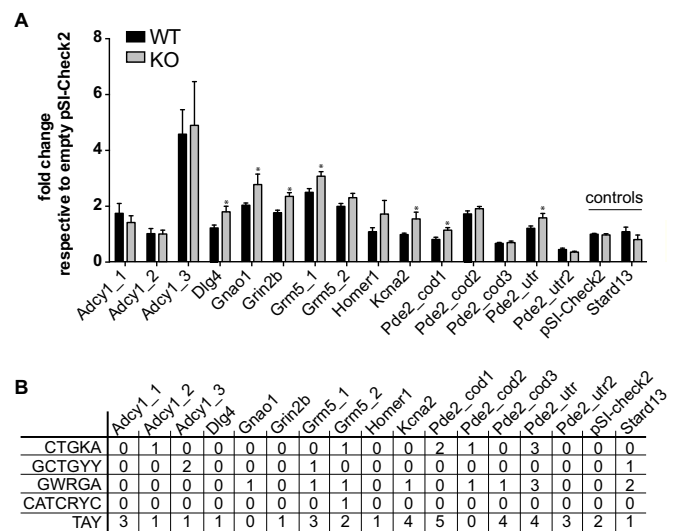


**Figure 4.** Role of RNA motifs bound by FMRP in translational regulation. (A) Influence of FMRP on luciferase reporter gene assay bearing motifs bound by FMRP or an unrelated control. pSI-CHECK-2 plasmids expressing Renilla carrying the various peak sequences in its' 3'-UTR were transfected in STEK cells expressing or not FMRP. At least three-independent experiments with two biological replicates, for each transfection were quantified. For each transfection Renilla luciferase activity was normalized with Firefly luciferase activity. Ratios for all conditions were divided by the mean of the ratio measured for the empty vector (pSI-CHECK-2). Results are presented as the mean  $\pm$ SEM (*t*-test, \**P* < 0.05). Empty vector and pSI-CHECK-2 carrying a sequence not bound by FMRP are named 'controls'. (B) Summary Table reporting the motifs present in the various sequence analyzed.

firming the results of CLIP. We sub-cloned in the 3'UTR of the luciferase reporter gene the peak sequence bound by FMRP in some of the best targets we identified and we transfected cell lines expressing or not *Fmr1* mRNA. As shown in Figure 4A and B, all the best motifs bound by FMRP behave by repressing the translation in the presence of FMRP. Indeed, in the absence of FMRP the activity of luciferase is increased when its mRNA is bound to one of the motifs we identified (Figure 4A). We could also verify by RT-qPCR that the relative levels of expression of the Renilla luciferase mRNA of each construct were identical in the presence and in the absence of FMRP (not shown) when

compared to the levels of the Firefly luciferase mRNA. The results we found using a reporter protein are consistent with the data of synaptic expression of the protein considered (26). For instance, PDE2A is overexpressed in the *Fmr1*-null cortical synapses of young mice [(26) and Figure 5] while the levels of Adenylate cyclase 1 are not different in the presence or in the absence of FMRP in the same extracts, even if its coding mRNA is bound by this protein. Suggesting that FMRP may modulate the metabolism of this mRNA in a step other than translation. We found that the *Pde2a* mRNA was the most enriched among the mRNAs co-immunoprecipitated with FMRP in cortex (Figure 3) and hippocampus (not shown). PDE2A is a phosphodiesterase involved in cAMP and cGMP degradation in various tissues including the brain (31–33). Interestingly, many of the pathways most represented in our IPA analysis are directly connected to cAMP/cGMP signaling and involve PDE2A (Supplementary Table S5). These findings suggest that the *Pde2a* mRNA is a crucial target of FMRP and may be involved in the physiopathology of FXS. While findings obtained using various approaches (34–37) highlight the presynaptic localization of PDE2A, we found that PDE2A is also post-synaptically located and partially co-localizes with PSD95 in dendritic spines of 17-day *in vitro* cultured cortical neurons (Supplementary Figure S4A). Furthermore, levels of *Pde2a* mRNA in cultured primary cortical neurons are increased *in vitro* upon neuron development (Supplementary Figure S4B). High-throughput sequencing showed that *Pde2a* mRNA levels are similar in the cortex of 13-day-old *Fmr1*-KO and WT mice (Supplementary Figure S4C) and, even if other PDEs are expressed in this brain area, *Pde2a* mRNA levels are the highest (Supplementary Figure S4C). An increased abundance of PDE2A was reported in synaptosomes prepared from the brain of mice at 17 days of age, but not at the adult age (26). Consistent with these results, we found that PDE2A protein levels are increased in highly purified synaptosomal fractions obtained from cortices and hippocampi of 13-day-old *Fmr1*-null mice compared with WT animals (Figure 5A, B). These data, together with the findings reported in Figure 4, suggested that FMRP negatively modulates the translation of the *Pde2a* mRNA. We thus carried out polyribosome fractionation on cortical extracts from 13-day-old WT and *Fmr1*-KO (Figure 5C) and measured *Pde2a* mRNA levels by RT-qPCR in pooled fractions (Figure 5D). We showed that, compared to WT cortical tissue, *Pde2a* mRNA is more abundantly associated with polyribosomes obtained from *Fmr1*-KO tissue. This result is consistent with an upregulated translation of this mRNA in the absence of FMRP. We assumed that a similar mechanism of FMRP-dependent regulation occurs in the hippocampus, since PDE2A levels are increased in *Fmr1*-KO hippocampi. To assess the implication of FMRP in the dendritic transport, the level of the *Pde2a* mRNA was measured by smFISH (38) both in WT and *Fmr1*-KO primary cortical neurons at 17 days *in vitro*. Compared to WT, the abundance of *Pde2a* mRNA was higher in neurites of *Fmr1*-KO neurons (Figure 5E–F) while no difference was observed in the soma (not shown). Collectively, these results strongly suggest that FMRP negatively modulates the translation of the *Pde2a* mRNA as well as its axonal/dendritic transport. An increased level of PDE2A is

predicted to impact on the intracellular amount of cAMP and cGMP both in cortex and hippocampus.

## DISCUSSION

Despite a wealth of research on FXS, the mechanistic action of FMRP (e.g. the RNA motifs that are targeted and the functional role of FMRP/RNA interaction) remains unclear and a specific and effective therapy for FXS is not yet available. With the purpose of addressing both of these issues, we define here a set of mRNA targets of FMRP at a critical step of postnatal development of the brain. We performed HITS-CLIP in mouse cerebellum, hippocampus and cortex at PND 13, when FMRP is most highly expressed (10,11) and the number of synapses reaches the highest level (12). We identified the largest set of FMRP mRNA targets in the mouse brain to date, including 1610 new targets, 57 of which have been previously linked to autism (SFARI list). Considering a restricted list of targets harboring at least 50 counts in the immunoprecipitated material from each tissue, we identified 193 new targets, 80 of which were found in the cerebellum IP and 36 in the hippocampus further illustrating the need to perform tissue-restricted CLIP analysis to identify a comprehensive set of FMRP RNA targets.

Indeed, another study considered only FMRP targets associated to polyribosomes (13), while we immunoprecipitated FMRP from various subcellular localizations. This confirms that FMRP is involved in functions other than translational regulation and suggests that this protein interacts with different RNAs at different steps of their metabolism. Indeed, we show here that FMRP negatively modulates both translation and transport of the *Pde2a* mRNA at the synapse. Overall, we identified fewer RNA targets than Ascano *et al.* (8) but their study used overexpression of FMRP in a cell line also expressing endogenous FMRP (8), overexpression that could have biased the mRNA binding repertoire of FMRP. Furthermore, even if HEK share a large proportion of their transcriptome with the brain tissue, the authors have probably identified RNA targets of FMRP that are not neuronally expressed.

## Molecular bases of FMRP/RNA interaction

The ACUK/WGGA motif (8) was previously shown to be necessary (at least in HEK cells) but not sufficient to mediate FMRP/RNA interaction (1,39,40). Our dataset shows an enrichment of G-4-forming structures in FMRP-bound RNA fragments, which further confirms the role of G-4 in mediating FMRP/RNA interaction. However, as now clearly established, not all FMRP mRNA targets harbor this motif (41). Indeed, we identified here a novel and very significantly enriched consensus motif (CTGKA) bound by FMRP, suggesting that we defined the prominent RNA motif driving FMRP-dependent translation modulation in brain. Among the less prominent motifs we found, two of them (TAY and GWRGA) are very similar to those identified by another study (30) combining results from the two previous CLIP assays (8,13). However, the other motifs we found appear specific to our study, suggesting that our approach (in different brain areas), combined with an anti-

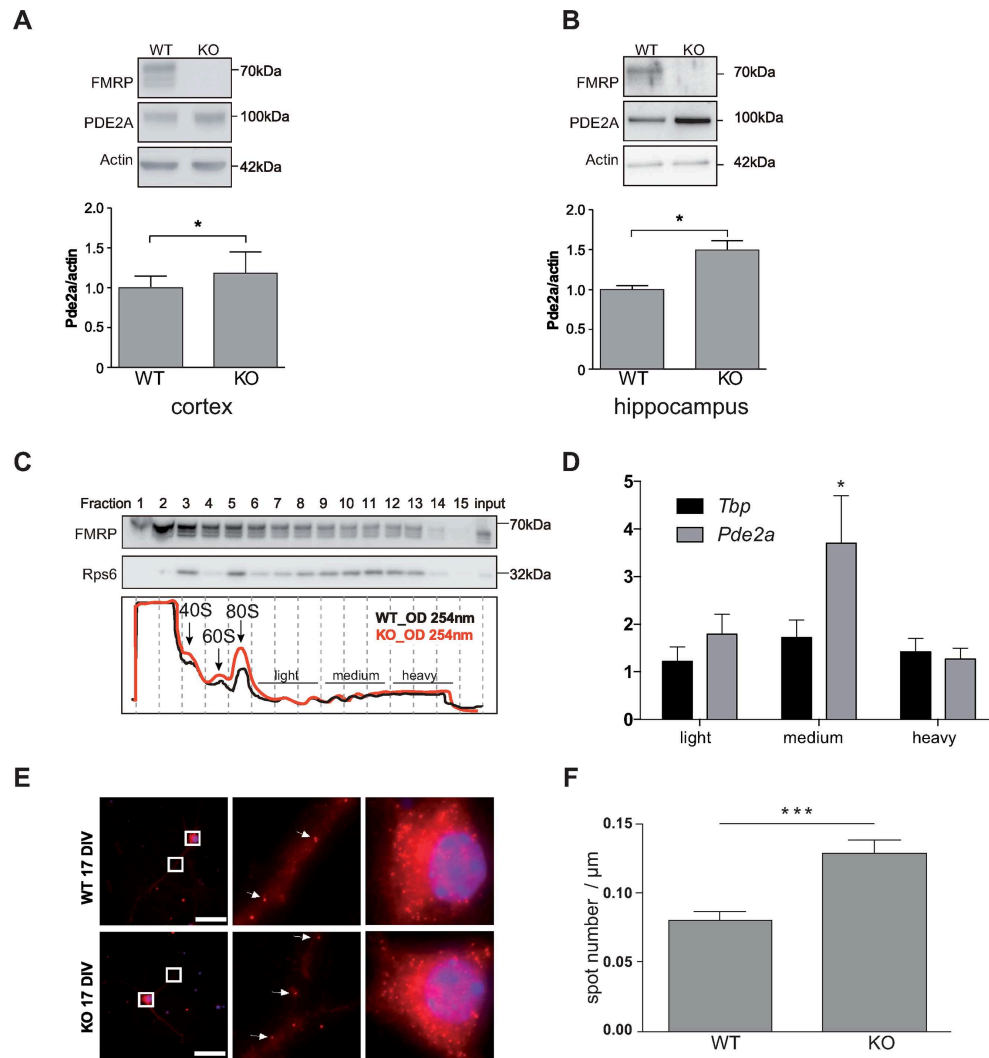


**Figure 5.** Characterization of Pde2A mRNA as predominant target of FMRP. (A) Synaptoneurosomes from 13 days old WT and *Fmr1*-KO cortices and (B) hippocampi were purified and proteins extracted as described in the ‘Material and Methods’ section. The presence of FMRP and PDE2A was revealed by western blot. Upper panels/representative western-blot of FMRP, PDE2A and  $\beta$ -Actin protein levels in synaptosomal extracts from cortex (A) and hippocampus (B). Densitometric quantification of immunoblots reveal that the absence of FMRP (KO) leads to a significant increase in PDE2A protein levels relative to controls (WT). Data are presented as mean  $\pm$  SEM of  $n = 4$  independent samples (Mann–Whitney test  $* P < 0.05$ ). (C) Cortical protein extracts from PND 13 WT and *Fmr1*-KO male mice were analyzed by sedimentation velocity through a 20–50% sucrose gradient. Fifteen fractions were generated. The integrity and distribution of polyribosomes were based on the 254 nm UV profile (in the lower panel representative profiles of two sucrose gradients preparations from WT and *Fmr1*-KO cortices, respectively, are shown). The distribution of polyribosomes was also verified by the presence of ribosomal protein S6 (rpS6), a core protein of the small ribosomal subunit. The presence of rpS6 and FMRP in the various fractions was detected by immunoblot (top panels) using specific antibodies for these two proteins. The name of the protein is indicated on the left while the molecular weight is indicated on the right of each immunoblot. RNAs purified from the indicated fractions were pooled and the abundance of *Pde2a* mRNA measured by qRT-PCR. (D) Fold changes in *Tbp* or *Pde2a* mRNA levels in the pooled fractions were measured as described in the ‘Materials and Methods’ section. Mean  $\pm$  SEM from three independent experiments (three WT and three *Fmr1*-KO brain were used) are shown. One sample *t*-test was performed for each mRNA in the pooled fractions,  $* P < 0.05$  (E) Left panels: representative pictures of cells expressing the *Pde2a* mRNA detected by smFISH in WT and *Fmr1*-KO cultured cortical neurons. Scale bar: 50  $\mu\text{m}$ . Images of cell bodies and dendrites boxed in this panel are enlarged (zoom 900 $\times$ ) in middle and right panels, respectively. Each dot corresponds to a single RNA molecule. White arrows indicate examples of individual mRNA molecules. (F) Number of transported mRNAs (spots) localized in the distal segment of dendrites of 17 days *in vitro* WT ( $n = 44$ ) or *Fmr1*-KO ( $n = 60$ ) neurons. Mean  $\pm$  SEM is shown. Statistical significance was calculated using the unpaired *t*-test,  $*** P < 0.0005$ .

body efficiently precipitating FMRP, allowed the identification not only of new targets (see later) but also of new binding-motifs. All the motifs (alone or in combination) are able to negatively modulate FMRP-driven translational regulation consistent with the well-established function of FMRP as a repressor of translation, even if some exceptions have been described (9,23,42). The fact that we found that

some RNA regions bound by FMRP do not have an impact on the FMRP-translational modulation (Figure 4A) suggests that their interaction with FMRP mediate a function other than translation regulation. Alternatively, additional co-factors are needed to achieve such a regulation in a given cell type or in a spatio/temporal control. In other cases, the reasons could be more complexes and suggest an im-

plication of FMRP in large number of regulation of RNA metabolism, not only including intracellular transport but possibly an implication in RNA folding and/or RNPs assembly. Also, the sequences we—and others—found are relatively short and this strongly indicate that their location in a special structural context is crucial for FMRP recognition, as we have already suggested (39). This suggestion is now validated by showing that three of the motifs bound by FMRP in brain, (CTGKA, GWRGA, TAY) are recognized in the context of a single strand RNA region (likely a loop structure). Interestingly, Taliaferro *et al.* recently showed that the structural context in which a given sequence motif is crucial for the specificity of binding of the cognate RNA-binding protein (43). Similar studies will be needed to decipher the determinants of this structural context that modulate FMRP binding onto its target sequences. The combinatorial recognition of its target sequence by FMRP may be explained by the presence of multiple RNA binding domains in this protein. On one hand, the RGG-box was already shown to recognize several structures and a combined sequence/structure (7,15,23,44) and, on the other hand, the KH2 domain was shown to recognize a complex structure, the kissing complex, (45). Even if a pathological mutation in the KH2 (e.g. I304N) does not prevent the ability of this protein to bind RNA (7), this mutant FMRP is not associated to polyribosomes, is localized in small RNase-resistant RNPs (46) and impacts the size and number of RNA granules (47,48). Furthermore, deletion of the RGG box resulted in a less efficient association to polyribosomes (49). Collectively, these findings suggest that, even if these two RNA binding domains can act in a modular manner, the precise recognition of the mRNA targets and their integration of functional RNPs depends on the integrity of both RNA-binding domains.

By analyzing the codon composition of FMRP binding sites in coding sequences we showed that, intriguingly, the GAC codon is overrepresented and GC-rich codons are underrepresented in these sequences. The GAC codon is not particularly rare and its corresponding tRNA has an average level of expression. We believe that this further argues in favor of the requirement of a structural motif (i.e. a sequence presented in a structure context) bound by FMRP. In addition to the presence of RNA motifs and its surrounding sequences, the specificity of binding of this protein might imply the action of FMRP-interacting proteins that are components of FMRP-containing RNPs and that can interfere (compete/cooperate/prevent) with the function of FMRP. In this context, we can only argue that to assess the functional significance of the FMRP/target interaction and the molecular role of RNA target encoded proteins in the pathophysiology of FXS, the critical targets of FMRP must be studied individually in the appropriate cellular context. Indeed, FMRP may play crucial regulatory roles in the metabolism of cell-specific transcripts even in cell types where it is not highly expressed. For this reason, we studied the cell origin of FMRP targets. Some of these previously overlooked targets include *Slc1a2* in astrocytes/ependymal cells, *Mef2c* in pyramidal cells from CA1, *Scd2* and *Marks* in oligodendrocytes, and *Rapgef4* in endothelial mural cells. These results also suggest the functional importance of FMRP in glia, even if in these cells its expression is lower

than in pyramidal neurons. Moreover, it is interesting that some FMRP RNA targets are particularly abundant in a given tissue, such as *Grm4*, *Fat2* or *Unc5C* that are specific to the cerebellum, *Camk2a*, *Kif5a* and *Agap2* that are more enriched in immunoprecipitations from hippocampi, or *Calml1* and *Encl1* that are more enriched in IPs from cortex. *Pde2a* is only bound by FMRP in cortex and hippocampus (Supplementary Table S1). Considering that the role of FMRP in the various steps of RNA metabolism is modulated through the presence of its interacting partners, as we have previously shown (23,43), we strongly believe that our results are critical to unravel cell-dependent FMRP regulations. In conclusion, we can predict that the functional relevance of each target can be studied individually. A similar approach was used to understand the role of the RNA G-4 in the molecular bases of FXS. This motif has been shown to modulate the FMRP-dependent translation (39,41) but not FMRP-dependent dendritic transport (50). Conversely, the complex with FXR1P (paralog of FMRP)/G-4 has also been involved in the control of RNA stability (51).

### Identification of mRNAs target of FMRP critical for FXS pathophysiology

Our approach allowed us to define the role of FMRP in various brain areas by investigating its implication in the regulation of mRNAs expressed in specific brain regions. A large overlap is observed between FMRP targets in cortex and in hippocampus, while targets from cerebellum appear more divergent. However, specific targets for each analyzed area have been found and these identifications could be possible only by the ‘regionalized’ approach. Gene Ontology analysis allowed to point out that FMRP targets several pathways in the brain like CREB signaling in neurons (Supplementary Table S5), axonal guidance, RAR activation, Rac signaling, regulation of p70s6k signaling and synaptic long-term depression and long-term potentiation. Of particular interest is the specificity of the *Gai* signaling in the hippocampus as well as the iNos and Tgf- $\beta$  signaling in the cortex. In addition, our analysis also pointed out that cAMP/cGMP is one the most prominent deregulated pathways in the *Fmr1*-KO mouse brain and that the *Pde2a* mRNA is one prominent target of FMRP. We show here that in the absence of FMRP the level of PDE2A is elevated both in cortex and hippocampus, implying a reduced level of cAMP and cGMP in those brain areas in *Fmr1*-null mice. Indeed, the PDE2A enzyme is involved in cGMP-dependent degradation of both cAMP and cGMP, two second messengers at the crossroad of many signaling pathways which modulate a large array of intracellular processes in neurons strongly impacting memory and cognition (52). In neurons, PDE2A is mainly synaptic and exerts both pre- and post-synaptic functions [this study and (37)] being involved in synaptogenesis (53) and synaptic plasticity (37,54). All these considerations suggest that this protein is a putative therapeutic target for an effective treatment of FXS.

We focused here on *Pde2a* mRNA, a mRNA target of FMRP in hippocampus and cortex, two brain areas whose dysfunction is most likely causative to cognitive and behavior deficits in FXS. However, we would like to underline

that it is known that altered cerebellum volume and connectivity are associated with etiology of Autism Spectrum Disorder (ASD) (55,56). However, specific cerebellar pathways involved in those pathophysiological mechanisms are poorly described. Thus, our analysis of the FMRP targets in this tissue may help in revealing them. For instance, the implication and regulation of (Estrogen Receptor) *Erb2* and *Erb3* by FMRP is very intriguing and, if extended to ASD, could provide a molecular clue to explain the 1 to 4 ratio between female and male ASD patients (57). In addition, for instance, one of the pathways specifically modulated by FMRP in cerebellum is the GDNF (Glial Cell Line-derived Neurotrophic Factor) that has been recently associated to normal cerebellar motor learning (58). In conclusion, all these pathways may contribute to cellular and/or behavioral phenotypes of FXS.

## DATA AVAILABILITY

Sequencing data have been submitted to GEO: GSE104269.

## SUPPLEMENTARY DATA

Supplementary Data are available at NAR Online.

## ACKNOWLEDGEMENTS

We thank E. Lalli and M. Capovilla for critical reading of the manuscript, M. Drozd for discussion and N. Durand for technical help.

## FUNDING

Université Côte d'Azur; INSERM; CNRS; Agence Nationale de Recherches [ANR-11-LABX-0028-01, ANR-12-BSV4-0020, ANR-12-SVSE8-0022, ANR-15-CE16-0015]; Fondation Jeéroôme Lejeune; Monaco Against Autism Foundation; FRM [DEQ20140329490 to B.B., FRM-ING20140129004 to B.B., T.M.]; FRAXA Foundation (to T.M.); 'Signalife Program' International PhD Fellowship (to S.C.). Funding for open access charge: FRM [DEQ20140329490].

*Conflict of interest statement.* None declared.

## REFERENCES

- Maurin, T., Zongaro, S. and Bardoni, B. (2014) Fragile X syndrome: from molecular pathology to therapy. *Neurosci. Biobehav. Rev.* **46**, 242–255.
- Bassell, G.J. and Warren, S.T. (2008) Fragile X syndrome: loss of local mRNA regulation alters synaptic development and function. *Neuron*, **60**, 201–214.
- Sidorov, M.S., Auerbach, B.D. and Bear, M.F. (2013) Fragile X mental retardation protein and synaptic plasticity. *Mol. Brain*, **6**, 15.
- Erickson, C.A., Davenport, M.H., Schaefer, T.L., Wink, L.K., Pedapati, E.V., Sweeney, J.A., Fitzpatrick, S.E., Brown, W.T., Budimirovic, D., Hagerman, R.J. *et al.* (2017) Fragile X targeted pharmacotherapy: lessons learned and future directions. *J. Neurodev. Disord.*, **9**, 7.
- van Karnebeek, C.D., Bowden, K. and Berry-Kravis, E. (2016) Treatment of neurogenetic developmental conditions: from 2016 into the future. *Pediatr. Neurol.*, **65**, 1–13.
- Castagnola, S., Bardoni, B. and Maurin, T. (2017) The search for an effective therapy to treat fragile X syndrome: dream or reality? *Front. Synaptic Neurosci.*, **9**, 15.
- Darnell, J.C., Jensen, K.B., Jin, P., Brown, V., Warren, S.T. and Darnell, R.B. (2001) Fragile X mental retardation protein targets G quartet mRNAs important for neuronal function. *Cell*, **107**, 489–499.
- Ascano, M. Jr, Mukherjee, N., Bandaru, P., Miller, J.B., Nusbaum, J.D., Corcoran, D.L., Langlois, C., Munschauer, M., Dewell, S., Hafner, M. *et al.* (2012) FMRP targets distinct mRNA sequence elements to regulate protein expression. *Nature*, **492**, 382–386.
- Tabet, R., Moutin, E., Becker, J.A., Heintz, D., Fouillen, L., Flatter, E., Krezel, W., Alunni, V., Koebel, P., Dembele, D. *et al.* (2016) Fragile X mental retardation protein (FMRP) controls diacylglycerol kinase activity in neurons. *Proc. Natl. Acad. Sci. U.S.A.*, **113**, E3619–E3628.
- Davidovic, L., Navratil, V., Bonaccorso, C.M., Catania, M.V., Bardoni, B. and Dumas, M.E. (2011) A metabolomic and systems biology perspective on the brain of the fragile X syndrome mouse model. *Genome Res.*, **21**, 2190–2202.
- Bonaccorso, C.M., Spatuzza, M., Di Marco, B., Gloria, A., Barrancotto, G., Cupo, A., Musumeci, S.A., D'Antoni, S., Bardoni, B. and Catania, M.V. (2015) Fragile X mental retardation protein (FMRP) interacting proteins exhibit different expression patterns during development. *Int. J. Dev. Neurosci.*, **42**, 15–23.
- Semple, B.D., Blomgren, K., Gimlin, K., Ferriero, D.M. and Noble-Haeusslein, L.J. (2013) Brain development in rodents and humans: Identifying benchmarks of maturation and vulnerability to injury across species. *Prog. Neurobiol.*, **106–107**, 1–16.
- Darnell, J.C., Van Driesche, S.J., Zhang, C., Hung, K.Y., Mele, A., Fraser, C.E., Stone, E.F., Chen, C., Fak, J.J., Chi, S.W. *et al.* (2011) FMRP stalls ribosomal translocation on mRNAs linked to synaptic function and autism. *Cell*, **146**, 247–261.
- Hafner, M., Landthaler, M., Burger, L., Khorshid, M., Hausser, J., Berninger, P., Rothballer, A., Ascano, M. Jr, Jungkamp, A.C., Munschauer, M. *et al.* (2010) Transcriptome-wide identification of RNA-binding protein and microRNA target sites by PAR-CLIP. *Cell*, **141**, 129–141.
- Spitzer, J., Hafner, M., Landthaler, M., Ascano, M., Farazi, T., Wardle, G., Nusbaum, J., Khorshid, M., Burger, L., Zavolan, M. *et al.* (2014) PAR-CLIP (Photoactivatable Ribonucleoside-Enhanced Crosslinking and Immunoprecipitation): a step-by-step protocol to the transcriptome-wide identification of binding sites of RNA-binding proteins. *Methods Enzymol.*, **539**, 113–161.
- Konig, J., Zarnack, K., Rot, G., Curk, T., Kayikci, M., Zupan, B., Turner, D.J., Luscombe, N.M. and Ule, J. (2010) iCLIP reveals the function of hnRNP particles in splicing at individual nucleotide resolution. *Nat. Struct. Mol. Biol.*, **17**, 909–915.
- Althammer, S., Gonzalez-Vallinas, J., Ballare, C., Beato, M. and Eyraes, E. (2011) Pyicos: a versatile toolkit for the analysis of high-throughput sequencing data. *Bioinformatics*, **27**, 3333–3340.
- Guo, J.U. and Bartel, D.P. (2016) RNA G-quadruplexes are globally unfolded in eukaryotic cells and depleted in bacteria. *Science*, **353**, aaf5371.
- Schaeffer, C., Bardoni, B., Mandel, J.L., Ehresmann, B., Ehresmann, C. and Moine, H. (2001) The fragile X mental retardation protein binds specifically to its mRNA via a purine quartet motif. *EMBO J.*, **20**, 4803–4813.
- Karabiber, F., McGinnis, J.L., Favorov, O.V. and Weeks, K.M. (2013) QuShape: rapid, accurate, and best-practices quantification of nucleic acid probing information, resolved by capillary electrophoresis. *RNA*, **19**, 63–73.
- Zeisel, A., Munoz-Manchado, A.B., Codeluppi, S., Lonnerberg, P., La Manno, G., Jureus, A., Marques, S., Munguba, H., He, L., Betscholtz, C. *et al.* (2015) Brain structure. Cell types in the mouse cortex and hippocampus revealed by single-cell RNA-seq. *Science*, **347**, 1138–1142.
- Bustin, S.A., Benes, V., Garson, J.A., Hellems, J., Huggett, J., Kubista, M., Mueller, R., Nolan, T., Pfaffl, M.W., Shipley, G.L. *et al.* (2009) The MIQE guidelines: minimum information for publication of quantitative real-time PCR experiments. *Clin. Chem.*, **55**, 611–622.
- Bechara, E.G., Didiot, M.C., Melko, M., Davidovic, L., Bensaid, M., Martin, P., Castets, M., Pognonec, P., Khandjian, E.W., Moine, H. *et al.* (2009) A novel function for fragile X mental retardation protein in translational activation. *PLoS Biol.*, **7**, e16.
- Castets, M., Schaeffer, C., Bechara, E., Schenck, A., Khandjian, E.W., Luche, S., Moine, H., Rabilloud, T., Mandel, J.L. and Bardoni, B. (2005) FMRP interferes with the Rac1 pathway and controls actin

- cytoskeleton dynamics in murine fibroblasts. *Hum. Mol. Genet.*, **14**, 835–844.
25. Tsanov, N., Samacoits, A., Chouaib, R., Traboulsi, A.M., Gostan, T., Weber, C., Zimmer, C., Zibara, K., Walter, T., Peter, M. *et al.* (2016) smiFISH and FISH-quant—a flexible single RNA detection approach with super-resolution capability. *Nucleic Acids Res.*, **44**, e165.
  26. Tang, B., Wang, T., Wan, H., Han, L., Qin, X., Zhang, Y., Wang, J., Yu, C., Berton, F., Francesconi, W. *et al.* (2015) Fmr1 deficiency promotes age-dependent alterations in the cortical synaptic proteome. *Proc. Natl. Acad. Sci. U.S.A.*, **112**, E4697–E4706.
  27. Cajigas, I.J., Tushev, G., Will, T.J., tom Dieck, S., Fuerst, N. and Schuman, E.M. (2012) The local transcriptome in the synaptic neuropil revealed by deep sequencing and high-resolution imaging. *Neuron*, **74**, 453–466.
  28. Lorenz, R., Bernhart, S.H., Honer Zu Siederdisen, C., Tafer, H., Flamm, C., Stadler, P.F. and Hofacker, I.L. (2011) ViennaRNA Package 2.0. *Algorithms Mol. Biol.*, **6**, 26.
  29. Bailey, T.L. (2011) DREME: motif discovery in transcription factor ChIP-seq data. *Bioinformatics*, **27**, 1653–1659.
  30. Anderson, B.R., Chopra, P., Suhl, J.A., Warren, S.T. and Bassell, G.J. (2016) Identification of consensus binding sites clarifies FMRP binding determinants. *Nucleic Acids Res.*, **44**, 6649–6659.
  31. Zaccolo, M. and Movsesian, M.A. (2007) cAMP and cGMP signaling cross-talk: role of phosphodiesterases and implications for cardiac pathophysiology. *Circ. Res.*, **100**, 1569–1578.
  32. Averaimo, S. and Nicol, X. (2014) Intermingled cAMP, cGMP and calcium spatiotemporal dynamics in developing neuronal circuits. *Front. Cell Neurosci.*, **8**, 376.
  33. Maurice, D.H., Ke, H., Ahmad, F., Wang, Y., Chung, J. and Manganiello, V.C. (2014) Advances in targeting cyclic nucleotide phosphodiesterases. *Nat. Rev. Drug Discov.*, **13**, 290–314.
  34. Russwurm, C., Zoidl, G., Koesling, D. and Russwurm, M. (2009) Dual acylation of PDE2A splice variant 3: targeting to synaptic membranes. *J. Biol. Chem.*, **284**, 25782–25790.
  35. Hu, F., Ren, J., Zhang, J.E., Zhong, W. and Luo, M. (2012) Natriuretic peptides block synaptic transmission by activating phosphodiesterase 2A and reducing presynaptic PKA activity. *Proc. Natl. Acad. Sci. U.S.A.*, **109**, 17681–17686.
  36. Boyken, J., Gronborg, M., Riedel, D., Urlaub, H., Jahn, R. and Chua, J.J. (2013) Molecular profiling of synaptic vesicle docking sites reveals novel proteins but few differences between glutamatergic and GABAergic synapses. *Neuron*, **78**, 285–297.
  37. Fernandez-Fernandez, D., Rosenbrock, H. and Kroker, K.S. (2015) Inhibition of PDE2A, but not PDE9A, modulates presynaptic short-term plasticity measured by paired-pulse facilitation in the CA1 region of the hippocampus. *Synapse*, **69**, 484–496.
  38. Tsanov, N., Samacoits, A., Chouaib, R., Traboulsi, A.M., Gostan, T., Weber, C., Zimmer, C., Zibara, K., Walter, T., Peter, M. *et al.* (2016) smiFISH and FISH-quant—a flexible single RNA detection approach with super-resolution capability. *Nucleic Acids Res.*, **44**, e165.
  39. Maurin, T., Melko, M., Abekhouch, S., Khalfallah, O., Davidovic, L., Jarjat, M., D'Antoni, S., Catania, M.V., Moine, H., Bechara, E. *et al.* (2015) The FMRP/GRK4 mRNA interaction uncovers a new mode of binding of the Fragile X mental retardation protein in cerebellum. *Nucleic Acids Res.*, **43**, 8540–8550.
  40. Suhl, J.A., Chopra, P., Anderson, B.R., Bassell, G.J. and Warren, S.T. (2014) Analysis of FMRP mRNA target datasets reveals highly associated mRNAs mediated by G-quadruplex structures formed via clustered WGGA sequences. *Hum. Mol. Genet.*, **23**, 5479–5491.
  41. Melko, M. and Bardoni, B. (2010) The role of G-quadruplex in RNA metabolism: involvement of FMRP and FMR2P. *Biochimie*, **92**, 919–926.
  42. Gross, C., Yao, X., Pong, D.L., Jeromin, A. and Bassell, G.J. (2011) Fragile X mental retardation protein regulates protein expression and mRNA translation of the potassium channel Kv4.2. *J. Neurosci.*, **31**, 5693–5698.
  43. Taliaferro, J.M., Lambert, N.J., Sudmant, P.H., Dominguez, D., Merkin, J.J., Alexis, M.S., Bazile, C. and Burge, C.B. (2016) RNA sequence context effects measured in vitro predict in vivo protein binding and regulation. *Mol. Cell*, **64**, 294–306.
  44. Bechara, E., Davidovic, L., Melko, M., Bensaid, M., Tremblay, S., Grosgeorge, J., Khandjian, E.W., Lalli, E. and Bardoni, B. (2007) Fragile X related protein 1 isoforms differentially modulate the affinity of fragile X mental retardation protein for G-quartet RNA structure. *Nucleic Acids Res.*, **35**, 299–306.
  45. Darnell, J.C., Fraser, C.E., Mostovetsky, O., Stefani, G., Jones, T.A., Eddy, S.R. and Darnell, R.B. (2005) Kissing complex RNAs mediate interaction between the fragile-X mental retardation protein KH2 domain and brain polyribosomes. *Genes Dev.*, **19**, 903–918.
  46. Zang, J.B., Nosyreva, E.D., Spencer, C.M., Volk, L.J., Musunuru, K., Zhong, R., Stone, E.F., Yuva-Paylor, L.A., Huber, K.M., Paylor, R. *et al.* (2009) A mouse model of the human fragile X syndrome I304N mutation. *PLoS Genet.*, **5**, e1000758.
  47. Schrier, M., Severijnen, L.A., Reis, S., Rife, M., van't Padje, S., van Cappellen, G., Oostra, B.A. and Willemsen, R. (2004) Transport kinetics of FMRP containing the I304N mutation of severe fragile X syndrome in neurites of living rat PC12 cells. *Exp. Neurol.*, **189**, 343–353.
  48. Levenga, J., Buijsen, R.A., Rife, M., Moine, H., Nelson, D.L., Oostra, B.A., Willemsen, R. and de Vrij, F.M. (2009) Ultrastructural analysis of the functional domains in FMRP using primary hippocampal mouse neurons. *Neurobiol. Dis.*, **35**, 241–250.
  49. Mazroui, R., Huot, M.E., Tremblay, S., Boilard, N., Labelle, Y. and Khandjian, E.W. (2003) Fragile X Mental Retardation protein determinants required for its association with polyribosomal mRNPs. *Hum. Mol. Genet.*, **12**, 3087–3096.
  50. Subramanian, M., Rage, F., Tabet, R., Flatter, E., Mandel, J.L. and Moine, H. (2011) G-quadruplex RNA structure as a signal for neurite mRNA targeting. *EMBO Rep.*, **12**, 697–704.
  51. Davidovic, L., Durand, N., Khalfallah, O., Tabet, R., Barbry, P., Mari, B., Sacconi, S., Moine, H. and Bardoni, B. (2013) A novel role for the RNA-binding protein FXR1P in myoblasts cell-cycle progression by modulating p21/Cdkn1a/Cip1/Waf1 mRNA stability. *PLoS Genet.*, **9**, e1003367.
  52. Gomez, L. and Breitenbucher, J.G. (2013) PDE2 inhibition: potential for the treatment of cognitive disorders. *Bioorg. Med. Chem. Lett.*, **23**, 6522–6527.
  53. Boess, F.G., Hendrix, M., van der Staay, F.J., Erb, C., Schreiber, R., van Staveren, W., de Vente, J., Prickaerts, J., Blokland, A. and Koenig, G. (2004) Inhibition of phosphodiesterase 2 increases neuronal cGMP, synaptic plasticity and memory performance. *Neuropharmacology*, **47**, 1081–1092.
  54. Domek-Lopacinska, K. and Strosznajder, J.B. (2008) The effect of selective inhibition of cyclic GMP hydrolyzing phosphodiesterases 2 and 5 on learning and memory processes and nitric oxide synthase activity in brain during aging. *Brain Res.*, **1216**, 68–77.
  55. Traut, N., Beggiato, A., Bourgeron, T., Delorme, R., Rondi-Reig, L., Paradis, A.L. and Toro, R. (2018) Cerebellar volume in autism: literature meta-analysis and analysis of the autism brain imaging data exchange cohort. *Biol. Psychiatry*, **83**, 579–588.
  56. Stoodley, C.J., D'Mello, A.M., Ellegood, J., Jakkamsetti, V., Liu, P., Nebel, M.B., Gibson, J.M., Kelly, E., Meng, F., Cano, C.A. *et al.* (2017) Altered cerebellar connectivity in autism and cerebellar-mediated rescue of autism-related behaviors in mice. *Nat. Neurosci.*, **20**, 1744–1751.
  57. Loomes, R., Hull, L. and Mandy, W.P.L. (2017) What is the male-to-female ratio in autism spectrum disorder? A systematic review and Meta-Analysis. *J. Am. Acad. Child Adolesc. Psychiatry*, **56**, 466–474.
  58. Sergaki, M.C., López-Ramos, J.C., Stagkourakis, S., Gruart, A., Broberger, C., Delgado-García, J.M. and Ibáñez, C.F. (2017) Compromised survival of cerebellar molecular layer interneurons lacking GDNF receptors GFR $\alpha$ 1 or RET impairs normal cerebellar motor learning. *Cell Rep.*, **19**, 1977–1986.

# Publication 4



ORIGINAL ARTICLE

# Involvement of Phosphodiesterase 2A Activity in the Pathophysiology of Fragile X Syndrome

Thomas Maurin <sup>1,2</sup>, Francesca Melancia<sup>3</sup>, Marielle Jarjat<sup>1,2</sup>, Liliana Castro <sup>4,5</sup>, Lara Costa<sup>6</sup>, Sébastien Delhaye<sup>1,2</sup>, Anouar Khayachi<sup>1</sup>, Sara Castagnola<sup>1,2</sup>, Elia Mota<sup>4,5</sup>, Audrey Di Giorgio<sup>7</sup>, Michela Servadio<sup>3</sup>, Malgorzata Drozd<sup>1,2</sup>, Gwénola Poupon<sup>1</sup>, Sara Schiavi<sup>3</sup>, Lara Sardone<sup>8</sup>, Stéphane Azoulay<sup>7</sup>, Lucia Ciranna<sup>8</sup>, Stéphane Martin<sup>9</sup>, Pierre Vincent <sup>4,5</sup>, Viviana Trezza<sup>3</sup> and Barbara Bardoni <sup>2,9</sup>

<sup>1</sup>Université Côte d'Azur, CNRS, IPMC, F-06560 Valbonne, France, <sup>2</sup>CNRS LIA «Neogenex», F-06560 Valbonne, France, <sup>3</sup>Department of Sciences, Università RomaTre, I-00145 Roma, Italy, <sup>4</sup>Sorbonne Université, CNRS, Biological Adaptation and Ageing, F-75005 Paris, France, <sup>5</sup>Labex BioPsy, F-75005 Paris, France, <sup>6</sup>Department of Clinical and Experimental Medicine, University of Messina, I-98122 Messina, Italy, <sup>7</sup>Université Côte d'Azur, CNRS, Institut de Chimie de Nice, F-06108 Nice, France, <sup>8</sup>Department of Biomedical and Biotechnological Sciences, University of Catania, I-95123 Catania, Italy and <sup>9</sup>Université Côte d'Azur, INSERM, CNRS, IPMC, F-06560 Valbonne, France

Address correspondence to Barbara Bardoni, Thomas Maurin, CNRS UMR7275, Institute of Molecular and Cellular Pharmacology, 660 Route des Lucioles, Sophia-Antipolis, 06560 Valbonne, France. Email: bardoni@ipmc.cnrs.fr (B.B.); maurin@ipmc.cnrs.fr (T.M.) [orcid.org/0000-0001-6411-1517](https://orcid.org/0000-0001-6411-1517)

Fancesca Melancia and Marielle Jarjat equally contributed; Liliana Castro, Lara Costa and Sébastien Delhaye equally contributed to this work; Lucia Ciranna, Stéphan Martin, Pierre Vincent and Viviana Trezza equally contributed to this work

## Abstract

The fragile X mental retardation protein (FMRP) is an RNA-binding protein involved in translational regulation of mRNAs that play key roles in synaptic morphology and plasticity. The functional absence of FMRP causes the fragile X syndrome (FXS), the most common form of inherited intellectual disability and the most common monogenic cause of autism. No effective treatment is available for FXS. We recently identified the *Phosphodiesterase 2A (Pde2a)* mRNA as a prominent target of FMRP. PDE2A enzymatic activity is increased in the brain of *Fmr1*-KO mice, a recognized model of FXS, leading to decreased levels of cAMP and cGMP. Here, we pharmacologically inhibited PDE2A in *Fmr1*-KO mice and observed a rescue both of the maturity of dendritic spines and of the exaggerated hippocampal mGluR-dependent long-term depression. Remarkably, PDE2A blockade rescued the social and communicative deficits of both mouse and rat *Fmr1*-KO animals. Importantly, chronic inhibition of PDE2A in newborn *Fmr1*-KO mice followed by a washout interval, resulted in the rescue of the altered social behavior observed in adolescent mice. Altogether, these results reveal the key role of PDE2A in the pathophysiology of FXS and suggest that its pharmacological inhibition represents a novel therapeutic approach for FXS.

**Key words:** autism spectrum disorder, *Fmr1*-KO mice, *Fmr1*-KO rats, fragile X syndrome, phosphodiesterase 2A

## Introduction

Fragile X syndrome (FXS) is a rare genetic neurodevelopmental disorder with a prevalence of 1:4000 males and 1:7000 females representing the most common form of inherited intellectual disability (ID) and a leading genetic cause of autism spectrum disorder (ASD). Patients may also exhibit a range of disabling neurological problems including hyperactivity, attention deficit, anxiety and epileptic seizures in addition to facial dysmorphisms and physical abnormalities (Bassell and Warren 2008; Maurin et al. 2014; Castagnola et al. 2017). FXS is caused by the absence of expression of the *FMR1* gene, which ultimately leads to the lack of its product, the fragile X mental retardation protein (FMRP), a translational modulator of synaptic proteins and a regulator of mRNA transport at the synapse. Consequently, neurons of both FXS patients and *Fmr1*-KO mice exhibit abnormal dendritic spines associated with altered forms of synaptic plasticity (Bassell and Warren 2008; Maurin et al. 2014; Castagnola et al. 2017). Furthermore, altered volumes of specific brain structures that develop prenatally or early postnatally in young FXS children (Gothelf et al. 2008; Hoefft et al. 2010) and *Fmr1*-KO pups (Lai et al. 2016) have been described. The abundance of many synaptic proteins is altered in the absence of FMRP and, consequently, multiple molecular pathways are dysregulated in *Fmr1*-KO neurons (Maurin et al. 2018). However, despite the research efforts made both at preclinical and clinical levels, approved therapies are not yet available for FXS (Budimirovic et al. 2017; Castagnola et al. 2017; Erickson et al. 2017). Towards this goal, it is essential to have a better understanding of the pathophysiology of FXS and of the role played by FMRP during brain development. Therefore, we used High Throughput Sequencing-Cross Linking Immuno-Precipitation (HITS-CLIP) to identify FMRP RNA targets at postnatal day (PND) 13, an early developmental stage of mouse brain, when FMRP is most highly expressed and synaptogenesis peaks (Maurin et al. 2018). At this age, in hippocampus and in cortex a prominent target of FMRP is the *Phosphodiesterase 2A* (*Pde2a*) mRNA (Maurin et al. 2018), which encodes an enzyme involved in cAMP and cGMP degradation (Maurice et al. 2014). PDE2A levels and activity are increased (Maurin et al. 2018 and this study) in *Fmr1*-KO, resulting in reduced levels of cAMP and cGMP, 2 intracellular secondary messengers having key roles in neuronal differentiation, development and function (Shelly et al. 2010; Park et al. 2014). Here, we unravel the pathophysiological relevance of PDE2A activity in FXS by combining *in vitro*, *ex vivo*, and *in vivo* experiments and using 2 rodent models of FXS. We conclude that PDE2A represents a novel therapeutic target to treat children affected by FXS.

## Materials and Methods

### Neuronal Cultures and Spine Morphology Analysis

Primary cortical neurons were prepared from embryos at E15.5 obtained from pregnant C57BL/6 *Fmr1*-KO and wild type (WT) mice as previously described (Khayachi et al. 2018). Neurons (17 days *in vitro*) were treated with 0.2  $\mu$ M BAY607550 or DMSO (control) for 24 h in total. After 5 h of pharmacological treatment, neurons were transduced with attenuated Sindbis viral particles pSinRep5(nsP2726)-expressing GFP at a multiplicity of infection (MOI) of 0.1. Transduced neurons (18 days *in vitro*) were washed twice in PBS at room temperature (RT) after 19 h of transduction, and then fixed (Devader et al. 2015). Sequential confocal images (512  $\times$  220 pixels; Zoom 3.0; Average 4; Speed 7) of GFP-expressing neurons were acquired with a 63X oil-immersion lens (Numerical Aperture NA 1.4) on an inverted Zeiss LSM780

confocal microscope. Z-series of 7–8 images of randomly selected secondary dendrites (3 independent cultures, 24–30 neurons per condition) were analyzed using NeuronStudio software, which allows for the automated detection of immature and mature spines (Rodriguez et al. 2008; Devader et al. 2015).

The dendritic spine morphology analysis was scored and analyzed by trained observers who were unaware of treatment conditions.

### cAMP and cGMP Detection

1) ELISA test: Frozen ground hippocampi from PND 13 mice, were resuspended in 10 volumes of 0.1 N HCl and centrifuged to remove debris. Supernatants were used directly for cGMP measurement. ELISA was then carried out according to the manufacturer's instructions (Direct cGMP ELISA kit; Enzo Life Science). 2) cAMP-Glo Max assay: Primary cortical neurons (17–21 days *in vitro*) cultured in 96 wells plates were stimulated in 2 biological replicates with 10  $\mu$ M Forskolin and 1  $\mu$ M BAY607550 in dPBS supplemented with CaCl<sub>2</sub> and MgCl<sub>2</sub> for 30 min at 37 °C. cAMP concentration was measured with the cAMP-Glo Max assay (Promega) according to the manufacturer's indications. 3) cAMP Biosensors: Brain slices were prepared from male mice at PND 7–11, transduced with Sindbis viral particles to express the cAMP biosensor Epac-S<sup>H150</sup> (Polito et al. 2013). Wide-field images were obtained with an Olympus BX50WI or BX1WI upright microscope with a 40 $\times$  0.8 NA water-immersion objective and an ORCA-AG camera (Hamamatsu). Images were acquired with iVision (Biovision, Exton, PA, USA). The excitation and dichroic filters were D436/20 and 455dxc. Signals were acquired by alternating the emission filters with a filter wheel (Sutter Instruments, Novato, CA, USA), HQ480/40 for the donor, and D535/40 for the acceptor. Images were analyzed with custom routines according to the IGOR Pro environment (Wavemetrics, Lake Oswego, OR, USA). The emission ratio was calculated for each pixel as F480/F535. The pseudocolor images display the ratio value coded in hue and the fluorescence of the preparation coded in intensity. The amplitudes of responses were quantified for each neuron as the fractional change in ratio from its own baseline and maximal final ratio response (in the presence of forskolin and IBMX). Responses obtained from CA1 neurons were averaged for each experiment (i.e., brain slice). Data were analyzed with SPSS statistical software version 22.0 (Chicago, IL, USA). Normality in variable distributions and homogeneity of variances across groups were assessed with the Shapiro–Wilk and Levene tests, respectively.

### Animals

The experiments were performed following the ARRIVE (Animals in Research: Reporting In Vivo Experiments) guidelines (Kilkenny et al. 2010). *Fmr1*-knockout (KO) and WT mice on a C57BL/6J congenic background were obtained from Prof. R. Willemsen (Mientjes et al. 2006), while *Fmr1*-KO and WT rats on a Sprague-Dawley background were purchased from Horizon Discovery (formerly SAGE Labs, USA). All animals were generated and housed in groups of 4 in standard laboratory conditions (22 °C, 55  $\pm$  10% humidity, 12-h light/12-h dark diurnal cycles) with food and water provided *ad libitum*.

### Behavior

Experimental testing was performed between 12:00 and 16:30 each day during the 12-h light period. Only male mice and rats were used. Animal care was conducted in accordance with the

European Community Directive 2010/63/EU. The experiments were approved by the local ethics committee (Comité d'Ethique en Expérimentation Animale CIEPAL-AZUR N. 00788.01; APAFIS#4985-2 016 032 314 169 426 v4APAFIS#8100-2 016 112 217 148 206 v3), by the French Ministry of Research and by the Italian Ministry of Health. The number of animals used in each experiment is indicated in the figure legends.

### Electrophysiology

Hippocampal slices were prepared from WT and *Fmr1*-KO mice on a C57BL/6J genetic background at PND 13 as previously described (Costa et al. 2012), following protocols approved by local ethics committee (OPBA, University of Catania) and by the Italian Ministry of Health (N. 35212016-PR). Data were acquired and analyzed with the Signal software (Cambridge Electronic Design, England). Excitatory Post Synaptic Current (EPSC) amplitude was measured as the difference between peak and baseline current. EPSC amplitude values were averaged over 1 min and expressed as % of baseline (mean EPSC amplitude calculated from EPSCs recorded during at least 15 min before [S]-3,5-Dihydroxyphenylglycine [DHPG] application). Different sets of values were compared using the appropriate statistical tests indicated in the corresponding figure legend. The amount of long-term depression (LTD) induced by metabotropic group I glutamate receptor (mGluR) was calculated 40 min after LTD induction by DHPG application and is expressed by indicating EPSC amplitude as percentage of baseline (% EPSC).

### Drug Treatment

BAY607550 (Cayman) was dissolved in 10% DMSO/8.75% Tween 80/8.75% polyethylene glycol/saline. For the behavioral experiments, BAY607550 or Lu AF64280 (or their vehicles) were administered intraperitoneally (i.p.) 30 min before testing. BAY607550 was administered at the doses of 0.05 mg/kg at infancy and 0.1 mg/kg at adolescence, while Lu AF64280 was administered at 0.5 mg/kg. Drug doses and pretreatment intervals were based on literature (Boess et al. 2004; Masood et al. 2008, 2009; Ding et al. 2014; Redrobe et al. 2014; Wang et al. 2017) and our pilot data showing that, at the doses used in the present study, drugs did not affect the behavior of WT animals. In one experiment, chronic treatment was carried out by a daily i.p. injection of 0.05 mg/kg BAY607550 to mice from PND 5–21 and mice were tested for social interaction after a washout interval of 9 days. One pup per litter from different litters per treatment group was used in the behavioral experiments, to control for any potential litter effect. Animals were randomly allocated to each treatment group. Coding of the drug solutions ensured that both during experimentation and behavior analysis, the experimenter was unaware of the treatment of the animals. The number of animals per group is indicated in the figure legends.

### The Isolation-Induced Ultrasonic Vocalizations Test

The test was performed as previously described (Servadio et al. 2016). Briefly, each pup (at PND 10 for mice and PNDs 5 and 9 for rats) was individually removed from the nest and placed into a black Plexiglas arena, located inside a sound-attenuating and temperature-controlled chamber. Pup ultrasonic vocalizations (USVs) were detected for 3 min by an ultrasound microphone (Avisoft Bioacoustics, Germany) sensitive to frequencies between 10 and 250 kHz and fixed at 10 cm above the arena. Pup axillary temperature was measured before and after the test by a digital thermometer. The emission of USVs was analyzed using Avisoft Recorder software (Version 5.1).

### Homing Behavior Test

At PND 14, the litter was separated from the dam and kept for 30 min in a temperature-controlled holding cage. Then, each mouse pup was placed into a Plexiglas box whose floor was covered for 1/3 with bedding from the pup's home cage and for 2/3 with clean bedding. The pup was located at the side of the box covered by clean bedding, and its behavior was videorecorded for 4 min for subsequent analysis. The following parameters were scored using the Observer 3.0 software (Noldus Information Technology): latency (s) to reach the home-cage bedding area; total time (s) spent by the pup in the nest bedding area.

### Social Interaction Test

The test was performed as previously described (Terranova and Laviola 2005; Jamain et al. 2008). The 28–30-day-old mice were individually habituated to the experimental apparatus (a Plexiglas cage measuring 30 × 30 × 30 cm<sup>3</sup>) for 5 min the day before testing. On the test day, the animals were isolated for 2 h before testing, to enhance their social motivation and thus facilitate the expression of social interaction during testing. The test consisted of placing 2 animals (same treatment and weight) into the test cage for 10 min.

The behavior of the animals was recorded using a video camera with zoom lens, DVD recorder and LCD monitor. Behavior was assessed per single animal and analyzed by a trained observer who was unaware of genotype and treatment conditions using the Observer XT software (Noldus, The Netherlands).

The following parameters were scored (Terranova and Laviola 2005; Jamain et al. 2008):

- a. Social activities:
  1. Social sniffing: sniffing any part of the body of the partner, including the anogenital area.
  2. Following: moving in the direction of or pursuing the partner, who moves away.
  3. Mutual circle: partners are mutually sniffing each other's anogenital region, while describing tight circles with their reciprocal following movements.
  4. Pushing past: the focal animal passes between the wall of the cage and the body of the partner by pushing its own body through the narrow space available.
  5. Crawling under/over: the focal animal crawls underneath or over the partner's body, crossing it transversely from one side to the other.
  6. Social grooming: chewing and licking the fur of the partner.
  7. Social rest: the focal animal is being groomed by the partner.
  8. Pushing under: the focal animal pushes its own snout or the whole anterior part of its body under the partner's body, and rests for at least 3 s.
  9. Social inactivity: the focal animal is lying flat or standing still (eyes closed or open) while maintaining close physical contact with the partner.
- b. Nonsocial activities:
  1. Running: the focal animal performs a sudden, rapid, vigorous, and erratic darting, characterized by frequent and sharp changes in direction and without any obvious target.
  2. Inactive: Self-explanatory.
  3. Exploring: Self-explanatory.

4. Digging: the focal animal is digging in the sawdust, pushing and kicking it around, using the snout and/or both the forepaws and hindpaws.

The average frequency of total social activities, quantified as number of events during the 10 min testing session, was graphed.

### Statistical Analysis

Results are expressed as mean  $\pm$  standard error of the mean (SEM). All statistical analyses were based on biological replicates. Appropriate statistical tests used for each experiment are described in the corresponding figure legends. All statistical analyses were carried out using the GraphPad Prism Version 6.0e.

## Results

### PDE2A Dysregulation is Involved in the Physiopathology of FXS

*Pde2a* is expressed both in cortex and hippocampus (e.g., supragranular layer of neocortex, CA1 and CA3 regions of hippocampus) (Stephenson et al. 2009, 2012), with a high and homogenous expression in the mouse CA1. To assess whether the increased

abundance of the PDE2A protein in the absence of FMRP that we described (Maurin et al. 2018) is associated with its elevated activity in hippocampus, we measured cAMP levels in single neurons of the CA1 area in *Fmr1*-KO and WT mouse brain slices. For this purpose, we used the Epac-S<sup>H150</sup> fluorescent biosensor that detects an increase in cAMP levels by a decrease in FRET between the donor and acceptor fluorophores (Polito et al. 2013). These changes were monitored in real-time by ratiometric fluorescence imaging. cAMP synthesis was first stimulated using forskolin, leading to a steady-state biosensor emission ratio. PDE2A was then activated using the NO donor DEANO, which decreased the biosensor ratio. PDE2A activity was then blocked by the addition of the potent and specific PDE2A inhibitor BAY607550 (Boess et al. 2004), which increased the biosensor ratio, revealing the effective contribution of PDE2A in cAMP degradation. A final application of forskolin and the nonselective phosphodiesterase inhibitor IBMX increased the biosensor ratio to its maximum. An example of this analysis in WT neurons is reported in Figure 1A, B. Then we performed these assays in hippocampal slices obtained from PND 7–11 WT and *Fmr1*-KO mice. cAMP levels elicited by forskolin and DEANO stimulation were significantly lower in the absence of *Fmr1* expression, consistent with an elevated PDE2A activity in the *Fmr1*-KO hippocampus (Fig. 1C). We confirmed these findings by a detailed analysis of cAMP

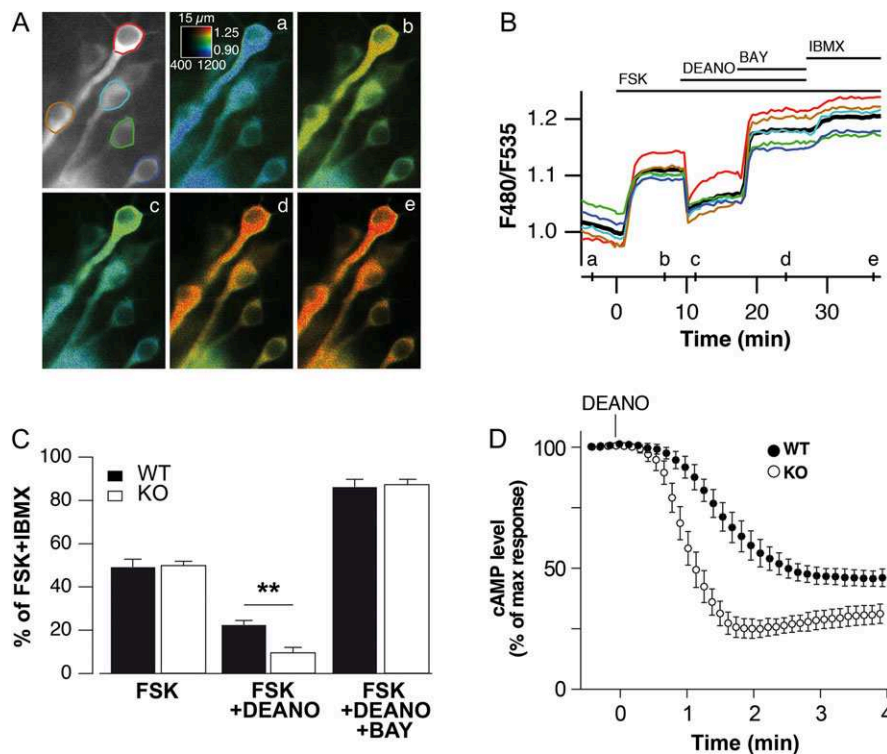


**Figure 1.** The increased activity of PDE2A results into decreased cAMP levels. (A) Hippocampal brain slices expressing the Epac-S<sup>H150</sup> biosensor were imaged with wide-field fluorescence microscopy (here exemplified with a measure in a WT brain slice). Images show the raw fluorescence intensity at 535 nm (in gray scale) and the ratio (in pseudocolor), reporting changes in cAMP concentration before stimulation and at different times of the recording during the different treatments (a–e), as indicated by the corresponding lines on the graph in panel “B”. The calibration square on the pseudocolor image indicates from left to right increasing fluorescence intensity levels, and from bottom to top increasing ratio values. The width of the square is used as a scale bar. Its size is indicated above it in micrometers. (B) Each trace on the graph indicates the F480/F535 emission ratio measured on the regions (neuron) delimited by the color contour drawn on the gray scale image (upper left panel). The black trace corresponds to the mean of the 5 colored traces. (C) Quantification of cAMP in WT and *Fmr1*-KO hippocampal slices: the successive responses to forskolin, DEANO and BAY607550 were quantified as a fraction of the maximal response measured in the presence of IBMX. (C) Average ratio response to forskolin (10  $\mu$ M), forskolin + DEANO (10  $\mu$ M) and forskolin + DEANO + BAY607550 (0.2  $\mu$ M) for WT and *Fmr1*-KO. Mean  $\pm$  SEM is shown. In each experiment (i.e., brain slices tested, one slice per animal) a variable number of neurons have been considered (between 1 and 6). Results from  $n = 12$  WT and  $n = 16$  *Fmr1*-KO experiments are shown. Two-way ANOVA followed by Bonferroni multiple comparisons post hoc test revealed a significantly lower level of cAMP in *Fmr1*-KO slices for the FSK + DEANO condition ( $F_{\text{treatment}(1,26)} = 640$ ,  $P < 0.001$ ;  $F_{\text{genotype}(1,26)} = 1.25$ ,  $P = 0.278$ ;  $F_{\text{genotype} \times \text{treatment}(1,26)} = 15.76$ ,  $P = 0.001$ ) followed by Bonferroni multiple comparisons post hoc test (adjusted  $P$  value  $**P < 0.01$ ). (D) Time course measurement of cAMP levels after DEANO application in the presence or in the absence of FMRP.

degradation kinetics in the presence and in the absence of FMRP upon PDE2A activation with DEANO: the decrease in biosensor ratio upon PDE2A stimulation with DEANO was significantly faster in *Fmr1*-KO neurons than in WT (Fig. 1D).

In addition, using an ELISA immuno-assay, we showed that cGMP levels are also significantly decreased in *Fmr1*-KO hippocampi (Supplementary Fig. S1). Collectively, these data indicate that there is an elevated activity of PDE2A in hippocampal *Fmr1*-KO neurons.

### Blocking PDE2A Activity Suppresses the Exaggerated LTD in *Fmr1*-KO hippocampus

A hallmark of FXS is the exaggerated LTD induced by mGluR activation in the hippocampal CA3-CA1 synapses (Huber et al. 2002). To assess whether inhibition of PDE2A can prevent the exaggerated synaptic plasticity characterizing FXS hippocampi, we measured LTD expression in the presence and in the absence of BAY607550. AMPA receptor-mediated excitatory postsynaptic currents (EPSCs) were recorded from CA1 pyramidal neurons under whole-cell patch clamp following stimulation of Schaffer collaterals, in the continuous presence of D-AP5 (50  $\mu$ M) and bicuculline (5  $\mu$ M). Bath application of DHPG (100  $\mu$ M, 5 min), an agonist of group I mGluRs, induced a LTD of EPSC amplitude that in WT was not modified in the presence of BAY607550 (50 nM; Fig. 2A,C). The amount of mGluR-LTD is exaggerated in *Fmr1*-KO hippocampi (EPSC amplitude:  $40 \pm 9\%$  vs.  $78 \pm 9\%$  in WT vs. *Fmr1*-KO treated with BAY607550; Fig. 2B,C), as previously reported (Costa et al. 2012; Castagnola et al. 2017). Intracellular BAY607550 (50 nM) in *Fmr1*-KO mouse hippocampal neurons reverted the exaggerated mGluR-LTD to a level that is not statistically different from WT control recordings (EPSC % amplitude:  $78 \pm 9\%$  vs.  $86 \pm 7\%$  in WT vs. *Fmr1*-KO treated with BAY607550; Fig. 2B,C). Remarkably, BAY607550 treatment (50 nM) had no effect on mGluR-LTD in WT slices (Fig. 2A-C). These results clearly show the implication of PDE2A-mediated regulation of cAMP and cGMP in the exaggerated mGluR-dependent LTD in *Fmr1*-KO mice.

### Inhibiting PDE2A Activity Restores Axonal Length and Spine Maturation in Cultured Cortical *Fmr1*-KO Neurons

The presence of abnormal immature dendritic spines in the brain of FXS patients and in primary neuronal cultures of mouse *Fmr1*-KO models of FXS (Comery et al. 1997; Irwin et al. 2000; Nimchinsky et al. 2001; Antar et al. 2005, 2006) is another hallmark associated with the functional absence of FMRP. Importantly, both cAMP and cGMP have been reported to exert an important role in axonal growth and dendritic spine maturation (Shelly et al. 2010; Shen and Cowan 2010; Averaimo and Nicol 2014; Akiyama et al. 2016). Therefore, to assess the involvement of PDE2A in synaptic morphology, we first analyzed cAMP levels in cultured cortical neurons in the absence or in the presence of PDE2A inhibitors (Supplementary Fig. S2). We then assessed the impact of an inhibition of PDE2A activity on the maturation of dendritic spines (Fig. 3) and on axonal growth (Fig. 4) in *Fmr1*-KO cultured cortical neurons. To quantify the activity of PDE2A in FXS neurons, we measured cAMP levels in cultured *Fmr1*-KO upon forskolin stimulation associated with pan-PDE inhibition with IBMX (Supplementary Fig. S2). This latter treatment led to a significant increase in cAMP levels both in the presence and in the absence of FMRP expression (Supplementary Fig. S2A), while treatment with Rolipram (a specific inhibitor of PDE4) did not (Supplementary

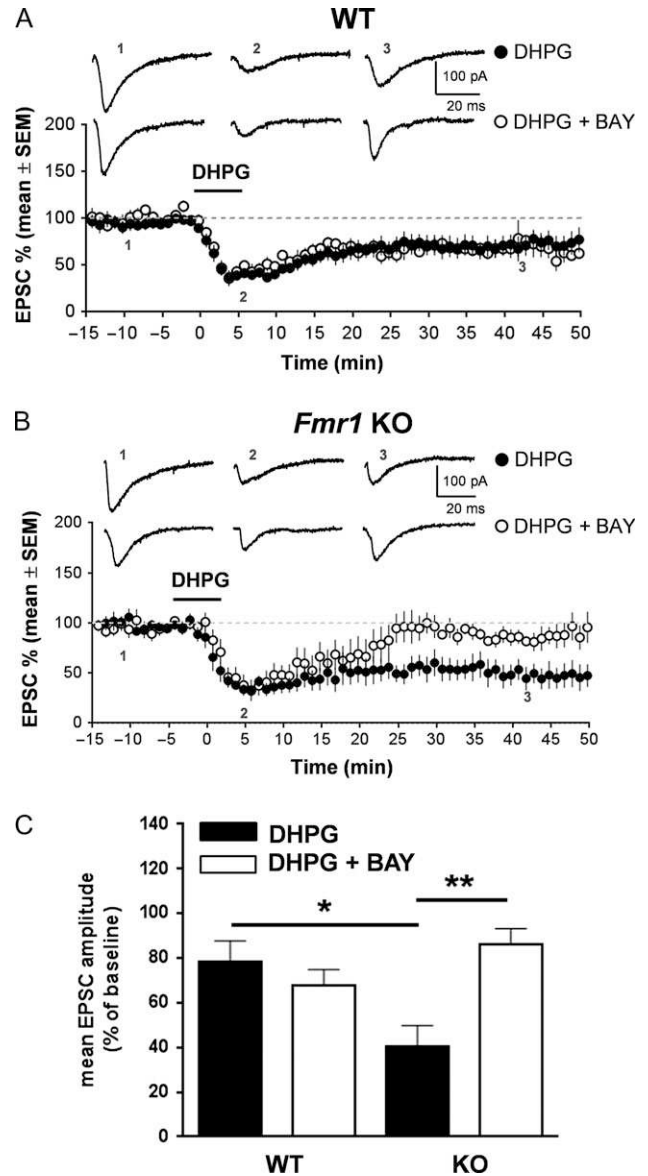


**Figure 2.** Blockade of PDE2A rescues the exaggerated hippocampal mGluR-dependent LTD in the *Fmr1*-KO brain. (A) DHPG (100  $\mu$ M, 5 min) induces a mGluR-LTD of EPSCs recorded from CA1 pyramidal neurons obtained from WT mouse slices ( $n = 6$ ). BAY607550 (50 nM, added intracellularly in the recording pipette) did not modify the amount of mGluR-LTD of EPSCs recorded from CA1 pyramidal neurons in WT slices ( $n = 6$ ). (B) In mouse *Fmr1*-KO slices ( $n = 9$ ), mGluR-LTD was reversed in the presence of intracellular BAY607550 (50 nM). (C) Bar graphs show % EPSC amplitude (mean  $\pm$  SEM from groups of neurons) 40 min after application of DHPG in control conditions or in the presence of intracellular BAY607550 (50 nM). Bar graphs show the mean  $\pm$  SEM values of EPSC % after the indicated pharmacological treatments. Two-way ANOVA were computed ( $F_{\text{genotype}(1,22)} = 1.159$ ,  $P = 0.2933$ ;  $F_{\text{treatment}(1,22)} = 3.919$ ,  $P = 0.2933$ ;  $F_{\text{genotype} \times \text{treatment}(1,22)} = 10.24$ ;  $P = 0.0041$ ) with Bonferroni's post-tests for multiple comparisons of data sets, using genotype (*Fmr1*-KO or WT) and treatment (BAY607550 or vehicle) as between-subjects factor (adjusted  $P$  value: \* $P = 0.0276$ ; \*\* $P = 0.0037$ ).

Fig. S2B). Conversely, the specific blockade of PDE2A activity by BAY607550 promoted a significant increase in cAMP levels in *Fmr1*-KO neurons without affecting its abundance in WT neurons (Supplementary Fig. S2C). This finding suggests a PDE2A-dependent regulation of cAMP levels in *Fmr1*-KO neurons.

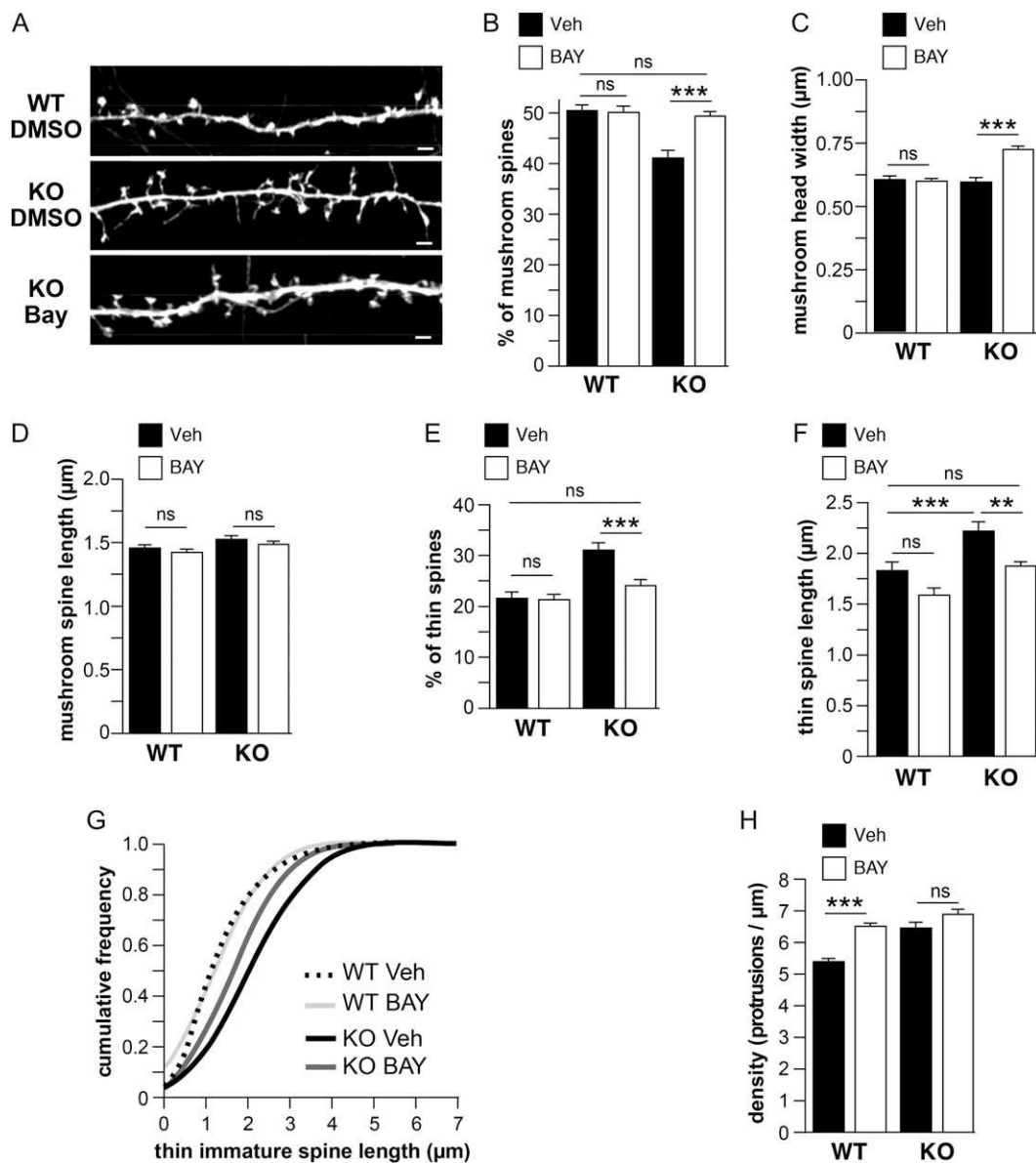


**Figure 3.** Inhibition of PDE2A activity improves *Fmr1*-KO dendritic spine morphology in cultured cortical neurons. (A) Representative high-resolution confocal images showing GFP-expressing WT and *Fmr1*-KO mouse secondary dendrites treated or not for 24 h with 0.2  $\mu$ M BAY607550 to block PDE2A activity. Spine morphology was assessed using NeuronStudio software 19 h post-transduction and compared with the measurement obtained from control DMSO-treated neurons. Scale bars: 2  $\mu$ m. All summary histograms present mean  $\pm$  SEM values, statistical significance was assessed with 2-way ANOVA. The percentage of mature mushroom spines ( $F_{\text{genotype}}(1,110) = 10.98$ ,  $P = 0.0012$ ;  $F_{\text{treatment}}(1,110) = 7.042$ ,  $P = 0.0091$ ;  $F_{\text{genotype} \times \text{treatment}}(1,110) = 8.984$ ;  $P = 0.0034$ ), (B) mushroom head width ( $F_{\text{genotype}}(1,1678) = 18.15$ ,  $P < 0.0001$ ;  $F_{\text{treatment}}(1,1678) = 22.06$ ,  $P < 0.0001$ ;  $F_{\text{genotype} \times \text{treatment}}(1,1678) = 28.41$ ;  $P < 0.0001$ ), (C) and mushroom spine length ( $F_{\text{genotype}}(1,1599) = 7.217$ ,  $P = 0.0073$ ;  $F_{\text{treatment}}(1,1599) = 3.665$ ,  $P = 0.0558$ ;  $F_{\text{genotype} \times \text{treatment}}(1,1599) = 0.002329$ ;  $P = 0.9615$ ) (D) measured in secondary dendrites of control and BAY607550-treated neurons. The percentage of immature thin spines ( $F_{\text{genotype}}(1,111) = 30.25$ ,  $P < 0.0001$ ;  $F_{\text{treatment}}(1,111) = 12.09$ ,  $P = 0.0007$ ;  $F_{\text{genotype} \times \text{treatment}}(1,111) = 8.911$ ;  $P = 0.0035$ ) (E) and thin spine length ( $F_{\text{genotype}}(1,878) = 23.16$ ,  $P < 0.0001$ ;  $F_{\text{treatment}}(1,878) = 17.37$ ,  $P < 0.0001$ ;  $F_{\text{genotype} \times \text{treatment}}(1,878) = 0.6166$ ;  $P = 0.4325$ ) (F) is presented. The consequence of the BAY607550 treatment on the distribution of the thin spine length is depicted as cumulative frequency curves in (G). (H) Histograms showing the mean  $\pm$  SEM values of protrusion frequency after the indicated pharmacological treatments. Two-way ANOVA were computed with Bonferroni post hoc test to assess the treatment effect in neurons from each genotype. (Adjusted P value: \*\* $P < 0.01$ ; \*\*\* $P < 0.001$ .  $N = \sim 1000$ .) Protrusions per condition (3 independent mouse cortical neuron cultures; 24–30 neurons per condition). ns, not significant.

In cultured *Fmr1*-KO neurons (Fig. 3A), the specific inhibition of PDE2A by BAY607550 strongly promoted spine maturation by increasing the number of mushroom spines (Fig. 3B) and reduced the number of immature filopodia (Fig. 3E) to normal WT levels. BAY607550 also had a positive impact on the maturity of *Fmr1*-KO neurons by increasing the head size of mushroom spines (Fig. 3C) and concomitantly reducing the length of thin immature spines to WT levels (Fig. 3F–G). Finally, the

BAY607550 treatment affected neither the length of mature spines (Fig. 3D) nor the density of dendritic protrusions (Fig. 3H) in *Fmr1*-KO neurons.

Abnormal axonal growth has been observed in the fly model of FXS (Morales et al. 2002). Since both cAMP and cGMP fulfill critical roles in axonal growth (Shelly et al. 2010; Shen and Cowan 2010; Averaimo and Nicol 2014; Akiyama et al. 2016), we assessed whether PDE2A activity regulates the length of axons.

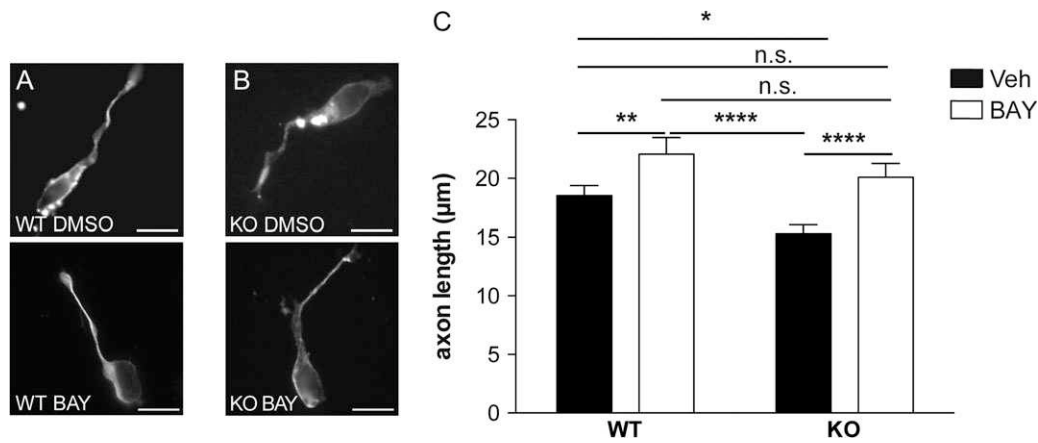


**Figure 4.** PDE2A activity is associated to axon growth regulation. (A, B) Representative pictures of 2 days in vitro cultured WT (A) and *Fmr1*-KO (B) primary cortical neurons treated with vehicle or 1  $\mu$ M BAY607550 as indicated (scale bar: 10  $\mu$ m). (C) Histogram of axon length of WT and *Fmr1*-KO neurons treated with vehicle or with 1  $\mu$ M BAY607550 for 24 h. Results show the mean axon length  $\pm$  SEM from 3 independent cultures on 73 randomly selected cells for each condition. Two-way ANOVA with Tukey post hoc test: DMSO:KO versus DMSO:WT. \*Adjusted P value = 0.0256; BAY:WT versus DMSO:WT. \*\*Adjusted P value = 0.0081; BAY:KO versus DMSO:WT. ns: Adjusted P value = 0.4114; BAY:WT versus DMSO:KO. \*\*\*\*Adjusted P value < 0.0001; BAY:KO versus DMSO:KO. \*\*\*\*Adjusted P value < 0.0001; BAY:KO versus BAY:WT. ns: Adjusted P value = 0.3547; ns, not significant.

Using an immunocytochemistry-based approach, we measured axon length of 2 days in vitro neurons and showed that *Fmr1*-KO neurons had significantly shorter axons than WT cells (Fig. 4A–C). The blockade of PDE2A for 24 h with BAY607550 was sufficient to fully rescue the axonal growth defect of FXS neurons (Fig. 4).

### Critical Role of PDE2A Activity in Defining Social Deficits Displayed by 2 Rodent Models of FXS

The *Fmr1*-KO mouse model of FXS recapitulates the main behavioral traits initially described in FXS patients, such as cognitive deficit and social interaction impairments (Mientjes et al. 2006; Maurin et al. 2014). Since we identified *Pde2a* mRNA as a target of FMRP during the early postnatal life in the mouse brain and since we showed that PDE2A expression was increased in *Fmr1*-KO brains (Maurin et al. 2018), we investigated whether an acute PDE2A blockade in vivo rescued the altered phenotype of *Fmr1*-KO infant (PND 10–14) and adolescent (PND 30) mice in FXS-relevant behaviors (Fig. 5). At infancy, *Fmr1*-KO pups displayed early communicative deficits, since they vocalized significantly less compared with WT pups when separated from the dam and siblings at PND 10 (Fig. 5A,B). Furthermore, *Fmr1*-KO animals showed early deficits in social discrimination, since they were unable to use olfactory cues to discriminate between a neutral odor and their own cage odor in the homing behavior test (Fig. 5C,D). BAY607550 has been shown to efficiently cross the blood-brain barrier when administered i.p., promoting comparable PDE2A inhibition levels as the intracranial injection route (Wang et al. 2017). Our results showed that inhibition of PDE2A activity through i.p. administration of BAY607550 normalized the altered USV profile displayed by PND 10 *Fmr1*-KO mice (Fig. 5B). Remarkably, we validated this result by inhibiting PDE2A with Lu AF64280, another highly specific PDE2A inhibitor (Redrobe et al. 2014). Similar to BAY607550, Lu AF64280 was able to revert the altered USV frequency displayed by *Fmr1*-null pups (Supplementary Fig. S3). This confirms that PDE2A blockade is able to rescue the communicative deficit displayed by *Fmr1*-KO mice in the USV test. Furthermore, we found that treatment with BAY607550 improved the performance of *Fmr1*-KO pups in the homing behavior test (Fig. 5C–E) without

altering the performance of WT pups. Our results pointed out that altered social behavior is a core phenotypic characteristic of the FXS mouse model. Accordingly, compared with WT animals, adolescent *Fmr1*-KO mice showed reduced social interaction, a phenotype that was rescued by PDE2A inhibition (Fig. 5F).

### PDE2A is a Therapeutic Target for FXS

The elevated activity of PDE2A may underlie the deficits in communicative and social domains displayed by *Fmr1*-KO mice throughout development. To confirm this possibility, we chronically treated *Fmr1*-KO mice with BAY607550 from PND 5 to PND21, and tested their social abilities after a washout interval of 9 days. Strikingly, early treatment with BAY607550 reversed the social deficits displayed by *Fmr1*-KO mice at PND 30, showing that the beneficial effects of early PDE2A pharmacological blockade are long-lasting (Fig. 5G). Importantly, the administration of BAY607550 had no effect on the behavior of WT mice (Fig. 5B,D–G), further indicating the specificity of this treatment for the FXS phenotype. Finally, chronically administered BAY607550 rescued the abnormal dendritic spine length in the CA1 region of the hippocampus of *Fmr1*-KO mice (Supplementary Fig. S4). To validate PDE2A as a therapeutic target for FXS, we extended the behavioral analysis to *Fmr1*-KO infant rats. Similar to *Fmr1*-KO mice, *Fmr1*-KO rats vocalized less than WT controls when separated from their mother and siblings at PND 5 and PND 9 (Fig. 6A,B). Remarkably, acute administration of BAY607550 also normalized their altered USV pattern (Fig. 6A,B) and the ability of these infant rats to communicate, without affecting the behavior of WT control animals (Fig. 6A,B).

## Discussion

### Role of PDE2A in Hippocampus and Cortex Development

We have shown that an elevated amount of the PDE2A protein is present in *Fmr1*-null cortex and hippocampus (Maurin et al. 2018). Due to the heterogeneous pattern of the expression level of PDE2A in these brain regions (Stephenson et al. 2009, 2012), we measured here the PDE2A activity at the single cell level demonstrating that the activity of PDE2A is also significantly increased

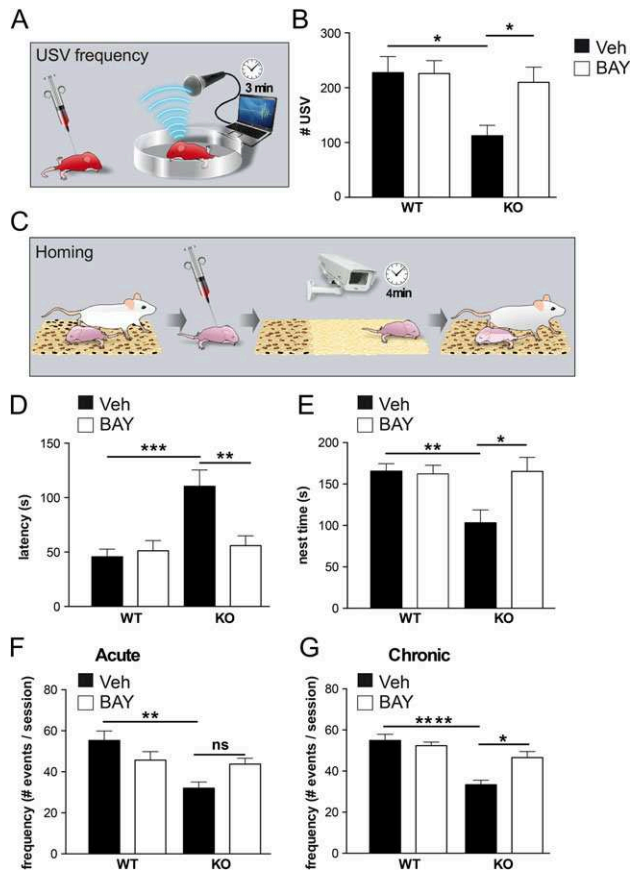


**Figure 5.** Inhibition of PDE2A activity rescues abnormal behaviors in infant and adolescent *Fmr1*-null mice. (A) Scheme of the USV test performed at PND 10. The 30 min after treatment with BAY607550 or vehicle, pups were separated from the dam and ultrasonic vocalizations (USV) were recorded for 3 min. (B) *Fmr1*-KO mice emit less USVs when removed from the nest at PND 10, and this communicative deficit is reversed upon BAY607550 injection ( $F_{\text{genotype}(1,63)} = 7.07$ ,  $P = 0.01$ ;  $F_{\text{treatment}(1,63)} = 3.80$ ,  $P = 0.05$ ;  $F_{\text{genotype} \times \text{treatment}(1,63)} = 4.09$ ;  $P = 0.04$ );  $n$ : WT-VEH = 17; WT-BAY = 17; KO-VEH = 16; KO-BAY = 17). (C) presentation of the homing test performed at PND 14; *Fmr1*-KO mice show (D) longer latency to reach the home-cage bedding ( $F_{\text{genotype}(1,45)} = 11.79$ ,  $P = 0.001$ ;  $F_{\text{treatment}(1,45)} = 5.86$ ,  $P = 0.02$ ;  $F_{\text{genotype} \times \text{treatment}(1,45)} = 8.81$ ;  $P = 0.005$ ) and (E) spend less time in the nest area ( $F_{\text{genotype}(1,45)} = 5.51$ ,  $P = 0.02$ ;  $F_{\text{treatment}(1,45)} = 5.37$ ,  $P = 0.02$ ;  $F_{\text{genotype} \times \text{treatment}(1,45)} = 6.63$ ;  $P = 0.013$ ) in the homing behavior test at PND 14 ( $n$ : WT-VEH = 14; WT-BAY = 16; KO-VEH = 9; KO-BAY = 10); both these parameters are normalized when *Fmr1*-KO mice are treated with BAY 607 550. (F, G) Social interaction was evaluated at PND 30, results are reported for acute (F) ( $n$ : WT-VEH = 18; WT-BAY = 22; KO-VEH = 12; KO-BAY = 9) ( $F_{\text{genotype}(1,57)} = 7.53$ ,  $P = 0.008$ ;  $F_{\text{treatment}(1,57)} = 0.05$ ,  $P = 0.82$ ;  $F_{\text{genotype} \times \text{treatment}(1,57)} = 5.43$ ;  $P = 0.02$ ), and chronic treatment (G) ( $n$ : WT-VEH = 11; WT-BAY = 14; KO-VEH = 8; KO-BAY = 7) ( $F_{\text{genotype}(1,36)} = 28.71$   $P < 0.0001$ ;  $F_{\text{treatment}(1,36)} = 4.358$   $P = 0.0440$ ;  $F_{\text{genotype} \times \text{treatment}(1,36)} = 9.539$   $P = 0.0039$ ). Data represent mean  $\pm$  SEM (adjusted  $P$  value: \* $P < 0.05$ , \*\* $P < 0.01$ , \*\*\* $P < 0.001$ ). Two-way ANOVA was used to assess the effects of BAY607550 in *Fmr1*-KO and WT mice, using genotype (*Fmr1*-KO or WT) and treatment (BAY607550 or vehicle) as between-subjects factor, followed by Tukey multiple comparison post hoc test where appropriate.

in the absence of FMRP. Since an important fraction of PDE2A is localized at the synapse (Russwurm et al. 2009; Maurin et al. 2018), we reasoned that its elevated activity in FXS neurons could impact local cAMP and cGMP homeostasis. It has been reported that the levels of both cAMP and cGMP have critical roles in axon elongation and guidance (Shelly et al. 2010; Akiyama et al. 2016) and in regulating the morphology and growth of dendritic spines

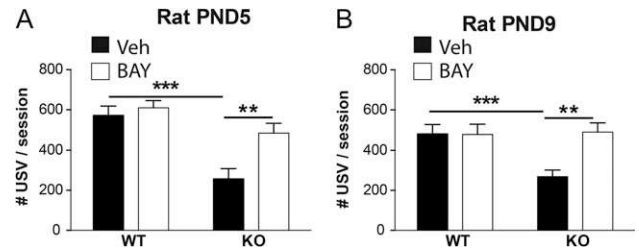


**Figure 6.** Inhibition of PDE2A activity rescues communication deficit in infant *Fmr1*-KO rats. *Fmr1*-KO rats emit less USVs when removed from the nest at PND 5 and 9, and this communicative deficit is reversed upon BAY607550 injection at (A) PND 5 ( $n$ : WT-Veh = 8; WT-Bay = 8; KO-Veh = 9; KO-Bay = 9) ( $F_{\text{genotype}(1,32)} = 5.67$ ,  $P = 0.023$ ;  $F_{\text{treatment}(1,32)} = 6.76$ ,  $P = 0.014$ ;  $F_{\text{genotype} \times \text{treatment}(1,32)} = 7.12$ ;  $P = 0.012$ ) and (B) at PND 9 ( $n$ : WT-Veh = 8; WT-Bay = 8; KO-Veh = 10; KO-Bay = 10) ( $F_{\text{genotype}(1,30)} = 22.72$ ,  $P < 0.001$ ;  $F_{\text{treatment}(1,30)} = 8.27$ ,  $P = 0.007$ ;  $F_{\text{genotype} \times \text{treatment}(1,30)} = 4.28$ ;  $P = 0.047$ ). Data represent the mean number of emitted USV ( $\pm$ SEM) per 3 min-recording session. (Adjusted  $P$  value \*\* $P < 0.01$ , \*\*\* $P < 0.001$ .) Two-way ANOVA was used to assess the effects of BAY607550 in *Fmr1*-KO and WT rats, using genotype (*Fmr1*-KO or WT) and treatment (BAY607550 or vehicle) as between-subjects factors, followed by Tukey multiple comparison post hoc test where appropriate.

(Dityatev and El-Husseini 2011). Indeed, *Fmr1*-KO neurons show an increased PDE2A activity as well as an increased density of spines compared with WT neurons. Blocking the excess of PDE2A activity in *Fmr1*-KO cells leads to spine maturation without decreasing the protrusion density. In WT cells, there is no effect of the BAY607550 on spine maturation but there is an increase in the density of protrusion suggesting separated roles of PDE2A activity in spine formation and maturation but not in spine elimination. This latter result is consistent with our recent findings showing that the density of spines is restored in *Fmr1*-KO olfactory neurons by depleting CYFIP1, a protein connecting FMRP with actin remodeling via Rac1 (Abekhoukh et al. 2017). Moreover, the reduced length of growing axons that we found in 2 DIV *Fmr1*-KO neurons may result from the elevated levels of PDE2A that lead, in turn, to a reduced concentration of axonal cAMP and cGMP. Indeed, the normal length of growing axons is restored after treatment with the specific PDE2A inhibitor BAY607550. Furthermore, it is known that cGMP stimulates synthesis of glutamate via phosphoglycerate kinase (PGK) (Neitz et al. 2011). Consistent with a reduction of cGMP, glutamate levels are reduced in the *Fmr1*-KO cortex (Davidovic et al. 2011) and hippocampus (Hebert et al. 2014). PDE2A is the only PDE identified so far at the presynaptic active zone, associated with docked vesicles and illustrating the importance of such a compartmentalized action (Maurin et al. 2018). Indeed, cAMP abundance coupled to PKA signaling is critical to modulate assembly/disassembly/priming/recycling of neurotransmitter vesicles and, consequently, for synaptic transmission and plasticity events (Crawford and Mennerick 2012) and basal synaptic transmission (Gomez and Breitenbucher 2013). Here we show that the pharmacological inhibition of PDE2A activity rescues the exaggerated mGluR-dependent LTD in *Fmr1*-KO hippocampal slices, a well-characterized hallmark of *Fmr1*-KO brain (Huber et al. 2002).

As we already explained, cGMP and cAMP are involved in axonal growth, spine maturation and synaptic plasticity. Since PDE2A modulates the level of both cAMP and cGMP, we can suggest that its elevated activity in the absence of FMRP contributes to the definition of a neuronal FXS phenotype characterized by altered dendritic morphology, altered axonal length and exaggerated mGluR-LTD.

## PDE2A has a Crucial and Evolutionarily Conserved Role in the Physiopathology of FXS

We show here that *Fmr1*-KO pups have profound deficits in both social communication and social discrimination from the first days of life, as revealed by their altered USV profile and impaired homing behavior, respectively. This, in turn, may alter the proper development of social behavior and social recognition (Terry and Johanson 1996; Melo et al. 2006). In line with this hypothesis, *Fmr1*-KO mice show deficits in social interaction at the adolescent age (Liu and Smith 2009; Dahlhaus and El-Husseini 2010; Kazdoba et al. 2014) that mirror the phenotype observed in FXS patients. Considering the impact of the pharmacological inhibition of PDE2A on the in vitro and ex vivo FXS phenotypes, we assessed whether the PDE2A inhibitor BAY607550 could revert the altered phenotype displayed by *Fmr1*-KO animals in social communication, social discrimination, and social interaction. Administration of BAY607550 normalizes the USV profile displayed by *Fmr1*-KO mice and rats. In addition, this treatment rescues the altered performance of *Fmr1*-KO pups in the homing behavior test, and increases the frequency of social interactions observed in *Fmr1*-KO mice to similar levels as WT animals. While PDE2A was previously linked to cognitive processes (Gomez and Breitenbucher 2013; Redrobe et al. 2014; Lueptow et al. 2016), here, for the first time, we associate its increased activity with altered social deficits. It is interesting to notice that PDE2A is coexpressed with FMRP in a specific class of neurons in the olfactory bulb (Korsak et al. 2017). These neurons have been shown to play a role in thermosensing and detecting stress in congeners as well as in pheromone sensing behavior (Juilfs et al. 1997). This can lead to the speculation that modulating PDE2A activity in these neurons may influence the social behavior. In conclusion, PDE2A may be an attractive target to simultaneously treat the social and communicative dysfunctions characterizing FXS patients. Importantly, mice chronically treated with BAY607550 during the early postnatal development period clearly benefit of the positive effect of this therapy when tested at adolescence. This result strongly suggests that inhibition of PDE2A during infancy has long-term positive effects and provides a strong preclinical rationale for a new therapeutic strategy for FXS patients. Remarkably, we used very low doses of BAY607550 that do not affect the behavior of WT animals. This is important not only because our approach targets a pediatric population but also because low doses should reduce possible toxic side effects of the drug. Interestingly, several trials have been performed in the past with various formulations and dosages of PF-05180999 to treat migraine. We note that the trial in which the highest dosage (360 mg) was tested was discontinued for safety issues, nevertheless former trials using lower doses (30 or 120 mg) were completed but results are yet to be published (<https://clinicaltrials.gov>; #NCT01429740 and #NCT01981499). These studies are however encouraging for future therapeutic intervention for central nervous system (CNS) disorders. Indeed, a phase 1 study has been conducted to investigate the pharmacological properties of TAK915 (another PDE2A inhibitor from Takeda pharmaceuticals (Nakashima et al. 2018)) in order to guide dosage in future clinical studies in schizophrenia (<https://clinicaltrials.gov/ct2/show/results/NCT02584569>). We would suggest that TAK915 may also be used to investigate other CNS disorders in the future.

Our data clearly highlight that PDE2A abundance has a pivotal role in the physiopathology of FXS (Maurin et al. 2018). While cGMP metabolism had never been studied in FXS, it has

already been proposed that the convergence of altered pathways in FXS neurons is responsible for an altered abundance of cAMP in this syndrome. All these pathways are mostly postsynaptic signaling cascades and their relevance for FXS up to date was only studied in adult *Fmr1*-KO mice (Choi et al. 2016; Sethna et al. 2017). Inhibition of *Pde4D* was recently shown to have positive effects on LTD, learning and memory in adult *Fmr1*-KO mice (Gurney et al. 2017). These results provide evidence for the crucial role of cAMP abundance in synaptic plasticity in *Fmr1*-KO mice. However, the PDE4 enzyme family modulates cAMP but not cGMP levels and does not appear to be directly involved in the pathophysiology of FXS since its expression is not deregulated in the synaptosomal preparations obtained from both young and adult *Fmr1*-KO mice (Tang et al. 2015). Furthermore, *Pde4D* mRNA is not a prominent FMRP target in all the CLIP assays that have been performed so far (Darnell et al. 2011; Ascano et al. 2012; Tabet et al. 2016; Maurin et al. 2018).

Also, up to now, most of the treatments proposed for FXS have been tested in adult mice and, even when successful, their translation to the clinic failed (Budimirovic et al. 2017; Castagnola et al. 2017; Erickson et al. 2017). Considering these unsuccessful results, an increasing amount of data suggests the need to treat patients affected by neurodevelopmental disorders at the earliest possible age (Khalfallah et al. 2017 for review, and this study) and for a long period of time (Erickson et al. 2017). Remarkably, BAY607550 treatment rescues the communication deficits in both *Fmr1*-KO mice and rats. This strongly argues in favor of a conserved contribution of PDE2A activity in the regulation of processes and/or communication circuits underpinning social behaviors. In the same direction, our findings showing the rescue of social interaction after 9 days of washout suggest that the chronic treatment performed in infancy of these mice was sufficient to modify circuits for an extended time-period. Even if these processes should be investigated in depth in the near future, overall these findings further reinforce the translation potential of this targeted therapeutic approach for FXS.

## Conclusions

PDE2A is an overlooked phosphodiesterase previously linked to cognitive processes (Boess et al. 2004; Redrobe et al. 2014; Mikami et al. 2017; Nakashima et al. 2018). Here, for the first time, we establish a relationship between its altered expression and defects in axonal growth, maturation of dendritic spines, mGluR-dependent hippocampal LTD and altered social communication, social discrimination and social interaction behaviors at early developmental ages in *Fmr1*-KO animals. FXS is the leading inherited cause of ID and ASD and the *Fmr1*-KO mouse and rat models are not only widely recognized animal models of FXS but also genetic models of ASD. Since we highlight here that PDE2A abundance has a pivotal role in the pathophysiology of FXS, an implication of PDE2A in other forms of autism can be hypothesized and therefore, targeting PDE2A could be considered a generalized pharmacological target to treat social deficits common to both ASD and FXS.

## Supplementary Material

Supplementary material is available at *Cerebral Cortex* online.

## Funding

Institut National de la Santé et de la Recherche Médicale (INSERM); Centre National de la Recherche Scientifique (CNRS); Université Côte d'Azur (UCA); Agence Nationale de la Recherche: ANR-12-BSV4-0020 to B.B. and ANR-15-CE16-0015 to B.B. and S.M. Fondation Recherche Médicale (FRM) DEQ20140329490 to BB and FRM-ING20140129004 to B.B. and T.M.; Fondation Jérôme Lejeune to B.B. and S.M. FRAXA Foundation to T.M. PV was supported (in part) by the Investissements d'Avenir program managed by the ANR under reference ANR-11-IDEX-0004-02 (LabEx Bio-Psy). VT was in part supported by Grant to Department of Science, Roma Tre University (MIUR-Italy Dipartimenti di eccellenza, ARTICOLO 1, COMMI 314-337 LEGGE 232/2016). S.C. and M.D. are recipient of international PhD fellowships "LabEx Signallife Program" by ANR-11-LABX-0028-01 (to B.B. and SM.).

## Author's Contribution

Li.C. and E.M. performed biosensor cAMP experiments under the guidance of P.V. T.M. performed cAMP and cGMP measures in cultured neurons as described in M&M. La.C. and L.S. performed LTD studies under the supervision of Lu.C. S.C. and M.D. performed cortical neuronal cultures under the guidance of T.M. and B.B. S.C. and M.J. performed RT-qPCR studies under the guidance of B.B. A.K. and G.P. performed dendritic spines analysis under the guidance of S.M. M.J. performed axonal studies under the guidance of T.M. and B.B. M.J., S.D., F.M., M.S., and S.S. performed behavioral studies under the supervision of V.T. M.J., S.D., and T.M. performed Golgi staining under the supervision of B.B. A.D.G. synthesized Lu AF64280 under the guidance of S.A. T.M. and B.B. designed the study, T.M., V.T., L.C., P.V., S.M., and B.B. analyzed the data and wrote the article.

## Notes

The authors are indebted with E. Lalli and M. Capovilla for critical reading of the article, M. Grossi, M. Beal and C. Gandin for technical help, F. Aguila for graphical artwork and I. Caillé for discussion and gift of some materials. *Conflict of interest:* The authors declare no competing financial interests.

## References

Abekhouk S, Sahin HB, Grossi M, Zongaro S, Maurin T, Madrigal I, Kazue-Sugioka D, Raas-Rothschild A, Doulazmi M, Carrera P, et al. 2017. New insights into the regulatory function of CYFIP1 in the context of WAVE- and FMRP-containing complexes. *Dis Model Mech.* 10:463–474.

Akiyama H, Fukuda T, Tojima T, Nikolaev VO, Kamiguchi H. 2016. Cyclic nucleotide control of microtubule dynamics for axon guidance. *J Neurosci.* 36:5636–5649.

Antar LN, Dichtenberg JB, Plociniak M, Afroz R, Bassell GJ. 2005. Localization of FMRP-associated mRNA granules and requirement of microtubules for activity-dependent trafficking in hippocampal neurons. *Genes Brain Behav.* 4:350–359.

Antar LN, Li C, Zhang H, Carroll RC, Bassell GJ. 2006. Local functions for FMRP in axon growth cone motility and activity-dependent regulation of filopodia and spine synapses. *Mol Cell Neurosci.* 32:37–48.

Ascano M Jr., Mukherjee N, Bandaru P, Miller JB, Nusbaum JD, Corcoran DL, Langlois C, Munschauer M, Dewell S, Hafner M, et al. 2012. FMRP targets distinct mRNA sequence elements to regulate protein expression. *Nature.* 492:382–386.

Averaimo S, Nicol X. 2014. Intermingled cAMP, cGMP and calcium spatiotemporal dynamics in developing neuronal circuits. *Front Cell Neurosci.* 8:376.

Bassell GJ, Warren ST. 2008. Fragile X syndrome: loss of local mRNA regulation alters synaptic development and function. *Neuron.* 60:201–214.

Boess FG, Hendrix M, van der Staay FJ, Erb C, Schreiber R, van Staveren W, de Vente J, Prickaerts J, Blokland A, Koenig G. 2004. Inhibition of phosphodiesterase 2 increases neuronal cGMP, synaptic plasticity and memory performance. *Neuropharmacology.* 47:1081–1092.

Budimirovic DB, Berry-Kravis E, Erickson CA, Hall SS, Hessler D, Reiss AL, King MK, Abbeduto L, Kaufmann WE. 2017. Updated report on tools to measure outcomes of clinical trials in fragile X syndrome. *J Neurodev Dis.* 9:14.

Castagnola S, Bardoni B, Maurin T. 2017. The search for an effective therapy to treat fragile X syndrome: dream or reality? *Front Syn Neurosci.* 9:15.

Choi CH, Schoenfeld BP, Bell AJ, Hinchey J, Rosenfelt C, Gertner MJ, Campbell SR, Emerson D, Hinchey P, Kollaros M, et al. 2016. Multiple drug treatments that increase cAMP signaling restore long-term memory and aberrant signaling in fragile X syndrome models. *Front Behav Neurosci.* 10:136.

Comery TA, Harris JB, Willems PJ, Oostra BA, Irwin SA, Weiler JJ, Greenough WT. 1997. Abnormal dendritic spines in fragile X knockout mice: maturation and pruning deficits. *Proc Natl Acad Sci USA.* 94:5401–5404.

Costa L, Spatuzza M, D'Antoni S, Bonaccorso CM, Trovato C, Musumeci SA, Leopoldo M, Lacivita E, Catania MV, Ciranna L. 2012. Activation of 5-HT7 serotonin receptors reverses metabotropic glutamate receptor-mediated synaptic plasticity in wild-type and Fmr1 knockout mice, a model of Fragile X syndrome. *Biol Psychiatry.* 72:924–933.

Crawford DC, Mennerick S. 2012. Presynaptically silent synapses: dormancy and awakening of presynaptic vesicle release. *Neuroscientist.* 18:216–223.

Dahlhaus R, El-Husseini A. 2010. Altered neuroligin expression is involved in social deficits in a mouse model of the fragile X syndrome. *Behav Brain Res.* 208:96–105.

Darnell JC, Van Driesche SJ, Zhang C, Hung KY, Mele A, Fraser CE, Stone EF, Chen C, Fak JJ, Chi SW, et al. 2011. FMRP stalls ribosomal translocation on mRNAs linked to synaptic function and autism. *Cell.* 146:247–261.

Davidovic L, Navratil V, Bonaccorso CM, Catania MV, Bardoni B, Dumas ME. 2011. A metabolomic and systems biology perspective on the brain of the fragile X syndrome mouse model. *Genome Res.* 21:2190–2202.

Devader C, Khayachi A, Veyssière J, Moha Ou Maati H, Roulot M, Moreno S, Borsotto M, Martin S, Heurteaux C, Mazella J. 2015. In vitro and in vivo regulation of synaptogenesis by the novel antidepressant spadin. *Br J Pharmacol.* 172:2604–2617.

Ding L, Zhang C, Masood A, Li J, Sun J, Nadeem A, Zhang HT, O'Donnell JM, Xu Y. 2014. Protective effects of phosphodiesterase 2 inhibitor on depression- and anxiety-like behaviors: involvement of antioxidant and anti-apoptotic mechanisms. *Behav Brain Res.* 268:150–158.

Dityatev A, El-Husseini A. 2011. *Molecular mechanisms of synaptogenesis.* New York; London: Springer.

Erickson CA, Davenport MH, Schaefer TL, Wink LK, Pedapati EV, Sweeney JA, Fitzpatrick SE, Brown WT, Budimirovic D, Hagerman RJ, et al. 2017. Fragile X targeted pharmacotherapy: lessons learned and future directions. *J Neurodev Disord.* 9:7.

- Gomez L, Breitenbucher JG. 2013. PDE2 inhibition: potential for the treatment of cognitive disorders. *Bioorg Med Chem Lett.* 23:6522–6527.
- Gothelf D, Furfaro JA, Hoeft F, Hoeft F, Eckert MA, Hall SS, O'Hara R, Erba HW, Ringel J, Hayashi KM, et al. 2008. Neuroanatomy of Fragile X syndrome is associated with aberrant behavior and the FragileX mental retardation protein (FMRP). *Ann Neurol.* 63:40–51.
- Gurney ME, Cogram P, Deacon RM, Rex C, Tranfaglia M. 2017. Multiple behavior phenotypes of the fragile-X syndrome mouse model respond to chronic inhibition of phosphodiesterase-4D (PDE4D). *Sci Rep.* 7:14653.
- Hebert B, Pietropaolo S, Meme S, Laudier B, Laugeray A, Doisne N, Quartier A, Lefeuvre S, Got L, Cahard D, et al. 2014. Rescue of fragile X syndrome phenotypes in Fmr1 KO mice by a BKCa channel opener molecule. *Orphanet J Rare Dis.* 9:124.
- Hoeft F, Carter JC, Lightbody AA, Cody Hazlett H, Piven J, Reiss AL. 2010. Region-specific alterations in brain development in one- to three-year-old boys with fragile X syndrome. *Proc Natl Acad Sci USA.* 107:9335–9339.
- Huber KM, Gallagher SM, Warren ST, Bear MF. 2002. Altered synaptic plasticity in a mouse model of fragile X mental retardation. *Proc Natl Acad Sci USA.* 99:7746–7750.
- Irwin SA, Galvez R, Greenough WT. 2000. Dendritic spine structural anomalies in fragile-X mental retardation syndrome. *Cereb Cortex.* 10:1038–1044.
- Jamain S, Radyushkin K, Hammerschmidt K, Granon S, Boretius S, Varoqueaux F, Ramanantsoa N, Gallego J, Ronnenberg A, Winter D, et al. 2008. Reduced social interaction and ultrasonic communication in a mouse model of monogenic heritable autism. *Proc Natl Acad Sci USA.* 105:1710–1715.
- Juilfs DM, Fülle HJ, Zhao AZ, Houslay MD, Garbers DL, Beavo JA. 1997. A subset of olfactory neurons that selectively express cGMP-stimulated phosphodiesterase (PDE2) and guanylyl cyclase-D define a unique olfactory signal transduction pathway. *Proc Natl Acad Sci USA.* 94:3388–3395.
- Kazdoba TM, Leach PT, Silverman JL, Crawley JN. 2014. Modeling fragile X syndrome in the Fmr1 knockout mouse. *Intractable Rare Dis Res.* 3:118–133.
- Khalifallah O, Jarjat M, Davidovic L, Nottet N, Cestele S, Mangegazza M, Bardoni B. 2017. Depletion of the fragile X mental retardation protein in embryonic stem cells alters the kinetics of neurogenesis. *Stem Cells.* 35:374–385.
- Khayachi A, Gwizdek C, Poupon G, Alcor D, Chafai M, Cassé F, Maurin T, Prieto M, Folci A, De Graeve F, et al. 2018. Sumoylation regulates FMRP-mediated dendritic spine elimination and maturation. *Nat Commun.* 9:757.
- Kilkenny C, Browne WJ, Cuthill IC, Emerson M, Altman DG. 2010. Improving bioscience research reporting: the ARRIVE guidelines for reporting animal research. *PLoS Biol.* 8:e1000412.
- Korsak LIT, Shepard KA, Akins MR. 2017. Cell type-dependent axonal localization of translational regulators and mRNA in mouse peripheral olfactory neurons. *J Comp Neurol.* 525:2201–2215.
- Lai JK, Lerch JP, Doering LC, Foster JA, Ellegood J. 2016. Regional brain volumes changes in adult male FMR1-KO mouse on the FVB strain. *Neurosci.* 318:12–21.
- Liu ZH, Smith CB. 2009. Dissociation of social and nonsocial anxiety in a mouse model of fragile X syndrome. *Neurosci Lett.* 454:62–66.
- Lueptow LM, Zhan CG, O'Donnell JM. 2016. Cyclic GMP-mediated memory enhancement in the object recognition test by inhibitors of phosphodiesterase-2 in mice. *Psychopharmacology (Berl).* 233:447–456.
- Masood A, Huang Y, Hajjhussein H, Xiao L, Li H, Sun J, Nadeem A, Zhang HT, O'Donnell JM, Xu Y. 2009. Anxiolytic effects of phosphodiesterase-2 inhibitors associated with increased cGMP signaling. *J Pharmacol Exp Ther.* 331:690–699.
- Masood A, Nadeem A, Mustafa SJ, O'Donnell JM. 2008. Reversal of oxidative stress-induced anxiety by inhibition of phosphodiesterase-2 in mice. *J Pharmacol Exp Ther.* 326:369–379.
- Maurice DH, Ke H, Ahmad F, Wang Y, Chung J, Manganiello VC. 2014. Advances in targeting cyclic nucleotide phosphodiesterases. *Nat Rev Drug Discov.* 13:290–314.
- Maurin T, Lebrigand L, Castagnola S, Paquet A, Jarjat M, Grossi M, Popa A, Rage F, Bardoni B. 2018. HITS-CLIP in various brain areas reveals new targets and new modalities of RNA binding by fragile X mental retardation protein. *Nucleic Acids Res.* 46:6344–6355.
- Maurin T, Zongaro S, Bardoni B. 2014. Fragile X syndrome: from molecular pathology to therapy. *Neurosci Biobehav Rev.* 2:242–255.
- Melo AI, Lovic V, Gonzalez A, Madden M, Sinopoli K, Fleming AS. 2006. Maternal and littermate deprivation disrupts maternal behavior and social-learning of food preference in adulthood: tactile stimulation, nest odor, and social rearing prevent these effects. *Dev Psychobiol.* 48:209–219.
- Mientjes EJ, Nieuwenhuizen I, Kirkpatrick L, Zu T, Hoogeveen-Westerveld M, Severijnen L, Rifé M, Willemsen R, Nelson DL, Oostra BA. 2006. The generation of a conditional Fmr1 knockout mouse model to study Fmrp function in vivo. *Neurobiol Dis.* 21:549–555.
- Mikami S, Sasaki S, Asano Y, Ujikawa O, Fukumoto S, Nakashima K, Oki H, Kamiguchi N, Imada H, Iwashita H, et al. 2017. Discovery of an orally bioavailable, brain-penetrating, in vivo active phosphodiesterase 2A inhibitor lead series for the treatment of cognitive disorders. *J Med Chem.* 60:7658–7676.
- Morales J, Hiesinger PR, Schroeder AJ, Kume K, Verstreken P, Jackson FR, Nelson DL, Hassan BA. 2002. Drosophila fragile X protein, DFXR, regulates neuronal morphology and function in the brain. *Neuron.* 34:961–972.
- Nakashima M, Imada H, Shiraishi E, Ito Y, Suzuki N, Miyamoto M, Taniguchi T, Iwashita H. 2018. Phosphodiesterase 2A inhibitor TAK-915 ameliorates cognitive impairments and social withdrawal in N-methyl-D-aspartate receptor antagonist-induced rat models of schizophrenia. *J Pharmacol Exp Ther.* 365:179–188.
- Neitz A, Mergia E, Eysel UT, Koesling D, Mittmann T. 2011. Presynaptic nitric oxide/cGMP facilitates glutamate release via hyperpolarization-activated cyclic nucleotide-gated channels in the hippocampus. *Eur J Neurosci.* 33:1611–1621.
- Nimchinsky EA, Oberlander AM, Svoboda K. 2001. Abnormal development of dendritic spines in FMR1 knock-out mice. *J Neurosci.* 21:5139–5146.
- Park AJ, Havekes R, Choi JH, Luczak V, Nie T, Huang T, Abel T. 2014. A presynaptic role for PKA in synaptic tagging and memory. *Neurobiol Learn Mem.* 114:101–112.
- Polito M, Klarenbeek J, Jalink K, Paupardin-Tritsch D, Vincent P, Castro LR. 2013. The NO/cGMP pathway inhibits transient cAMP signals through the activation of PDE2 in striatal neurons. *Front Cell Neurosci.* 7:211.
- Redrobe JP, Jorgensen M, Christoffersen CT, Montezinho LP, Bastlund JF, Carnerup M, Bundgaard C, Lerdrup L, Plath N. 2014. In vitro and in vivo characterisation of Lu AF64280, a novel, brain penetrant phosphodiesterase (PDE) 2A inhibitor: potential relevance to cognitive deficits in schizophrenia. *Psychopharmacology (Berl).* 231:3151–3167.

- Rodriguez A, Ehlenberger DB, Dickstein DL, Hof PR, Wearne SL. 2008. Automated three-dimensional detection and shape classification of dendritic spines from fluorescence microscopy images. *PLoS One*. 3:e1997.
- Russwurm C, Zoidl G, Koesling D, Russwurm M. 2009. Dual acylation of PDE2A splice variant 3: targeting to synaptic membranes. *J Biol Chem*. 284:25782–25790.
- Servadio M, Melancia F, Manduca A, di Masi A, Schiavi S, Cartocci V, Pallottini V, Campolongo P, Ascenzi P, Trezza V. 2016. Targeting anandamide metabolism rescues core and associated autistic-like symptoms in rats prenatally exposed to valproic acid. *Transl Psychiatry*. 6:e902.
- Sethna F, Feng W, Ding Q, Robison AJ, Feng Y, Wang H. 2017. Enhanced expression of ADCY1 underlies aberrant neuronal signalling and behaviour in a syndromic autism model. *Nat Commun*. 8:14359.
- Shelly M, Lim BK, Cancedda L, Heilshorn SC, Gao H, Poo MM. 2010. Local and long-range reciprocal regulation of cAMP and cGMP in axon/dendrite formation. *Science*. 327:547–552.
- Shen K, Cowan CW. 2010. Guidance molecules in synapse formation and plasticity. *Cold Spring Harb Perspect Biol*. 2:a001842.
- Stephenson DT, Coskran TM, Kelly MP, Kleiman RJ, Morton D, O'Neill SM, Schmidt CJ, Weinberg RJ, Menniti FS. 2012. The distribution of phosphodiesterase 2A in the rat brain. *Neurosci*. 226:145–155.
- Stephenson DT, Coskran TM, Wilhelms MB, Adamowicz WO, O'Donnell MM, Muravnick KB, Menniti FS, Kleiman RJ, Morton D. 2009. Immunohistochemical localization of phosphodiesterase 2A in multiple mammalian species. *J Histochem Cytochem*. 57:933–949.
- Tabet R, Moutin E, Becker JA, Heintz D, Fouillen L, Flatter E, Krężel W, Alunni V, Koebel P, Dembélé D, et al. 2016. Fragile X mental retardation protein (FMRP) controls diacylglycerol kinase activity in neurons. *Proc Natl Acad Sci USA*. 113: E3619–E3628.
- Tang B, Wang T, Wan H, Han L, Qin X, Zhang Y, Wang J, Yu C, Berton F, Francesconi W, et al. 2015. *Fmr1* deficiency promotes age-dependent alterations in the cortical synaptic proteome. *Proc Natl Acad Sci USA*. 112:E4697–E4706.
- Terranova ML, Laviola G. 2005. Scoring of social interactions and play in mice during adolescence. *Curr Protoc Toxicol*. Chapter. 13: 13.10.1–13.10.11.
- Terry LM, Johanson IB. 1996. Effects of altered olfactory experiences on the development of infant rats' responses to odors. *Dev Psychobiol*. 29:353–377.
- Wang L, Xiaokaiti Y, Wang G, Xu X, Chen L, Huang X, Liu L, Pan J, Hu S, Chen Z, et al. 2017. Inhibition of PDE2 reverses beta amyloid induced memory impairment through regulation of PKA/PKG-dependent neuro-inflammatory and apoptotic pathways. *Sci Rep*. 7:12044.

# Publication 5



# New Insights Into the Role of Ca<sub>v</sub>2 Protein Family in Calcium Flux Deregulation in *Fmr1*-KO Neurons

Sara Castagnola<sup>1,2</sup>, Sébastien Delhaye<sup>1,2</sup>, Alessandra Folci<sup>1</sup>, Agnès Paquet<sup>1</sup>, Frédéric Brau<sup>1</sup>, Fabrice Duprat<sup>3</sup>, Marielle Jarjat<sup>1,2</sup>, Mauro Grossi<sup>1,2</sup>, Méline Béal<sup>1,2</sup>, Stéphane Martin<sup>3</sup>, Massimo Mantegazza<sup>3</sup>, Barbara Bardoni<sup>2,3</sup> and Thomas Maurin<sup>1,2\*</sup>

<sup>1</sup>Université Côte d'Azur, CNRS UMR7275, IPMC, Valbonne, France, <sup>2</sup>CNRS LIA "Neogenex", Valbonne, France, <sup>3</sup>Université Côte d'Azur, INSERM, CNRS UMR7275, IPMC, Valbonne, France

Fragile X syndrome (FXS), the most common form of inherited intellectual disability (ID) and a leading cause of autism, results from the loss of expression of the *Fmr1* gene which encodes the RNA-binding protein Fragile X Mental Retardation Protein (FMRP). Among the thousands mRNA targets of FMRP, numerous encode regulators of ion homeostasis. It has also been described that FMRP directly interacts with Ca<sup>2+</sup> channels modulating their activity. Collectively these findings suggest that FMRP plays critical roles in Ca<sup>2+</sup> homeostasis during nervous system development. We carried out a functional analysis of Ca<sup>2+</sup> regulation using a calcium imaging approach in *Fmr1*-KO cultured neurons and we show that these cells display impaired steady state Ca<sup>2+</sup> concentration and an altered entry of Ca<sup>2+</sup> after KCl-triggered depolarization. Consistent with these data, we show that the protein product of the *Cacna1a* gene, the pore-forming subunit of the Ca<sub>v</sub>2.1 channel, is less expressed at the plasma membrane of *Fmr1*-KO neurons compared to wild-type (WT). Thus, our findings point out the critical role that Ca<sub>v</sub>2.1 plays in the altered Ca<sup>2+</sup> flux in *Fmr1*-KO neurons, impacting Ca<sup>2+</sup> homeostasis of these cells. Remarkably, we highlight a new phenotype of cultured *Fmr1*-KO neurons that can be considered a novel cellular biomarker and is amenable to small molecule screening and identification of new drugs to treat FXS.

## OPEN ACCESS

### Edited by:

Regina Dahlhaus,  
Friedrich-Alexander-Universität  
Erlangen-Nürnberg, Germany

### Reviewed by:

Maija Liisa Castrén,  
University of Helsinki, Finland  
Christina Gross,  
Cincinnati Children's Hospital Medical  
Center, United States

### \*Correspondence:

Thomas Maurin  
maurin@ipmc.cnrs.fr

**Keywords:** Fragile X syndrome, Ca<sub>v</sub>2.1, calcium homeostasis, ratiometric calcium imaging, *Cacna1a*

## INTRODUCTION

Fragile X syndrome (FXS) is the most common form of inherited intellectual disability (ID) and the leading identified monogenic cause of autism (Maurin et al., 2014; Castagnola et al., 2017). FXS is caused by the silencing of the *Fmr1* gene encoding the Fragile X Mental Retardation Protein (FMRP), an RNA-binding protein modulating the expression of thousands of mRNAs primarily at the translational level in particular, it has been shown to regulate translation at the synaptic level. Furthermore, FMRP has been reported to be involved in different steps of RNA metabolism, indeed it is a component of various ribonucleoproteic complexes (mRNPs), including the RNA granules, the mRNP involved in transport along neurites (Maurin et al., 2014, 2018a).

Several reports have shown that FMRP binds multiple RNAs encoding regulators of ion homeostasis and more particularly involved in the calcium ion pathway (Brown et al., 2001; Miyashiro et al., 2003; Darnell et al., 2011; Ascano et al., 2012; Maurin et al., 2018a).

**Received:** 16 April 2018

**Accepted:** 30 August 2018

**Published:** 27 September 2018

### Citation:

Castagnola S, Delhaye S, Folci A, Paquet A, Brau F, Duprat F, Jarjat M, Grossi M, Béal M, Martin S, Mantegazza M, Bardoni B and Maurin T (2018) New Insights Into the Role of Ca<sub>v</sub>2 Protein Family in Calcium Flux Deregulation in *Fmr1*-KO Neurons. *Front. Mol. Neurosci.* 11:342. doi: 10.3389/fnmol.2018.00342

Furthermore, the search for FMRP-interacting proteins has resulted into the identification of dozens of partners, including ion channels (Bardoni et al., 2006; Ferron, 2016; and this study). Consistently with these findings, ion homeostasis defects in FXS neurons have been described (Chen et al., 2003; Meredith et al., 2007; Brown et al., 2010; Deng et al., 2013; Ferron et al., 2014; Hebert et al., 2014; Zhang et al., 2014; Contractor et al., 2015; Myrick et al., 2015; Wahlstrom-Helgren and Klyachko, 2015; Achuta et al., 2018). In particular, FMRP has been reported to directly interact with two members of the Voltage Gated Calcium Channels (VGCC) family, namely Ca<sub>v</sub>2.1 and Ca<sub>v</sub>2.2 (Ferron et al., 2014).

Cytosolic calcium concentration is set by the balance between calcium influx and efflux as well as by the exchange of calcium ion with internal stores. Calcium homeostasis is tightly controlled and involves multiple protein complexes such as ATPase pumps, transporters and ion channels in various cellular compartments (Clapham, 2007).

VGCCs respond to plasma membrane depolarization by allowing extracellular calcium ions to flow into cells according to their concentration gradient. Calcium can then act as a second messenger of cell depolarization activating various key intracellular signaling pathways, inducing contraction in muscle cells, protein phosphorylation, secretion and synaptic transmission. VGCCs are heteromers composed by the assembly of a pore-forming subunit (encoded by the corresponding  $\alpha$ 1 gene) and auxiliary  $\beta$  and  $\alpha$ 2 $\delta$  proteins (Dolphin, 2016). VGCCs can be distinguished as L-, N-, R- and P/Q-type channels depending on the identity of the pore-forming subunit. L- and T-type VGCCs are found in a great variety of cells, while N-, P/Q- and R-type are mostly expressed in neurons (Catterall, 2011).

The *Cacna1a* gene encodes the P/Q-type VGCC Ca<sub>v</sub>2.1, which is critical for the depolarization-evoked release of neurotransmitters at the presynaptic terminals (Simms and Zamponi, 2014). Ca<sub>v</sub>2.1 is mostly expressed in the cerebellum, consequently mutations in the *Cacna1a* gene are associated with several neurological disorders such as episodic ataxia and spino-cerebellar ataxia (Zhuchenko et al., 1997). More recently, new mutations in this gene have been identified in four unrelated families with ID, attention deficit, hyperactivity and autism spectrum disorder (Damaj et al., 2015). This suggests that Ca<sub>v</sub>2.1 may play a previously under-appreciated role in brain regions other than the cerebellum and could have been implicated roles in cognition, memory and social interaction regulation. Indeed, regulation of Ca<sub>v</sub>2.1 channels by calcium sensor proteins is required for normal short-term synaptic plasticity, LTP, and spatial learning and memory in mice (Nanou et al., 2016).

We thus investigated calcium homeostasis using ratiometric calcium imaging in *Fmr1*-KO neurons. Our results show that neurons lacking FMRP are not only more sensitive to Ca<sub>v</sub>2.2 inhibition but also less sensitive to Ca<sub>v</sub>2.1 inhibition compared to wild-type (WT) neurons and this is a consequence of an impaired membrane expression of this channel in the absence of FMRP. We propose here a model in which FMRP is involved in the regulation of the relative membrane expression of P/Q- and N-type VGCCs.

## MATERIALS AND METHODS

### Primary Neuronal Cultures

Cultures were prepared from the cortex of embryonic stage E14.5 WT and *Fmr1*-KO embryos as previously described (Abekhokh et al., 2017; Maurin et al., 2018a). Neurons (250,000 cells) were plated on ornithine-coated glass coverslips (35 mm diameter) and cultivated in complete medium: Neurobasal (Invitrogen) supplemented with B-27 (Invitrogen) and glutamax (Invitrogen). Neurons were fed weekly by removing 10% of the culture medium and replacing it with fresh complete medium.

### Ratiometric Calcium Imaging

Primary cortical neurons Day-*In-Vitro* 19–23 (DIV 19–23; 13 independent cultures) grown on coverslips were incubated in neurobasal containing 20  $\mu$ M Fura2-AM (Invitrogen) for 30 min at 37°C. After two washes with HEPES-buffered Tyrode's calcium solution (in mM: 139 NaCl, 15 glucose, 1.25 Na<sub>2</sub>HPO<sub>4</sub> dibasic heptahydrate, 1.8 MgSO<sub>4</sub> heptahydrate, 1.6 CaCl<sub>2</sub> dihydrate, 3 KCl, 10 HEPES), coverslips were placed in a metal chamber on an inverted microscope (AxioObserver, Carl Zeiss) equipped with a 300W Xenon lamp (Sutter Instruments) and a Fluor 40 $\times$  NA 1.4 oil immersion objective. Cells were perfused at 22°C throughout the recording with Tyrode's calcium solution. The pharmacological stimulations were performed by supplementing the calcium recording solution with either DiHydroxyPhenylGlycine (DHPG, 100  $\mu$ M) or KCl (50 mM) or VGCC antagonist ( $\omega$ -agatoxin-Iva (100 nM);  $\omega$ -conotoxin GV1a (1  $\mu$ M); Nitrendipine (1  $\mu$ M)) or VGCC antagonist (same concentrations) + KCl. A calibration step was performed at the end of every recording by applying successively 0 Ca<sup>2+</sup> (in mM: 129 NaCl, 15 glucose, 1.25 Na<sub>2</sub>HPO<sub>4</sub> dibasic heptahydrate, 1.8 MgSO<sub>4</sub> heptahydrate, 0.5 EGTA, 3 KCl, 10 HEPES), then 0 Ca<sup>2+</sup> + ionomycin (5  $\mu$ M) and finally 10 Ca<sup>2+</sup> + ionomycin (5  $\mu$ M; in mM: 129 NaCl, 15 glucose, 1.25 Na<sub>2</sub>HPO<sub>4</sub> dibasic heptahydrate, 1.8 MgSO<sub>4</sub> heptahydrate, 10 CaCl<sub>2</sub> dihydrate, 3 KCl, 10 HEPES) solutions. This calibration step allows to quantify the lowest and the highest probe fluorescence F<sub>340/380</sub> ratio for every Region of Interest (ROI); the maximal value was used subsequently to normalize the fluorescence F<sub>340/380</sub> measurements. Every recording experiment followed the same protocol:

Tyrode's—40 s; Tyrode's + DHPG—40 s; Tyrode's—60 s; Tyrode's + KCl—20 s; Tyrode's—60 s; Tyrode's + KCl—20 s; Tyrode's—60 s; Tyrode's + VGCC antagonist—60 s; Tyrode's + KCl + VGCC antagonist—20 s; Tyrode's + VGCC antagonist—60 s; Tyrode's + KCl + VGCC antagonist—20 s; Tyrode's + VGCC antagonist—60 s; Tyrode's + KCl + VGCC antagonist—20 s; Tyrode's + VGCC antagonist—60 s; Tyrode's (0 Calcium)—80 s; calibration (see above).

Fura2 was sequentially excited at 340 nm and 380 nm, and the emission monitored at 510 nm. Images were acquired with a cascade 512 EMCCD camera every 2 s using the Metafluor software (Roper Scientific). For each recorded cell, the intracellular calcium concentration [Ca<sup>2+</sup>]<sub>i</sub> was estimated by measuring the F<sub>340/380</sub> nm ratio of fluorescence normalized to the

maximal probe fluorescence measured when cells were perfused with the 10 Calcium + ionomycin solution.  $\omega$ -agatoxin-IVA and  $\omega$ -conotoxin GVIA were purchased from Smarttox, Nitrendipine from Sigma-Aldrich. Resting calcium levels (“baseline”) were measured as the average fluorescence from the first 40 s of each recording. For KCl stimulation, for each cell analyzed we report the results of the mean of two maximal  $F_{340/380}$  in two consecutive stimulations. The Drug Response (DR) represents the mean of the two max  $F_{340/380}$  in two consecutive stimulations over the mean of the three max  $F_{340/380}$  in three consecutive stimulations in the presence of antagonist. The results of the pharmacological stimulations (DHPG, KCl) are reported as fold change over baseline levels. Only cells for which the DHPG stimulation elicited a fold change greater than 1.1 times the baseline levels in  $F_{340/380}$  ratio were considered responsive cells.

## Immunoprecipitation

Cerebella from WT and *Fmr1*-KO mice were grinded in liquid nitrogen into fine powder and resuspended in 5 v/w with PBS containing 1% Igepal. Samples were cleared with 15  $\mu$ l of naked Dynabeads A (ThermoFisher) for 30 min at 4°C on a rotating wheel. During this time, 30  $\mu$ l of Dynabeads A were incubated with anti-FMRP primary antibody for 1 h at room temperature on a rotating wheel, with 100  $\mu$ g of tRNA, ssDNA and BSA. The “pre-clear” beads were then removed and samples were centrifuged for 10 min at 14,000 rpm at 4°C. Supernatants were incubated with antibody-coated beads overnight at 4°C on a rotating wheel. Beads were washed three times with PBS containing 0.1% Igepal and incubated for 15 min at 55°C with 100 mM dithiothreitol and 2 $\times$  Laemmli sample buffer. Eluted proteins were then resolved on 4%–12% gradient SDS-PAGE using MOPS buffer (Invitrogen).

## Biotinylation

Primary neurons plated at the density of 200,000 cells per well were used for biotinylation experiments at DIV 15. Neurons were washed twice with PBS and incubated with EZLink Sulfo-NHS-LC-Biotine (0.3 mg/ml in PBS, Thermo Scientific) for 10 min at 4°C. After a quick wash with PBS, unbound biotin molecules were quenched with 50 mM NH<sub>4</sub>Cl for 5 min. After two washes with ice-cold PBS, proteins were extracted using lysis buffer containing 10 mM Tris-HCl pH 7.5, 10 mM EDTA, 150 mM NaCl, 1% Triton X-100, 0.1% SDS and 1% mammalian protease inhibitor cocktail (Sigma-Aldrich). Two-hundred microgram of proteins from each condition were incubated overnight at 4°C with streptavidin-conjugated beads (Sigma-Aldrich). Beads were then washed three times with lysis buffer and resuspended in Laemmli buffer. Proteins were separated in 7% acrylamide-bis-acrylamide gel. Primary antibodies anti  $\beta$ -Actin (Sigma, #A5441; 1/1,000), anti-Ca<sub>v</sub>2.1 (Alomone Labs, #ACC-001; 1/1,000) and anti  $\beta$ 3-tubulin (Synaptic Systems, #302302; 1/1,000) were used.

RNA extraction and RT-qPCR were performed as previously described (Maurin et al., 2018a). The sequences of the primers used in this study are provided in **Table 1**.

**TABLE 1** | Sequences of the primers used in this study.

	Forward	Reverse
<i>Cacna1a</i>	GAGTATGACCCTGCTGCCTG	TGCAAGCAACCCTATGAGGA
<i>Cacna1b</i>	TGCGTTCTCGAGCTTCATGG	CGCTTGATGGTCTTGAGGGG
<i>Cacna1c</i>	GAACCATATCCTAGGCAATGCAG	AAGAGCCCTTGTGCAGGAAA
<i>Cacna1e</i>	TGAGTTTGTCCGTGTCTGGG	GAGGGACATCTCTTGCCGAG
<i>c-Kit</i>	GGAGTGTAAAGCCCTCCAACG	TGGGCCTGGATTTGCTCTTT
<i>Klf4</i>	CAGGATTCATCCCCATCCG	TGGCATGAGCTCTTGATAATGGA
<i>Gfap</i>	CAGATCCGAGGGGGCAAAA	TGAGCCTGTATTGGGACAACT
<i>Dlg4</i>	GGCGGAGAGGAACCTGTCC	AGAATTGGCCTTGAGGGAGGA
<i>Tbp</i>	AGGCCAGACCCCAACTC	GGTGTGTCCTGGCAA

Sequences are presented from 5' to 3' end.

## Polyribosome Fractionation

Samples from polyribosome fractionation were described previously (Maurin et al., 2018a). Polyribosome fractionation was performed as described previously (Bechara et al., 2009) on 20%–50% (w/w) continuous sucrose gradients. Fractions were separated on a BR-188 Density Gradient Fractionation System (Brandel). Fold changes in *Cacna1a* mRNA levels between WT and *Fmr1*-KO were assessed by RT-qPCR and were calculated for individual fractions 6–14 according to the formula  $2^{-ddCp}$  where ddCp is  $(Cp\ Pde2a\ KO\ fraction_x - Cp\ Gapdh\ KO\ fraction_x) - (Cp\ Pde2a\ WT\ fraction_x - Cp\ Gapdh\ WT\ fraction_x)$ . Results from fractions 6 to 8 (light), 9 to 11 (medium) and 12 to 14 (heavy) were pooled and analyzed together.

## Protein Extraction and Western Blot Analysis

Cells and tissues extracts were processed as described previously (Maurin et al., 2018a). Primary antibodies anti  $\beta$ -Actin (Sigma, clone AC-74; 1/1,000) and anti-Ca<sub>v</sub>2.1 (Alomone Labs, #ACC-001; 1/1,000) were incubated overnight at 4°C in PBS 0.05%.

## Immunocytochemistry on Primary Neurons

Primary neurons grown on glass coverslips were washed three times with PBS at room-temperature and then fixed using 4% Paraformaldehyde (PFA) in PBS for 10 min at room temperature. After rinsing briefly with PBS, free aldehydes were blocked with 50 mM NH<sub>4</sub>Cl in PBS for 5 min. Then, a saturation step was performed with PBS containing 10% Fetal Bovine Serum and 0.1% Triton X-100 for at least 20 min. Neurons were incubated with antibodies diluted in PBS containing 10% Fetal Bovine Serum and 0.1% Triton X-100 in a humidified chamber overnight at 4°C. After three PBS washes, neurons were incubated with secondary antibodies for 1 h at RT. After three PBS washes cells were incubated for 3 min in a PBS solution containing DAPI (10  $\mu$ g/ml). The glass coverslips were finally washed once with ddH<sub>2</sub>O and mounted (Dako Fluorescent Mounting Medium) on glass slides and stored in the dark at 4°C. The polyclonal anti-Ca<sub>v</sub>2.1 (Alomone Labs, #ACC-001) antibody was used at a dilution of 1/50. The 1C3 antibody against FMRP was used at a dilution of 1/200 (Castets et al., 2005). Colocalization quantifications of FMRP and Ca<sub>v</sub>2.1 in one confocal plan (average of three scans) were carried out using the JACoP plugin for ImageJ (Bolte and Cordelières, 2006). Cells were examined on a TCS SP5 confocal microscope (Leica).

## Cell Shape Analysis

We designed an ImageJ (Schneider et al., 2012) dedicated macro to analyze simultaneously the cell shape and the Fura2 fluorescence ratio variations (in time) obtained by sequential excitation at 340 and 380 nm. First, kinetics images of 340 and 380 nm excitation were stacked together and any lateral drift was corrected using the StackReg plugin (Thévenaz et al., 1998). A mask and a list of ROIs for each cell was obtained on the last 340 nm image after a filtering (recursive TopHat followed by an unsharp mask) and a Huang intensity thresholding. Then the 340 and 380 nm images were separated in two stacks and their  $F_{340/380}$  ratio calculated after a background measurement and subtraction in each image of the stack. The ROIs were then used on the 340/380 stack to get individual cell measurements of shape parameters (Aspect Ratio, Roundness, Area, Solidity) and  $F_{340/380}$  fluorescence ratios during time.

## Multivariate Analysis of the Cell Morphology Parameters

Baseline and KCl data were extracted and normalized to the maximal calcium value obtained for each cell with the 10 mM Calcium + ionomycin solution and combined to cell morphology parameters extracted from the images. Both cell morphology, normalized baseline and KCl data were then used for unsupervised analysis. Data were first log<sub>10</sub> transformed, then mean-centered and scaled. Then, dimension reduction was performed using Barnes-Hut implementation of t-Distributed Stochastic Neighbor Embedding (tSNE), with perplexity parameter set to 40. K-means clustering was performed on the two-dimension tSNE projection and the optimal number of clusters was determined using the Gap statistic. Significance of the differences between continuous variable distributions was assessed using either Mann-Whitney or Kruskal-Wallis rank sum tests as appropriate. All analyses and graphical representations were performed using the R statistical package or Prism Software 6-2 version (GraphPad Software, Inc., San Diego, CA, USA).

## Statistics

The Kolmogorov-Smirnov test was used to assess the normality of the distribution of the datasets. To compare non-normally distributed data, two non-parametric tests were used: the Mann-Whitney test was applied to data of two unpaired samples, while the Kruskal-Wallis test was used to examine the significance of four unpaired groups. Data are expressed as mean ± SEM, and the *P* values (or adjusted *P* values) < 0.05 were considered statistically significant. RT-qPCR analysis of mRNA expression were analyzed using ANOVA TWO WAY with Sidak's multiple comparisons *post hoc* test. The statistical analysis was performed using Prism Software 6-2 version (GraphPad Software, Inc.).

## Animal Experiments

The experiments were performed following the ARRIVE (Animals in Research: reporting *in vivo* Experiments) guidelines (Kilkenny et al., 2010). Animal care was conducted in accordance with the European Community Directive

2010/63/EU. The experiments were approved by the local ethics committee (Comité d'Ethique en Expérimentation Animale CIEPAL-AZUR N. 00788.01; APAFIS#4985-2016032314169426 v4APAFIS#8100-2016112217148206 v3).

## RESULTS

### Calcium Homeostasis Is Impaired in *Fmr1*-KO Cells

We investigated calcium homeostasis using Fura2 ratiometric imaging in primary neuron cultures derived from the cortex of E14.5 WT and *Fmr1*-KO embryos. According to our immunocytochemistry results, these cultures are enriched in neurons and have limited mature astrocyte content (less than 10% of cells) that are mostly present in cell aggregates (**Supplementary Figures S1A,B**). Therefore, these regions were avoided in subsequent calcium recordings. RT-qPCR analysis of the expression of GFAP and PSD95 markers showed that the absence of FMRP does not affect the relative amounts of astrocytes and neurons in *Fmr1*-KO cultures compared to WT (**Supplementary Figure S1C**). We systematically applied a series of consecutive drug treatments followed by a calibration step that allowed us to quantify the minimum and maximum fluorescence of Fura2 in each analyzed cell. We used the normalized fluorescence ratio ( $[F_{340/380}]/\max[F_{340/380}]$ ) as an indirect quantification of the actual intracellular calcium concentration. By this imaging approach we investigated the functionality of several key parameters of calcium homeostasis in neurons in the presence or in the absence of FMRP.

### Cellular Analysis

Our imaging data clearly show the heterogeneity of the neuronal types present in primary neuron cultures (**Figures 1A–C**). Cells differ in size, shape, resting intracellular calcium levels and maximum calcium entry upon KCl stimulation. We wondered whether the absence of FMRP could have different impacts on calcium homeostasis in different cell types. The Fura2 fluorescence ratio and the shape analysis of the ROIs were simultaneously quantified by an ImageJ lab-made macro giving the shape descriptors for each ROI (area, roundness, solidity, circularity). Roundness reflects how circular a ROI is, while solidity and circularity indicate how soft (high scores) or rough (low scores) are the contours of the region. We then performed an unsupervised multivariate analysis (**Supplementary Figures S2A,B**) to group cells according to their size, shape and calcium homeostasis parameters (baseline levels, maximum calcium levels upon KCl stimulation) identifying four distinct and homogeneous groups of cells (**Supplementary Figures S2C–H**). Representative images of ROIs detected in each cluster are shown in **Supplementary Figure S3**. Cells in group 1 and 3 differ in size and in the complexity of their contour, have a higher resting calcium concentration and high calcium entry upon KCl stimulation. Group 2 cells are small with rough contours and display a limited calcium entry following KCl stimulation, characteristics that suggest an astrocytic lineage. Group 4 ROI are small elongated objects that mostly correspond

to neurites (**Supplementary Figure S3**). We considered the repartition of WT and *Fmr1*-KO cells in these clusters and our results indicate a homogeneous distribution of cells from the two genotypes in all clusters (**Supplementary Figures S2I–L**). The number of DHPG-responding cells was also similar in both genotypes (**Supplementary Figure S4**). We focused our analysis on cells belonging to group 1 and 3 which according to this analysis, have neuron characteristics. These cells were subsequently analyzed together. The steady state intracellular Ca<sup>2+</sup> concentration, measured prior to any pharmacological treatment during the first 40 s of the recording, is elevated in the absence of FMRP (Mann-Whitney test,  $P < 0.0001$ ; **Figure 1D**).

The metabotropic Glutamate receptor pathway has been described to be deregulated in FXS (Huber et al., 2002; Bear et al., 2004). The activation of this pathway with pharmacological agonists like DHPG triggers calcium release from internal stores through IP<sub>3</sub> receptors as a consequence of the activation of the Phospholipase C and IP<sub>3</sub> second messenger pathway. The calcium ion release from intracellular stores in response to DHPG is variable and not significantly different in the absence of FMRP compared to WT cells at the population level (Mann-Whitney test,  $P = 0.9963$ , not significant; **Figure 1E**).

We next induced cell depolarization by applying a 50 mM KCl solution onto the cultures, as in these conditions VGCCs are the main determinants of calcium entry in neurons (Mao et al., 2001). VGCCs respond to cell depolarization, upon which they open and allow calcium ion entry through their pore-forming subunit. We thus analyzed for each cell the fold change in  $F_{340/380}$  induced by KCl over baseline levels. Our results show that calcium entry through voltage-dependent plasma membrane channels upon KCl-induced neuron depolarization is slightly decreased in *Fmr1*-KO neurons (Mann-Whitney test,  $P < 0.0001$ ; **Figure 1F**). Last, we observed that after the KCl stimulations *Fmr1*-KO neurons had significantly higher mean  $F_{340/380}$  ratio over the 40 s that followed the KCl stimulation compared to WT, suggesting a deregulated return to baseline levels in the absence of FMRP (Mann-Whitney test,  $P < 0.005$ ; **Figure 1G**).

Highly specific pharmacological blockers have been identified for all these VGCC subfamilies (Zamponi et al., 2015). For instance, we used specific pharmacological blockers of VGCCs: dihydropyridines, such as nitrendipine, block L-type VGCCs (Peterson et al., 1996) by binding to transmembrane domains of the  $\alpha 1$  subunit hence affecting the gating mechanism of the L-type VGCCs.  $\omega$ -Conotoxin-GV1a (Conotoxin) blocks N-type VGCCs (Ichida et al., 2005) by interacting with the channel pore.  $\omega$ -Agatoxin IVa (Agatoxin) inhibits P/Q-type VGCCs (Adams et al., 1993) by binding to two extracellular loops of the  $\alpha 1$  subunit that are close to the sensor domain of the P/Q-channel. Thus, we used some of these blockers in order to further investigate the molecular determinants of such calcium homeostasis deregulations. Within each neuron expressing or not FMRP, we measured the DR as the ratio of the mean of the maximal depolarization-induced Ca<sup>2+</sup> entry in the presence of a VGCC-specific antagonist on the mean calcium entry in the absence of a

VGCC-specific antagonist. All the antagonists tested significantly reduced calcium ion entry upon KCl stimulation. Indeed, each antagonist treatment produced a DR that was statistically different from 1, the DR value expected for a drug having no effect (one sample *t*-test,  $P < 0.0001$ ; **Figures 2A–C**). Nevertheless, Nitrendipine (1  $\mu$ M) reduced KCl-triggered calcium ion entry similarly in WT and *Fmr1*-KO cells (Mann Whitney test, n.s.:  $P = 0.2968$ ; **Figure 2A**). The  $\omega$ -Conotoxin-GV1a (Conotoxin; 1  $\mu$ M) was more efficient in *Fmr1*-KO cells (Mann Whitney test,  $P < 0.0001$ ; **Figure 2B**). On the contrary, the  $\omega$ -Agatoxin IVa (Agatoxin; 100 nM) had a fainter effect in *Fmr1*-KO than in WT cells (Mann Whitney test,  $P < 0.0001$ ; **Figure 2C**). These findings strongly suggest that N- and P/Q-type channels are deregulated in *Fmr1*-KO neurons. These results are recapitulated in **Table 2**.

### ***Cacna1a* Expression Is Altered in *Fmr1*-KO Primary Neurons**

The pore forming unit of P/Q-type VGCC is encoded by the *Cacna1a* gene, whose mRNA is a target of FMRP (Darnell et al., 2011), in particular also during early brain development (at Post-Natal Day 13, PND 13; Maurin et al., 2018a). We therefore investigated how FMRP regulates *Cacna1a* expression in *Fmr1*-KO primary cultured neurons and in cortical extracts of *Fmr1*-KO mouse. We precisely characterized the time course of various  $\alpha 1$  gene expression in WT and *Fmr1*-KO primary neurons by RT-qPCR. *Cacna1a* is the most upregulated  $\alpha 1$  gene of the Ca<sub>v</sub>2 family between DIV 14 and 21, and its expression is reduced in *Fmr1*-KO neurons (**Figures 3A–D**) at DIV 21 compared to WT cells. We therefore investigated whether FMRP modulates *Cacna1a* mRNA half-life by measuring *Cacna1a* stability together with control RNAs in primary neurons treated with the polymerase II inhibitor Actinomycin D. We observed that, consistent with a previous report (Sharova et al., 2009), Actinomycin D treatment triggers a strong decrease in *Klf4* transcript expression (**Figure 3E**) which is not due to cell toxicity, as we could show that in the same conditions *c-Kit* expression is stable over time (**Figure 3F**). In these conditions, *Cacna1a* expression is affected to a similar extent in WT and *Fmr1*-KO neurons (**Figure 3G**), excluding a role of FMRP in regulating *Cacna1a* mRNA stability. We concluded that the decreased expression levels of *Cacna1a* mRNA in *Fmr1*-KO cells do not depend on the half-life of this mRNA in the absence of FMRP but it is likely due to a decreased transcription level. Thus, we analyzed *Cacna1a* translation in the cortex of WT and *Fmr1*-KO mice by quantifying *Cacna1a* mRNA levels in different fractions of polyribosome preparations obtained from WT and *Fmr1*-KO PND 13 mouse cortex. Our results show that *Cacna1a* mRNA polyribosome association is increased in the light and medium polyribosome fractions, which argues in favor of an increased translation of this mRNA in the absence of FMRP (**Figure 3H**).

Western blot analysis of total Ca<sub>v</sub>2.1 protein levels in DIV 17–21 primary neurons showed no statistically significant difference between WT and *Fmr1*-KO cells (Mann-Whitney test,  $P = 0.7$ , not significant; **Figures 4A,B**). We also analyzed Ca<sub>v</sub>2.1 expression at the plasma membrane of *Fmr1*-KO and

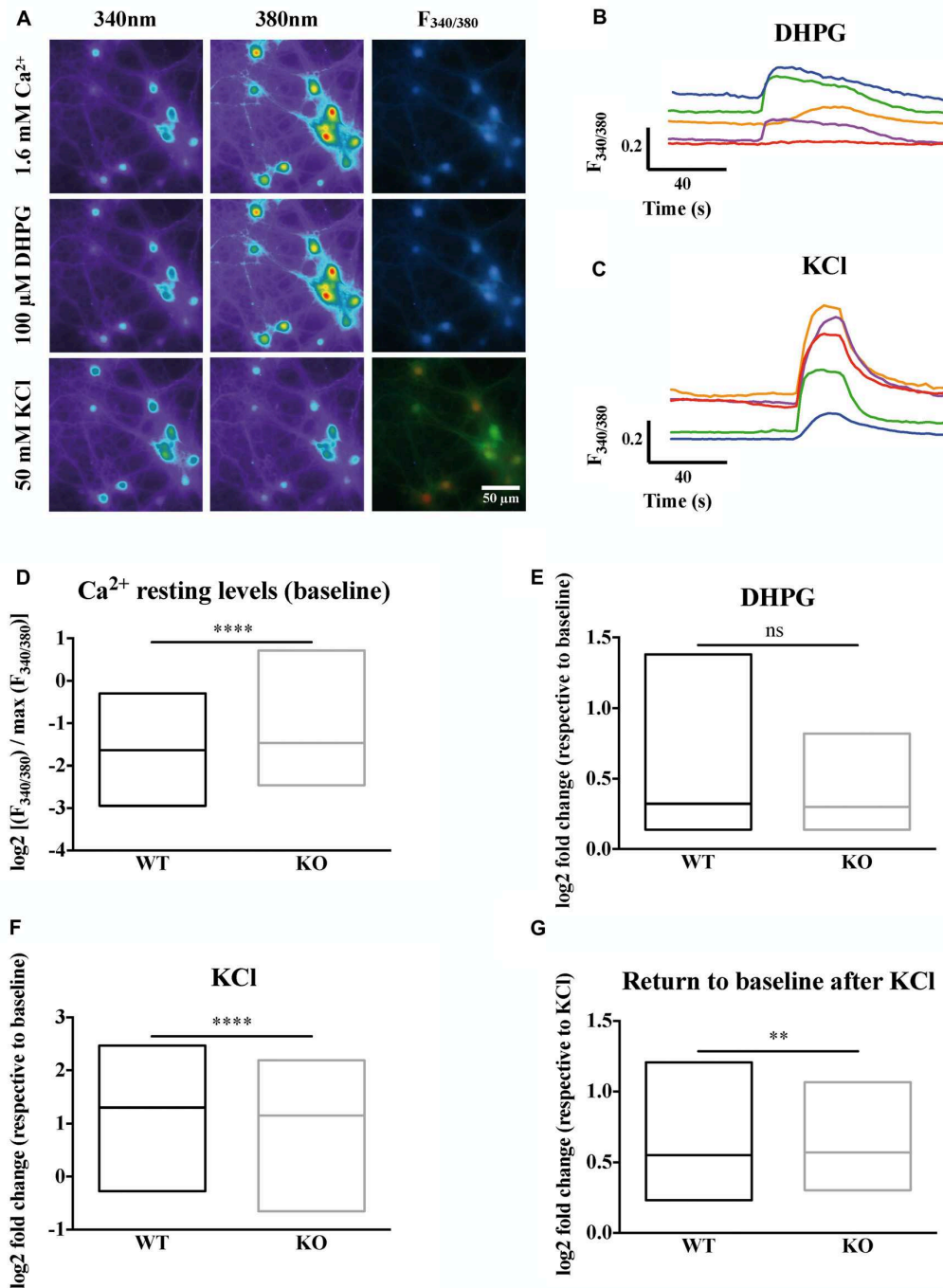
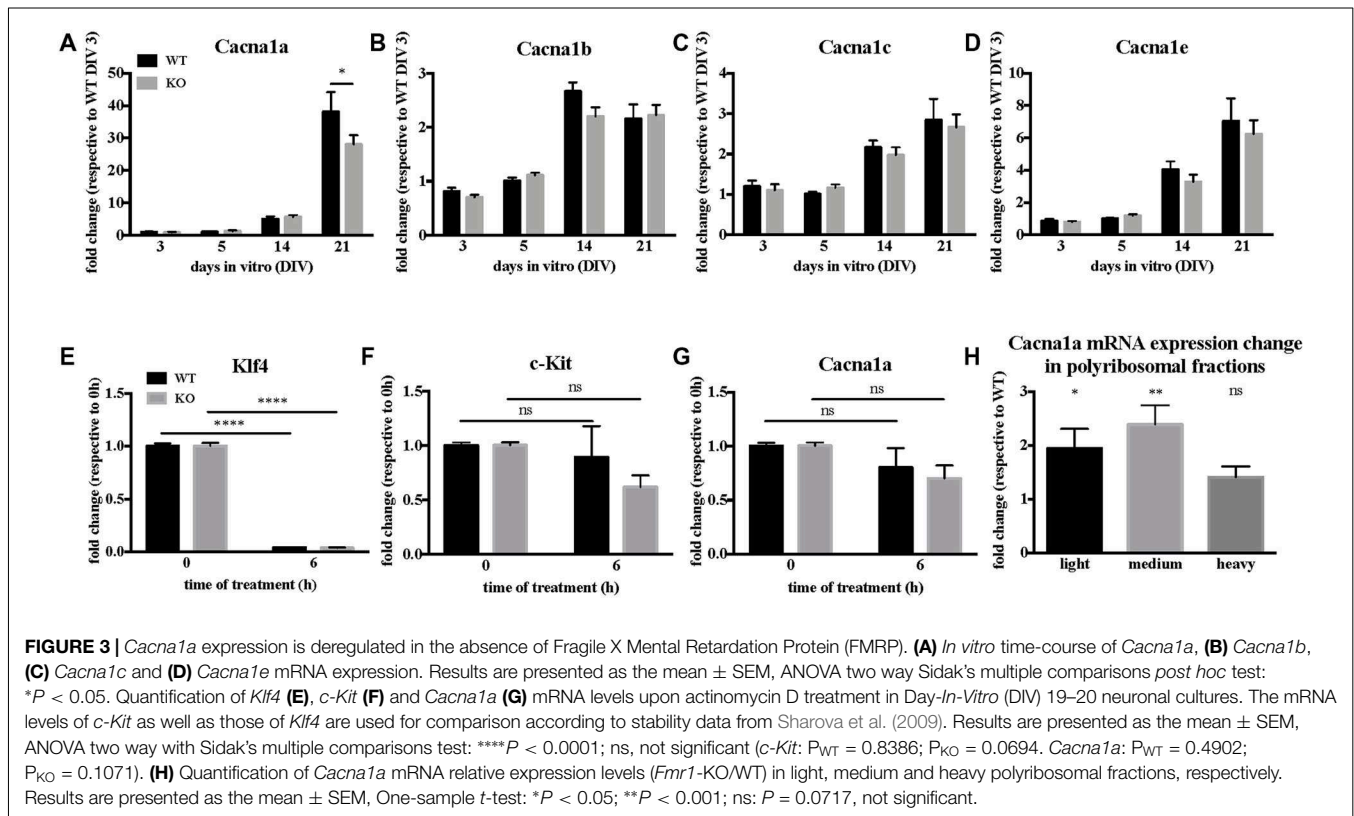
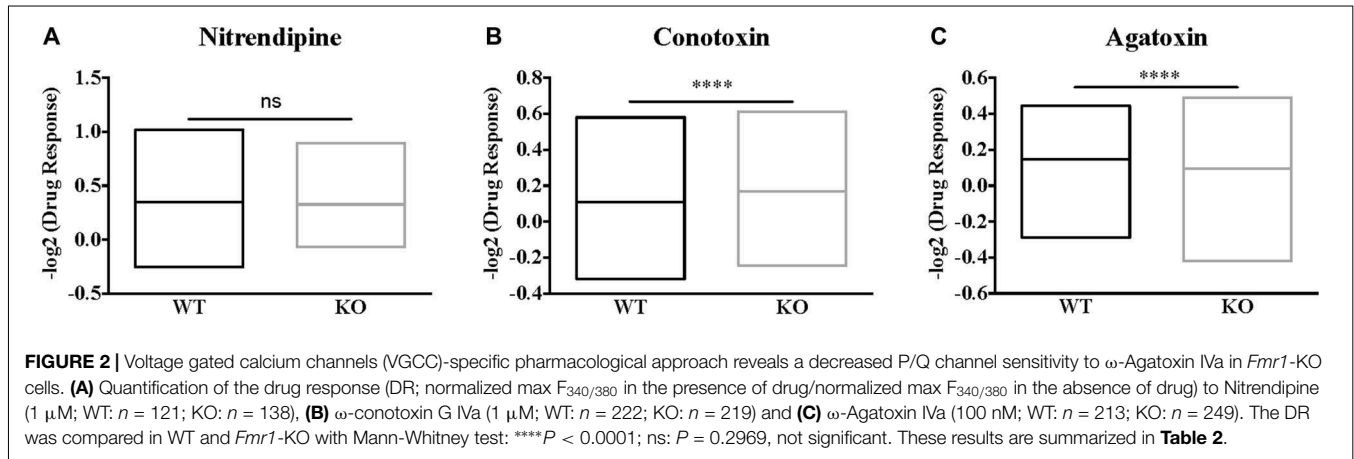


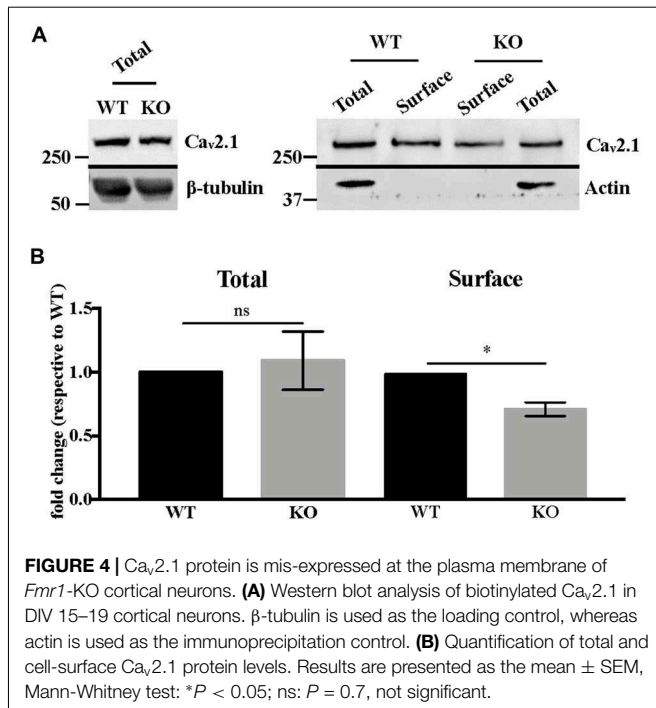
**FIGURE 1** | Calcium homeostasis is deregulated in Fragile X mental retardation 1-knockout (*Fmr1*)-KO neurons. **(A)** Profiles of the ratiometric calcium imaging response. Left panels show the emission of Fura2 at 340 nm. Middle panels show the emission of Fura2 at 380 nm. Right panels show the 340 nm/380 nm ratio of fluorescence (F<sub>340/380</sub>). Upper panels show the emission of Fura2 upon 1.6 mM Ca<sup>2+</sup> perfusion. Middle panels show the emission of Fura2 upon 100 μM DiHydroxyPhenylGlycine (DHPG) perfusion. Lower panels show the emission of Fura upon 50 mM KCl perfusion. The scale bar of each panel is 50 μm. **(B)** Sample traces of Fura2 recording upon metabotropic glutamate receptor stimulation with DHPG (100 μM) or **(C)** depolarization with KCl (50 mM) in wild-type (WT) cells. For each cell recorded, the Fura2 fluorescence at each time was normalized to the maximum Fura2 fluorescence ratio observed in the presence of a solution containing 10 mM CaCl<sub>2</sub> and ionomycin (5 μM). The mean stabilized F<sub>340/380</sub> ratio of Fura2 fluorescence during the first 40 s of recording in the absence of any stimulation is represented in **(D)**. The log<sub>2</sub> fold change in normalized F<sub>340/380</sub> after 100 μM DHPG stimulation over baseline normalized ratio is presented in **(E)**. The log<sub>2</sub> fold change in normalized F<sub>340/380</sub> after 50 mM KCl stimulation over baseline normalized ratio is presented in **(F)**. The return to baseline following a KCl stimulation is shown for WT and *Fmr1*-KO neurons **(G)**. Mann-Whitney test: \*\*\*\**P* < 0.0001; \*\**P* < 0.005; ns: *P* = 0.9963, not significant. WT*n* = 697; KO*n* = 744. These results are summarized in **Table 2**.

**TABLE 2** | Results summary.

	Mean ± SEM WT (n)	Mean ± SEM KO (n)	P value	P value significance
<b>Figure 1D</b> resting	-1.636 ± 0.016 (697)	-1.459 ± 0.0141 (744)	<0.0001	****
<b>Figure 1E</b> DHPG	0.3221 ± 0.0150 (222)	0.2989 ± 0.0105 (211)	0.9963	ns
<b>Figure 1F</b> KCl	1.297 ± 0.0142 (697)	1.154 ± 0.0147 (744)	<0.0001	****
<b>Figure 1G</b> After KCl	0.5509 ± 0.0054 (697)	0.5709 ± 0.0051 (744)	0.0038	**
<b>Figure 2A</b> Nitrendipine response	0.3497 ± 0.0215 (121)	0.3273 ± 0.0196 (138)	0.2968	ns
<b>Figure 2B</b> Conotoxin response	0.1088 ± 0.0087 (222)	0.1681 ± 0.0090 (219)	<0.0001	****
<b>Figure 2C</b> Agatoxin response	0.1478 ± 0.0085 (213)	0.0961 ± 0.0087 (249)	<0.0001	****

Mann-Whitney test was used to assess statistical significance.



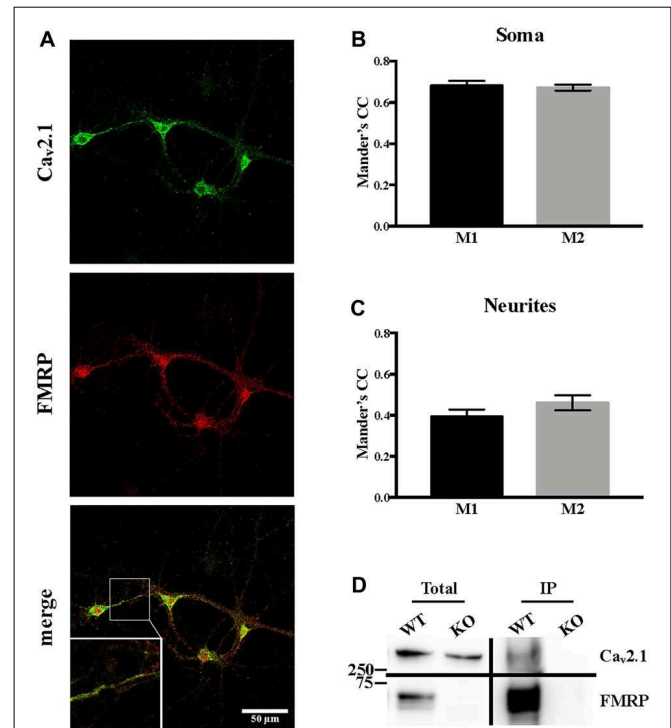


WT primary neurons by performing biotinylation assay. Our results show that Ca<sub>v</sub>2.1 protein is less expressed at the cell surface of *Fmr1*-KO neurons (Mann-Whitney test, *P* < 0.05; **Figures 4A,B**).

Since it was reported that, when overexpressed, FMRP directly interacts with both Ca<sub>v</sub>2.1 and Ca<sub>v</sub>2.2 (Ferron et al., 2014), we assessed whether Ca<sub>v</sub>2.1 and FMRP are colocalized in cortical neurons. Using double immunofluorescent staining and confocal microscopy, we observed and quantified their colocalization using Mander's coefficients both in soma and in neurites (**Figures 5A–C**). These findings were also confirmed by biochemistry experiments performed on cerebellar extracts from PND 13 mice in which we showed that endogenous Ca<sub>v</sub>2.1 co-immunoprecipitates with FMRP (**Figure 5D**).

## DISCUSSION

We and others have shown that among the FMRP mRNA targets many encode ion channels, sensors of intracellular ion concentration and other regulators of ion homeostasis (Brown et al., 2001; Darnell et al., 2011; Maurin et al., 2018a). Nonetheless, the direct interaction of FMRP with ion channels has been reported previously (Brown et al., 2010; Ferron et al., 2014; Myrick et al., 2015; Ferron, 2016). Also, it is not surprising that deregulations of expression levels as well as activities of ion channels have been shown in *Fmr1*-KO neurons (Chen et al., 2003; Meredith et al., 2007; Brown et al., 2010; Deng et al., 2013; Ferron et al., 2014; Zhang et al., 2014; Deng and Klyachko, 2016), some directly implicating VGCC deregulation in FXS (Chen et al., 2003; Meredith et al., 2007; Deng et al., 2013; Ferron et al., 2014; Zhang et al., 2014). Even if some of the conclusions of various studies were not completely convergent (Meredith et al.,



2007; Ferron et al., 2014; Zhang et al., 2014), collectively these works suggest that the Ca<sup>2+</sup> signaling-associated pathways may be involved in the physiopathology of FXS. For this reason, we decided to study calcium homeostasis in live, cultured neurons in the presence and in the absence of FMRP, using calcium imaging.

2007; Ferron et al., 2014; Zhang et al., 2014), collectively these works suggest that the Ca<sup>2+</sup> signaling-associated pathways may be involved in the physiopathology of FXS. For this reason, we decided to study calcium homeostasis in live, cultured neurons in the presence and in the absence of FMRP, using calcium imaging.

## FMRP Regulates VGCC Expression and Function

VGCCs play key roles in neurons, notably by regulating membrane excitability, neurotransmitter release and gene expression modulation (Simms and Zamponi, 2014). Alterations in the plasma membrane expression of these channels lead to pathological phenotypes, ranging from ataxia, ID, ASD and epilepsy (Yue et al., 1997; Damaj et al., 2015). Thus, to gain further insight in the Ca<sup>2+</sup> pathway-associated molecular pathology in FXS, we carried out a pharmacological approach using VGCC-specific antagonists in our cellular model. We showed that both N- and P/Q-type VGCC inhibition differently affected KCl-mediated entry in WT and *Fmr1*-KO neurons. Indeed, blocking N-type VGCCs was more efficient in *Fmr1*-KO than in WT neurons and conversely, P/Q-type inhibition had less effect in *Fmr1*-KO neurons, suggesting that both Ca<sub>v</sub>2.2

and Ca<sub>v</sub>2.1 activities are deregulated in the absence of FMRP. Interestingly, *Cacna1a* mRNA is a target of FMRP in various brain regions (Maurin et al., 2018a) and here we show that:

1. The membrane levels of Ca<sub>v</sub>2.1 channels are reduced in *Fmr1*-KO neurons, consistent with the reduced sensitivity to P/Q-type VGCC inhibition with Agatoxin. Since the intracellular levels of Ca<sub>v</sub>2.1 do not appear to be altered (**Figure 4**), we conclude that Ca<sub>v</sub>2.1 direct interaction with FMRP could play a role in its function/localization in the absence of the partner. Also, the altered actin cytoskeleton organization described in different FXS cell lines (Castets et al., 2005; Nolze et al., 2013; Abekhoukh and Bardoni, 2014; Abekhoukh et al., 2017) may explain the reduced membrane expression of Ca<sub>v</sub>2.1, since cytoskeleton is the route for the correct subcellular localization of mRNAs (Bramham and Wells, 2007). It is worth reminding that altered sublocalization of membrane proteins (encoded by mRNA targets of FMRP) have been already described, such as diacylglycerol lipase- $\alpha$  (DGL- $\alpha$ ; Jung et al., 2012), Homer 1 (Giuffrida et al., 2005; Aloisi et al., 2017) and Kv4.2, (Gross et al., 2011). Similarly, Ca<sub>v</sub>2.1 could be one of the deregulated elements. Interestingly, FMRP binds the mRNAs of other of its interacting proteins such as FMRP, CYFIP2, FXR1, Ca<sub>v</sub>2.2 (Darnell et al., 2011; Maurin et al., 2018a), suggesting a tight regulation of a FMRP-containing complex in a FMRP-dependent manner. Furthermore, the multiple mRNA targets of FMRP likely generate a network of interactions among FMRP-dependent pathways whose functional consequences are not easily predictable only considering the main role of FMRP as a translational repressor.
2. Even if the level of the mRNA encoding *Cacna1a* is slightly decreased in *Fmr1*-KO neurons at DIV21 (**Figure 3A**), the translational upregulation of this mRNA (as predicted by the increased polyribosome association of Ca<sub>v</sub>2.1 mRNA in *Fmr1*-KO brain compared with WT; **Figure 3H**) counterbalances the reduced mRNA level of *Cacna1a* in mature neurons. As in a yin-yang effect, this leads to unaltered total Ca<sub>v</sub>2.1 levels. We did not find any FMRP-dependent effect on RNA stability of *Cacna1a*, leading to the conclusion that the reduced level of *Cacna1a* mRNA in *Fmr1*-KO neurons is rather due to an indirect transcriptional deregulation.

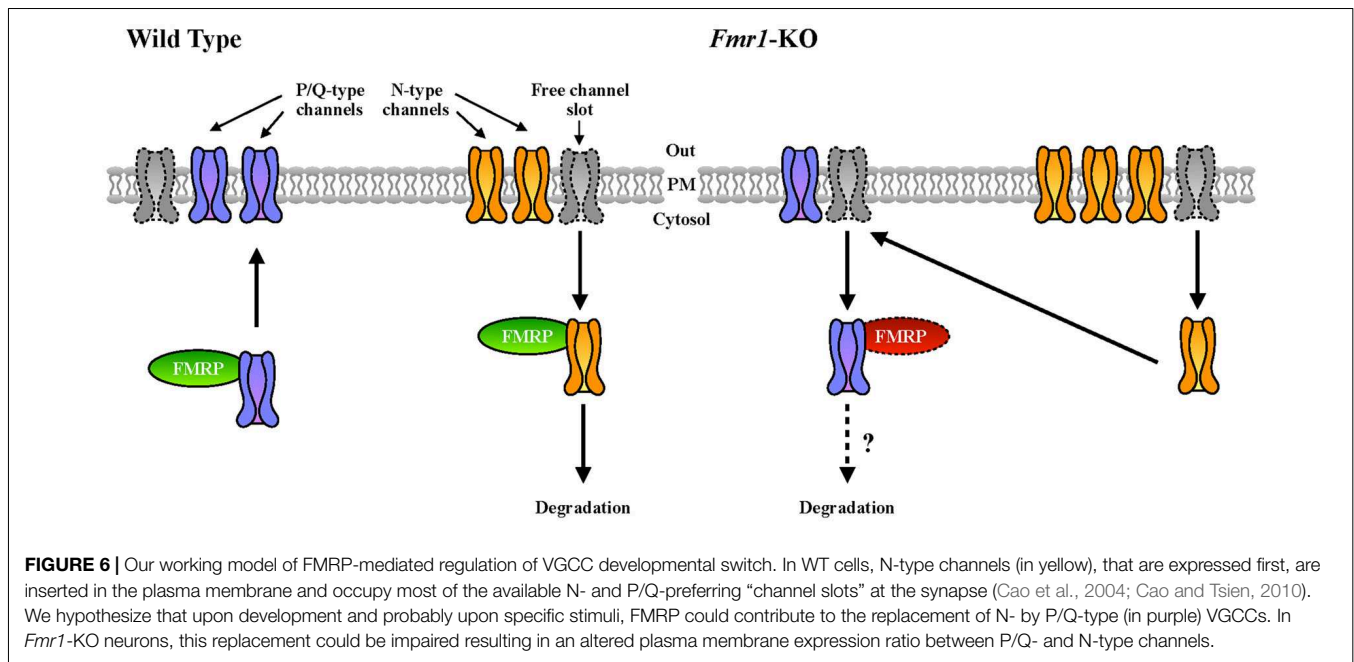
## Pre-synaptic Calcium Channels in FXS and ASD

Ca<sub>v</sub>2.2 was previously described to be more expressed and present at the plasma membrane of cells in the absence of FMRP (Ferron et al., 2014). This is consistent with the increased sensitivity to conotoxin that we observed in *Fmr1*-KO neurons compared to WT. At the molecular level, this abnormality was explained on the basis of the interaction (by overexpression) between FMRP and both Ca<sub>v</sub>2.2 and Ca<sub>v</sub>2.1 channels (Ferron et al., 2014). Interestingly, we confirmed here this latter finding by showing that the interaction between the endogenous proteins also occurs in brain (**Figure 5D**). Remarkably, we showed here that in *Fmr1*-KO cells Ca<sub>v</sub>2.1

expression deregulation is opposite to the one of Ca<sub>v</sub>2.2 (Ferron et al., 2014). As we already stated, FMRP also binds Ca<sub>v</sub>2.1 mRNA transcripts, indeed strongly suggesting a central role of FMRP in the regulation of P/Q- and N-type channels relative expression. Interestingly, it was shown that in cultured hippocampal synapses, P/Q- and N-type channels have preferred plasma membrane slots (Cao et al., 2004; Cao and Tsien, 2010) and according to this model, there are exclusive N-type channel slots and P/Q- preferring slots that can be used by N-type channels. For instance, in neurons expressing mutated P/Q-channels that lead to familial hemiplegic migraine type disease, N-type channel currents are increased, either by an increased release probability or rather by an increased N-type expression at the plasma membrane (Cao and Tsien, 2010). Collectively, these findings suggest that some P/Q-type channel slots can actually be occupied by N-type channels upon P/Q-type deficiency. Since FMRP has been shown previously to regulate N-type expression by targeting this channel to the proteasome (Ferron et al., 2014), it is tempting to speculate that FMRP is a molecular adaptor regulating the relative plasma membrane expression of N- and P/Q-type channels. In addition, by regulating the subcellular mRNA localization and/or translation of these channel types, it may also directly modulate their presence at the plasma membrane (**Figure 6**). Future studies will clarify the precise molecular mechanisms underpinning this deregulation in FXS, but it is interesting to underline here that an imbalance between the levels and the activities of N- and P/Q-type channels, could have some impacts on the physiopathology of FXS. Indeed, the differences in N- and P/Q-type inactivation kinetics, their various effects on short term plasticity (Inchauspe et al., 2004) and their different sensitivity to G-protein-coupled receptor-mediated inhibition of neurotransmitter release may have strong impacts on the functioning of synapses (Bourinet et al., 1996). Noteworthy, P/Q-type channel activity, but not N-type, mediates GABA release in fast spiking interneurons in rat pre-frontal cortex (Zaitsev et al., 2007). This suggests that abnormal GABA secretion at the temporoammonic branch of the perforant path in the *Fmr1*-KO mouse model (Wahlstrom-Helgren and Klyachko, 2015) could be related to Ca<sub>v</sub>2.1 expression defects. Furthermore, it was reported that the maximal inhibition by the GABAB receptor agonist baclofen was greater for EPSCs mediated by N-type channels than for those mediated by P/Q-type channels (Ishikawa et al., 2005). Consequently, in *Fmr1*-KO mice it is likely that the compensation of P/Q- by N-type channels have strong consequences on GABAB inhibition by weakening its effect on presynaptic release, likely leading to network hyper-excitability.

## Impairment of Calcium Homeostasis as a New Phenotype of *Fmr1*-KO Neurons. Is It a Novel Biomarker?

Implications of our findings are twofold, biological and clinical. Indeed, the FXS research field actively seeks new treatments and biomarkers to evaluate their efficiency (Castagnola et al., 2017; Maurin et al., 2018b) and, to date, the main cellular



biomarker of cultured *Fmr1*-KO neurons is represented by their abnormal dendritic spine morphology, whose analysis requires exquisite expertise (Khayachi et al., 2018). Conversely, using spectroscopy, calcium concentration measurements can be routinely performed in most laboratory settings, making it an easy and robust marker to monitor drug efficacy. Here, we applied this technique to primary cultured neurons but it will also be possible to perform it in iPS-derived neurons thus obtaining, for the first time, a molecular marker that can be functionally quantified. This can be useful for diagnostic purposes and particularly as a follow-up for specific therapies. Indeed, the search for specific and easily measurable biomarkers for FXS as well as for ASD is urgent. For instance, since 2009 one of the conclusions of the Outcome Measures Working Groups for Fragile X was “. . .research on biomarkers for detecting treatment response in FXS was in its infancy, but this was an area of utmost importance” (Berry-Kravis et al., 2013). More recently, the accurate analysis of 22 double-blind controlled clinical trials in FXS finalized between 2008 and 2015 led to the conclusion that the readouts employed to evaluate the outcome of treatments were in general of moderate/poor quality (Budimirovic et al., 2017). Last but not least, this cellular biomarker could be used as the readout for screenings of small-molecule (singular) libraries (Bardoni et al., 2017) to define new treatments opportunities for FXS.

### Study Limitations

There are several limitations of this study that one may consider:

1. Our ImageJ macro analysis resulted in the identification of four types of cells, which is clearly underestimating the complexity of the cell population. We nevertheless trust that this approach will be useful to identify a cell type of

interest in the future, associating morphological parameters with molecular/physiological determinants; interestingly, Ota et al. (2018) very recently published a study highlighting the benefits of identifying cells according to their shape;

2. In agreement with the expression levels of Ca<sub>v</sub>2.1, we focused our study on mature neuron cultures. This VGCC deregulation may not be observed in different culture settings;
3. The polyribosome fractionation experiments were performed on cortex extracts from PND 13 mice, preventing the identification of actively translating ribosomes through pharmacological inhibition. Therefore, we can only speculate that the increased presence of *Cacna1a* mRNA in light and medium fractions reflects an increased translation of this mRNA in *Fmr1*-KO mice;
4. The working model describing the putative role of FMRP in the regulation of N- and P/Q-type VGCCs at the plasma membrane (Figure 6) awaits a molecular mechanism and therefore is speculative. It nevertheless may be considered as a starting point for future analyses.

### AUTHOR CONTRIBUTIONS

TM, FD and AF designed the experiments. SC, SD, AF, MB, MJ, MG and TM performed the experiments. FB designed and wrote the macro in ImageJ. AP performed the unsupervised multivariate analysis. TM, SC, AF, AP, MM, SM and BB analyzed the data. TM, SC and BB wrote the manuscript.

### FUNDING

This study was supported by Université Côte d’Azur (UCA); Institut National de la Santé et de la Recherche Médicale

(INSERM); Centre National de la Recherche Scientifique (CNRS); Agence Nationale de la Recherche: ANR-12-BSV4-0020, ANR-12-SVSE8-0022 and Fondation pour la Recherche Médicale (FRM) DEQ20140329490 to BB; Investments for the Future, through the LABEX SIGNALIFE program: #ANR-11-LABX-0028-013, Fondation Jérôme Lejeune and ANR-15-CE16-0015 to BB and SM; FRM-ING20140129004 to BB and TM; FRAXA Foundation to TM. Bioinformatics analysis were performed at the UCAGenomiX platform of the IPMC, a member of the national infrastructure “France Génomique” (ANR-10-Infra-01). SC is recipient of an international Ph.D. fellowship from the “LABEX SIGNALIFE program.”

## ACKNOWLEDGMENTS

The authors are grateful to Prof. M. Lazdunski, M. Doghman and M. Drozd for discussion.

## SUPPLEMENTARY MATERIAL

The Supplementary Material for this article can be found online at: <https://www.frontiersin.org/articles/10.3389/fnmol.2018.00342/full#supplementary-material>

**FIGURE S1** | Cortical primary neuronal cultures show a negligible level of astrocytic growth. **(A)** Fluorescent analysis showing the level of GFAP (in green) in Day-In-Vitro (DIV) 12 WT primary neuronal cultures compared to the total number of cells (DAPI staining in blue for nuclei). **(B)** Percentage of GFAP-positive cells (20 imaged regions;  $n = 261$  DAPI-positive cells;  $n = 23$  GFAP-positive cells).

## REFERENCES

- Abekhouk, S., and Bardoni, B. (2014). CYFIP family proteins between autism and intellectual disability: links with Fragile X syndrome. *Front. Cell. Neurosci.* 8:81. doi: 10.3389/fncel.2014.00081
- Abekhouk, S., Sahin, H. B., Grossi, M., Zongaro, S., Maurin, T., Madrigal, I., et al. (2017). New insights into the regulatory function of CYFIP1 in the context of WAVE- and FMRP-containing complexes. *Dis. Model. Mech.* 10, 463–474. doi: 10.1242/dmm.025809
- Achuta, V. S., Moykkynen, T., Peteri, U. K., Turconi, G., Rivera, C., Keinänen, K., et al. (2018). Functional changes of AMPA responses in human induced pluripotent stem cell-derived neural progenitors in Fragile X syndrome. *Sci. Signal.* 11:eaa8784. doi: 10.1126/scisignal.aan8784
- Adams, M. E., Myers, R. A., Imperial, J. S., and Olivera, B. M. (1993). Toxotyping rat brain calcium channels with omega-toxins from spider and cone snail venoms. *Biochemistry* 32, 12566–12570. doi: 10.1021/bi00210a003
- Aloisi, E., Le Corf, K., Dupuis, J., Zhang, P., Ginger, M., Labrousse, V., et al. (2017). Altered surface mGluR5 dynamics provoke synaptic NMDAR dysfunction and cognitive defects in Fmr1 knockout mice. *Nat. Commun.* 8:1103. doi: 10.1038/s41467-017-01191-2
- Ascano, M. Jr., Mukherjee, N., Bandaru, P., Miller, J. B., Nusbaum, J. D., Corcoran, D. L., et al. (2012). FMRP targets distinct mRNA sequence elements to regulate protein expression. *Nature* 492, 382–386. doi: 10.1038/nature11737
- Bardoni, B., Capovilla, M., and Lalli, E. (2017). Modeling Fragile X syndrome in neurogenesis: an unexpected phenotype and a novel tool for future therapies. *Neurogenesis* 4:e1270384. doi: 10.1080/23262133.2016.1270384
- Bardoni, B., Davidovic, L., Bensaid, M., and Khandjian, E. W. (2006). The Fragile X syndrome: exploring its molecular basis and seeking a treatment. *Expert Rev. Mol. Med.* 8, 1–16. doi: 10.1017/s1462399406010751

**(C)** Quantification of *Gfap* and *Psd95* (*Dlg4* transcript) mRNA levels in DIV 20 cortical neurons ( $n = 3$  independent cultures). Results are presented as the mean  $\pm$  SEM, Mann-Whitney test: ns, not significant (*Gfap*:  $P = 0.3701$ ; *Psd95*:  $P = 0.6200$ ).

**FIGURE S2** | Unsupervised analysis of the shape and calcium homeostasis parameters of primary neuron cultures leads to the identification of four different groups of Regions-of-Interest (ROIs). Shape and calcium homeostasis parameters were first visualized in 2-dimension space using t-Distributed Stochastic Neighbor Embedding (t-SNE), then K-means clustering was performed on the 2-dimension t-SNE projection, and the optimal number of clusters, was determined using the Gap statistic. **(A)** t-SNE representation of the data, with cells colored by genotype. The distribution of WT (black dots) and *Fmr1*-KO (red dots) is homogeneous and vastly overlapping in all clusters. **(B)** t-SNE representation of the data, with cells colored by cluster. The distribution of the parameters of interest by clusters are presented using boxplots. The boxplots are defined as 25th percentile–75th percentile, the horizontal line corresponds to the median value, and whiskers extend to the min-max values. **(C)** Area covered by the cells, **(D)** cell circularity, **(E)** cell solidity, **(F)** cell roundness, **(G)** cell resting intracellular calcium concentration and **(H)** maximal KCl-triggered intracellular calcium concentration. **(I–L)** Number of cells from each genotype in the various experiments:  $\omega$ -agatoxin-IVa (Aga),  $\omega$ -conotoxin GV1a (Cono), Nitrendipine (Nitren) or in the absence of VGCC antagonist (NoDrug) show the homogeneous WT and *Fmr1*-KO cell distribution in all identified clusters.

**FIGURE S3** | Representative images of ROIs identified using the ImageJ macro. Left panels are pseudo-colored images of stabilized unstimulated cells **(a, d, g, j)**. Middle panels represent the same cells during KCl stimulation **(b, e, h, k)**. Right panels show the macro output result **(c, f, i, l)**. The ROIs are encircled by a yellow line and the numbers indicate to which cluster ROI were attributed.

**FIGURE S4** | The percentage of DHPG-responding cells is similar in WT and *Fmr1*-KO neurons. Cells in which the pharmacological stimulation elicited at least a 1.1 fold change in the  $F_{340/380}$  ratio compared to baseline  $F_{340/380}$  were considered DHPG-responsive and were counted in each cell cluster.

- Bear, M. F., Huber, K. M., and Warren, S. T. (2004). The mGluR theory of Fragile X mental retardation. *Trends Neurosci.* 27, 370–377. doi: 10.1016/j.tins.2004.04.009
- Bechara, E. G., Didiot, M. C., Melko, M., Davidovic, L., Bensaid, M., Martin, P., et al. (2009). A novel function for Fragile X mental retardation protein in translational activation. *PLoS Biol.* 7:e16. doi: 10.1371/journal.pbio.1000016
- Berry-Kravis, E., Hessler, D., Abbeduto, L., Reiss, A. L., Beckel-Mitchener, A., Urv, T. K., et al. (2013). Outcome measures for clinical trials in Fragile X syndrome. *J. Dev. Behav. Pediatr.* 34, 508–522. doi: 10.1097/DBP.0b013e31829d1f20
- Bolte, S., and Cordelières, F. P. (2006). A guided tour into subcellular colocalization analysis in light microscopy. *J. Microsc.* 224, 213–232. doi: 10.1111/j.1365-2818.2006.01706.x
- Bonaccorso, C. M., Spatuzza, M., Di Marco, B., Gloria, A., Barrancotto, G., Cupo, A., et al. (2015). Fragile X mental retardation protein (FMRP) interacting proteins exhibit different expression patterns during development. *Int. J. Dev. Neurosci.* 42, 15–23. doi: 10.1016/j.ijdevneu.2015.02.004
- Bourinet, E., Soong, T. W., Stea, A., and Snutch, T. P. (1996). Determinants of the G protein-dependent opioid modulation of neuronal calcium channels. *Proc. Natl. Acad. Sci. U S A* 93, 1486–1491. doi: 10.1073/pnas.93.4.1486
- Bramham, C. R., and Wells, D. G. (2007). Dendritic mRNA: transport, translation and function. *Nat. Rev. Neurosci.* 8, 776–789. doi: 10.1038/nrn2150
- Brown, V., Jin, P., Ceman, S., Darnell, J. C., O'Donnell, W. T., Tenenbaum, S. A., et al. (2001). Microarray identification of FMRP-associated brain mRNAs and altered mRNA translational profiles in fragile X syndrome. *Cell* 107, 477–487. doi: 10.1016/s0092-8674(01)00568-2
- Brown, M. R., Kronengold, J., Gazula, V. R., Chen, Y., Strumbos, J. G., Sigworth, F. J., et al. (2010). Fragile X mental retardation protein controls gating of the sodium-activated potassium channel Slack. *Nat. Neurosci.* 13, 819–821. doi: 10.1038/nn.2563

- Budimirovic, D. B., Berry-Kravis, E., Erickson, C. A., Hall, S. S., Hessel, D., Reiss, A. L., et al. (2017). Updated report on tools to measure outcomes of clinical trials in fragile X syndrome. *J. Neurodev. Disord.* 9:14. doi: 10.1186/s11689-017-9193-x
- Cao, Y. Q., Piedras-Renteria, E. S., Smith, G. B., Chen, G., Harata, N. C., and Tsien, R. W. (2004). Presynaptic Ca<sup>2+</sup> channels compete for channel type-preferring slots in altered neurotransmission arising from Ca<sup>2+</sup> channelopathy. *Neuron* 43, 387–400. doi: 10.1016/j.neuron.2004.07.014
- Cao, Y. Q., and Tsien, R. W. (2010). Different relationship of N- and P/Q-type Ca<sup>2+</sup> channels to channel-interacting slots in controlling neurotransmission at cultured hippocampal synapses. *J. Neurosci.* 30, 4536–4546. doi: 10.1523/JNEUROSCI.5161-09.2010
- Castagnola, S., Bardoni, B., and Maurin, T. (2017). The search for an effective therapy to treat fragile X syndrome: dream or reality? *Front. Synaptic Neurosci.* 9:15. doi: 10.3389/fnsyn.2017.00015
- Castets, M., Schaeffer, C., Bechara, E., Schenck, A., Khandjian, E. W., Luche, S., et al. (2005). FMRP interferes with the Rac1 pathway and controls actin cytoskeleton dynamics in murine fibroblasts. *Hum. Mol. Genet.* 14, 835–844. doi: 10.1093/hmg/ddi077
- Catterall, W. A. (2011). Voltage-gated calcium channels. *Cold Spring Harb. Perspect. Biol.* 3:a003947. doi: 10.1101/cshperspect.a003947
- Chen, L., Yun, S. W., Seto, J., Liu, W., and Toth, M. (2003). The fragile X mental retardation protein binds and regulates a novel class of mRNAs containing U rich target sequences. *Neuroscience* 120, 1005–1017. doi: 10.1016/s0306-4522(03)00406-8
- Clapham, D. E. (2007). Calcium signaling. *Cell* 131, 1047–1058. doi: 10.1016/j.cell.2007.11.028
- Contractor, A., Klyachko, V. A., and Portera-Cailliau, C. (2015). Altered neuronal and circuit excitability in fragile X syndrome. *Neuron* 87, 699–715. doi: 10.1016/j.neuron.2015.06.017
- Damaj, L., Lupien-Meilleur, A., Lortie, A., Riou, E., Ospina, L. H., Gagnon, L., et al. (2015). CACNA1A haploinsufficiency causes cognitive impairment, autism and epileptic encephalopathy with mild cerebellar symptoms. *Eur. J. Hum. Genet.* 23, 1505–1512. doi: 10.1038/ejhg.2015.21
- Darnell, J. C., Van Driesche, S. J., Zhang, C., Hung, K. Y., Mele, A., Fraser, C. E., et al. (2011). FMRP stalls ribosomal translocation on mRNAs linked to synaptic function and autism. *Cell* 146, 247–261. doi: 10.1016/j.cell.2011.06.013
- Deng, P. Y., and Klyachko, V. A. (2016). Increased persistent sodium current causes neuronal hyperexcitability in the entorhinal cortex of Fmr1 knockout mice. *Cell Rep.* 16, 3157–3166. doi: 10.1016/j.celrep.2016.08.046
- Deng, P. Y., Rotman, Z., Blundon, J. A., Cho, Y., Cui, J., Cavalli, V., et al. (2013). FMRP regulates neurotransmitter release and synaptic information transmission by modulating action potential duration via BK channels. *Neuron* 77, 696–711. doi: 10.1016/j.neuron.2012.12.018
- Dolphin, A. C. (2016). Voltage-gated calcium channels and their auxiliary subunits: physiology and pathophysiology and pharmacology. *J. Physiol.* 594, 5369–5390. doi: 10.1113/JP272262
- Ferron, L. (2016). Fragile X mental retardation protein controls ion channel expression and activity. *J. Physiol.* 594, 5861–5867. doi: 10.1113/jp270675
- Ferron, L., Nieto-Rostro, M., Cassidy, J. S., and Dolphin, A. C. (2014). Fragile X mental retardation protein controls synaptic vesicle exocytosis by modulating N-type calcium channel density. *Nat. Commun.* 5:3628. doi: 10.1038/ncomms4628
- Giuffrida, R., Musumeci, S., D'Antoni, S., Bonaccorso, C. M., Giuffrida-Stella, A. M., Oostra, B. A., et al. (2005). A reduced number of metabotropic glutamate subtype 5 receptors are associated with constitutive homer proteins in a mouse model of fragile X syndrome. *J. Neurosci.* 25, 8908–8916. doi: 10.1523/JNEUROSCI.0932-05.2005
- Gross, C., Yao, X., Pong, D. L., Jeromin, A., and Bassell, G. J. (2011). Fragile X mental retardation protein regulates protein expression and mRNA translation of the potassium channel Kv4.2. *J. Neurosci.* 31, 5693–5698. doi: 10.1523/JNEUROSCI.6661-10.2011
- Hebert, B., Pietropaolo, S., Meme, S., Laudier, B., Laugeray, A., Doisne, N., et al. (2014). Rescue of fragile X syndrome phenotypes in Fmr1 KO mice by a BKCa channel opener molecule. *Orphanet J. Rare Dis.* 9:124. doi: 10.1186/s13023-014-0124-6
- Huber, K. M., Gallagher, S. M., Warren, S. T., and Bear, M. F. (2002). Altered synaptic plasticity in a mouse model of Fragile X mental retardation. *Proc. Natl. Acad. Sci. U S A* 99, 7746–7750. doi: 10.1073/pnas.122205699
- Ichida, S., Abe, J., Komoike, K., Imanishi, T., Wada, T., Masuko, T., et al. (2005). Characteristics of omega-conotoxin GVI A and MVIIC binding to Cav 2.1 and Cav 2.2 channels captured by anti-Ca<sup>2+</sup> channel peptide antibodies. *Neurochem. Res.* 30, 457–466. doi: 10.1007/s11064-005-2681-5
- Inchauspe, C. G., Martini, F. J., Forsythe, I. D., and Uchitel, O. D. (2004). Functional compensation of P/Q by N-type channels blocks short-term plasticity at the calyx of Held presynaptic terminal. *J. Neurosci.* 24, 10379–10383. doi: 10.1523/JNEUROSCI.2104-04.2004
- Ishikawa, T., Kaneko, M., Shin, H. S., and Takahashi, T. (2005). Presynaptic N-type and P/Q-type Ca<sup>2+</sup> channels mediating synaptic transmission at the calyx of Held of mice. *J. Physiol.* 568, 199–209. doi: 10.1113/jphysiol.2005.089912
- Jung, K. M., Sepers, M., Henstridge, C. M., Lassalle, O., Neuhofer, D., Martin, H., et al. (2012). Uncoupling of the endocannabinoid signalling complex in a mouse model of fragile X syndrome. *Nat. Commun.* 3:1080. doi: 10.1038/ncomms2045
- Khayachi, A., Gwizdek, C., Poupon, G., Alcor, D., Chafai, M., Casse, F., et al. (2018). Sumoylation regulates FMRP-mediated dendritic spine elimination and maturation. *Nat. Commun.* 9:757. doi: 10.1038/s41467-018-03222-y
- Kilkenny, C., Browne, W. J., Cuthill, I. C., Emerson, M., and Altman, D. G. (2010). Improving bioscience research reporting: the ARRIVE guidelines for reporting animal research. *PLoS Biol.* 8:e1000412. doi: 10.1371/journal.pbio.1000412
- Mao, B. Q., Hamzei-Sichani, F., Aronov, D., Froemke, R. C., and Yuste, R. (2001). Dynamics of spontaneous activity in neocortical slices. *Neuron* 32, 883–898. doi: 10.1016/s0896-6273(01)00518-9
- Maurin, T., Lebrigand, K., Castagnola, S., Paquet, A., Jarjat, M., Popa, A., et al. (2018a). HITS-CLIP in various brain areas reveals new targets and new modalities of RNA binding by Fragile X mental retardation protein. *Nucleic Acids Res.* 46, 6344–6355. doi: 10.1093/nar/gky267
- Maurin, T., Melancia, F., Jarjat, M., Castro, L., Costa, L., Delhay, S., et al. (2018b). Involvement of phosphodiesterase 2A activity in the pathophysiology of fragile X syndrome. *Cereb. Cortex* doi: 10.1093/cercor/bhy192 [Epub ahead of print].
- Maurin, T., Zongaro, S., and Bardoni, B. (2014). Fragile X syndrome: from molecular pathology to therapy. *Neurosci. Biobehav. Rev.* 46, 242–255. doi: 10.1016/j.neubiorev.2014.01.006
- Meredith, R. M., Holmgren, C. D., Weidum, M., Burnashev, N., and Mansvelder, H. D. (2007). Increased threshold for spike-timing-dependent plasticity is caused by unreliable calcium signaling in mice lacking Fragile X gene FMR1. *Neuron* 54, 627–638. doi: 10.1016/j.neuron.2007.04.028
- Miyashiro, K. Y., Beckel-Mitchener, A., Purk, T. P., Becker, K. G., Barret, T., Liu, L., et al. (2003). RNA cargoes associating with FMRP reveal deficits in cellular functioning in Fmr1 null mice. *Neuron* 37, 417–431. doi: 10.1016/s0896-6273(03)00034-5
- Myrick, L. K., Deng, P. Y., Hashimoto, H., Oh, Y. M., Cho, Y., Poidevin, M. J., et al. (2015). Independent role for presynaptic FMRP revealed by an FMR1 missense mutation associated with intellectual disability and seizures. *Proc. Natl. Acad. Sci. U S A* 112, 949–956. doi: 10.1073/pnas.1423094112
- Nanou, E., Scheuer, T., and Catterall, W. A. (2016). Calcium sensor regulation of the Cav2.1 Ca<sup>2+</sup> channel contributes to long-term potentiation and spatial learning. *Proc. Natl. Acad. Sci. U S A* 113, 13209–13214. doi: 10.1073/pnas.1616206113
- Nolze, A., Schneider, J., Keil, R., Lederer, M., Hüttelmaier, S., Kessels, M. M., et al. (2013). FMRP regulates actin filament organization via the armadillo protein p0071. *RNA* 19, 1483–1496. doi: 10.1261/rna.037945.112
- Ota, S., Horisaki, R., Kawamura, Y., Ugawa, M., Sato, I., Hashimoto, K., et al. (2018). Ghost cytometry. *Science* 360, 1246–1251. doi: 10.1126/science.aan0096
- Peterson, B. Z., Tanada, T. N., and Catterall, W. A. (1996). Molecular determinants of high affinity dihydropyridine binding in L-type calcium channels. *J. Biol. Chem.* 271, 5293–5296. doi: 10.1074/jbc.271.10.5293
- Schneider, C. A., Rasband, W. S., and Eliceiri, K. W. (2012). NIH Image to ImageJ: 25 years of image analysis. *Nat. Methods* 9, 671–675. doi: 10.1038/nmeth.2089
- Sharova, L. V., Sharov, A. A., Nederezov, T., Piao, Y., Shaik, N., and Ko, M. S. (2009). Database for mRNA half-life of 19 977 genes obtained by DNA microarray analysis of pluripotent and differentiating mouse embryonic stem cells. *DNA Res.* 16, 45–58. doi: 10.1093/dnares/dsn030

- Simms, B. A., and Zamponi, G. W. (2014). Neuronal voltage-gated calcium channels: structure, function and dysfunction. *Neuron* 82, 24–45. doi: 10.1016/j.neuron.2014.03.016
- Thévenaz, P., Ruttimann, U. E., and Unser, M. (1998). A pyramid approach to subpixel registration based on intensity. *IEEE Trans. Image Process.* 7, 27–41. doi: 10.1109/83.650848
- Wahlstrom-Helgren, S., and Klyachko, V. A. (2015). GABA<sub>B</sub> receptor-mediated feed-forward circuit dysfunction in the mouse model of fragile X syndrome. *J. Physiol.* 593, 5009–5024. doi: 10.1113/jp271190
- Yue, Q., Jen, J. C., Nelson, S. F., and Baloh, R. W. (1997). Progressive ataxia due to a missense mutation in a calcium-channel gene. *Am. J. Hum. Genet.* 61, 1078–1087. doi: 10.1086/301613
- Zaitsev, A. V., Povysheva, N. V., Lewis, D. A., and Krimer, L. S. (2007). P/Q-type, but not N-type, calcium channels mediate GABA release from fast-spiking interneurons to pyramidal cells in rat prefrontal cortex. *J. Neurophysiol.* 97, 3567–3573. doi: 10.1152/jn.01293.2006
- Zamponi, G. W., Striessnig, J., Koschak, A., and Dolphin, A. C. (2015). The physiology, pathology, and pharmacology of voltage-gated calcium channels and their future therapeutic potential. *Pharmacol. Rev.* 67, 821–870. doi: 10.1124/pr.114.009654
- Zhang, Y., Bonnan, A., Bony, G., Ferezou, I., Pietropaolo, S., Ginger, M., et al. (2014). Dendritic channelopathies contribute to neocortical and sensory hyperexcitability in *Fmr1*<sup>-/-</sup> mice. *Nat. Neurosci.* 17, 1701–1709. doi: 10.1038/nn.3864
- Zhuchenko, O., Bailey, J., Bonnen, P., Ashizawa, T., Stockton, D. W., Amos, C., et al. (1997). Autosomal dominant cerebellar ataxia (SCA6) associated with small polyglutamine expansions in the  $\alpha$  1A-voltage-dependent calcium channel. *Nat. Genet.* 15, 62–69. doi: 10.1038/ng0197-62

**Conflict of Interest Statement:** The authors declare that the research was conducted in the absence of any commercial or financial relationships that could be construed as a potential conflict of interest.

Copyright © 2018 Castagnola, Delhaye, Folci, Paquet, Brau, Duprat, Jarjat, Grossi, Béal, Martin, Mantegazza, Bardoni and Maurin. This is an open-access article distributed under the terms of the Creative Commons Attribution License (CC BY). The use, distribution or reproduction in other forums is permitted, provided the original author(s) and the copyright owner(s) are credited and that the original publication in this journal is cited, in accordance with accepted academic practice. No use, distribution or reproduction is permitted which does not comply with these terms.